

CHARACTERIZATION OF MINERAL OIL, COAL TAR AND SOIL PROPERTIES
AND INVESTIGATION OF MECHANISMS THAT AFFECT COAL TAR
ENTRAPMENT IN AND REMOVAL FROM POROUS MEDIA

A thesis
Presented to
The Academic Faculty

By
Lingjun Kong

In Partial Fulfillment
of the Requirements for the Degree
Doctor of Philosophy in Environmental Engineering
School of Civil and Environmental Engineering

Georgia Institute of Technology
July 2004

Copyright ©2004 by Lingjun Kong

CHARACTERIZATION OF MINERAL OIL, COAL TAR AND SOIL PROPERTIES
AND INVESTIGATION OF MECHANISMS THAT AFFECT COAL TAR
ENTRAPMENT IN AND REMOVAL FROM POROUS MEDIA

Approved by:

Dr. Kurt D Pennell, Chairman

Dr. William J. Koros

Dr. Ching-Hua Huang

Dr. James A. Mulholland

Dr. Sotira Yiacoumi

Date Approved: June 15th, 2004

Dedicated to my parents

Jiancheng Kong
and
Biying Huang

*whose steadfast belief in me has
always encouraged me to
persue my dream
and whose deep love will be supporting me
to achieve my goal*

ACKNOWLEDGEMENTS

At this moment when I am wrapping up my Ph.D. research work, I am so excited and grateful. There have been so many people with me throughout the whole journey to my PhD degree. I would like to acknowledge all the individuals for their support and understanding.

First, I want to address my sincere appreciation to my Ph.D. advisor, Dr. Kurt D. Pennell. Thank you for giving me the opportunity to come to Georgia Tech. Thank you for your support and understanding all these years. Thank you for all the valuable guidance and thoughtful advice.

Dr. Kevin H. Gardner, who was my advisor at Case Western Reserve University, opened the door to the United States for me. He is young, smart and considerate. He made it so easy for me to become accustomed to the life in the US. I enjoyed the time working with him, and I treasure the friendship between us.

Dr. William J. Koros, my minor advisor, is a respected professor with brilliant achievements in his academic career and a great personality. I want to express my heartfelt gratitude to him for agreeing to serve as a committee member and all the thoughtful inputs and constructive comments on my research and professional career. Also, I want to thank all the other committee members, Dr. James A. Mulholland, Dr. Ching-Hua Huang and Dr. Sotira Yiacoumi, for their interest in my research, their valuable suggestions and kind encouragements.

Much appreciation is expressed to my dearest friends, Jianzhong, Huichun (Judi) and Pinghong, Hongying (Cherry) and Yongtao, Jin and Xinyan, Di and Jin. Thanks for the support during my hard times. They made my happy times much happier, my tough times much easier. They are not only my friends, they are like family to me. Special thanks are also given to Lei and Xiaobing, Liuchun and Jie, Dongsheng, Haoming (Mary) and Yizhong, Ning and Duyuan (David), I couldn't get where I am without their friendship. I wish them the best in the future.

Speaking of friends, one person I cannot forget is Dr. Guangxuan Zhu. Besides all his assistance and help in the lab, I particularly appreciate his advice and suggestions in my everyday life and professional development. To me, he is like a teacher, a father and a friend.

My current or former labmates, Ahmet, Andrew, Jed, Eric, Dave, Mike Young and Charlotte, deserve tons of appreciation. They are all friendly, cooperative and responsible people. I am so lucky to be one of them. Ahmet helped me start in the lab. I enjoyed the time working and talking with him. I am deeply grateful for his friendship and encouragement. Andrew is such a gentleman. He is so nice and never hesitates to give me a hand. Jed has shown his steadfast support during my Ph.D. studies. I truly thank him for his continuous help on my research, and I will never forget all the discussions and conversations. He is like a big brother to me. Thank you, Jed. Eric is young and smart. I enjoy the time working with him and appreciate all his help.

Also, I would like to express my appreciation to all the other faculty, staff and students in environmental engineering program at Georgia Tech. They made my time at Georgia Tech more valuable. DoHyong is such a cool guy. I enjoyed all the

conversations, and thanks for all the wonderful rides. Youlboong is very friendly. He deserves much appreciation. James is so nice and always ready to help. I am so grateful for all his assistance.

At last, I want to thank my family, my mom, dad and two younger brothers, for all their love and support. I love them, miss them, I have been always wanted them to be proud of me.

TABLE OF CONTENTS

ACKNOWLEDGEMENTS	iv
LIST OF TABLES	xii
LIST OF FIGURES	xvi
LIST OF NOMENCLATURE AND SYMSBOLS	xxii
SUMMARY	xxvi
CHAPTER I. INTRODUCTION	1
CHAPTER II. LITERATURE REVIEW	6
Background	6
Nonaqueous Phase Liquid (NAPLs)	7
NAPL Entrapment in Porous Media	8
Interfacial Tension	13
Wettability	15
NAPL Residual Saturation	20
Capillary Pressure	22
Capillary Pressure-Saturation Relationship	28
NAPL Displacement in Porous Media	32
NAPL Source Zone Remediation Technologies	40
Surfactant Enhanced Aquifer Remediation	45
Surface Active Agents	45
Micellar Solubilization	46
NAPL Mobilizaton	46
Surface Enhanced Aquifer Remediation	50
Thermal Remediation	51
CHAPTER III. OBJECTIVES	55
CHAPTER IV. EVALUATION OF MINERAL OIL RESIDUAL SATURATION IN POROUS MEDIA	57
Introduction	57

Materials and Methods	61
Materials	61
Methods	62
Oil Density	62
Viscosity	62
Surface Tension	63
Interfacial Tension	64
Particle Size Analysis	65
Particle Density	67
Total Carbon	68
Specific Surface Area	68
Moisture Release Curves	69
Two-Phase (Oil-Water) Residual Oil Saturation Experiments	71
Three-Phase (Air-Oil-Water) Residual Oil Saturation Experiments	74
Results and Discussion	78
Physical Properties of Mineral Oil	78
Physical Properties of Soil	80
Moisture Release Curves of Soil Samples	81
Residual Mineral Oil Saturation in Two-Phase (Two-Phase) Systems	85
Residual Mineral Oil Saturation in Three-Phase (Air-Oil-Water) Systems	98
Summary and Conclusions	110
CHAPTER V. EVALUATION OF COAL TAR RESIDUAL SATURATION IN POROUS MEDIA	112
Introduction	112
Materials and Methods	118
Material	118
Methods	118
Particle Size Analysis	119
Particle Density	120
Total Carbon	120
Specific Surface Area	120
Cation Exchange Capacity	120
Moisture Release Curves	121
Tar Density	123
Viscosity	123
Surface Tension	123

Interfacial Tension	123
Two-Phase (Water-Tar) Residual Saturation Experiments	124
Results and Discussion	126
Soil Properties	126
Moisture Release Curves	129
Coal Tar Properties	134
Residual Tar Saturation in Two-Phase (Water-Tar) Systems	139
Dimensionless parameter Estimation	147
Summary and Conclusions	155
CHAPTER VI. SOLUTION CHEMISTRY EFFECTS ON THE INTERFACIAL PROPERTIES OF COAL TAR-WATER-SILICA SYSTEMS AND RESIDUAL COAL TAR SATURATION IN POROUS MEDIA	157
Introduction	157
Materials and Methods	165
Material	165
Methods	166
Solution Preparation	166
Contact Angle Measurements	167
Interfacial Tension	170
Zeta-Potential Measurements	170
Asphaltene Separation and Quantification	171
Acid Number Determination	172
Base Number Determination	174
Capillary Pressure-Residual Saturation Experiment	175
Results and Discussion	177
Characterization of Coal Tar Acid/Basic Properties	177
Asphaltene Quantification	177
Point of Zero Charge	180
Acid Number and Base Number	182
Effect of pH and Ionic Strength on Contact Angle	188
Effect of pH on Contact Angle	188
Effect of Organic Acid or Base Addition on Contact Angle	197
Effect of Ionic Strength on Contact Angle	203
Effect of pH and Ionic Strength on Tar-Water IFT	205
Effect of pH on Tar-Water IFT	205
Effect of Organic Acid/Base Addition on Tar-Water IFT	210
Effect of Ionic Strength on IFT	219
Effect of pH on Capillary Pressure-Saturation Relationships in Coal Tar-Water-Silica Sand System	220

Summary and Conclusions	233
CHAPTER VII. EFFECTS OF TEMPERATURE AND SURFACTANT ADDITION ON COAL TAR PROPERTIES, RESIDUAL SATURATION AND RECOVERY FROM POROUS MEDIA	236
Introduction	236
Materials and Methods	241
Materials	241
Methods	242
Effect of Temperature on Coal Tar Properties	242
Phase Behavior (salinity scan)	244
IFT Measurements	246
Permeability Measurement	246
Coal Tar Displacement Experiment	249
Results and Discussion	251
Effect of Temperature on Coal Tar and Displacing Solution Properties	251
Effect of Temperature on Density	251
Effect of Temperature on Viscosity	253
Effect of Temperature on IFT	255
Effect of Temperature on Contact Angle	257
Residual Coal Tar Saturation during Tar Displacement Experiments	260
Effect of Temperature on Coal Tar Residual Saturation	260
Surfactant Screening	262
Effects of Surfactant Flushing on Residual Coal Tar Saturation	266
Polymer Solution Viscosity and Rheology	268
Dimensionless Parameter Analysis of Coal Tar Displacement	271
Summary and Conclusions	276
CHAPTER VIII. CONSLUCIONS AND RECOMMENDATIONS	278
APPENDIX A. PRIMARY VOLATILE AND SEMIVOLATILE ORGANICS IN AUBURN COAL TAR	286
APPENDIX B. PRIMARY VOLATILE AND SEMIVOLATILE ORGANICS IN CAPE MAY COAL TAR	287
APPENDIX C. PRIMARY VOLATILE AND SEMIVOLATILE ORGANICS IN CHARLESTON COAL TAR	288

APPENDIX D. PRIMARY VOLATILE AND SEMIVOLATILE ORGANICS IN FAIRFIELD COAL TAR	289
APPENDIX E. PRIMARY VOLATILE AND SEMIVOLATILE ORGANICS IN SARANAC COAL TAR	290
APPENDIX F. PRIMARY VOLATILE AND SEMIVOLATILE ORGANICS IN SHIPPENSBURG COAL TAR	291
REFERENCES	292
VITA	309

LIST OF TABLES

Table 2-1:	Relevant properties and MCL for selected organic contaminants.	9
Table 2-2:	Relevant physical properties of representative NAPLs.	11
Table 2-3:	Reported contact angle values of NAPLs on different substrate in aqueous media	21
Table 2-4:	Residual NAPL saturation (S_{Nr}) in various subsurface systems.	23
Table 2-5:	Expressions for capillary number and Bond number.	35
Table 2-6:	Correlations between residual NAPL saturation and soil and NAPL properties (Chevalier and Fonte, 2000).	38
Table 2-7:	Comparison of representative remediation technologies.	48
Table 4-1:	Opening size of ASTM sieves used in particle size analysis.	66
Table 4-2:	Comparison of relevant properties for EPRI mineral oil, “Old” and “New” Franklin mineral oil, and dodecane (reference organic liquid).	79
Table 4-3:	Physical properties of soils obtained from particle size (sieve), surface area, and total carbon analysis.	83
Table 4-4:	Summary of soil water retention parameters obtained for van Genuchten and Brooks-Corey equations.	86
Table 4-5:	Summary of EPRI mineral oil residual saturation values in two-phase (water-oil) systems.	90
Table 4-6:	Linear Correlations between residual oil saturation and representative individual parameters in two-phase (water-oil) systems.	94
Table 4-7:	Selected linear correlations between residual oil saturation and parameter combinations in two-phase (water-oil) systems.	95
Table 4-8:	Representative nonlinear correlations between residual oil	96

	saturation and parameter combinations in two-phase(water-oil) systems.	
Table 4-9:	Summary of EPRI mineral oil residual saturation values in three-phase (air-water-NAPL) systems.	103
Table 4-10:	Summary of Franklin mineral oil residual saturation values in three-phase (air-water-oil) systems.	104
Table 4-11:	Linear Correlations between residual oil saturation and representative individual parameters in there-phase (air-water-oil) systems.	105
Table 4-12:	Selected linear correlations between residual oil saturation and parameter combinations in there-phase (air-water-oil) systems.	106
Table 4-13:	Representative nonlinear correlations between residual oil saturation and parameter combinations in there-phase (air-water-oil) systems.	107
Table 5-1:	Reported physical properties of coal tar.	115
Table 5-2:	Representative organic concentration in coal tar.	116
Table 5-3:	Example of major organic components of the coal tar.	116
Table 5-4:	Amounts of soil and coal tar samples received from participating utilities.	122
Table 5-5:	Experimental matrix for two-phase (water-tar) residual saturation experiments.	127
Table 5-6:	Physical properties of soils based on particle size (sieve) analysis.	132
Table 5-7:	Physical-chemical properties of nine MGP-site soil samples (sieved through No. 20 sieve).	133
Table 5-8:	Soil water retention characteristics obtained from van Genuchten and Brooks-Corey equations.	137
Table 5-9:	Physical properties of coal tar samples.	141
Table 5-10:	Summary of coal tar residual saturation measurements in two-phase (water-tar) systems.	142
Table 5-11:	Linear Correlations between residual tar saturation and	149

representative individual parameters in two-phase (water-tar) systems (all data).

Table 5-12:	Selected linear correlations between residual tar saturation and parameter combinations in two-phase (water-tar) systems (all data).	150
Table 5-13:	Selected nonlinear correlations between residual oil saturation and parameter combinations in two-phase (water-tar) systems (all data).	151
Table 5-14:	Selected correlations between residual tar saturation and parameters in paired and unpaired two-phase (water-tar) systems.	152
Table 5-15:	Capillary number, Bond number and total trapping numbers in coal tar soil columns.	154
Table 6-1:	Chemical specification for 5-indanol, 1-naphtoic acid and quinoline.	168
Table 6-2:	Stock buffer solution used in this study.	168
Table 6-3:	Asphaltene content, acid and base number, as well as point of zero charge of the six coal tar samples.	178
Table 6-4:	Contact angles of the six coal tar samples on glass slides as a function of aqueous solution pH.	189
Table 6-5:	Parameters used in interaction energy estimation.	194
Table 6-6:	Effect of 5-indanol concentration on contact angle of Saranac coal tar on glass slides in 0.01 M NaCl solution.	199
Table 6-7:	Effect of quinoline concentration on contact angle of Saranac coal tar on glass slides in 0.01 M NaCl solution.	200
Table 6-8:	Effect of NaCl concentration on the contact angle of Saranac coal tar (amended with 10% (wt) quinoline) on glass slides.	206
Table 6-9:	Tar-water IFT as a function of pH for six coal tar samples.	208
Table 6-10:	Effect of 5-indanol concentration on IFT between Saranac coal tar (added with 10% wt 5-indanol) and water with 0.01 M NaCl.	212
Table 6-11:	Effect of quinoline concentraton on IFT between Saranac coal tar (amended with 10% (wt) quinoline) and water with 0.01 M NaCl	213

Table 6-12:	Effect of NaCl concentration on the IFT between Saranac coal tar and water.	221
Table 6-13:	Effect of NaCl concentration on the IFT between Saranac coal tar (amended with 10% (wt) quinoline) and water.	221
Table 6-14:	Comparison of measured and predicted drainage capillary pressure entry pressure in Saranac tar-water-Ottawa sand system.	228
Table 6-15:	Comparison of residual saturation of water and coal tar during water drainage and imbibition process.	229
Table 6-16:	Parameters fitted to van Genuchten equation in air-water-F-70 and tar-water-F-70 systems using different scaling factors	230
Table 7-1:	Characteristics of surfactants used in study.	243
Table 7-2:	Effect of surfactant and salt on tar-water IFT and viscosity of Charleston coal tar at room temperature ($22 \pm 1^\circ\text{C}$).	264
Table 7-3:	Dimensionless Parameter Analysis of Coal Tar Displacement.	274

LIST OF FIGURES

Figure 2-1:	Typical Distribution of nonaqueous-phase liquid (NAPL) in the subsurface (a) LNAPL; (b) DNAPL (Lowe et al., 1999).	12
Figure 2-2:	Standard chemical potential of surface active molecules at an interface (the polar head is shown as a circle, and the non-polar tail by a short strait line) (after Davis and Rideal, 1963).	16
Figure 2-3:	Contact angle (ω).	18
Figure 2-4:	Equilibrium at a curved air-water interface (Bear 1972).	25
Figure 2-5:	Force balance in a capillary tube (a) air-water; (b) LNAPL-water; (c) DNAPL-water.	27
Figure 2-6:	Capillary pressure-saturation curve (Pankow and Cherry, 1996).	29
Figure 2-7:	Schematic diagram of the pore entrapment model that corresponding coordinate system (Pennell et al., 1996).	33
Figure 2-8:	PCE desaturation as a function of total trapping number (Pennell et al. 1996).	39
Figure 2-9:	Temperature range of soil heating and phenomenon significantly impacted (modified from Smith and Hinchee, 1993).	44
Figure 2-10:	Typical phase behavior with variation of electrolyte concentration (Baran et al., 1994).	43
Figure 2-11:	Generalized plot of viscosity for anionic surfactant solutions (Ramsburg, 2002).	44
Figure 4-1:	Tempe cells used to measure water retention characteristics (moisture release curves) of the soil samples.	70
Figure 4-2:	Residual mineral oil saturation experiments in (a) oil-water two-phase and (b) air-oil-water three-phase systems.	75
Figure 4-3:	Schematic diagram of experimental column apparatus used for water and oil residual saturation measurements.	76

Figure 4-4:	Textural classification of soils based on the Universal Soil Classification System (USCS).	82
Figure 4-5:	Soil water retention (release) curves of soils.	87
Figure 4-6:	Relationship between residual water saturation and particle density and porosity in air-water-soil systems.	88
Figure 4-7:	Representative van Genuchten (VG) and Brook-Corey (BC) fitting curves for MRC (Mead/Bell).	89
Figure 4-8:	Residual mineral oil saturation in oil-water two-phase system.	91
Figure 4-9:	Representative correlations between residual oil saturation and soil or oil properties in two-phase (water-oil) systems (solid lines represent fit curves and dash lines represent 95% confidence level) (a) linear correlations (Case 4-7-10); (b) nonlinear correlations (Case 4-8-8).	97
Figure 4-10:	Mineral oil saturation during the oil-drainage process in an air-oil-water three-phase system(dots represent EPRI data, and Squares represent Franklin (New) data).	99
Figure 4-11:	Residual mineral oil saturation in three-phase (air-oil-water) systems (a) EPRI mineral oil; (b) Franklin mineral oil.	102
Figure 4-12:	Representative correlations between residual mineral oil saturation and oil/soil properties in there-phase (air-water-oil) systems (solid lines represent fit curves and dash lines represent 95% confidence level) (a) linear correlations (Case 4-12-7); (b) nonlinear correlations (Case 4-13-5).	108
Figure 4-13:	Residual mineral oil saturation in both two- and three-phase systems.	109
Figure 5-1:	Glass (Teflon endplates) and aluminum (stainless steel endplates) columns used to measure coal tar residual saturation.	125
Figure 5-2:	Textural classification of soils collected from nine MGP sites based on the Universal Soil Classification System (USCS).	130
Figure 5-3:	Particle size distribution curves of soil samples collected from nine MGP sites.	131
Figure 5-4:	Soil water retention (release) curves of soils collected from nine MGP sites (a) normal scale; (b) semi-log scale.	132

Figure 5-5:	Representative van Ganuchten (VG) and Brook-Corey (BC) fitting curves for MRC.	136
Figure 5-6:	Residual saturation and residual concentration of six coal tar samples in two-phase (water-tar) systems.	143
Figure 5-7:	Images of air-dry and water-saturated Cape May (clean), and the extruded soil core at residual coal tar saturation.	144
Figure 5-8:	Images of air-dry and water-saturated Charleston soil (clean), and the extruded soil core at residual coal tar saturation.	145
Figure 5-9:	Images of air-dry and water-saturated Winsted soil (clean), and the extruded soil core at residual coal tar saturation (Shippensburg coal tar).	146
Figure 5-10:	Representative linear correlations between residual tar saturation and soil/tar properties (solid lines represent fit curve and dash lines represent 95% confidence level) (a) all data; (b) paired samples; (c) unpaired samples.	153
Figure 6-1:	Hypothetical structure of a petroleum asphaltene (Chemical formula: $(C_{79}H_{92}N_2S_2O)_3$, molecular weight: 3449 g/mole) (Bunger and Li, 1981).	161
Figure 6-2:	Contact angle measurements (a) Sessile drop method for contact angle measurement; (b) Representative digitized images obtained from goniometer.	169
Figure 6-3:	Capillary pressure-saturation experimental apparatus used for Saranac coal tar-water-Ottawa sand system at pH 4.7, 7.0 and 10.0.	176
Figure 6-4:	Viscosity (a) and density (b) versus asphaltene content (Solid lines represent the linear regression curve, and the dash lines represent 95% confidence levels).	179
Figure 6-5:	Zeta potential as a function of pH for Saranac tar.	181
Figure 6-6:	Acid- and base number determination by potentiometric titration.	184
Figure 6-7:	Correlations between acid and base numbers.	185
Figure 6-8:	Acid and base numbers as functions of asphaltene contents (wt%) for coal tar and crude oil samples.	186

Figure 6-9:	PZC as a function of BN/AN ratio (straight line represents the fitting curing for Zheng's data (2000)).	187
Figure 6-10:	Overall interaction energy between silica glass slide and coal tar as a function of separation distance accounting for electrostatic and van der Waals forces (DLVO forces); (b) Both DLVO forces and hydration force.	195
Figure 6-11:	Static contact angle as a function of pH for coal tar from six MGP sites.	196
Figure 6-12:	Contact angle as a function of pH with the addition of 5-indanol (a) and quinoline (b) to Saranac coal tar.	201
Figure 6-13:	Correlations between contact angle and AN, BN and addition of quinoline.	202
Figure 6-14:	Contact angles of Saranac tar (a) and Saranac tar amended with 10% (wt) quinoline on microscope glass slide as a function of aqueous pH at different NaCl concentrations.	207
Figure 6-15:	Interfacial tension (IFT) as a function of pH for six coal tar samples.	209
Figure 6-16:	IFT as a function of pH with the addition of 5-indanol (a) or quinoline (b) to Saranac tar.	214
Figure 6-17:	Correlations between tar-water IFT and the amount of 5-indanol or quinoline added to Saranac tar at pH 7.0 ($R^2=0.92$ for linear fit of data with 5-indanol addition, and $R^2=0.97$ for linear fit of data with quinoline addition).	215
Figure 6-18:	Comparison of IFT reduction with the addition of quinoline or 5-indanol to Saranac tar as a function of pH.	216
Figure 6-19:	Correlations between IFT and AN, BN, addition of 5-indanol to Saranac coal tar.	217
Figure 6-20:	Correlations between IFT and AN, BN, addition of quinoline to Saranac coal tar.	218
Figure 6-21:	IFT between Saranac and water as a function of pH at two different NaCl concentrations (a) Saranac tar without quinoline amended; (b) Saranac tar amended with 10% quinoline; (c) benzen amended with 10% quinoline.	222

Figure 6-22:	Capillary pressure-saturation relationships in coal tar-water-F-70 Ottawa sand system at pH 4.7, 7.0, 10.0.	227
Figure 6-23:	Scaled capillary pressure-saturation relationships (lines represents predicted P_c - S relationships from that in air-water system, dots represents experimental data). (a)(b) Case I; (c)(d) Case II; (e)(f) Case III.	231
Figure 6-24:	Root Mean Square Error (RMSE) of three different scaling approaches at pH 4.7, 7.0 and 10.0.	232
Figure 7-1:	Representative salinity scan experiment with 10% MA-80I surfactant, 1g/L CaCl_2 and NaCl.	245
Figure 7-2:	Schematic shape of a pendant drop of one fluid formed in another (d_e is the equatorial diameter of the pendant droplet, and d_s is the diameter measured at a distance d_e up from the bottom of the drop).	247
Figure 7-3:	Representative KI tracer BTCs for determining the residual coal tar saturation in Charleston tar-water-Ottawa sand (20-30 mesh) system (Retardation factors R_F are 1.01, 0.71 and 0.78 for system before coal tar injection, after water flood without surfactant, and after water flood with surfactant, respectively).	250
Figure 7-4:	Measured density of coal tar, surfactant solution (10% MA-80I + 1g/L CaCl_2 + 3 g/L NaCl) and water (0.01 M as a function of temperature in the range of 22 to 50°C (error bars are smaller than symbols).	252
Figure 7-5:	Temperature effect on viscosity (a) viscosity of coal tar (Charleston, Fairfield and Cape May), surfactant solution (10% MA-80I + 1 g/L CaCl_2 + 3 g/L NaCl) and water (0.01 M NaCl) as a function of temperature (22 to 50°C) (error bars are smaller than symbols). (b) Comparison of viscosity of coal tar to that of white oils and crude oils (white oil and crude oil data are from Ekmondson, 1965).	254
Figure 7-6:	Charleston tar-water, surfactant solution IFT as a function of temperature (a) Tar-water IFT as a function of temperature at different pHs; (b) Comparison of tar-water IFT and tar-surfactant solution IFT as a function of temperature at pH 7.0.	256
Figure 7-7:	Contact angle of glass slides in Charleston tar-water and tar-10% MA80-I surfactant solution systems as a function of temperature (a) Contact angle of Charleston coal tar on glass slide in water; (b) Comparison of contact angle of Charleston	258

coal tar on glass slide in water and surfactant solution.

Figure 7-8:	Temperature effect on Charleston coal tar removal in Ottawa sand (a) F-70 Ottawa sand; (b) 20-30 mesh Ottawa sand.	261
Figure 7-9:	IFT and viscosity as a function of salinity in Charleston coal tar-surfactant solution system (a) IFT as a function of salinity; viscosity as a function of salinity (error bars are smaller than symbols).	265
Figure 7-10:	Comparison of Charleston coal tar residual saturation after different surfactant solution flushing at 22°C (“initial” means the initial coal tar saturation, “water” refers to the residual tar saturation after water (0.01M NaCl) flood, and “surfactant” corresponds to the residual tar saturation after surfactant flushing).	267
Figure 7-11:	Effect of shear rate, temperature and concentration on xanthan gum solution viscosity.	270
Figure 7-12:	Permeability changes in column during various stage of the flushing process (“Water”, “CS-330” and “CS+XG” correspond to the permeability after water (0.01 M NaCl, CS-330 and CS-330/Xanthan gum solution flushing).	273
Figure 7-13:	Relationships between residual coal tar saturation and capillary number, (b) total trapping number, and dimensionless group F (Solid or dash lines in (c) represent data for crude oil (Abrams, 1975).	275

LIST OF ACRONYMS AND SYMBOLS

Acronyms

AN	acid number
ANOVA	analysis of variance
ASTM	American Society for Testing and Materials
BETX	benzene, toluene, ethyl benzene, and xylenes
BN	base number
CA	contact angle
CAA	Clean Air Act
CAS	Chemical Abstracts Service
CEC	cation exchange capacity
CERLA Act	Comprehensive Environmental Response, Compensation, and Liability Act
CHOX	chemical oxidation
DNAPL	dense nonaqueous phase liquid
DV	drop volume
EO	ethylene oxide
HPLC	high performance liquid chromatograph
HSWA	Hazardous and Solid Waste Amendments
IFT	interfacial tension
LLE	liquid-liquid equilibria
LNAPL	light nonaqueous phase liquid
MCL	maximum contaminant level
MCLG	maximum contaminant level goal
MGP	manufactured gas plant
MP	micellar/polymer flushing
MRC	moisture release curve
MW	molecule weight
NAPL	nonaqueous phase liquid
NPL	National Priority List
NPDWR	National Primary Drinking Water Regulations
PAH	polycyclic aromatic hydrocarbon (or polynuclear aromatic hydrocarbons)
PCBs	polychlorinated biphenyls
PCE	tetrachloroethene
PO	propylene oxide
PTFE	polytetrafluoroethylene
PV	pore volume
PZC	point of zero charge
RT	ring tensiometer
SARA	Superfund Amendments and Reauthorization Act

SEAR	surfactant enhanced aquifer remediation
SMCL	secondary maximum contaminant level
SSA	specific surface area
SSM	solid sample module
ST	surface tension
TC	total carbon
TCE	trichloroethene
TOC	total organic carbon
USCS	Universal Soil Classification System
USDA	United States Department of Agriculture
USEPA	United States Environmental Protection Agency

Symbols

A	Hamaker constant [J]
a_i	activity of species i [mol L^{-1}]
c_i	bulk solution concentration of species i [mol L^{-1}]
C	mean circumference of the du Nouy ring
cF	correction factor [dimensionless]
C_g	coefficient of gradation [dimensionless]
c_i	aqueous concentration of chemical i [mol L^{-1}]
c_s	surface concentration [mol L^{-1}]
C_u	coefficient of uniformity [dimensionless]
D	separation distance between two parallel surfaces [m]
d	inner diameter of the tip [m]
d_e	equatorial diameter of the pendant drop [m]
d_s	diameter measured at a distance d_e up from the bottom of the pendant drop [m]
d_m	median particle size [mm]
d_{50}	the size with 50% of the particles pass through [mm]
d_{60}	the size with 60% of the particles pass through [mm]
d_{10}	the size with 10% of the particles pass through [mm]
E	standard desorption free energy (J)
E_p	polar group desorption energy (J)
E_{np}	nonpolar group desorption energy (J)
F	dimensionless group
H	shape dependent quantity.
h	negative pressure [cm of water]
k	intrinsic permeability [m^2]
K	conductivity [m s^{-1}]
k_{rw}	NAPL relative permeability [dimensionless]
K_d	partitioning coefficient
k_w	wetting coefficient
m	mobility ratio [dimensionless]
N	molarity
N_B	bond number [dimensionless]

N_{Ca}	capillary number [dimensionless]
N_T	total trapping number [dimensionless]
P_c	capillary pressure [cm of water]
P_N	pressure in nonwetting phase [cm of water]
P_w	pressure in wetting phase [cm of water]
q	Darcy's velocity [$m\ s^{-1}$]
Q	flow rate [$m^3\ s^{-1}$]
R	radius of the du Nouy ring and the wire of ring [cm]
r	radius of the wire of the du Nouy ring [cm]
r_1, r_2	radii of curvature [m]
r^*	mean radius of curvature [m]
R_F	retardation factor [dimensionless]
S	saturation [$cm^3\ cm^{-3}$]
S_e	effective saturation [dimensionless]
S_{Nr}	residual NAPL saturation [$cm^3\ cm^{-3}$]
S_r	residual saturation [dimensionless]
S_s	saturated saturation [dimensionless]
S_{wr}	residual water saturation [dimensionless]
S_{wri}	antecedent water saturation [$cm^3\ cm^{-3}$]
S^s	interfacial entropy per unit area [$J\ m^{-2}$]
T	temperature [K]
U	electrophoretic mobility
V_d	average volume of oil droplets [cm^3]
V_{napl}	volume of NAPL in porous medium [cm^3]
V_{void}	volume of void in porous medium [cm^3]
W	weight [g]
W_{edk}	electric double layer interaction energy [J]
W_{hyd}	hydration interaction energy [J]
W_{vdw}	van der Waals interaction energy [J]
z	valency of ion [dimensionless]

Greek symbols

α	fitting parameter in van-Genuchten equation
β	angle of inclination from horizontal [$^\circ$]
γ	interfacial tension [dynes cm^{-1}]
κ	Debye-Hückel parameter [m^{-1}]
λ	pore size distribution parameter
Γ_i	surface excess of specie I [$mol\ m^{-2}$]
μ	chemical potential [$J\ mol^{-1}$]
η	viscosity [cP]
η_o	oil phase viscosity [cP]
η_w	water phase viscosity [cP]
ϕ_0	electric potential of surface [mv]
ϕ	porosity [$cm^3\ cm^{-3}$]
ρ	density [$g\ cm^{-3}$]

ρ_b	bulk density [g cm^{-3}]
ρ_{CT}	coal tar density [g cm^{-3}]
ρ_o	oil density [g cm^{-3}]
ρ_s	solid density [g cm^{-3}]
ρ_w	water density [g cm^{-3}]
θ	volumetric water content [$\text{cm}^3 \text{ cm}^{-3}$]
θ_{sat}	saturated volumetric water content [$\text{cm}^3 \text{ cm}^{-3}$]
θ_{res}	residual volumetric water content [$\text{cm}^3 \text{ cm}^{-3}$]
τ	shear stress [N m^{-2}]
γ	shear rate [s^{-1}]
ε	permittivity [$\text{C N}^{-1} \text{ m}^{-1}$]
ζ	zeta potential (mV)
ω	contact angle ($^\circ$)

SUMMARY

Mineral oil is one of the most widely spilled petroleum products. Coal tar was a significant by-product of the former manufactured gas plants (MGPs). Mineral oil and coal tar are mixture nonaqueous phase liquids (NAPLs). Polycyclic aromatic hydrocarbons (PAHs), most of which are known to be carcinogenic and mutagenic, appear as either impurities in mineral oil or primary constituents in coal tar. Therefore, the appearance of mineral oils or coal tars in the subsurface can serve as long-term sources of ground water contamination. However, very limited data are available on the entrapment and removal of mixture NAPLs (i.e., mineral oil and coal tar) in porous media. Data about coal tar behavior in porous media are particularly lacking. Current remediation technologies are ineffective, especially to coal tar contaminated sites, and a lot of former MGP sites remain unaddressed.

The overall objective of this research was to evaluate the behavior of mineral oil and coal tar in porous media, develop correlations between the residual NAPL saturation and NAPL and soil properties, and investigate the mechanisms governing NAPL entrapment and recovery from porous media.

The quantification of properties of three commercial mineral oils and six MGP coal tars reveals that mineral oils are light nonaqueous phase liquids (LNAPLs) with densities lower than water ($\sim 0.88 \text{ g/cm}^3$) and viscosities ranging from 10 to 20 cP at 22°C , whereas coal tars are dense nonaqueous phase liquids (DNAPLs) with densities slightly greater than water ($1.052\text{-}1.104 \text{ g/cm}^3$) and viscosities much higher than water

(32-425 cP at 22°C). The interfacial tensions (IFT) between oil or tar and water were lower than that of pure NAPLs. Properties of 16 field soil samples (soil particle size distribution, specific surface area, total carbon content, cationic exchange capability and soil moisture release curve) were also characterized. Correlations between residual NAPL saturation and NAPL and soil properties were developed. The results show that the entrapment of mineral oil and coal tar in porous media is dependent upon soil particle size distribution, total carbon content, oil (tar) viscosity and oil (tar)-water IFT.

Asphaltenes, which are believed to be the constituents containing acidic and basic functional groups in coal tars, were quantified. Coal tar density and viscosity show significant dependence upon asphaltene contents, which is attributed to the asphaltene aggregation. Other parameters indicating acidic and basic properties, including acid and base number and point of zero charge, were also measured for each coal tar sample.

Coal tar contact angle on silica glass slides and tar-water IFT were measured as a function of aqueous pH, ionic strength and organic acid or base addition. Based on the contact angle data, the silica surface exhibited slightly increased water-wetting condition (i.e., contact angle reduction) when pH is greater than 7 or lower than 4. At high pH (>7), the contact angle reduction was attributed to the electrostatic repulsive force between negatively charged silica glass surface and deprotonated organic acid in coal tar. At low pH, the hydration force overweighed the electrostatic force and resulted in the contact angle reduction. Interfacial tension exhibited a reduction at both low and high pH, suggesting the dissociation of acid or base constituents was responsible. These mechanisms governing the contact angle and IFT change with pH were further evaluated by addition of 5-indanol and quinoline into the coal tar phase. From the contact angle and

IFT measurements with the addition of 5-indanol and quinoline, 5-indanol addition did not affect the contact angle, while the addition of quinoline resulted in a more oil-wetting condition, especially at low pH (< 4.5). These observations are consistent with the hypothesis that wettability change stems from the electrostatic interaction between the coal tar phase and silica surface. The fact that the contact angle decreased slightly when pH was less than 4.5 indicates that the hydration force cannot be neglected. With the addition of quinoline, this trend became less pronounced and no longer observed following the addition of quinoline addition greater than 5%, confirming the existence of the hydration force. The overall energy caused by van der Waals, electrostatic and hydration forces between the coal tar and glass slide surface was plotted against the separation distance between these two surfaces. The resulted curves at pH 2.6 and 3.4 exhibit energy barriers for the coal tar to overcome in order to approach the glass surface, indicating a more water-wetting conditions (contact angle reduction). For tar-water IFT, 5-indanol and quinoline acted as surface active species which accumulated at the tar-water interface, and consequently decreased the IFT. The effect of ionic strength is believed to be determined by the “salting-out” effect and electrostatic interaction, and this effect is negligible when the ionic strength below 0.5 M, indicating ionic strength is not a significant factor on coal tar entrapment in typical ground water system.

Capillary pressure-saturation relationships were investigated for F-70 Ottawa sand at three different pH (4.7, 7.0 and 10.0). Experimental results show that residual tar saturation in F-70 Ottawa sand at pH 4.7, pH 7.0 and pH 10.0 were 0.38, 0.18 and 0.10 cm^3/cm^3 , respectively, corresponding to the contact angle decrease. Scaling analysis indicates the viscosity effect cannot be neglected.

The effect of temperature and surfactant or surfactant/polymer addition on coal tar removal was investigated by conducting coal tar displacement experiments at three different temperatures (22, 35, and 50°C) with series flushing of water, surfactant and surfactant/polymer. Coal tar removal from porous media was enhanced by elevating the temperature. The coal tar removal increased approximately 4% in F-70 Ottawa sand and 11% in 20-30 mesh Ottawa sand as temperature increased from 22 to 50°C. In the surfactant flushing studies, three anionic surfactants, Aerosol MA-80I, Steol CS-330 and Dowfax 8390, were tested for the ability to reduce the tar water IFT, and two surfactant solutions were utilized in coal tar displacement experiments. CS-330 with a Na₂CO₃ concentration of 21.2 g/L (0.2 M) was found to be more effective than Aerosol MA-80I with the addition of 1 g/L CaCl₂ and 3 g/L NaCl, which indicates the efficiency of surfactant flushing was dependent not only upon the surfactant-NAPL combination, but also upon salt type and concentration. Xanthan gum was used as the polymer combined with surfactant solution for the purpose of mobility control. Positive results were found at a xanthan gum concentration of 500 ppm. Dimensionless parameter analysis reveals that the residual saturation of coal tar was still as high as 17% when the capillary number, total trapping number and F value were 1×10^{-2} , which is consistent with published data on viscous crude oils. These results imply that coal tars are very difficult to remove from porous media.

Overall, the property quantification and correlation development in this study provide tools in predicting NAPL entrapment in porous media from measurable NAPL and soil properties. Aqueous chemistry (i.e., pH and ionic strength) influences NAPL entrapment in porous media, but is not enough to cause significant removal of residual

coal tar in the evaluated systems. Thermal technique and surfactant/polymer flushing, or their combination exhibited great potential in MGP site remediation, but may still require flux and plum management.

CHAPTER I

INTRODUCTION

With the development of the energy industry, petroleum- or coal-derived products have become widespread in the subsurface as a result of accidental spills, leaks and improper disposal. Mineral oil is one of the most widely spilled petroleum products. Coal tar is a significant by-product of the former manufactured gas plants (MGPs), where gas fuels were produced from coal. Mineral oils and coal tars are complex nonaqueous phase liquids (NAPLs), containing polycyclic aromatic hydrocarbons (PAHs). PAHs exist as impurities in mineral oils, and are the primary constituents in coal tar. Many PAH compounds are known to be carcinogenic and mutagenic, while others are suspected carcinogens (Irwin et al., 1997; Peters et al. 1999). Consequently, the presence of mineral oils and coal tars in the subsurface has the potential to cause adverse risk to human health and environment, and degrade ground water resources. However, very limited data are available to evaluate the mineral oil and coal tar entrapment in the subsurface, and even less effort have been employed to investigate the mechanisms controlling the entrapment and removal of these NAPLs in the porous media.

The NAPL entrapment caused by capillary pressure is defined as residual NAPL saturation. In the petroleum industry, the volume of oil trapped and not recoverable from oil reservoirs has been of great concern, and a lot of data were published on the oil

residual saturation in petroleum reservoirs. In environmental engineering, the residual NAPL saturation data are focused on pure NAPLs, such as benzene, trichloroethen (TCE) and tetrachlorethan (PCE) (Mercer and Cohen, 1990). Due to their unique physical chemical properties, including composition, viscosity and interfacial tension (IFT), mineral oils and coal tars can behave very differently from the pure NAPLs in porous media or oil in oil reservoirs. For example, the existence of asphaltenes, which consist of condensed aromatic nuclei systems with numerous polar functional groups containing N, O, S atoms, can increase the coal tar viscosity due to asphaltene aggregation (Sheu and Storm, 1995). At the same time, the polar functional groups, which could serve as organic acids or bases and surface active molecules, could cause the variation of coal tar spreading or adhere on the solid surface (wettability) and tar-water interfacial tension (Zheng, 2001a, b, c; Zheng and Powers, 2003). However, available data of residual coal tar saturations are very limited and vary significantly. Hugaboom and Powers (2002) reported residual tar saturations ranging from 0.29 to 0.47 in a relatively uniform coarse sand, while Barranco and Dawson (1999) got much higher values (0.52-0.77) under similar laboratory conditions. Due to the lack of residual saturation data, the correlations between residual NAPL saturation and NAPL and soil properties, which can provide useful tools to predict the amount of trapped NAPLs based on a limited set of measurable soil and NAPL properties, are rarely investigated. The few correlations available were based on low viscosity organics in synthetic polytetrafluoroethylene (PTFE) cores (Steff et al., 1997) or silica sand (Chevalier and Fonte, 2000). No investigation has been found to address the correlations between residual saturation of highly viscous NAPL and properties of NAPL and natural soils.

Although the quantification of NAPL entrapment and characterization of site conditions is essential, the ultimate goal is to reduce or removal the residual NAPL from the subsurface. Speaking to the NAPL contaminated site remediation, pump and treat is one of the most widely used source zone remediation technologies (Mackay and Cherry, 1989). The conventional pump and treat technology extracts groundwater through extraction wells and treats the extracted water above ground prior to disposal. Pump and treat often requires lengthy periods of time to achieve cleanup objectives. For DNAPLs, conventional pump-and-treat remediation technologies, which rely on transport of the NAPL or dissolution of the contaminant into the aqueous phase, are less effective. First, DNAPLs are much harder to remove when at the bottom of an aquifer. The second reason for the reduction of the effectiveness of pump and treat remediation stems from the extreme low solubility of organics, such as PAHs, in water. Some forms of chemical enhancement for pump-and-treat has been proved to be necessary at some remediation sites, especially to highly viscous fluids. Surfactant enhance aquifer remediation (SEAR) has been proved to be a promising technology under many circumstances (Villaume, 1985; Pennell et al., 1993; Pennell et al., 1994; Bettahar et al., 1999; Dwarakanath et al., 1999; Ramsburg, 2002). Due to the solubilization of organic chemicals by the surfactant micelle and reduction of interfacial tension by the surfactant, NAPL removal can be greatly enhanced. For better results, cosolvent and/or polymer are used with surfactant. The injection of cosolvent can drastically increase the solubility, and polymers can increase the displacing phase viscosity and decrease the mobility ratio, thereby facilitating their removal from the subsurface.

Thermal methods have been widely used in enhance oil recovery (EOR) (Lake, 1989) and some NAPL contaminant sites (McGowan et al., 1996; USEPA, 2000). McGowan et al. (1996) reported that coal tars were could be removed at soil temperatures above 400°C. But these high temperatures are hard to achieve in the subsurface system and are very energy-consuming. High temperatures may also cause unexpected reactions of coal tar constituents, which could lead to unexpected harm to human health and contamination of the environment. Considering the fact that viscosity decreased exponentially with increasing temperature (Lake, 1989), thermal technology at relative low temperature would benefit the removal of highly viscous coal tar from the porous media.

The overall objective of this research is to quantify the properties of commercial mineral oils, MGP coal tars and representative natural soils, evaluate the residual saturation of mineral oil and coal tar in porous media, and investigate the mechanisms controlling NAPL entrapment and removal in the porous media.

This thesis begins with a background and literature review in order to provide general information for the research topic (Chapter II). The overall and specific objectives are outlined in Chapter III. In Chapter IV, results from property quantification of three commercial mineral oils and seven field soil samples, investigation of residual mineral oil saturation in saturated and unsaturated porous media, and development of correlations between residual oil saturation and properties of mineral oils and soils are presented. Properties of six coal tar samples and nine soil samples from former MGP sites were evaluated. Coal tar residual saturations in soils were quantified. Correlations between residual coal tar saturation and representative tar and soil properties were

developed. All these results are described in Chapter V. Investigation of the effect of pH and ionic strength on wettability and tar-water interfacial tension (IFT) are incorporated in Chapter VI. Contact angle and tar-water IFT were measured as a function of pH, ionic strength and organic acid or base concentration. Coal tar acid/base properties were evaluated by determining acid/base number, and point of zero charge (PZC) of each coal tar samples. In Chapter VII, the effects of heating and surfactant or surfactant/polymer flushing on coal tar recovery are discussed, and dimensionless parameter analysis on coal tar displacement are presented. Chapter VIII provides a summary of the present research, including recommendations for future work.

CHAPTER II

LITERATURE REVIEW

Background

Although water covers nearly three quarters of the earth's surface, only 4.9% of the world's natural water is considered to be fresh water suitable for direct human consumption. Two thirds of this fresh water is groundwater (Bachmat, 1994). Groundwater is widely available throughout the United States, and is one of the nation's most valuable natural resources. It is used primarily for irrigation and drinking. More than 50% percent of the U.S. population uses groundwater as the primary source of drinking water. The use of groundwater increased significantly over the past century, from 34 billion gallons per day in 1950 to 80 billion gallons per day in 1990 (Ahmed et al., 1997).

Groundwater contaminations mainly result from leachate from landfills and dumps, leakage from underground storage tanks, accidental spills and improper disposal of organic solvents, and surface application of herbicides, fertilizers, insecticides. All these direct or indirect interference of humans can lead to degradation of groundwater quality and endanger the environment and public health. In addition, due to their high toxicity even at extremely low concentrations, these contaminant sources can act as long-term sources of groundwater contamination. Table 2-1 presents common organic liquid

contaminants and their relevant properties, as well as the Maximum Contaminant Level (MCL) regulated by the National Primary Drinking Water Regulations (NPDWR) (USEPA, 1995). Although the aqueous solubilities of these organic compounds are very low, they are still several orders-of-magnitude higher than the MCL. Therefore, protection of the groundwater system from NAPL contamination has been becoming more and more urgent to meet the requirement of expanding population and economy.

In this chapter, general background information and a review of literature related to the research topic are provided. Information relevant to specific research tasks is covered in the introduction section of Chapter IV through VII.

Nonaqueous Phase Liquids (NAPLs)

Organic contaminants released into the subsurface may exist as a separate liquid phase, which is referred to as a nonaqueous phase liquid (NAPL). Organic liquids, which possess a lower density than water, are referred to as light nonaqueous phase liquids (LNAPLs), such as benzene, toluene, ethylbenzene, xylene, mineral oil, gasoline, jet fuel and heating oil. Organic liquids that have a greater density than water are referred to as dense nonaqueous phase liquids (DNAPLs), such as trichloroethene (TCE), tetrachloroethene (PCE), coal tar, and creosote. Nonaqueous phase liquid (NAPL) can exist as either a single component or a complex mixture. For instance, TCE and PCE are pure form NAPLs, whereas mineral oils, coal tars and creosotes are composed of a wide variety of hydrocarbons. It is also possible to find constituents with a pure liquid density less than water in a DNAPL, and constituents denser than water in a LNAPL. The overall density of the NAPL phase depends on the fraction and density of all the

constituents. In general, the densities of LNAPLs range from 0.7 to 0.9 g/cm³, while most DNAPLs encountered have densities ranging from 1.03 to 1.40 g/cm³ (Lowe et al., 1999) (Table 2-2). The viscosities of NAPLs vary depending on the composition, origins, weathering and other factors. For example, the viscosity of TCE and PCE is 1.46 and 1.63 centipoise (cP), respectively (Pankow and Cherry, 1996), while the viscosity of coal tar could vary from approximately 10 to over 1000 cP (Lee et al., 1992b; Barranac and Dawson, 1997; Zheng, 2001).

NAPL Entrapment in Porous Media

When released into the subsurface, a NAPL will migrate downward through the unsaturated zone, leaving residual liquid trapped in the pore spaces. Upon reaching the water table, LNAPL will tend to spread laterally along the capillary fringe above the water table. In contrast, DNAPLs will continue to migrate downward through the ground water until a lense of low permeability is encountered. When a spill is large enough, DNAPLs can migrate downward until they reach the impermeable aquiclude (Mercer and Cohen, 1990; Pankow and Cherry, 1996; Lowe et al., 1999) (Figure 2-1). At many sites, NAPLs exist in the unsaturated zone (air-water-NAPL, three-phase) and saturated zone (water-NAPL, two-phase) as disconnected organic blobs or “ganglia” (residual saturation). If sufficient volume has been released, excess NAPL may also accumulate as free liquid in the subsurface, which is referred to as NAPL pool. When encountering groundwater flow, both the residual and pooled NAPL constituents can dissolve into the water phase and form NAPL plume, resulting in a larger area of dissolution plume contamination of the subsurface.

Table 2-1. Relevant properties and MCL for selected organic contaminants.

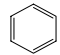
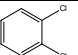
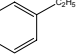
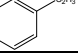
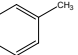
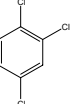
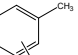
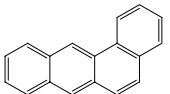
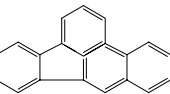
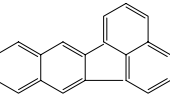
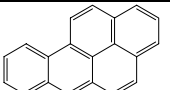
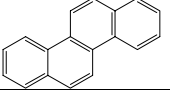
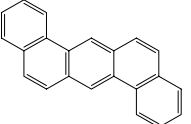
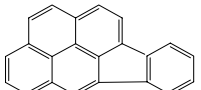
Organic Compounds	Structure	MW (g/mole)	C _s (mg/L)	Log (K _{ow})	MCL (mg/L)
Benzene		78	1780	1.99	0.005
Carbon Tetrachloride	CCl ₄	154	1200	2.62-2.83	0.005
<i>o</i> -Dichlorobenzene		147	140	3.38	0.6
Ethylbenzene		106	140 (15°C)	3.15	0.7
Styrene		104	310	2.95	0.1
Tetrachloroethylene (PCE)	Cl ₂ C=CCl ₂	166	200	3.40	0.005
Toluene		92	526	2.69	1
1,2,4-trichlorobenzene		183.5	30	4.02	0.070
Trichloroethylene (TCE)	ClCH=CCl ₂	131.5	1100	2.29	0.005
Vinyl chloride (VC)	ClCH=CHCl	97	2700	0.6	0.002
Xylenes (total)		88	175	3.12-3.2	10
Benz[a]anthracene		228	0.011	5.52	(0.0001)
Benzo[b]fluoranthene		252	0.0015	6.11	(0.0002)
Benzo[k]fluoranthene		252	0.0008	6.11	(0.0002)

Table 2-1. Relevant properties and MCL for selected organic contaminants (continued)

Organic Compounds	Structure	MW (g/mole)	C _s (mg/L)	Log (K _{ow})	MCL (mg/L)
Benzo[a]pyrene		252	0.004	6.11	0.0002
Chrysene		228	0.002	5.52	(0.0002)
Dibenz[a,h]anthracene		278	0.0005	6.70	(0.0003)
Indeno[1,2,3-c,d]pyrene		276	0.062	6.7	(0.0004)

MW=Molecular Weight

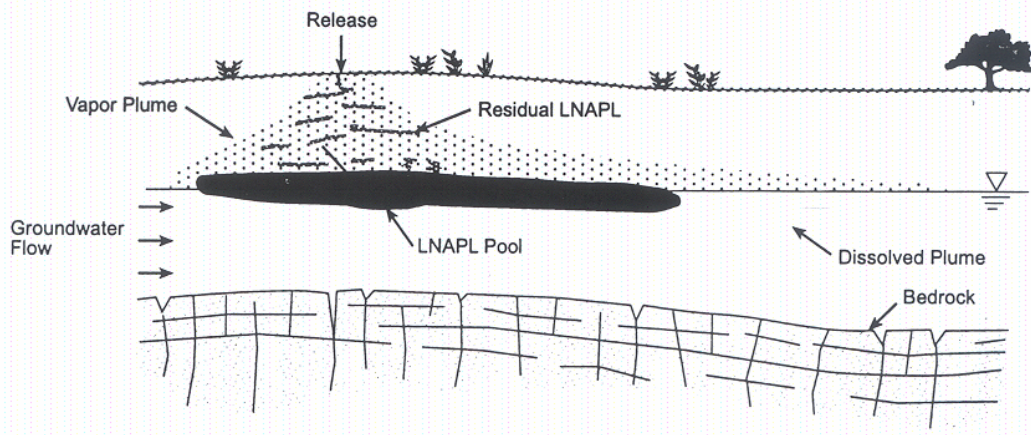
C_s=aqueous solubility at 25°C

K_{ow}=octanol-water partition coefficient (Syracuse Research Corporation, 2004)

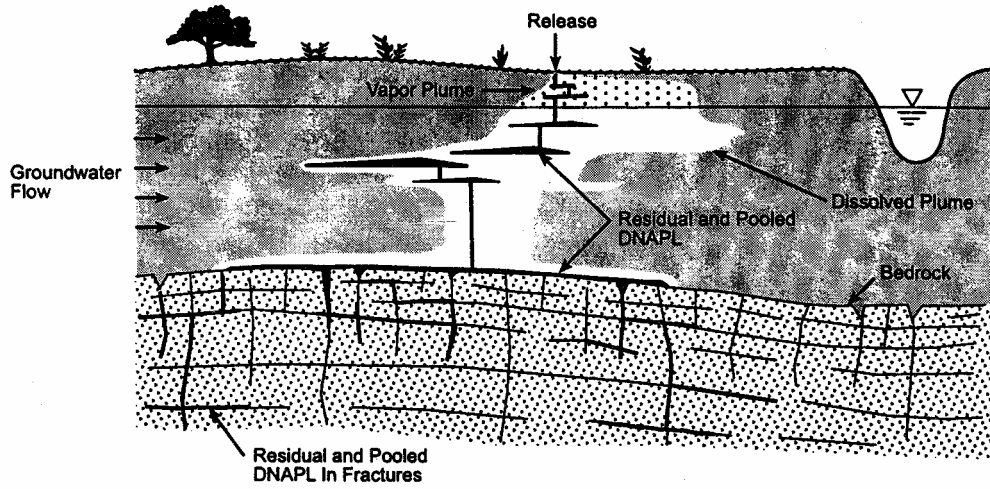
Table 2-2. Relevant physical properties of representative NAPLs.

NAPL	Density (g/cm ³)	Viscosity (cP)	References
Water *	0.998 (22°C)	0.9548 (22°C)	Weast et al., 1986-1987
Benzene	0.87 (25°C)	0.60 (25°C)	Mercer and Cohen, 1990
Chlorobenzene (CB)	1.10 (25°C)	0.72 (30°C)	Mercer and Cohen, 1990
Tetrachloroethene (PCE)	1.63 (15°C)	1.93 (15°C)	Mercer and Cohen, 1990
Trichloroethene (TCE)	1.47 (20°C)	0.57 (20°C)	Mercer and Cohen, 1990
Aroclor 1221	1.18 (25°C)	40 (38°C)	Mercer and Cohen, 1990
No 5 white oil	0.86 (10°C)	34 (21°C)	Ekmondson, 1965
Gasoline	0.73 (20°C)	0.45 (25°C)	Hunt et al., 1988a
Crude oil	0.70-0.98 (20°C)	8-87 (10°C)	Mercer and Cohen, 1990
Coal Tar from Stroudsburg, PA	1.017 (15.5°C)	19.0 (7°C)	Villaume, 1985
Coal Tar from META	1.06-1.43 (24°C)	34-6600 (40°C)	Lee et al., 1992b
Coal Tar from Pennsylvania	1.051 (25°C)	19.4 (25°C)	Hugaboom and Powers, 2002

* water is used a reference aqueous phase.



(a)



(b)

Figure 2-1. Typical Distribution of nonaqueous-phase liquid (NAPL) in the subsurface (a) LNAPL; (b) DNAPL (Lowe et al., 1999).

Interfacial Tension

Interfacial Tension (IFT) refers to the tensile force that exists at the interface of two immiscible fluid phases. Interfacial tension results from the difference between the mutual attraction of like molecules within each liquid, and the attraction of dissimilar molecules across the fluid interface (Davies and Rideal, 1963; Mercer and Cohen, 1990; Lowe et al., 1999). The IFT between a liquid phase and a gas phase is usually called surface tension. Interfacial tension is an important factor determining the capillary pressure, which causes the NAPL entrapment in porous media. Interfacial tension is also directly related to the wettability of the solid phase. In general, low NAPL-water IFT results in low NAPL entrapment in porous media (Mercer and Cohen, 1990). For miscible liquids, the NAPL-water IFT is zero. For NAPLs commonly found in subsurface, NAPL-water IFTs generally range from 5 to 50 dynes/cm (Mercer and Cohen, 1990; Lowe et al., 1999). For pure NAPL, such as TCE and PCE, the IFT is on the order of 40 to 50 dynes/cm, for complex mixture such as coal tar, the IFT is much lower (~ 20-30 dynes/cm). The reduction of IFT between mixture NAPL and water compared to that of pure NAPL-water is attributed to the accumulation of surface active constituents in complex NAPLs at the NAPL-water interface (Davies and Rideal, 1963; Barranco et al., 1997; Lord et al., 1997; Standal et al., 1999; Zheng and Powers, 2003). The IFT reduction at constant temperature can be quantitatively described by the Gibbs adsorption equation, which could be expressed as (Adamson, 1990):

$$\Gamma_i = -\left(\frac{\partial\gamma}{\partial\mu_i}\right)_T \quad (2-1)$$

or

$$\Gamma_i = -\frac{1}{RT} \left(\frac{\partial \gamma}{\partial \ln a_i} \right) \quad (2-2)$$

where Γ_i is the surface excess of species i (mol/m²), γ is the interfacial tension (N/m²), R is the universal gas constant, T is the absolute temperature (K), μ_i is the chemical potential of species i adsorbed at the interface (J/mol), and a_i is the activity of species i adsorbed at the interface (mol/m³), which is equal to the bulk phase concentration (c_i) in dilute systems. Thus if $\frac{\partial \gamma}{\partial \ln a_i}$ is negative, Γ_i is then positive, indicating an excess of component i present at the surface, otherwise, Γ_i is negative, which means a deficiency of component i present at the surface. Literature reported that the IFT reduction in oil-water system is caused by the adsorption of the surface active species at the oil-water interface (positive surface excess) (Lord et al., 1997; Standal et al., 1999). The application of surfactants in petroleum industry and environmental remediation to enhance the oil recovery and reduce the NAPL entrapment is caused by the IFT reduction due to the accumulation of surfactants at the oil-water or NAPL-water interface based on the Gibbs adsorption equation.

Davies and Rideal (1963) proposed a more instructive expression to relate the adsorption of surface active molecules to their structure (Equation 2-3). Assuming equilibrium, the adsorption isotherm can be expressed as:

$$\frac{c_s}{c} = \exp\left(\frac{\mu^0 - \mu_s^0}{RT}\right) = \exp\left(-\frac{E}{RT}\right) \quad (2-3)$$

where μ^0 and μ_s^0 are the chemical potential at standard state of bulk solution and interface, respectively, E is the standard free energy of adsorption. When E is negative, surface active molecules tend to accumulate at the oil-water interface. If E is a positive

value, indicating a tendency for surface active molecules to desorb (Figure 2-2). For a surface active molecule with ionizable polar moiety (i.e. $-\text{COO}^-$, $-\text{SO}_4^{2-}$, $-\text{NH}_3^+$), its adsorption energy (E) at the oil-water interface is consist of three terms (Davies and Rideal, 1963):

$$E = E_p + E_{np} + ze\varphi_0 \quad (2-4)$$

where, E_p and E_{np} are the energies of adsorption that contributed by polar group and nonpolar chain, respectively, z is the valence of the surface-active ion, φ_0 is the electrical potential of the surface and e is the electronic charge. Since Z and φ_0 are always of the same sign, the electrostatic term is always positive, which acts to reduce the adsorption. Davies and Rideal (1963) gave the values E_p , E_{np} and $ze\varphi_0$ of 1 mM sodium lauryl sulfate (SLS) with no salt addition (Case I) and 0.01 mM SLS with 0.145 M NaCl addition (Case II). The E_p and E_{np} values are the same, while the electrostatic term of Case I is nearly three times higher than that of Case II, which results in a overall positive value of adsorption energy in Case I, whereas in Case II, the adsorption energy value remains negative. That means the IFT reduction caused by SLS in case II would be greater than that in Case I. Equation 2-3 and 2-4 indicate that the efficiency of IFT reduction is not only dependent on the amount of surface active molecules accumulating at the NAPL-water interface, but also the surfactant structure and surfactant solution composition such as salinity.

Wettability

Wettability is the term used to describe the relative adhesion of two fluids to a solid surface. In a porous media containing two or more immiscible fluids, wettability is a

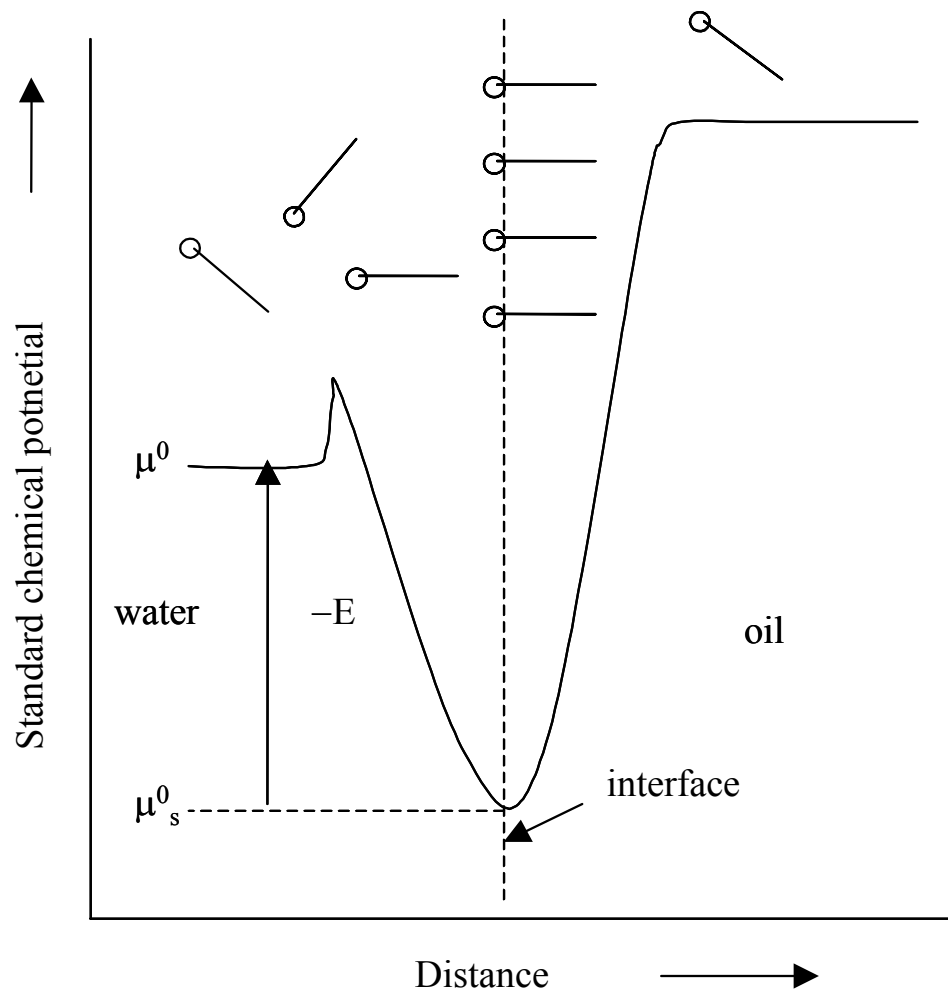


Figure 2-2. Standard chemical potential of surface active molecules at an interface (the polar head is shown as a circle, and the non-polar tail by a short strait line) (after Davis and Rideal, 1963).

measure of the tendency of one of the fluids to wet (spread or adhere) the surface relating to fluid. Wettability is typically quantified with contact angle, ω , which was defined as Young's equation (Adamson, 1990):

$$\cos \omega = \frac{\gamma_{ns} - \gamma_{ws}}{\gamma_{nw}} \quad (2-5)$$

Equation (2-5) shows that contact angle is a function of the IFT between nonwetting-wetting phase (γ_{nw}), wetting phase-solid (γ_{ws}) and nonwetting phase-solid (γ_{ns}). Using the convention that contact angle is measured through the aqueous phase, small contact angles ($\omega < 70^\circ$) are associated with water-wetting solids while large contact angles ($\omega > 110^\circ$) are indicative of oil-wetting surfaces. When contact angles are between 70° and 110° , the surfaces are referred to as intermediate wetting (Mercer and Cohen, 1990) (Figure 2-3).

Most of the natural porous medium are water-wetting (Anderson, 1986). The available contact angle data of pure organics (i.e., PCE, trichlorobenzene (TCB), chloroform and chlorobenzene (CB)) and a mixture DNAPL (primarily composed of tetrachlorobenzene, TCBs, PCE, hexachlorocyclopentadiene and octachlorocyclopentene) on clay or Ottawa fine to coarse sand in water medium are in the range of 15 to 50° (Table 2-3) (Mercer and Cohen, 1990). However, with the variation of NAPL Phase and solid substrate, things could be very different. Morrow (1976) reported that 39 of 55 petroleum reservoirs were in oil-wetting conditions. In general, the oil-wetting conditions of the reservoir were attributed to sorption of high-molecular weight polar components in the crude oil, primarily asphaltenes. The efficiency of a water flood in a mixed- and oil-

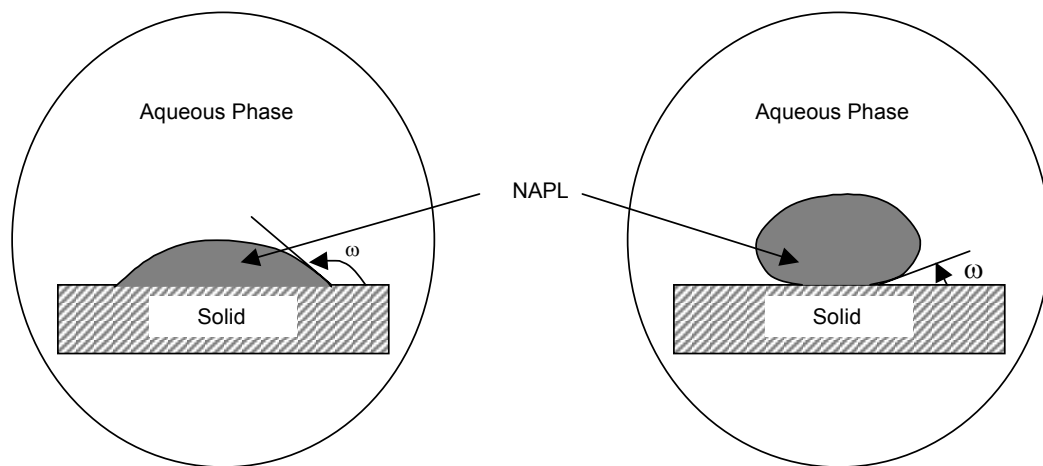


Figure 2-3. Contact angle (ω)

wet rock could be 20% lower than that in a water-wet or weakly water-wet rock (Morrow, 1990). Coal tar from a MGP site in Stroudsburg, PA was found to preferentially spread on quartz slides in the presence of water ($\omega = 125^\circ$) (Villaume, 1985). Wettability of solid surface in the presence of NAPL and water can be influenced by several factors such as polar constituents in NAPL, surfactant addition and aqueous pH. Asphaltene molecules, which are characterized by both aromatic and aliphatic regions with numerous polar functional groups containing nitrogen (N), sulfur (S), and oxygen (O) atoms, have been identified as one of the primary components in crude oil that affect the wettability of reservoir rocks (Morrow, 1990). Powers and Tamblin (1995) investigated the wettability of gasoline on quartz surfaces (quartz slides and Ottawa sand). Contact angle measurements of isooctane with different additives show that contact angles ranged from 26° with 0.1% (wt) *o*-toluidine addition to 162.8° with the addition of 1% (wt) dodecylamine (DDA). Powers et al. (1996) assessed the wettability of quartz slides and quartz sand exposed to petroleum products (mobil gasoline, diesel fuel oil, crude oil etc), coal-derived products (creosote and cola tar) and neat solvents (toluene, TCE and isooctane) using three different techniques (bottle test, contact angle measurement and capillary pressure curve). The results showed that NAPLs composed of higher molecular weight constituents such as creosote and coal tar, or surfactant such as gasoline, had a greater impact on the system wettability than lower molecular weight NAPLs such as TCE. Neat solvents (i.e., toluene, TCE and isooctane) were found to have no significant impact on the wettability of quartz surface because they do not have the impurities and surface active agents and generally have high interfacial tension. Dwarakanath et al. (2002) reached a very similar conclusion that NAPLs with a

combination of high equivalent alkane carbon number values and high viscosities, such as creosote, coal tar and fuel hydrocarbons are more likely to change the wettability of solid surface. Villaume (1985) found the hysteresis effect of contact angle; that is, the contact angle was less when NAPL advances over an initially water-saturated medium than when NAPL recedes from a NAPL-contaminated medium. Mercer and Cohen (1990) reported that the contact angle of the previously mentioned mixture NAPL on a NAPL-contaminated fine sand ranged from 45 to 105° (Table 2-3).

NAPL Residual Saturation

Residual saturation of NAPL (S_N) is the volumetric saturation ($V_{\text{NAPL}}/V_{\text{voids}}$) at which NAPL becomes discontinuous and is held by capillary forces under ambient groundwater flow conditions. The entrapped NAPLs in the subsurface system always present in the form of liquid blobs and fingers (ganglia), which have been separated from the continuous NAPL body by invading water. Residual NAPL does not move with the flowing ground water. Instead, it acts as a distributed, immobile source for dissolved-phase partitioning into the contiguous ground water and lead to the formation of contaminant plume. Most organic solvents have solubilities several orders-of-magnitude higher than the concentrations at which there is concern for human health (MCL). Residual saturations in two-phase (water-NAPL) systems generally range from 0.15 to 0.50, and from 0.10 to 0.20 in three-phase (air-water-NAPL) systems (Table 2-4) (Mercer and Cohen, 1990). Very limited data have been reported for mixed NAPL residual saturations, and most of these data were obtained in relatively coarse silica sands. Core flood tests performed on Berea sandstone showed that the residual coal tar saturation in

Table 2-3. Reported contact angle values of NAPLs on different substrate in aqueous medium

NAPL	Substrate	Contact angle (°)	Reference
Toluene	Quartz slide	52	Powers et al., 1996
isooctane	Quartz slide	28	Powers et al., 1996
PCE	clay	23-48	Mercer and Cohen, 1990
TCB	Clay	28-38	Mercer and Cohen, 1990
CB	Clay	27-34	Mercer and Cohen, 1990
Chloroform	Clay	29-31	Mercer and Cohen, 1990
Mixed DNAPL	Clay	20-37	Mercer and Cohen, 1990
Mixed DNAPL	Fine sand and silt	30-40	Mercer and Cohen, 1990
Mixed DNAPL	Ottawa fine to coarse sand	33-50	Mercer and Cohen, 1990
Mixed DNAPL	Stainless steel	131-154	Mercer and Cohen, 1990
Mixed DNAPL	NAPL contaminated fine sand	45-105	Mercer and Cohen, 1990
Mobile gasoline	Quartz slide	72	Powers et al., 1996
BP gasoline	Quartz slide	66	Powers et al., 1996
Diesel fuel	Quartz slide	31	Powers et al., 1996
Crude oil	Quartz slide	99	Powers et al., 1996
Fuel oil	Quartz slide	45	Powers et al., 1996
Creosote	Quartz slide	163	Powers et al., 1996
Coal tar	Quartz slide	125	Villaume, 1985
Coal tar	Quartz slide	8-18	Barranco and Dawson, 1999

Stroudsburg, PA is 0.30 to 0.35 (Villaume, 1985). Barranco et al. (1997) found the residual saturation of coal tar in medium quartz sand is approximately 0.77, 0.66 and 0.52 at pH 3, 7 and 12, respectively. Hugaboom and Powers (2002) reported residual coal tar saturations values of 0.47, 0.30 and 0.29 at very similar conditions (pH 4.7, 7.2, 9.9).

Capillary Pressure

The trapped NAPL blobs or ganglia of various sizes and shapes are held in the inter-granular spaces by capillary forces. Capillary pressure is a property that causes porous media to imbibe wetting fluids and repel nonwetting fluids (Bear, 1972). Capillary pressure is defined as the difference between the nonwetting fluid pressure and the wetting fluid pressure. For a water-NAPL system, capillary pressure, P_c , can be expressed as:

$$P_c \equiv P_N - P_w \quad (2-6)$$

where P_N and P_w are the pressures of NAPL phase and water phase (cm of water), respectively.

Figure 2-4 illustrates an infinitesimal element of a curved interface between two immiscible fluids. The normal component of fluid pressure is discontinuous at the interface. The pressure difference caused by the interface tension is the capillary pressure. The Laplace formula for capillary pressure can be expressed as (Bear, 1972):

$$P_c = P_2 - P_1 = \gamma_{12} \left(\frac{1}{r_1} + \frac{1}{r_2} \right) = \frac{2\gamma_{12}}{r^*} \quad (2-7)$$

where, subscripts 1 and 2 represent two immiscible fluids, the γ_{12} is the interfacial tension between these two fluids, r_1 and r_2 are the radii of curvature of the interface (m),

Table 2-4. Residual NAPL saturation (S_{Nr}) in various subsurface systems.

Residual Fluid	System	Medium	S_{Nr} (cm^3/cm^3)	References
water	vad.	sand	0.10	Mercer and Cohen, 1990
water	vad.	loamy sand	0.14	Mercer and Cohen, 1990
water	vad.	sandy loam	0.16	Mercer and Cohen, 1990
water	vad.	loam	0.18	Mercer and Cohen, 1990
water	vad.	silt loam	0.15	Mercer and Cohen, 1990
water	vad.	silt	0.07	Mercer and Cohen, 1990
water	vad.	sandy clay loam	0.26	Mercer and Cohen, 1990
water	vad.	clay loam	0.23	Mercer and Cohen, 1990
water	vad.	silty clay loam	0.19	Mercer and Cohen, 1990
water	vad.	clayey soil	0.18	Mercer and Cohen, 1990
gasoline	vad.	coarse sand	0.15-0.19	Mercer and Cohen, 1990
gasoline	vad.	medium sand	0.12-0.27	Mercer and Cohen, 1990
gasoline	vad.	fine sand	0.19-0.60	Mercer and Cohen, 1990
Mineral oil	N-A	Ottawa sand ($d_m=0.5\text{mm}$)	0.110	Mercer and Cohen, 1990
Mineral oil	N-A	glacial till	0.15-0.28	Mercer and Cohen, 1990
Mineral oil	vad.	glacial till	0.12-0.21	Mercer and Cohen, 1990
Mineral oil	vad.	alluvium	0.19	Mercer and Cohen, 1990
Paraffin oil	vad.	coarse sand	0.12	Mercer and Cohen, 1990

Table 2-4. Residual NAPL saturation (S_{Nr}) in various subsurface systems (continued).

Residual Fluid	System	Medium	S_{Nr} (cm^3/cm^3)	References
Paraffin oil	vad.	fine sediments	0.52	Mercer and Cohen, 1990
Crude oil	sat.	sandstone	0.16-0.47	Mercer and Cohen, 1990
Benzene	sat.	Sand (92% sand 5% silt, 3% clay)	0.24	Mercer and Cohen, 1990
o-xylene	sat.	Sand (92% sand 5% silt, 3% clay)	0.19	Mercer and Cohen, 1990
TCE	vad.	medium sand	0.20	Mercer and Cohen, 1990
TCE	vad.	fine sand	0.151-0.20	Mercer and Cohen, 1990
TCE	vad.	loamy sand	0.08	Mercer and Cohen, 1990
PCE	sat.	coarse Ottawa sand	0.15-0.25	Mercer and Cohen, 1990
n-Decane	sat.	Safety Bay sand	0.187	Steffy et al., 1997
n-Decane	vad.	Safety Bay sand	0.175	Steffy et al., 1997
Diesel	Sat.	Safety Bay sand	0.45	Steffy et al., 1997
Soltrol 170	Vad.	sand	0.22	Lenhard and Parker, 1988
Kerosene	Sat.	Selvilleta sand	0.263±0.022	Wilson et al., 1990
PCE	Sat.	Selvilleta sand	0.270±0.014	Wilson et al., 1990
Coal tar	sat.	Berea sandstone	0.30-0.35	Villaume, 1985
Coal tar	sat.	quartz sand	0.52-0.77	Barranaco, 1998
Coal tar	sat	Quartz sand	0.29-0.47	Hugaboom and Powers, 2002

vad. Refers to unsaturated systems (NAPL-water-air) or (water-air);

sat. refers to saturated systems (NAPL-water);

N-A refers to NAPL-air unsaturated systems (no water);

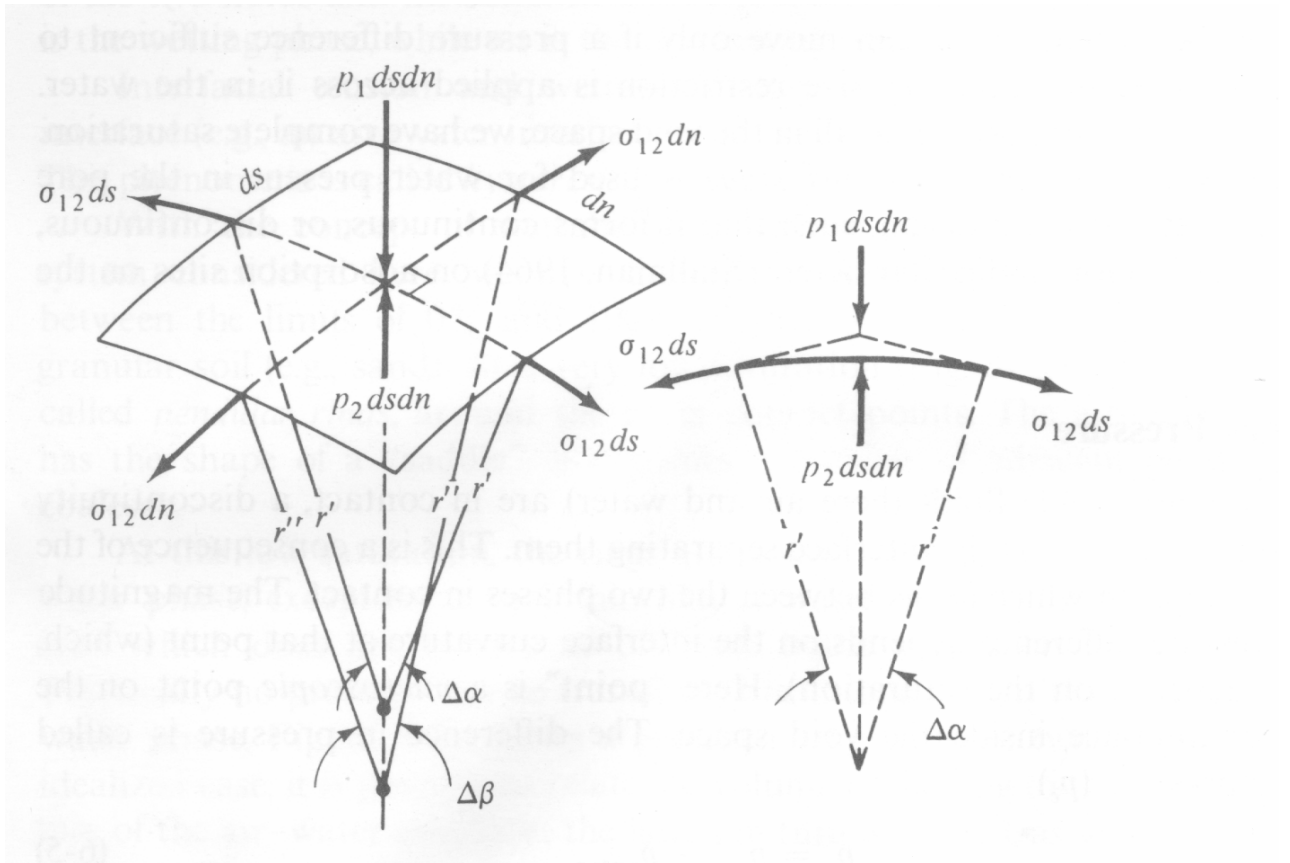


Figure 2-4. Equilibrium at a curved air-water interface (Bear 1972).

and r^* is the mean radius of curvature defined by $\frac{1}{r^*} = 2\left(\frac{1}{r_1} + \frac{1}{r_2}\right)$. The capillary pressure (P_c) is thus related to IFT, contact angle, and pore size. By analyzing the forces acting on the water column in the capillary tube as shown in Figure 2-5a, it can be found that the gravitational force of the water column in the capillary tube is balanced by the capillary force:

$$h_c \pi r^2 \rho g = 2\pi r \gamma \cos \omega \quad (2-8)$$

where h_c is the water height in the capillary tube, r is the radius of the tube, γ denotes surface tension and ρ is the water density. Simplify equation (2-8) and yield:

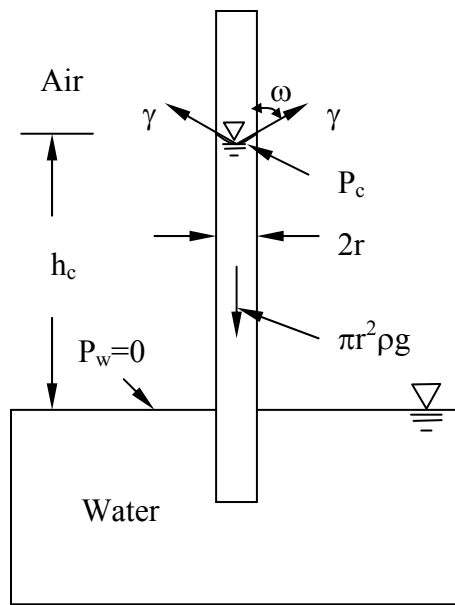
$$P_c = h_c = \frac{2\gamma \cos \omega}{r} \quad (2-9)$$

In the case of NAPL entrapment in porous media, the water-wetting aquifer materials tend to be coated with water film. The capillary pressure, which is produced due to the contact of immiscible fluids, causes the NAPL to be snapped off and entrapped as a separate droplet. Applying the capillary tube model into the NAPL–water system, the force balance on a LNAPL-water interface (Figure 2-5b) and a DNAPL-water interface (Figure 2-5c) can be expressed as Equation 2-10 and 2-11, respectively:

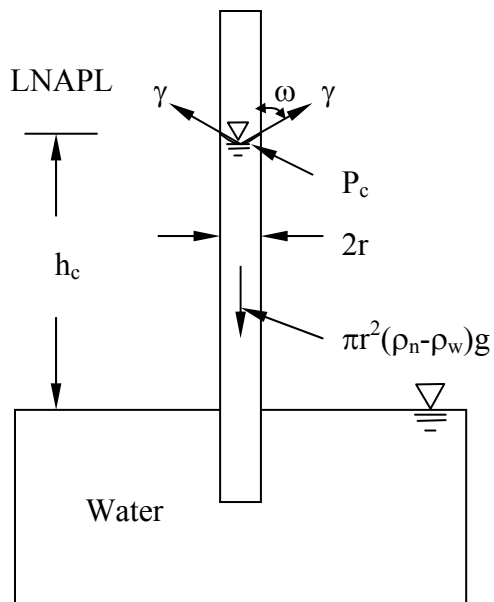
$$P_c \pi r^2 = h_c \pi r^2 (\rho_n - \rho_w) g = 2\pi r \gamma \cos \omega \quad (2-10)$$

$$P_c \pi r^2 = -h_c \pi r^2 (\rho_n - \rho_w) g = 2\pi r \gamma \cos \omega \quad (2-11)$$

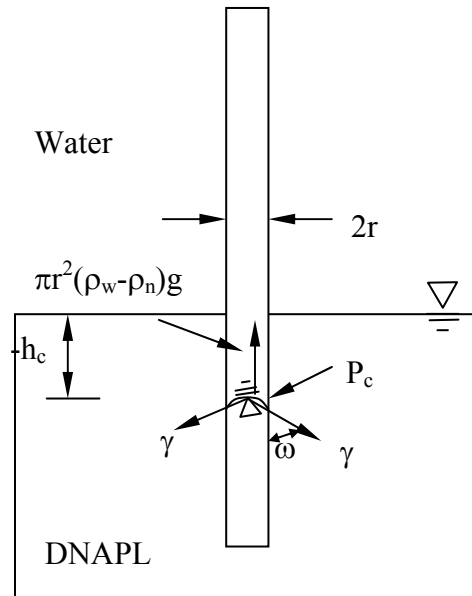
where, ρ_n and ρ_w represent the density of NAPL and water, respectively. Equations (2-10) and (2-11) show that the critical pressure head for the NAPL to enter a water-saturated media is $h_c = \frac{2\gamma \cos \omega}{rg|\rho_n - \rho_w|}$.



(a)



(b)



(c)

Figure 2-5. Force balance in a capillary tube (a) air-water; (b) LNAPL-water; (c) DNAPL-water

Capillary Pressure-Saturation Relationship

For a NAPL-water (two-phase) system, the capillary pressure-saturation (P_c - S) relationship is shown as Figure 2-6 (Pankow and Cherry, 1996). The water saturation at any particular capillary pressure is less during the wetting process than during drainage due to the hysteresis. The quantity ($I-S_w$) is known as the residual NAPL saturation S_N .

In two-phase (air-water or NAPL-water) systems, several functions have been proposed to empirically describe the capillary pressure-water saturation (P_c - S_w) relationship in unconsolidated porous media. One of the most popular functions was developed by Brooks and Corey (1964), referred to as the BC-equation:

$$\begin{aligned} S_e &= (\alpha h)^{-\lambda} & (\alpha h > 1) \\ S_e &= 1 & (\alpha h \leq 1) \end{aligned} \quad (2-12)$$

where, S_e is the effective degree of saturation ($S_e = \frac{\theta - \theta_r}{\theta_s - \theta_r} = \frac{S - S_r}{1 - S_r}$), θ , θ_r , and θ_s are water content, residual water content and saturated water content (cm^3/cm^3), respectively. S and S_r is the water saturation at a specific capillary pressure and residual water saturations ($P_c = 0$), respectively; α is an empirical parameter (cm^{-1}) whose inverse is often referred to as the non-wetting phase entry pressure or displacement pressure, λ is a pore-size distribution parameter effecting the slope of the retention function, and h is the negative pressure head (suction) (cm of water).

van Genuchten (1980) developed a smooth function to improve the description of water retention near saturation.

$$S_e = \frac{1}{[1 + (\alpha h)^n]^{(1-1/n)}} \quad (2-13)$$

where α and n are fitting parameters affecting the shape of the retention curve.

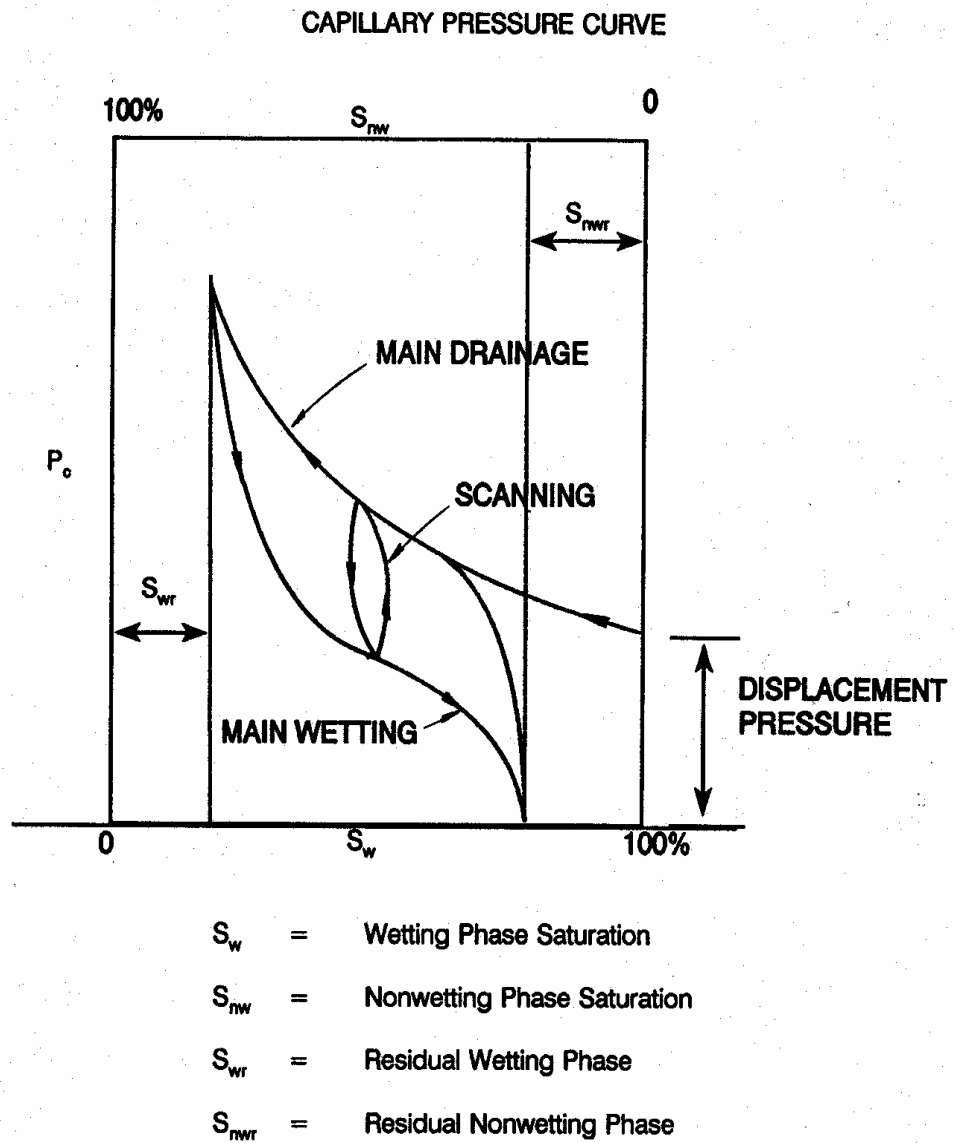


Figure 2-6. Capillary pressure-saturation curve (Pankow and Cherry, 1996).

Leverett's function proposed a way to obtain the P_c - S relationship of an unknown two-fluid, and three-fluid system from a known two-fluid system, such as air-water system.

$$J(S_w) = \frac{P_{c1}}{\gamma_1(k_1/\phi_1)^{1/2}} = \frac{P_{c2}}{\gamma_2(k_2/\phi_2)^{1/2}} \quad (2-14)$$

where, $J(S_w)$ is the leverett's function, S_w is the saturation of the wetting phase, k is the intrinsic permeability of the porous medium, ϕ is the porosity, and the subscripts 1 and 2 denote the different non-wetting phase. When the systems have the same permeability and porosity ($k_1 = k_2$, $\phi_1 = \phi_2$), Leverett's function is simplified to

$$J(S_w) = \frac{P_{c1}}{\gamma_1} = \frac{P_{c2}}{\gamma_2} \quad (2-15)$$

or,

$$P_{c2} = P_{c1} \frac{\gamma_1}{\gamma_2} \quad (2-16)$$

The interfacial tension ratio herein is also called scaling factor. That is, the capillary pressure at a given saturation for an unknown two-fluid system can be generated from another two-fluid system by knowing the ratio of the liquid-liquid interfacial tensions of the system. Dumore and Schols (1974) successfully scaled data in heptane-water and toluene-water systems using the IFT ratio as the scaling factor (Equation 2-16). Lenhard and Parker (1988) showed experimentally the validation of theory of extending two-phase (air-water, and NAPL-water) P_c - S data to three-phase (air-NAPL-water) systems for monotonic drainage paths in unconsolidated sand system. In this system, the NAPL phase was a 1 : 9 (vol) mixture of 1-iodoheptane and Soltrol 170 (a hydrocarbon solvent), and the sand was composed of 4.8, 94.7, 0.4 and 0.3% fine gravel, sand, silt, and clay

sizes, respectively. Based on the hypothesis that a dependence on the interfacial properties not only of the liquid-liquid interface, but also of the solid-liquid interfaces, the contact angle is incorporated into the scaling factor as:

$$P_{c2} = P_{c1} \frac{\gamma_2 f(\omega_2)}{\gamma_1 f(\omega_1)} \quad (2-17)$$

The most frequently used functional form of $f(\omega)$ is $\cos\omega$. Morrow (1976) observed that as the contact angle (ω) increased, the goodness of scaling using IFT ratio decreased in air-organic liquid-consolidated Teflon system, and concluded that a function of ω needs to be included in the scaling function. Demond and Roberts (1991) scaled the P_c - S relationship in air-water and pure organic-water systems, and found that discrepancy between the measured and predicted values using IFT ratios increased with decreasing interfacial forces. Scaling factor, including $\cos(\omega)$, improved the scaling to imbibition curve, and scaling of the P_c - S relationships was best achieved by including a correction based on the magnitude of contact angles for both interface curvature and roughness. Bradford and Leij (1995) investigated the P_c - S data in both two- and three-phase systems with scaling. Scaling was shown to be improved by incorporating the interfacial tension and the advancing and receding contact angles in air-water, air-oil and oil-water systems. The Leverett scaling could accurately predict the P_c - S curves in air-water-oil three-phase system from two-fluid data in hydrophilic media, but was inadequate for hydrophobic media due to the discontinuity of the intermediate fluid (Bradford and Leij, 1995). Lord et al. (1997) found that the P_c - S relationship could be scaled using surface or interfacial tension only in the air-water-silica and *o*-xylene-water-silica systems, which were strongly hydrophilic under all conditions. Karagunduz et al., (2001) found scaling factor

incorporating both IFT and contact angle accurately predicted the P_c - S relationships in air-water and air-surfactant solution in F-70 Ottawa sand, and also developed a single fitting parameter to scale the P_c - S relationships. However, all these scalings are conducted in systems with fluid viscosities very similar to that of water. Abrams (1975) proposed the possibility of including the viscosity ratio into the scaling factors, but no work has been published with respect to the scaling in highly viscous fluid systems.

NAPL Displacement in Porous Media

At residual NAPL saturation, the displacement of NAPL from aquifer requires that the capillary forces trapping the NAPL are exceeded by externally imposed forces (Pennell et al., 1996). In a NAPL-water two-phase system, the advective force due to the viscosity of the flowing groundwater and the gravity force due to NAPL density can act to displace NAPL blob or ganglia. Shear forces are customarily assumed to not play a substantial role in this system and can be neglected (Ng, et al., 1978). Figure 2-7 illustrates a NAPL globule entrapped in a single pore. The pore is oriented in a direction 1, which makes an arbitrary angle, α . Therefore, the force balance on the NAPL drop in the direction 1 of the pore can be expressed as:

$$P_R(\pi r_b^2) - P_A(\pi r_b^2) - \rho_o g(\pi r_b^2) \Delta l \sin \alpha = P_c(\pi r_b)^2 \quad (2-18)$$

where P_R and P_A are the pressure force on the receding and advancing side globule, respectively. Δl is the average length of the globule, ρ_o is the NAPL density, g is the gravity acceleration constant, and πr_b^2 is the globule area normal to the vector 1. Assuming a uniform internal pressure in the globule, substitute the capillary force with the Laplace's equation (Equation 2-7), and write Equation 2-18 in vector notation as:

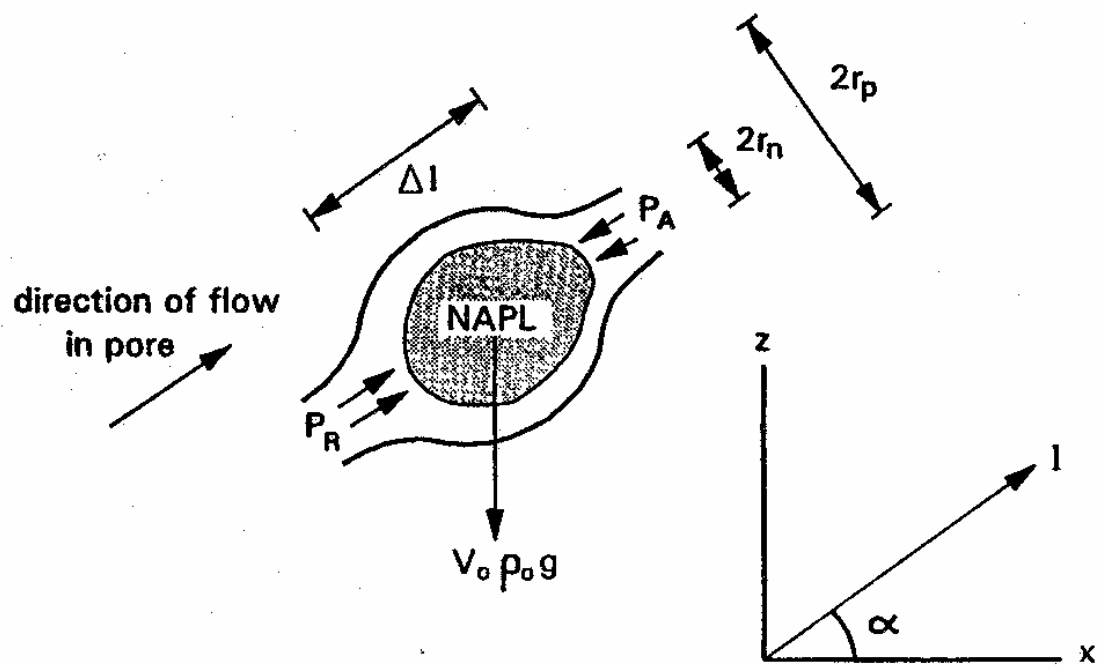


Figure 2-7. Schematic diagram of the pore entrapment model that corresponding coordinate system (Pennell et al., 1996).

$$-\nabla\hat{P}\cdot\hat{1}\Delta l - \rho_o g\hat{k}\cdot\hat{1}\Delta l = \frac{2\beta\sigma_{ow}\cos\theta}{r_n} \quad (2-19)$$

where, ∇P is the pressure gradient (vector), $\hat{1}$ and \hat{k} are the unit vectors in the x and z directions, respectively, $\beta = 1 - \frac{r_n}{r_b}$, where, r_n and r_b are the radii of pore neck and pore body, respectively. Mobilization will occur when the vector sum of the forces on the left side exceeds the capillary forces that hold discrete NAPL in place in soil porous media.

Substituting the pressure gradient obtained from Darcy's law (Equation 2-10) into Equation 2-19 and rearranging, Equation (2-21) was obtained:

$$\hat{q}_w = -\frac{kk_{rw}}{\eta_w}(\nabla\hat{P} + \rho_w g\hat{k}) \quad (2-20)$$

$$\frac{q_w\eta_w}{\gamma_{ow}\cos\omega} - \frac{\Delta\rho gkk_{rw}}{\gamma_{ow}\cos\omega}\sin\alpha = \frac{2\beta\sigma_{ow}\cos\theta}{r_n} \quad (2-21)$$

where q_w is the Darcy velocity, η_w is water viscosity, γ_{ow} is the interfacial tension between the NAPL and water, and ω is the contact angle at the solid-water-NAPL interface.

Therefore, the capillary number (N_{Ca}), which represents the ratio of viscous to capillary force, and the Bond number, which refers to the ratio of gravity to capillary forces, are defined as (Pennell et al., 1996):

$$N_{Ca} = \frac{q_w\eta_w}{\gamma_{ow}\cos\omega} \quad (2-22)$$

$$N_B = \frac{\Delta\rho g(k/\phi)}{\gamma_{ow}\cos\omega} \quad (2-23)$$

There are several other expressions of N_{Ca} and N_B used to predict the NAPL entrapment in porous media (Table 2-5) (Morrow and Songkran, 1981; Chatzis and Morrow, 1984; Dawson and Roberts, 1997), many of which are equivalent.

Table 2-5. Expressions for capillary number and bond number.

Dimensionless Parameters	Expression	Reference
Capillary Number (N_{Ca})	$N_{Ca} = \frac{k_w \Delta P}{\gamma_{ow} \cos \omega}$	Reed and Healy, 1976
	$N_{Ca} = \frac{q_w \eta_w}{\gamma_{ow}}$	Morrow and Songkran, 1981
	$N_{Ca} = \frac{k_w \Delta P}{\gamma_{ow}}$ $N_{Ca} = \frac{k_a \Delta P}{\gamma_{ow}}$	Chatzis and Morrow, 1984
	$N_{Ca} = \frac{q_w \eta_w}{\gamma_{ow} \cos \omega}$	Pennell et al. 1996
Bond Number (N_B)	$N_B = \frac{\Delta \rho g r^2}{\gamma_{ow} \cos \omega}$ $N_B = \frac{\Delta \rho g k}{\gamma_{ow} \cos \omega}$	Morrow and Songkran, 1981
	$N_B = \frac{\Delta \rho g (k / \phi)}{\gamma_{ow} \cos \omega}$	Dawson and Roberts, 1997
	$N_B = \frac{\Delta \rho g (k / \phi)}{\gamma_{ow} \cos \omega}$	Pennell et al. 1996

K_w and k_a are permeabilities of NAPL to water and air, respectively.

ΔP is the pressure gradient.

ϕ is the porosity of media.

For example, the two expressions for N_B defined by Morrow and Songkran (1981) can be related to one another through the Kozeny-Carman equation (Bear, 1972):

$$k = \frac{d_m^2 \phi^3}{180(1-\phi)^2} \quad (2-24)$$

where d_m is the mean particle size.

Compared all the N_{Ca} and N_B expressions, Equation (2-22) and (2-23), which are derived from force balance on NAPL globule, should better explain the NAPL displacement. Based on the capillary number and Bond number, Pennell et al. (1996) proposed another dimensionless parameter, total trapping number (N_T), which can be expressed as:

$$N_T = \sqrt{N_{Ca}^2 + 2N_{Ca}N_B \sin \alpha + N_B^2} \quad (2-25)$$

where α is the angle the flow makes with the positive x axis (counter-clockwise). For case of horizontal flow ($\alpha = 0^\circ$), the expression for N_T simplified to:

$$N_T = \sqrt{N_{Ca}^2 + N_B^2} \quad (2-26)$$

For vertical flow ($\alpha = 90^\circ$), in the direction of the buoyancy force, the expression for N_T becomes:

$$N_T = |N_{Ca} + N_B| \quad (2-27)$$

The critical value of N_T required to initiate PCE mobilization fell within the range of 2×10^{-5} to 5×10^{-5} , while complete displacement of PCE was observed as N_T approached 1×10^{-3} , as shown in Figure 2-8 (Pennell et al., 1996). Efforts to relate the residual saturation to capillary number or Bond number or total trapping number were also made. Morrow and Songkran (1981) showed that NAPL saturation is inversely

correlated with Bond Number (N_B). Chevalier and Fonte (2000) developed three correlation models between the residual saturation and soil and fluid properties from the experimental data (Table 2-6).

These results imply that mechanisms that increase the total trapping number (N_T) will decrease NAPL residual saturation and enhance the NAPL displacement. That is, methods such as increasing the water-flooding velocity, lowering the NAPL-water interfacial tension by surfactant addition, reducing the contact angle will benefit the residual NAPL mobilization (displacement) in porous media.

All the dimensionless parameters (N_{Ca} , N_B , and N_T) discussed here are obtained under the assumption that the shear forces, which are functions of the viscosity contrast between the aqueous and NAPL phase (Ng et al., 1978; Pennell et al., 1996), can be neglected. For viscous NAPL such as coal tar and other viscous oils, shear forces cannot be neglected (Ng et al., 1978). In oil recovery industry, where highly viscous oil is encountered, another parameter, mobility ratio (m), is proposed (Dullien, 1992):

$$m = \frac{k_{2r}\eta_1}{k_{1r}\eta_2} \quad (2-28)$$

where the subscripts 2 and 1 refers to the displacing and displaced phase, respectively, k_r is the relative permeability, and η is the viscosity. For miscible displacement the mobility ratio is simply the viscosity ratio η_2/η_1 . In the displacement process, lower mobility ratios favor NAPL recovery from porous media.

Table 2-6. Correlations between residual NAPL saturation and soil and NAPL properties (Chevalier and Fonte, 2000).

System Information	Conditions	Correlations	R ²
<u>NAPL:</u> Soltrol (mixed hydrocarbon solvent) <u>Sand:</u> FS Mix 1 (> 0.212 mm) FS Mix 2 (90% FS Mix 1+10% 0.150-0.212 mm) FS Mix 3 (80% FS Mix 1+20% 0.150 mm) FS 50 (0.355-0.425 mm)	$N_{Ca} < 2 \times 10^{-6}$	$S_n = -11.59 \left(\frac{C_u N_B}{C_g} \right)^2 + 0.182$	0.972
FS Mix 4 (30% FS Mix 1+10% FS 50+30%0.212-0.300 mm+20%0.180-0.212mm+10%0.150-0.180mm) FS Mix 5 (10% FS Mix 1+70% FS 50+30%0.212-0.300 mm+5%0.180-0.212mm+15%0.150-0.180mm) Coarse Silica Stock (CS Stock) CS 20 (0.850-1.18 mm CS Stock)	$2 \times 10^{-6} < N_{Ca} < 4.13 \times 10^{-5}$	$S_n = -10.58 \left(\frac{C_u N_B}{C_g} \right)^2 + 0.1247 N_{Ca}^{-0.03}$	0.934
	all	$S_n = 0.0371 C_u^{-0.1118} C_g^{0.1071} N_T - 0.1417$	0.824

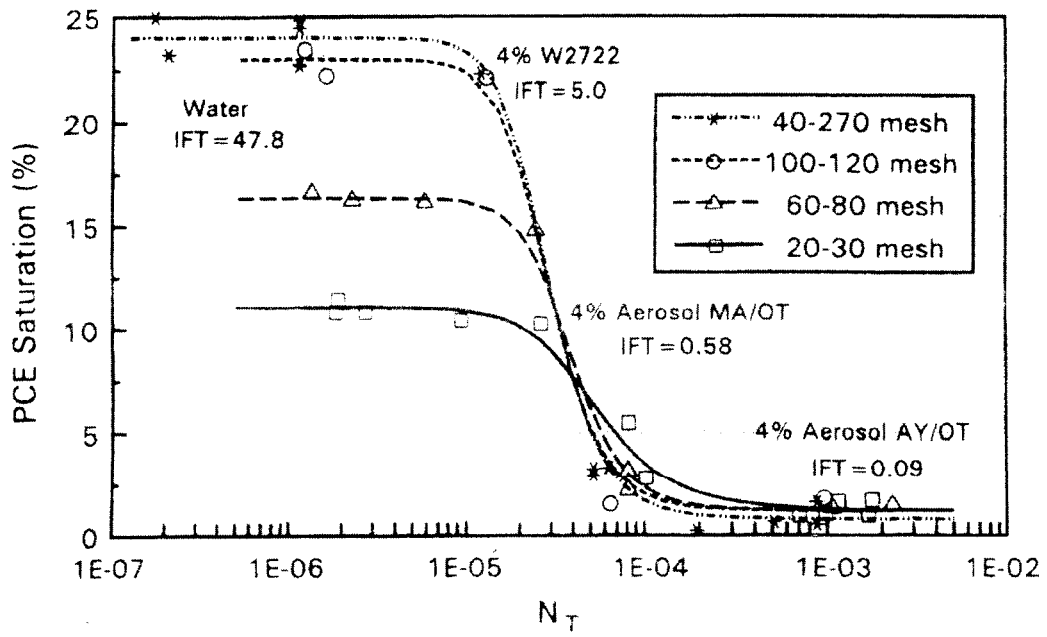


Figure 2-8. PCE desaturation as a function of total trapping number (Pennell et al. 1996).

NAPL Source Zone Remediation Technologies

Remediation of NAPL contaminated sites is primarily driven by regulatory pressure, contaminants transfers and releases into the environment, particularly via groundwater migration. Three categories of regulations issued by USEPA need to be considered during the contaminant sites remediation (Mahjoub et al., 2000): i) the Resource Conservation and Recovery Act (RCRA) of 1976, as amended by the hazardous and Solid Waste Amendments of 1984 (HSWA); ii) Comprehensive Environmental Response, Compensation and liability Act of 1980 (CERCLA), as amended by the Superfund Amendments and Reauthorization Act of 1986 (SARA); and iii) The Clean Air Act (CAA). Although some of the NAPL contaminated sites are not governed by RCRA or superfund, remediation usually follows similar guidelines. For example, most of the former manufactured gas plant sites (MGPs) are not CERCLA or Superfund. The Ashland/Northern States Powers Lakefront site (former MGP site), Ashland, Wisconsin, was proposed to the National Priority List (NPL) based on the evidence that Benzo(a)pyrene, benzoanthracene, xylenes, ethylbenzen, and other VOCs from former MGP operations have contaminated soils and underlying ground water (USEPA, 2001). The selection of appropriate remediation technology to meet the cleanup standards at reasonable cost is every important. However, each remediation technology has its advantages and limitations (Table 2-7). Under most circumstances, various technologies are used together to meet the strict cleanup standards.

Pump and treat remediation is one of the most widely used source zone remediation technologies. The conventional pump and treat technology removes groundwater through extraction wells and treats the extracted water above ground prior to

disposal. Pump and treat often requires lengthy periods of time to achieve cleanup objectives (Mackay and Cherry, 1989; MacDonald and Kavanaugh, 1994). For DNAPLs, conventional pump-and-treat remediation technologies, which rely on dissolution of the contaminant into the aqueous phase, are less effective. First, DNAPLs are much harder to remove when at the bottom of an aquifer. The second reason for the reduction of the effectiveness of pump and treat remediation stems from the extremely low solubility of many organic hydrophobic compounds in water (Mackay and Cherry, 1989).

Due to the inefficiency of traditional pump-and-treat technologies, new methodologies, such as the addition of surfactant or cosolvent to the subsurface prior to the pump-and-treat, are being investigated or have been developed. These methods facilitate the NAPL removal by reduce the NAPL-water IFT or increase the NAPL solubility in aqueous phase (Pennell et al., 1993, 1994; Lowe et al., 1999; Dwarakanath et al., 1999, 2000; Rouse et al., 2001; Roy et al., 1995; Kilbane, 1997). The surfactant enhanced aquifer remediation will be addressed in more detail in the next section.

Thermal methods have been widely used in enhanced oil recovery (EOR) processes. The steam methods account for nearly 80% of the EOR (Lake, 1989). There are four basic ways to apply thermal methods: hot water flooding, steam soak, steam drive, and *in situ* combustion. Figure 2-9 illustrates the *in situ* remediation processes that may be enhanced by soil heating and the applicable temperature ranges. Due to the higher cost and current de-emphasis by EPA, high-temperature incineration systems are not recommended (McGowan et al., 1996).

Chemical oxidation (CHOX) is an *in situ* technology developed to transform contaminants into benign products. Three major oxidants used in CHOX are hydrogen

peroxide, ozone, and hypochlorites. The most common form of this technology utilizes hydrogen peroxide in conjunction with an iron catalyst, which forms highly reactive hydroxyl radicals via Fenton's chemistry. The hydroxyl radicals are strong oxidants and react with surrounding molecules.

The primary advantage of chemical oxidation is the transformation of the pollutant, which is attractive because it may offer a solution to the question of ultimate disposal existing contaminants. Further, reaction rates are extremely high, indicating that the remediation time may be short. The limitations are the lack of reaction specificity, effect on microbes, and mass transport or deliverability (Bassel and Nelson, 2000).

Some of the wastes and by-products of MGP sites are believed to be degraded by biological processes (Ramaswami et al., 1994; Field et al., 1995; Grimberg et al., 1996; Jimenez and Bartha, 1996; Ramaswami and Luthy, 1997; Ramaswami et al., 1997; Ramaswami et al., 2001; Guerin, 2002). *In-situ* biodegradation is affected by several factors such as, soil hydraulic conductivity, depth of groundwater, infiltration rates, soil temperature, soil aeration and the low solubility and bioavailability of PAHs. The rate of removal for constituents of concern is limited. However, the effects of the PAH concentration on microorganism activities are not clear.

Capping is also referred to as containment, which does not provide source reduction but prevents or significantly reduces the migration of contaminants into the environment. Stabilization is similar to capping, as it attempts to prevent the spread of contaminants. Reagents, such as fly ash and Portland cement, are mixed with the soil to reduce permeability. This technique has been used widely for metals. Its use with organics is more problematic and it is clearly not appropriate for high concentration MGP

Table 2-7. Comparison of representative remediation technologies.

Remediation Technologies	Advantages	Disadvantages
Pump-and-treat	Easy to operate, relatively low cost	Long remediation time. Cannot achieve complete contaminant removal.
Thermal remediation	Minimal disruption to site operations. Benefit highly viscous NAPLs.	Difficulty distributing heat evenly throughout the contaminated zone. Utility cost may be high.
Chemical oxidation	Completely transformation of contaminants. High reaction rates	Lack of reaction specificity, effect on microbes, and mass transport or deliverability
Bioremediation	Generally inexpensive. Minimal disruption of existing operations	Uncertain about the toxicity of contaminants to microbials. Limited rate. Unsuitable for source zone remediation.
Capping (containing)	Quick installation. Prevents human and animal exposure. Relatively low cost	Does not reduce contaminant concentration. Uncertain long-term reliability

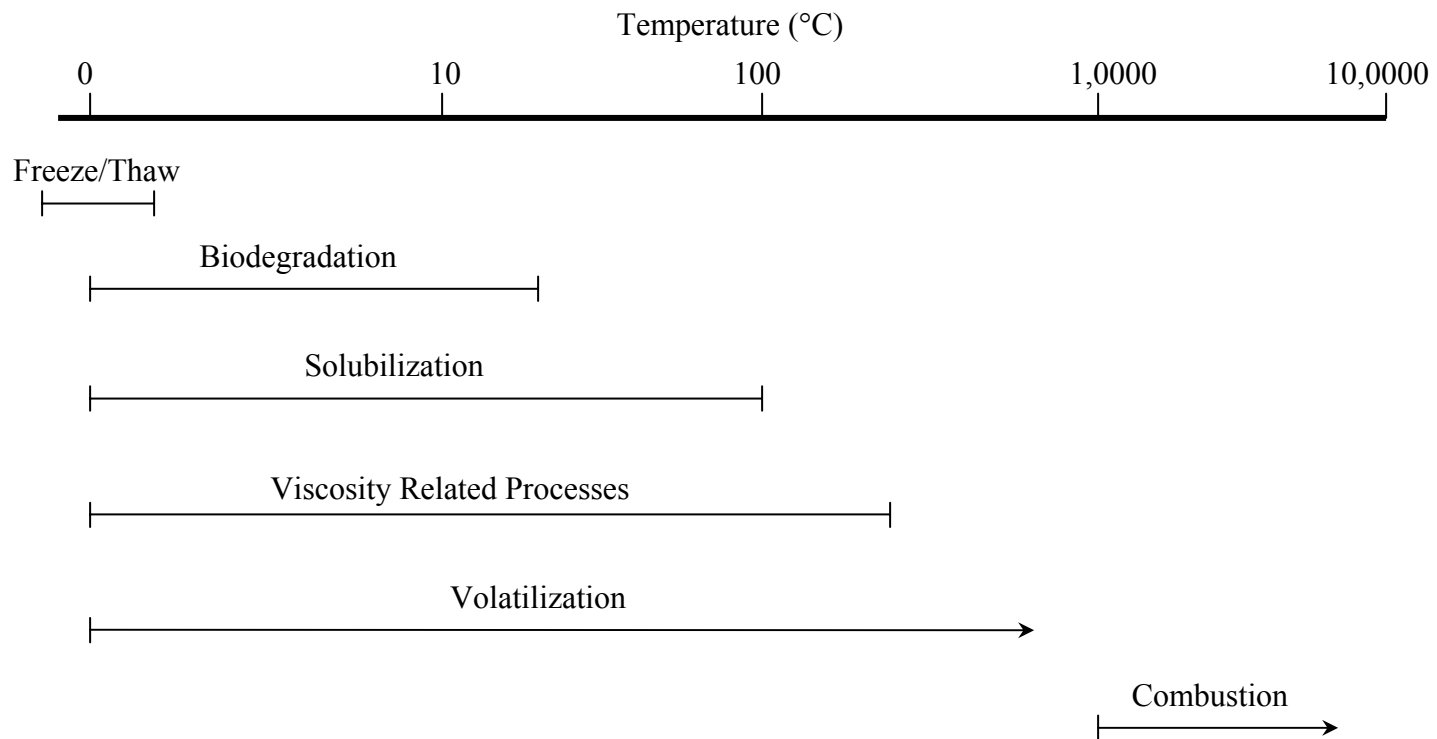


Figure 2-9. Temperature range of soil heating and phenomenon significantly impacted (modified from Smith and Hinchee, 1993).

coal tars (McGowan et al., 1996).

Surfactant Enhanced Aquifer Remediation

Because of the limitations of pump-and treat technology, the feasibility of surfactant to improve its efficiency has been widely investigated. Surfactants have been widely used in the petroleum industry (Lake, 1989; Taugbol et al., 1995; Hirasaki and Zhang, 2003; Schramm et al., 2003; Standnes et al., 2003). The application in environmental remediation is a relatively new technology (Villaume, 1985; Pennell et al., 1993; Pennell et al., 1994; Dwarakanath et al., 1999; Lowe et al., 1999; Dwarakanath et al., 2000; Rouse et al., 2001; Ramsburg, 2002).

Surface Active Agents

Surface active agents, or surfactants, are a class of chemical compounds that have the potential to alter the fluid interfacial properties. A typical surfactant monomer is an amphiphilic molecule, which is composed of a hydrophilic portion or moiety and a hydrophobic moiety. In a NAPL-water system, the competition between the hydrophilic and hydrophobic portion results in the accumulation of surfactant molecules at the NAPL-water interface.

Surfactants are classified into four groups according to the nature of the hydrophilic group. Anionic surfactants have negatively charged hydrophilic groups. They are relatively resistant to retention, stable and cheaper, and hence are the most widely used surfactants in petroleum industry (Lake, 1989; Hirasaki and Zhang, 2003). Cationic surfactants contain positively charged polar moiety. Since cationic surfactants tend to

adsorb on the anionic surfaces and are toxic, they are rarely used in groundwater system. Nonionic surfactants are have also been widely used in enhanced oil recovery and usually combined with other surfactants as cosurfactants. Nonionic surfactants are generally not sensitive to salinity compared to anionics (Lake, 1989; Lowe et al., 1999). Zwitterionic surfactant is the class of surfactants can be ionized to both positively and negatively charges groups in aqueous phase. So far, these surfactants are rarely used in oil recovery and contaminant remediations (Lake, 1989; Lowe et al., 1999).

Micellar Solubilization

When sufficient amounts of surfactants are added to the aqueous phase, the hydrophobic moieties of the surfactant molecule tend to associate to themselves to form aggregates or micellars, which orient with the hydrophobic groups pointed toward the interior of the micelle and the hydrophilic part outward. Therefore, the hydrophobic inner of the micelle becomes a good solvent for organic chemicals and results in an increasing of the organic chemical aqueous solubility, which is referred to as micellar solubilization. In general, the micellar solubilization can increase the aqueous solubility of common organic contaminants to 10- to 100 fold higher (Lowe et al., 1999).

NAPL Mobilization

Due to the accumulation of surfactant molecules at the NAPL-water interface, the oil-water IFT can be greatly reduced, which will lead to the reduction of capillary forces. Since the residual NAPL is retained by the capillary force. The reduction of IFT can result in the mobilization of NAPL in the subsurface.

In general, the IFT can be reduced to 1-5 dynes/cm (Lowe et al., 1999), but this value is not low enough to remove the residual saturation. In order to significantly lower the oil-water IFT, except for selecting the right NAPL-surfactant combination, the use of mixed surfactants or cosolvents or salinity modification is essential (Laker, 1989; Lowe et al., 1999).

Surfactant phase behavior is strongly dependent on the salinity. Figure 2-10 shows the typical phase behavior with variation of electrolyte concentration in an oil-water-surfactant system (Baran et al., 1994). At low salinity, surfactant exhibits good aqueous-phase solubility and poor oil-phase solubility. Thus, an aqueous continuous lower-phase microemulsion (o/w, Winsor Type I) is formed in equilibrium with excess oil. With the increase of salinity, more oil is incorporated into the microemulsion phase until reaches salinity S^* , which is referred to as the optimum salinity. At this salinity, equal volume of aqueous and oleic phases are incorporated in the microemulsion. With salinity continuing to increase, electrostatic forces decrease the surfactant's solubility in the aqueous phase, and the system reverts to an upper-phase oil continuous microemulsion (w/o, Winsor Type II) system in equilibrium with excess aqueous phase. Between the Winsor Type I and Type II is the Winsor Type III system, which describes a middle-phase microemulsion existing in equilibrium with excess aqueous and oil phase. Winsor Type III systems generally produce ultra low IFT between the middle surfactant rich phase and aqueous phase and oil phase. Viscosity of the Type III microemulsion is also relatively low (Figure 2-11).

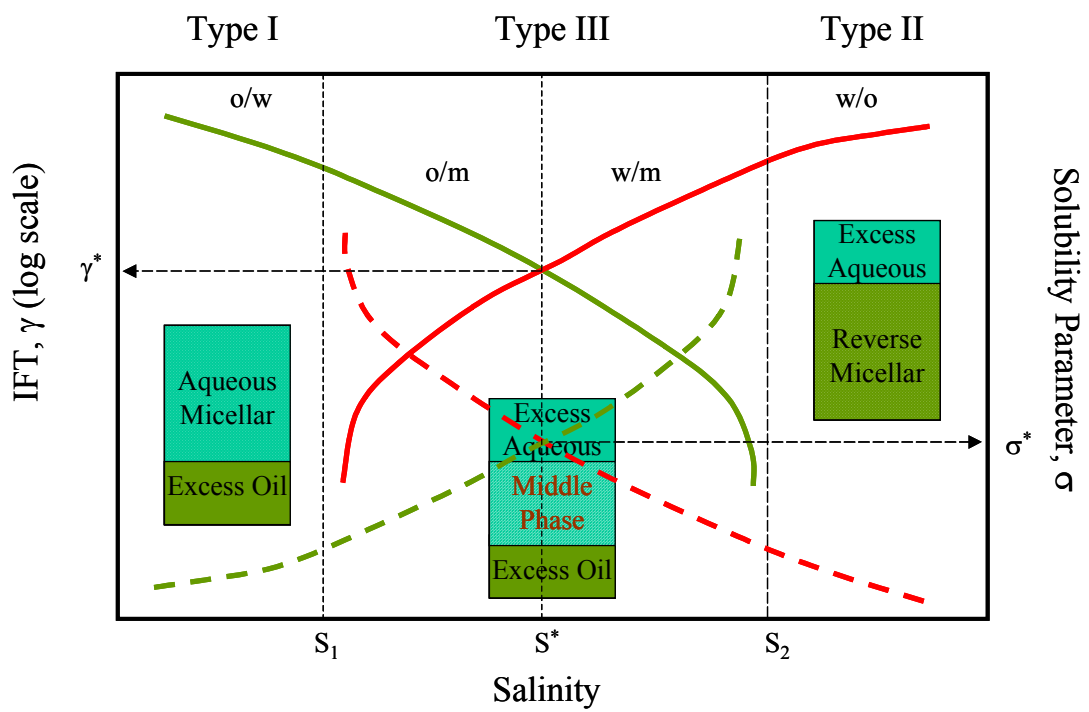


Figure 2-10. Typical phase behavior with variation of electrolyte concentration (Baran et al., 1994)

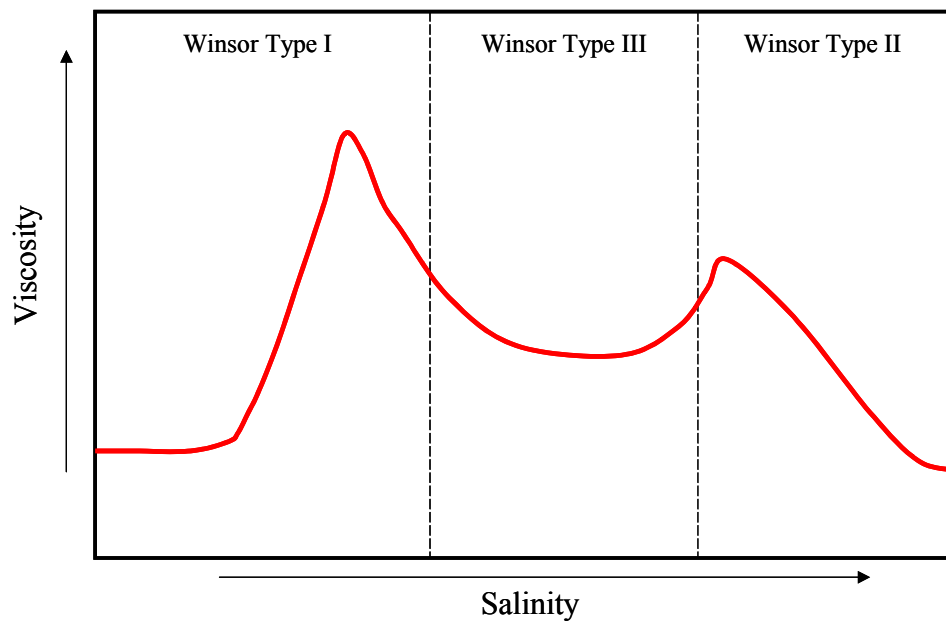


Figure 2-11. Generalized plot of viscosity for anionic surfactant solutions (Ramsburg, 2002).

Surfactant Enhanced Aquifer Remediation

There are two general mechanisms by which surfactants can enhance the removal of nonaqueous phase liquid (NAPL) source from both unsaturated and saturated zone. One is solubilization of organic phase due to micelle formation; the other is mobilization of NAPLs resulting from lowering the IFT using surfactant.

A lot of work has been conducted on the surfactant solubilization on pure NAPL (i.e. PCE, TCE) (Pennell et al., 1993, 1994; Dwarakanath et al., 1999; Lowe et al., 1999; Ramsburg, 2002). Recently, more research is focused on the effect of surfactant on aromatic organic chemicals and organic mixtures such as petroleum oils and coal tars (Dwarakanath et al., 1999, 2002; Rouse et al., 2001; Young et al. 2002). Yeom et al. (1995) investigated the nonionic surfactant solubilization to PAHs in coal tar contaminated soils, and predicted 55-70% removal of individual PAHs at dosages as high as 1 g(surfactant)/g(soil). If count in the mass-transfer limitation, the removal percentage was expected to be much lower. The kinetics of surfactant solubilization of soil-bound PAHs was also investigated and it was suggested that the release of PAHs not only determined by the micellar solubilization, but also the swelling of soil-tar matrix caused by surfactant sorption (Yeom et al., 1996). Paterson et al. (1999) investigated the use of five nonionic surfactants for desorption of PAHs from a coal tar-contaminated soil and found that the extraction efficiency was the order of increasing ethylene oxide (EO)/propylene oxide (PO) compositional ratio. Link (2000) also found the dissolution rate of PAHs (naphthalene, phenanthrene, fluoranthene, pyrene and benzo(a)pyrene) in coal tar were enhanced by the presence of Tween 20 and Tween 21, and the more hydrophobic surfactant, Tween 21 caused a greater enhancement than Tween 20.

Remediation based on micellar solubilization usually requires large quantity of surfactant solution, whereas mobilization has the advantage of significantly less flushing volumes (Dwarakanath et al., 1999; Ramsburg, 2002). Surfactants can adsorb to NAPL-water interfaces and significantly decrease the interfacial tension and alter the wetting properties of the soil matrix. The reduction of NAPL-water IFT decreases the capillary forces trapping the NAPL in place and results in greater mobility of the NAPL. Taugbøl et al. (1995) reported that it is possible to recover more than 50% of water flooded residual oil by performing a surfactant and polymer combination flood on oil (n-heptane) and seawater system in Berea sandstone cores. Jayanti et al. (2002) used custom-designed anionic surfactants to remove NAPLs, including PCE, gasoline and fuel oil, and very low NAPL saturation were achieved by forming Winsor Type III microemulsions. Acevedo et al. (2001) observed that Bitumen-water IFT decreased to low than 0.1 dynes/cm within the pH range of 9-12 when natural surfactant adsorpt at the Bitumen/water interface with the addition of Na_2CO_3 and emulsification was observed at pH 11.5. Under conditions of ultra low IFTs, capillary forces are substantially reduced and implicate NAPL displacement facilitation. Villaume (1985) reported a 7 to 10% of residual coal tar recovery after several pore volumes of polymer alkali solution injection at the MGP site, Stroudsburg, PA.

Thermal Remediation

Thermal methods such as steam injection and hot water flooding have been widely used for decades in enhanced oil recovery (EOR). The steam methods account for nearly 80% of the EOR (Lake, 1989). Some of the thermal techniques have been

proposed or performed in NAPL contaminated site remediation (Smith and Hincsee, 1993). However, the objectives of the NAPL remediation process are very different from those in EOR. In environmental remediation, the goal of thermal technologies is to meet the stringent groundwater and drinking water standards. The performance of a thermal technology in NAPL remediation requires the knowledge of the effect of temperature on NAPL and soil properties and NAPL-soil interactions.

The rise in temperature of the system influenced many variables such as density and viscosity of individual phases, interfacial properties including liquid-liquid IFT and solid wettability (Ekmondson, 1965; Davidson, 1969; Lake, 1989; Grant and Salehzadeh, 1996; She and Sleep, 1998; Rao, 1999; Grant, 2003). The most pronounced effect of temperature on fluid properties is viscosity. For most liquids, the viscosity displays an exponential decrease with the increasing temperature (Lake, 1989):

$$\eta = Ae^{B/T} \quad (2-29)$$

where η is the viscosity, T is the absolute temperature, A and B are empirical parameters. This relationship benefits the NAPL removal through enhancing the mobility of high viscosity fluid (displaced phase) by increasing the temperature.

Temperature effects on interfacial tension (IFT) and wettability are not very clear. Grant and Salehzadeh (1996, 2003) proposed several equations (Equation 2-33, 31) to describe the temperature dependence of IFT, wettability from chemical-thermodynamic analysis (Grant and Salehzadeh, 1996). However, since these general relationships include entropy and enthalpy, which are hard to quantify, the application of these relationships to practice is doubtful.

$$S^s = -A_s \frac{d\gamma}{dT} \quad (2-30)$$

$$\frac{dk}{dT} = \frac{1}{\gamma} \left(\frac{k_{\theta} \gamma + \Delta H}{T} - k \frac{d\gamma}{dT} \right) \quad (2-31)$$

where S^s is the interfacial entropy per unit area ($\text{J mol}^{-1} \text{m}^2$), γ is the IFT (N m^{-2}), and T is the absolute temperature (K), k_{ω} is the wetting coefficient defined by $k_{\omega} = \cos \omega$, and ΔH is the enthalpy of immersion per unit area (J m^{-2}).

Experimental results on the temperature effect on IFT, wettability and capillary pressure-saturation relationship are not consistent. McCaffery (1972) observed n-alkanes with 6-12 carbon atoms had a approximate 1 dyne/cm decrease of IFT for a 10°C increase in temperature, whereas for viscous mineral oil and tetradecane showed a decrease of 0.7-0.3 dynes/cm per 10°C . Davis (1994) found no significant different between the IFT at a temperature of 10 and 30°C at the 95% confidential level by using the Student's t-test. With respect to contact angle, Poston et al. (1970) observed a contact angle change of $-0.27^{\circ}/^{\circ}\text{C}$ for an organic-water-glass system. Sinnokrot et al., (1971) found a contact angle change of $-0.29^{\circ}/^{\circ}\text{C}$ for bayol-water-siliconed glass system, and $-0.13^{\circ}/^{\circ}\text{C}$ for and air-water-naphthalene system. Rao and Karyampudi (1998) observed that a quartz surface in a heavy oil-brine system remained strongly water-wetting in the temperature range of 20 to 162°C , and exhibited strongly oil-wetting at 196°C . The contact angle in an air-water-silica system was found to be near zero (Davis, 1994; Bradford and Leij, 1995); consequently, decreases in contact angle caused by increasing temperature are constrained to be very small.

Although temperature dependent of IFT and wettability is not clear, residual NAPL saturation, which is decided by the capillary pressure, generally was observed to decrease with the increasing temperature. Edmondson (1965) investigated the residual

saturation two refined oil (White oil) and two crude oil during water flooding and found the residual oil saturation of white oil No.15 decreased from over 44% to less than 30% when temperature increased from 38 to 260°C, and recovery of crude oil A increased from 32 to 50% as temperature increased from 22 to 139°C. Davis (1994) evaluated the residual oil (Paraffinic Oil) saturation variations in a relatively low temperature range (10 and 30°C). The measured residual oil saturation decreased approximately 10% in 20-30 mesh silica sand, ~5% in a mixed silica sand (1:1:1 of three sands with particle size in the range of 0.85 -0.50, 0.50-0.25, and 0.25-0.106 mm, respectively) when temperature increased from 10 to 30°C. She and Sleep (1998) found the PCE residual saturation decreased from 22.6 to 6.0% when the temperature increase from 20 to 80°C, while the water residual saturation increased from 0.8 to 27.1% in the same system. Overall, thermal remediation techniques are very promising technologies in environmental remediation, particularly to viscous NAPLs.

CHAPTER III

OBJECTIVES

The overall objective of this research was to evaluate the behavior of mineral oil (LNAPL) and coal tar (DNAPL) in porous media. To date, only limited data related to the residual saturation and recovery of complex mixture NAPLs in porous media are available, especially in three-phase (air-NAPL-water) systems. This research investigated the residual saturation of two commercial mineral oils and six MGP coal tars in sixteen natural soils, and related measured residual saturation data to NAPL and soil properties, including NAPL viscosity, interfacial tension, soil organic content, and soil particle size distribution. Based on the potential NAPL migration mechanisms, investigations were carried out on the effects of IFT, wettability, and viscosity ratio on coal tar entrapment and removal from the porous media. Heating was employed to reduce the coal tar viscosity, while a polymer was utilized to increase the displacing phase (aqueous phase) viscosity for the purpose of mobility control. Surfactant was used to reduce the oil-water interfacial tension and hence increase the NAPL removal from porous media. Overall, this research intended to provide useful tools in the prediction of the NAPL behavior in subsurface porous media and selection of appropriate remediation strategies to contaminated sites.

The specific objectives were to:

1. Quantify the properties of three commercial mineral oils (oil density, viscosity, surface tension and interfacial tension) and seven natural soil samples (particle density, particle size distribution, specific surface area, total carbon content, and soil moisture release curves), investigate the residual mineral oil saturation in soils in both two-phase (water-oil) and three-phase (air-water-oil) systems, and develop correlations between the residual oil saturation and oil/soil properties (Chapter VI).
2. Characterize the properties of six coal tars (tar density, viscosity, surface tension and interfacial tension) and nine soil samples (particle density, particle size distribution, specific surface area, total carbon content, cation exchange capacity, and soil moisture release curves) from former MGP sites, evaluate the residual tar saturation in the soil samples in two-phase systems (water-tar), and relate the measured residual tar saturation to representative tar and soil properties. (Chapter V).
3. Quantify the acid/base properties of each coal tar sample, including asphaltene content, acid and base number, and point of zero charge, and investigate the effect of aqueous chemistry (pH and ionic strength) on wettability, interfacial tension and capillary pressure-saturation relationships in coal tar-water-solid systems (Chapter VI).
4. Investigate the effect of temperature and surfactant or surfactant/polymer addition on contact angle, interfacial tension, viscosity and residual tar saturation, and evaluate potential technologies such as thermal method and surfactant or surfactant/polymer flushing to former MGP sites (Chapter VII).

CHAPTER IV

EVALUATION OF MINERAL OIL RESIDUAL SATURATION IN POROUS MEDIA

Introduction

Mineral Oils (MO), also known as liquid petrolatums, liquid paraffins or white mineral oils, are tasteless, odorless (when cold), transparent, oily liquids that are insoluble in both water and alcohol (Irwin et al., 1998). As highly refined petroleum product, mineral oils are produced in large quantities and used extensively in fuels, lubrication, pharmaceuticals, cosmetics, as well as textile and food industries. The composition of mineral oils varies depending on the crude oil source, the refining process, and additives, but the constituents are primarily saturated hydrocarbons. Possible hazards associated with mineral oil include impurities, such as PAHs, which are carcinogens. In modern mineral oil refining, solvent extraction, catalytic hydrotreating or both technologies are applied in order to remove PAHs (Irwin et al., 1998). However, PAHs have been detected in samples of mineral oil for medicinal and cosmetic use (National Library of Medicine, 1994). Hence, there are various opportunities for people to be exposed to mineral oil products. However, the most adverse risk comes from accidental spillage or leakage and improperly disposal of mineral oils, which can result in extensive and lasting contaminations of subsurface system.

Mineral oils, as less dense than water nonaqueous phase liquids (LNAPLs), could be spilled or improperly disposed on the surface, then migrate downward through the vadose zone (unsaturated zone) and spread laterally upon reaching the water table. Also, they could be released into the unsaturated or saturated zone due to the leakage from storage tanks or underground distribution pipelines. At an underground fuel tank site in San Jose, California, adjacent to two 1000-gallon storage tanks containing gasoline and diesel fuel, several inches of oil were found floating on the water table (Kostecki and Calabrese, 1991). As one of the most commonly spilled petroleum products in the United States, the fate and transport of mineral oil in the subsurface, including both the vadose zone and the saturated zone, is very important. The NAPL pools can generally removed by water flood, while the residual NAPL remains after the water floods and exists as immobile blobs or ganglias within the porous media. In two-phase (water-oil) systems, residual LNAPL saturations result from the imbibition of the wetting phase and occur when capillary pressure equals zero. In three-phase (air-water-oil) systems, residual LNAPL saturations are formed during the wetting-phase drainage process and are functions of an equilibrated capillary pressure (Pankow and Cherry, 1996; Steffy et al., 1997). Residual LNAPL saturations are typically higher in saturated two-phase system (pores completely filled with water) than in unsaturated three-phase system (pores contain air). In two-phase systems, residual LNAPL saturations are reported to be in the range from 0.15 to 0.50, while in three-phase systems, residual LNAPL saturations are generally between 0.10 and 0.20 (Mercer and Cohen, 1990; Steffy et al., 1997). Rathmell et al. (1973) reported the residual saturation of mineral oil in two-phase (water-oil) systems in sandstone to be in the range of 0.35-0.43. Pfannkuch (1983) observed that

residual mineral oil saturations in glacial till in vadose zone (three-phase system) ranged from 0.12 to 0.21. Mercer and Cohen (1990) attributed the difference of residual NAPL saturation between two-phase and three-phase systems to two phenomena: i) the buoyancy effect is higher in the unsaturated zone (three-phase) because the fluid density ratio is higher in three-phase systems (NAPL/air) than that in two-phase systems (NAPL/water); and ii) in two-phase water-wetting systems, NAPLs are the nonwetting phase compared to water and are trapped in larger pores. In three-phase systems, NAPLs are intermediate wetting phase, so NAPLs forms thin films on the water surface.

Several mathematical capillary-saturation (P_c - S) models have been used to simulate the water drainage and imbibition process in both saturated (two-phase) and unsaturated (three-phase) systems, and it was found that these models were reasonable approaches under the tested experimental conditions (Kool and Parker, 1987; Parker and Lenhard, 1987; Lenhard and Parker, 1988; Lenhard, 1992). In these models, NAPL entrapment in porous media is controlled by the capillary pressure, which is a function of interfacial tension (IFT), contact angle (or wettability) and pore dimensions. At the same time, residual NAPL saturation is dependent on the saturation history, which is referred to as hysteresis phenomena (Mualem, 1974; Mualem and Morel-Seytoux, 1978; Parker and Lenhard, 1987). That means the starting point of the water imbibition (NAPL drainage) process is important. van Geel and coworkers (1997; 2002) investigated the residual heptane (LNAPL) saturation in three-phase (heptane-water-air) system, and found that it was important to incorporate the effect of the residual NAPL saturation immediately prior to water imbibition, which referred to as the initial NAPL saturation, on the final residual NAPL saturation at the end of water imbibition process. An

analogous conclusion was reached by Steffy et al. (1997) that the residual LNAPL saturation was linearly dependent on the antecedent moisture content (S_{wi}) in decane-water-air and diesel-water-air three-phase systems, while the antecedent moisture content and initial NAPL saturation (S_{Ni}) is generally linearly related ($S_{wi}+S_{Ni}=I-S_a$), where S_a is the air saturation, and does not change during the water imbibition process. However, correlation models that related the residual NAPL saturation to common soil and NAPL properties are very limited. These kinds of correlations will provide useful tools in predicting the amount of NAPL entrapped based on measurable soil and NAPL properties. Steff et al. (1997) found strong correlations between residual oil saturation and surface tension in pure organic-air systems in synthetic polytetrafluoroethylene (PTFE) cores. Chevalier and Fonte (2000) performed more correlation analysis based on the experiments using Soltrol as the oil phase and seven uniform sized quartz fine sands as porous medium (Table 2-6). Three correlation models were proposed at three different capillary number ranges, and strong statistic correlations were found between the experimental and model predicted residual oil saturation values. However, these correlations were not tested in natural systems with complex NAPL and natural soils.

Overall, the lack of comprehensive understanding of the NAPL and aquifer characteristics, as well as the paucity of residual NAPL saturation data makes it very difficult to investigate the NAPL entrapment mechanism and select appropriate remedial alternatives at a particular NAPL contamination site. For complex mixture NAPLs, the situation is even worse. Hence, the purpose of this study was to quantify residual saturation of mineral oils in saturated and unsaturated soils. Properties of three commercial mineral oils, including density, viscosity, surface tension and interfacial

tension (IFT) were evaluated. Characteristics of seven field soil samples, including particle density, particle size distribution, total carbon content, N₂/BET specific surface area and pressure-saturation relationships were investigated. The residual mineral oil saturation was evaluated in both oil-water (two-phase) and air-oil-water (three-phase) systems for each soil, and the pressure-saturation relationships were investigated in air-oil-water (three-phase) systems. Correlations between the residual saturation and mineral oil and soil properties were developed to provide tools for predicting the residual saturation based on knowledge of soil and liquid properties.

Materials and Methods

Materials

Three Insulating Mineral Oils, designated as EPRI mineral oil, “new” Franklin mineral oil and “old” Franklin oil, were provided by Tetra Tech, Inc. and used as the nonaqueous phase liquid (NAPL) for the residual oil saturation experiments. Seven soil samples, referred to as Mead/Bell, Kalispell, Olympia, FR-9, LAI-3, CS-1, and TS-2, were supplied by Tetra Tech, Inc. All the soils were pretreated after received. Large stones, dried branches or foreign particles (e.g., broken glass) were removed by hand. The soils were spread on plastic film and ventilated place for at least a week, and turned over once a day. The air-dried soils were gently grounded in a ceramic mortar with a pestle, and stored in wide-mouth glass jars. F-70 (40-270 mesh) Ottawa sand, obtained from U.S. Silica Company (Berkeley Springs, WV), was used as a reference soil.

Reagents, including potassium chloride (KCl), potassium iodide (KI) and calcium chloride (CaCl₂), were obtained from Fisher Scientific Company (Pittsburg, PA). All the solutions were prepared with deionized-distilled water that was treated with a Barnsted Nanopure System (Dubeque, IA) to remove any residual organic contaminants. The Nanopure water was de-aired prior to use by a combination of heating and vacuum application.

Methods

Oil Density

The density of each mineral oil sample was determined using 25 mL glass pycnometers (Fisher Scientific, Pittsburg, PA). Prior to each use, the pycnometers were calibrated gravimetrically (Mettler-Toledo, AG245 analytical balance) based on the mass of Nanopure water required to fill the vessel at 22°C. Calibration measurements were performed in quintuplet, with the average mass and density of water at 22°C used to determine the volume of the pycnometer. Mineral oil densities were determined from the mass of oil filling the pycnometer and the calibrated volume. Measurements were performed in triplicates at 22°C for each mineral oil.

Viscosity

Viscosities of mineral oil samples were determined using a rheometer (Rheostress, Model RS75, Haake, Paramus, NJ) equipped with double gap cylinder sensor (Model DG 41). The temperature was maintained at 22°C using a recirculating water bath (Model C25, Haake, Paramus, NJ). The instrument was calibrated by

measuring the viscosity of Nanopure DI water at 22°C. Viscosity of each mineral oil was measured at a shear rate of 200 s⁻¹ in duplicate.

Surface Tension

The surface tension (ST) of mineral oil was determined by the du Nouy ring method. The experimental apparatus consisted of a Cahn DCA 322 dynamic contact analysis system (ThermoHaake, Paramus, NJ) connected to a personal computer. The ring was made of platinum-iridium. Prior to use, the ring was burned in a flame to remove any residual organic contaminants and cooled down to room temperature. The ring was immersed in mineral oil completely and retracted until completely out of the oil phase into the air phase. The surface tension was calculated from the measured force required to pull the ring through the mineral oil surface. The equation used to calculate the surface tension of the liquid is expressed as follow:

$$\gamma = \gamma^* \times cF \quad (4-1)$$

where γ^* is the raw surface tension reading from the measurement (dynes/cm), and cF is the correction factor, which is used to correct for the amount of liquid attached to the bottom of the ring during the pulling process of the experiment.

$$cF = 0.7250 + \sqrt{\frac{1.452\gamma^*}{C^2(\rho_d - \rho_l)} + 0.04534 - \frac{1.679}{R/r}} \quad (4-2)$$

where C is the mean circumference of the ring, ρ_d and ρ_l are the densities of the heavier and lighter liquid, respectively, R and r are the radius of the ring and the wire of ring, respectively.

The instrument was calibrated by measuring the surface tension of water (72.6 dynes/cm) following the protocol described above, until the difference between the measured and actual value was within $\pm 3\%$. The surface tension of each mineral oil was measured in triplicate.

Interfacial Tension

Interfacial tension (IFT) of mineral oil was measured using both drop volume method and a ring tensiometer. For the drop volume method, a syringe pump (Harvard Apparatus, 22) was used to force mineral oil through a tungsten-carbide tip (Caiser Tool Company, CA) with an inner diameter of 254 μm and wall thickness of 17 μm at the orifice into a Nanopure DI water solution in an upflow mode. The tip was located at the bottom of a glass column (1.7 cm in diameter by ~ 4.5 cm in height) containing with water. The time required for 5 drops to form and detach from the end of the tip immersed in the Nanopure DI water solution was recorded. A total of 30 drops were counted during each measurement. The IFT between mineral oil and water was calculated using the following equation (Hool et al., 1992):

$$\gamma = V_d \Delta \rho g / \pi d \quad (4-3)$$

where γ is the oil-water interfacial tension (dynes/cm), V_d is the average droplet volume (cm^3) ($V_d = \text{flow rate} \times \text{time} / \text{number of drops}$), $\Delta \rho$ is the difference in density between the two liquid phases (g cm^{-3}), g is the constant of gravity (cm s^{-2}) and d is the inner diameter of the tip orifice (cm). By using the tip with ultra thin wall at the orifice, the front facial area surrounding the orifice was minimized; thus, the Harkins correction factor could be neglected (Harkins et al., 1919; Hool et al., 1992). The drop volume method was checked

by measuring the surface tension of Nanopure DI water until the difference between the measured and actual surface tension value of water was within $\pm 5\%$.

The oil-water IFT was also determined by the du Nouy ring method (Adamson, 1990). The apparatus is the same as in surface tension measurements, but the procedure is more complicated. The ring was first immersed completely in the heavier phase (DI water). Mineral oil was added slowly into the beaker to form an oil phase on top of the water phase. The oil-water IFT was calculated from the measured force, required to pull the ring out of the oil-water interface (Equation 4-1, 2). The ring passed only once between the interface of the two liquids, typically from the heavier to the lighter liquid. The instrument was calibrated by measuring the Nanopure DI water surface tension and dodecane-water IFT. Each of oil-water IFT was measured in triplicate.

Particle Size Analysis:

Particle size distributions were analyzed using the sieve analysis method (Gee and Bauder, 1986). Empty sieves and pan were weighed (Mettler PM4000, Rite-Weight, Inc.) prior to soil sieving. Each pretreated soils as described in the material section was poured into the top sieve of a stack of sieves with openings of decreasing size from top to bottom (the pan was placed below the stack). The ASTM sieves and corresponding opening size are listed in Table 4-1. The stack of sieves was shaken by hand. Each sieve and pan was weighed after the soil sieving to determine the mass of soil retained on each sieve and pan. The cumulative weight passing through each sieve size was plotted as the ordinate (arithmetic scale) and sieve opening size as the abscissa (logarithmic scale), which was referred to as the particle size distribution curve. Soil retained on the No. 5 sieve (4 mm)

Table 4-1. Opening sizes of ASTM sieves used in particle size analysis.

ASTM Sieve No.	Opening (mm)
5	4.00
10	2.00
20	0.850
30	0.600
40	0.425
60	0.250
100	0.150
140	0.106
200	0.075
270	0.053

was discarded, and the remainder composited and mixed thoroughly. The air-dried soils were stored in 1 L wide-mouth glass jars and for subsequent analysis. Soil samples used for particle density, total carbon and surface area analysis were further sieved through No. 20 sieve (0.85 mm) prior to use.

Particle Density

The density of each soil sample was determined by the pycnometer method (Blake and Hartge, 1986) using 25 mL glass wide-mouth cylindrical pycnometers (Fisher Scientific, Pittsburg, PA). Prior to each measurement, the pycnometer was weighed (W_a). Approximately 10 g of soil was then added to the pycnometer and weighed (W_s). Soil adhering to the inside of the neck was rinsed into the body of the pycnometer with Nanopure water. Water was added until the pycnometer was about one-half full. Trapped air was removed from soil pores by gentle agitation of the contents, and enough Nanopure water was added to completely fill the pycnometer. The glass stopper was inserted and the outside of the pycnometer was thoroughly dried and cleaned with a tissue. The pycnometer and its contents (soil and water) were then weighed (W_{sw}). The pycnometer was then cleaned and filled with Nanopure water. The stopper was inserted and the outside of the pycnometer was thoroughly dry and weighed (W_w). The particle density was calculated as follows:

$$\rho_s = \rho_w (W_s - W_a) / [(W_s - W_a) - (W_{sw} - W_w)] \quad (4-4)$$

where, ρ_s and ρ_w are density of soil particle and water, respectively (g cm^{-3}). Density measurement for each soil sample was run in triplicate.

Total Carbon

The total carbon (TC) content of soils was determined using a Shimadzu Model 500 Total Organic Carbon (TOC) Analyzer equipped with a Solid Sample Module (SSM) and an infrared detector for CO₂ measurement (Shimadzu Instruments, Kyoto, Japan). Approximately 1g of soil samples were placed in a ceramic cell and combusted at 900°C in the SSM unit. The calibration of SSM module was made using anhydrous Dextrose powder containing 40.0% carbon by weight. Each soil sample was measured for TC in duplicate.

Specific Surface Area

Specific surface area (SSA) measurements were performed using a Micromeritics Accelerated Surface Area and Porosimetry System (ASAP) 2010 surface area analyzer (Micromeritics, Norcross, GA). Soil samples for surface area analysis were oven-dried at 105°C for 2 hours prior to use. Approximately 1 to 2 g of oven-dried soil samples were placed in a sample tube and degassed with Helium at 105°C using an automatic degas mode for 2-4 hours. The sample tube was transferred to a liquid N₂ bath (77°K) and exposed to different pressures of N₂ using an automated control system. Specific surface area values were then determined by fitting the N₂ adsorption data to the Brunauer, Emmett and Teller (BET) equation (Equation 4-5) (Adamson, 1990) over a relative vapor pressure range of 0.05 to 0.35.

$$\frac{P}{V(P_0 - P)} = \frac{1}{V_1 C} + \frac{(C-1)P}{V_1 C P_0} \quad (4-5)$$

where V is the volume of gas (N_2) adsorbed at pressure P (cm^3), V_1 is the volume of a single layer of adsorbed molecules over the entire surface of the soil particles (cm^3), P_0 is the pressure required for monolayer saturation at the temperature of the experiments (Pa), and C is a constant. The volume V_1 can be obtained by plotting $\frac{P}{V(P_0 - P)}$ versus $\frac{P}{P_0}$, hence the surface area covered by the N_2 gas, which is considered to be the N_2 /BET specific surface area of soil can be calculated. F-70 Ottawa sand with a surface area of $0.16 \text{ m}^2/\text{g}$ was used as the reference sample. Surface area analysis of each soil sample was performed in duplicate.

Moisture Release Curve:

Soil water saturation-capillary pressure relationships were determined using a Tempe cell system (Soil Moisture Equipment Corp., Santa Barbara, CA) (Klute, 1986) (Figure 4-1). Tempe cell contained a brass column (6 cm height by 5.4 cm inner diameter) and two Plexiglas end plates. A porous ceramic plate with a bubbling pressure of 1 bar (1033.6 cm of water) was placed on the bottom end plate. The endplates were fitted with Viton o-rings to provide a watertight seal between the soil column and the endplates. The Tempe cells were packed with air-dried soil through No 5 sieve ($< 4 \text{ mm}$) under gentle vibration in 1-cm increments. The packed Tempe cells were flushed with CO_2 to allow for more rapid dissolution for the entrapped gas phase. The Tempe cells were then saturated with 500 mg/L (0.0045 M) $CaCl_2$ degassed background solution using a low-speed piston pump (Model QG-20, Fluid Metering Inc., Syosset, NY) equipped with a stainless steel pump head module at a flow rate of 1 mL/min for ~ 10 pore volumes. Air pressure was applied to top of the cells in increments over a pressure



Figure 4-1. Tempe cells used to measure water retention characteristics (moisture release curves) of the soil samples

range of 0 to 1 bar. At each pressure increment, the cell was removed from the apparatus and weighed. The soil water content was determined gravimetrically using a digital balance with a resolution of 0.01 g (Mettler PM 4000, Rite-Weight, Inc.). Equilibrium conditions were assumed when the weight difference of the cells over two consecutive days was less than 0.1 g. Each MRC was run in duplicate or triplicate. F-70 Ottawa sand was used as a reference soil. The experimental moisture release curve data (negative pressure head and corresponding volumetric water content) were fitted to Brooks Corey and van Genuchten mode using Retention Curve (RETC) Code (van Genuchten et al., 1991).

Two-Phase (Oil-Water) Residual Oil Saturation Experiments

Kontes borosilicate glass columns with a 4.8 cm diameter and adjustable endplate were used for residual saturation experiments in oil-water two-phase system (Figure 4-2a). Each endplate was fitted with one 40 mesh (425 μm) polytetrafluoroethylene (PTFE) screen. The top endplate was lined with a 0.22 μm pore size Teflon filter paper (Osmonics Inc.) to obtain organic-wetting conditions, while the bottom endplate was lined with Whatman No. 42 filter paper (Fisher Scientific Co.) to obtain water-wetting conditions.

Air-dried soil (< 4 mm) was poured into the glass column in 1 cm increments and packed under gentle vibration. To reduce layering within the column, a small spatula was used to mix the soil after each increment addition. A bed length of 5 cm was used for each column. Soil properties, including porosity and bulk density, were determined gravimetrically.

Prior to water saturation, the column was flushed with CO₂ gas for about 20 minutes to facilitate dissolution of entrapped air during the saturation process. The soil column was then oriented vertically and saturated with 500 mg/L (0.0045 M) de-aired CaCl₂ background solution using a Rainin HPLC pump (Mode Dynamix SD-200). The water was pumped through the soil column in an upflow mode at a rate of 1-2 ml/min for approximately 20 pore volumes to ensure complete saturation of the soil with water. The porosity of the porous medium was again determined based on the water-saturated column mass and the density of water. The completely water saturated soil column was then performed a non-reactive tracer (KI) experiment. A KI non-reactive tracer solution (0.01 M) was injected at a flow rate of 1 mL/min using a Rainin HPLC pump. The effluent solution was collected using an ISCO fraction collector in 4-5 mL intervals (depending on the pore volume of the column. In general, 10 samples per pore volume were collected). After the injection of ~1.5 pore volumes of tracer solution, the influent solution was switched to 0.01 M KCl for about 3.5 pore volumes. The concentration of KI in effluent solution was analyzed using a Hewlett-Packard series 1100 high-pressure liquid chromatograph (HPLC) equipped with a 250 mm Supercosil LC-18-DB (Supelco reverse phase column (4.6 mm of i.d. and average particle size of 5 μm).

Following the tracer experiment, ~1.0 pore volume of mineral oil was introduced from top of column in a down-flow mode at a flow rate of 1 mL/min using a syringe pump (Model 22, Harvard Apparatus). Upon completion of mineral oil injection, the CaCl₂ background solution (500 mg/L) was pumped through the column at a flow rate of 5ml/min using the Rainin HPLC pump until no oil was observed in the effluent.

A second non-reactive tracer study was conducted after the water flushing to determine the residual oil saturation. Residual saturation of mineral oil was determined in two ways. The first method involved a pre- and post-entrapment gravimetric method, based on the difference in densities of fluids and the weight of the column before and after mineral oil entrapment.

$$S_{Nr} = \frac{W_{pre} - W_{post}}{(\rho_w - \rho_o)PV} \quad (4-6)$$

where, S_{Nr} is the residual LNAPL saturation ($\text{cm}^3 \text{ cm}^{-3}$) W_{pre} is the weight of column saturated with water before the mineral oil injection (g), and W_{post} is the weight of column after oil entrapment and water flushing (g). ρ_w and ρ_o are the densities of water and oil, respectively (g cm^{-3}), and PV is the total pore volume of the column (cm^3).

The second method was based on analysis of pre- and post-entrapment tracer tests. The tracer breakthrough curves (BTCs) before mineral oil injection and after water flushing were fit using CXTFIT2 computer code (Toride et al., 1995) to obtain the retardation factor. For non-reactive tracer, the equilibrium convection-dispersion equation (CDE) (Equation 4-7) was utilized.

$$R_F \frac{\partial c}{\partial t} = D \frac{\partial^2 c}{\partial x^2} - v \frac{\partial c}{\partial x} \quad (4-7)$$

where R_F is the retardation factor (dimensionless), c is the tracer concentration (mol L^{-1}), t is time (s), and v is the pore-water velocity (m s^{-1}).

The calculations of residual saturation were as following:

$$V_{res} = (R_{F,bef} - R_{F,af}) \times PV \quad (4-8)$$

$$S_{Nr} = V_{res} / PV \quad (4-9)$$

where, V_{res} is residual mineral oil volume (cm^3), $R_{F,bef}$ and $R_{F,aft}$ are retardation factors before mineral oil injection and after water flushing, respectively.

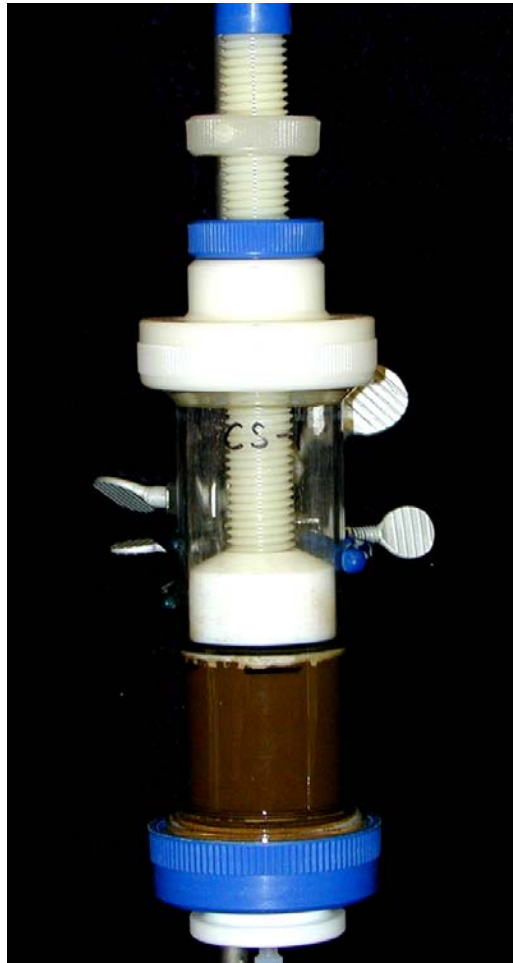
Residual saturations of water and oil were measured in duplicate for each soil.

Three-Phase (Air-Oil-Water) Residual Oil Saturation Experiments

Custom designed and manufactured soil columns and endplates were used in three phase (air-oil-water) experiments (Figure 4-2b). The soil columns were constructed from aluminum tubing, approximately 5.0 cm in length and 5.2 cm in inside diameter. Stainless steel endplates were fitted with viton o-rings to provide a watertight seal between the soil column and the endplate. Stainless steel mesh (425 μm opening) (McMaster Carr) and nylon mesh screens (212 μm opening) (Spectrum Laboratories, Inc.) were placed at the bottom endplate to hold the porous media in the column and to achieve uniform dispersed fluid flow across the column cross-sectional area. The three-phase experimental set up is shown in Figure 4-3.

The saturation experiments were conducted following an existing protocol developed to generate uniform distributions of both residual water and organic liquid in three-phase (air-oil-water) systems (Wilkins et al., 1995). The procedure involved three steps: i) uniform packing of the column with air-dried soil, ii) water imbibition and drainage to residual water saturation, and iii) oil imbibition and drainage to residual oil saturation.

Air-dried soil (< 4 mm) was added to the column in 1.5 cm increments under vibration and gentle tapping with a fitted dowel. When the column was filled with soil, Whatman No 42 filter paper was seated and the top endplate was fastened to the column.



(a)



(b)

Figure 4-2. Residual mineral oil saturation experiments in (a) oil-water two-phase and (b) air-oil-water three-phase systems.

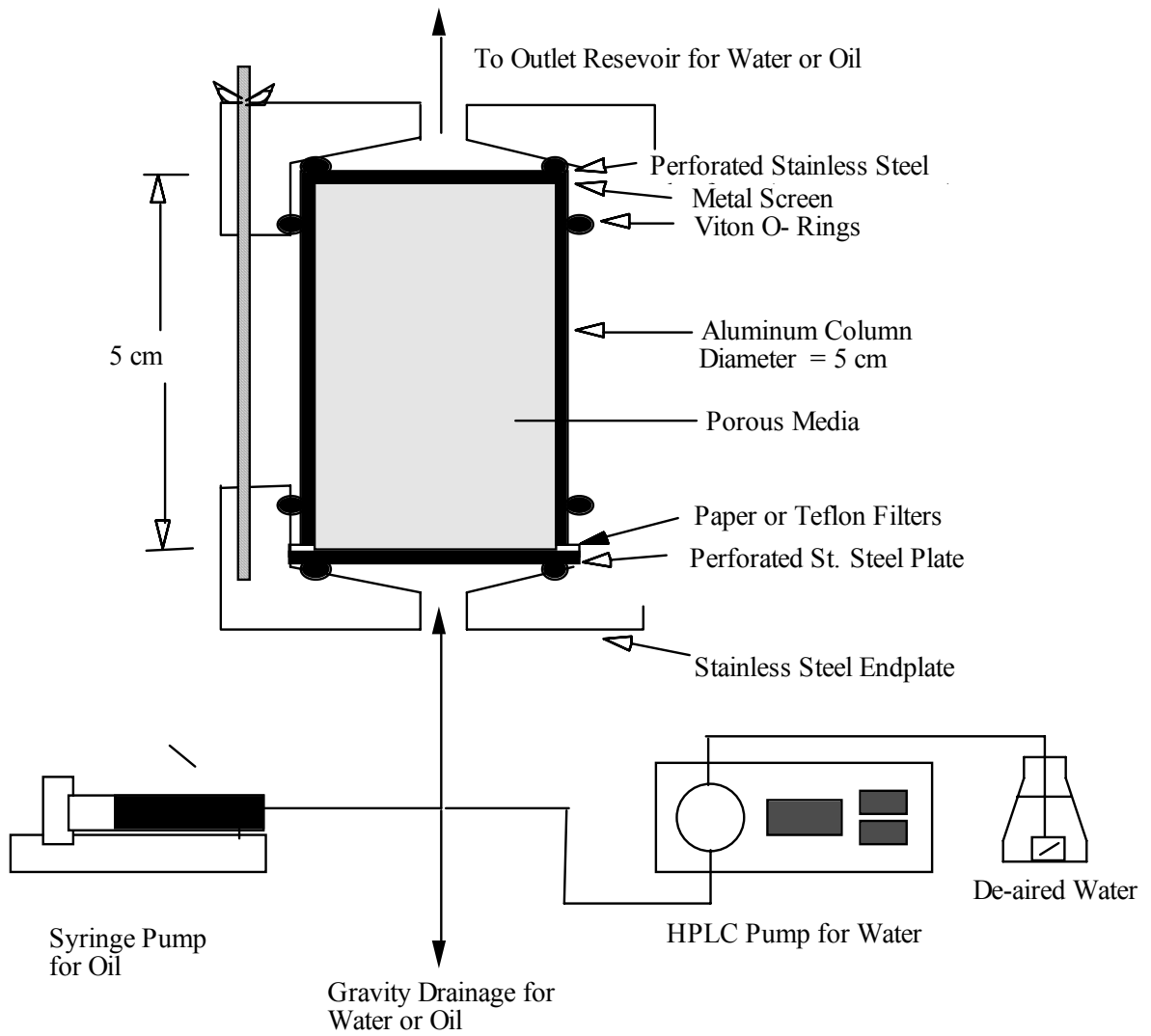


Figure 4-3. Schematic diagram of experimental column apparatus used for water and oil residual saturation measurements.

Soil properties, including porosity and bulk density, were determined gravimetrically.

Prior to water saturation, the soil column was flushed with CO₂ gas, and then saturated with 500 mg/L de-aired CaCl₂ solution as described in the two-phase experimental section. The soil column was then allowed to drain under a negative pressure head (suction) of either -100 cm of water (Mead/Bell, Kalispell, Olympia, FR-9 and LAI-3) or -305 cm of water (CS-1 and TS-2). The higher suction was required for the CS-1 and TS-2 samples because the water did not reach a residual state at a suction of 100 cm. The negative pressure was maintained with a pressure-vacuum regulator and monitored over time using a mercury manometer. The soil columns were weighed daily until the change in column weight was less than 0.1 g between two measurements. Upon the completion of water drainage, the residual water saturation was determined gravimetrically based on the density of water and the difference between dry-packed soil column weight and the soil column weight at residual water saturation.

After establishing the residual water saturation, the nylon mesh screen (0.45 μm pore size) at the bottom endplate was replaced with a hydrophobic Teflon filter (0.22 μm pore size) (Osmonics, Inc.). Prior to placement in the bottom endplate, the Teflon filter was saturated with mineral oil to prevent air entrapment. A syringe pump was then used to inject mineral oil (50-70 ml) into the column in an upflow mode at a flow rate of 1.0 ml/min. After the oil injection step was completed, the soil column was allowed to drain under three negative pressures (-50, -150, and -250 cm) for Mead/Bell, Kalispell, and Olympia soils, and a single negative pressure head (suction) of -90 cm for FR-9 and LAI-3 or -265 cm for CS-1 and TS-2. The Teflon filters were oil-wetting, and therefore allowed for oil drainage while preventing the passage of water. The soil columns were

weighed daily until the change in column weight was less than 0.1 g between two measurements. When oil drainage ceased, the residual oil saturation was determined gravimetrically based upon the oil density and the difference between the soil column weight before and after oil entrapment.

Residual saturations of water and oil were measured in duplicate for each soil.

Results and Discussion

Physical Properties of Mineral Oils

Liquid density, viscosity, surface tension and oil-water interfacial tension were measured for three mineral oil samples, including EPRI mineral oil and “New” and “Old” Franklin mineral oils, at room temperature ($22 \pm 1^\circ\text{C}$). Relevant mineral oil properties are listed in Table 4-2, with dodecane used as a reference LNAPL. The densities of the three samples were very similar, approximately 0.88 g/cm^3 , which is higher than that of dodecane, but lower than that of water. Viscosities at a shear rate of 200 s^{-1} ranged from 13.3 to 17.1 centipoise (cP). These viscosity values are greater than those of water and other pure NAPLs commonly encountered in the subsurface, including PCE, TCE, CB. Therefore, mineral oils could be classified as slightly viscous, light nonaqueous phase liquids (LNAPLs).

Measured surface tensions were in the range of 19.9-31.2 dynes/cm, considerably lower than the surface tension of water (72.6 dynes/cm). The IFT between EPRI mineral oil and water was relatively high, (~ 40 dynes/cm), and is similar as the IFT between PCE or TCE and water, which implicate that EPRI mineral oil is highly refined. The IFTs between the two Franklin mineral oils and water were much lower (~ 23 -36 dynes/cm),

Table 4-2. Comparison of relevant properties for EPRI mineral oil, “Old” and “New” Franklin mineral oil, and dodecane (reference organic liquid).

Physical-Chemical Property	EPRI Mineral Oil (2002)	“Old” Franklin Mineral Oil (1998)	“New” Franklin Mineral Oil (2002)	Dodecane (reference)
Liquid density (g/cm ³), 22°C	0.883 (±0.002)*	0.868 (±0.003)	0.868 (±0.000)	0.75 [‡]
Liquid density (g/cm ³), 24°C	---	0.875 [†]	---	---
Viscosity (cP), shear rate = 200 1/s, 20°C	18.72 (±0.09)	15.89 (±0.13)	14.51 (±0.03)	1.38 [‡]
Viscosity (cP), shear rate = 200 1/s, 22°C	17.09 (±0.08)	14.9 [†]	13.34 (±0.05)	
Viscosity (cP), 25°C	---		---	
Molecular weight (g/mole)	257 [†]	257 [†]	257 [†]	170.34 [‡]
Surface Tension, DV [§] (dyne/cm), 22°C	31.24 (±0.06)	29.92 (±0.30)	30.13 (±0.15)	27.22 (±1.68)
Surface Tension, RT [§] (dyne/cm), 22°C	27.96 (±0.69)	27.95 (±0.69)	27.04 (±0.22)	24.14 (±0.01)
Surface Tension (dyne/cm), 25°C	---	33.5 [†]	---	24.9 [‡]
Interfacial Tension, DV [§] (dynes/cm), 22°C	48.74 (±0.35)	30.39 (±0.51)	31.44 (±0.17)	48.27 (±0.14)
Interfacial Tension, RT [§] (dynes/cm), 22°C	40.36 (±0.33)	23.82 (±1.43)	36.13 (±0.74)	46.72 (±2.69)
Interfacial Tension (dynes/cm), 25°C	---	33.5 [†]	---	52.8 [‡]

* standard deviation (s. d. = $\sigma/\sqrt{N-1}$)

[†] TetraTech values

[‡] Literature values

[§] Drop Volume (DV); Ring Tensiometer (RT)

which is typical for the complex commercial mineral oils. The lower IFTs of mineral oil-water compared to pure organic-water IFTs could result from the accumulation of surface active constituents in the mineral oils at the oil-water interface.

Physical Properties of Soils

Based on the particle size analysis of all the seven soil samples, these soil samples were primarily sandy soils, with most of the soil particle size in range of 2-0.05 mm (sand), as shown in Table 4-3. The sand fractions in soils ranged from 55.98% for CS-1 soil to 99.48% for FR-70 soil. The CS-1, LAI-3 and TS-2 soils contained relatively high gravel portion (> 2 mm), which was 42.70%, 28.03% and 29.10%, respectively. The silt and clay particles (< 0.05 mm) were not found in Mead/Bell soil, and very low in FR-9 (0.49%) and LAI-3 (0.32%). For the other four soil samples (Kalispell, Olympia, CA-1 and TS-2), the silt and clay particles were less than 4%. Particle size distributions are plotted in Figure 4-4, classified according to United States Department of Agriculture (USDA) soil classification system. The calculated coefficient of uniformity ($C_u = \frac{d_{60}}{d_{10}}$) ranged from 2.28 for FR-9 and 23.0 for CS-1. Coefficient of uniformity is used to describe the uniform degree of soil, and lower values represent more uniform particle size distribution (Hillel, 1998). Therefore, FR-9 was a relatively uniform soil, while CS-1 ($C_u = 23.0$) and TS-2 ($C_u = 12.0$) have a broad particle size distribution. Another parameter, coefficient of gradation ($C_g = \frac{d_{30}^2}{d_{10}d_{60}}$), is also used to reflect the particle size distribution. In general, when C_g is $\sim 1-3$, the soil is considered to be well-graded, which means the soil contains a continuous particle size from largest to smallest. For the seven

soil samples examined in this study, the coefficient of gradation ranged from 0.37 for CS-1 soil to 1.93 for Kalispell soil, which indicates that CS-1 and TS-2 soils ($C_g = 0.59$) are poorly graded. The total carbon content of the seven soil samples ranged from 0.12% for Mead/Bell to 10.59% for TS-2 soil. Also TS-2 soil were much darker in appearance, which indicates appreciate amounts of organic carbon. Kalispell and CS-1 soils also contained relatively high total carbon content, which was 5.25% and 4.16%, respectively. The N_2 /BET surface area analysis was performed to three of the seven soil samples, including Mead/Bell, Kalispell and Olympia. The surface area values were 3.77, 5.94 and 5.44 m^2/g , respectively, which is higher than the F-70 Ottawa sand (0.16 m^2/g), but much lower than those of hydrous mica (167 m^2/g) and montmorillonite (677 m^2/g) (Marshall et al., 1996). Particle density of the seven soil samples ranged from 2.08 g/cm^3 for TS-2 to 2.74 g/cm^3 for Mead/Bell, which were typical densities for the field soil samples (Table 4-4).

Moisture Release Curves of Soil Samples

Average physical properties of Tempe cells packed with Mead/Bell, Kalispell, Olympia, FR-9, LAI-3, CS-1, and TS-2 soils are given in Table 4-4. Column bulk density ranged from 0.978 g/cm^3 for TS-2 to 1.792 g/cm^3 for Mead/Bell, which resulted in the pore volume (void volume) of TS-2 and Olympia (75.6 cm^3 and 81.6 cm^3 , respectively) was nearly twice as large as the pore volume obtained for Mead/Bell soil (44.4 cm^3). Water saturations ranged from 0.594 cm^3/cm^3 for Olympia to 0.324 cm^3/cm^3 for Mead/Bell soil.

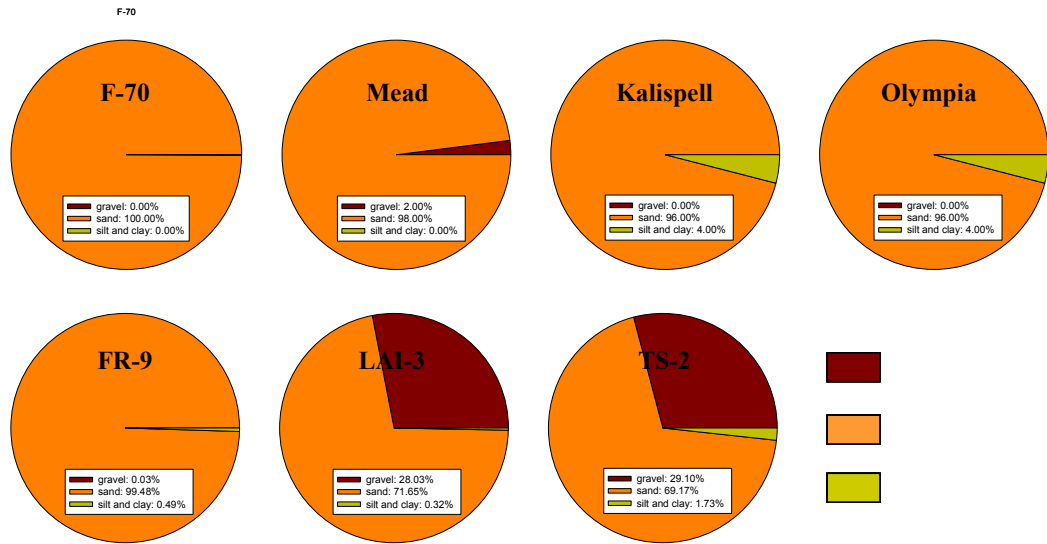


Figure 4-4. Textural classification of soils based on the Universal Soil Classification System (USCS) (Gravel: 76.2-4.75 mm; Sand: 4.75-0.075 mm; Silt and Clay: < 0.075 mm).

Table 4-3. Physical properties of soils obtained from particle size (sieve), surface area, and total carbon analysis.

Soil Identifier	d ₆₀ (mm)	d ₅₀ (mm)	d ₁₀ (mm)	C _u	C _g	USDA Particle Size Classification			N ₂ /BET Surface Area (m ² /g)	Total Carbon (%)
						% Gravel > 2 mm	% Sand 2-0.05 mm	% Silt+Clay < 0.05 mm		
F-70 OS	0.31	0.28	0.18	1.72	0.95	0.00	100.00	0.00	0.16	ND [‡]
Mead/Bell	0.46	0.40	0.20	2.30	0.98	2.00	98.00	0.00	3.77 (±0.37)*	0.12 (±0.01)
Kalispell	0.25	0.22	0.06	4.17	1.93	0.00	96.00	4.00	5.97	2.19 (±0.01)
Olympia	0.35	0.29	0.06	5.47	1.79	0.00	96.00	4.00	5.44 (±0.18)	5.25 (±0.12)
FR-9	0.41	0.37	0.18	2.28	1.83	0.03	99.48	0.49	NA	1.14(±0.00) ND [†]
CS-1	2.30	1.43	0.12	23.00	0.37	42.70	55.98	1.32	NA	4.16 (±0.30) 5.3 [†]
LAI-3	0.93	0.66	0.28	3.32	1.16	28.03	71.65	0.32	NA	0.14 (±0.01) 0.08 [†]
TS-2	1.44	1.08	0.10	12.00	0.59	29.10	69.17	1.73	NA	10.59 (±0.26) 10.7 [†]

* standard deviation (s. d. = $\sigma/\sqrt{n-1}$)

[†] TetraTech values

[‡] ND – none detected (below detection limit of 0.01% TC).

Soil moisture release curve (MRC) describes the capillary pressure-saturation (P_c - S_w) relationship in air-water-soil system. The comparisons of MRC primarily lie on three aspects: i) the bubbling pressure or air entry pressure, h_b , which refers to the capillary pressure at which movement of the air into the pores first occurs, ii) the steepness of the curve right after the bubbling pressure, which indicates the pore size distribution of the soils, and iii) the residual saturation corresponding to the saturation without changing with the increasing capillary pressure (Davis, 1994).

Comparing the MRCs shown in Figure 4-5 of the seven soil samples, Kalispell, Olympia and CS-1 exhibited relative higher pressures when the volumetric water contents started to drop, which are in agreement with bubbling pressure (air entry pressure) values. From the RECT fit of the MRC data (Table 4-4), the bubbling pressures (h_b) of Kalispell, Olympia and CS-1 soils were 94.3, 86.2 and 101.1 cm, respectively, while the bubbling pressure of FR-9 and LAI-1 soils were 6.0 and 5.6 cm, respectively. This observation indicates that the non-wetting phase fluid could enter the FR-9 and LAI-1 soils much easier than the Kalispell, Olympia and CS-1 soils. The volumetric water contents were also observed dropping sharply at low capillary pressure (or negative pressure, or suction) for Mead/Bell, Kalispell, Olympia, FR-9 and LAI-1 soils, which were well-graded soil. For CS-1 and TS-2 the decrease in water content with capillary pressure was gradual, which were consistent with the low C_g values as discussed in the soil properties section. When the capillary pressure exceeded ~ 200 cm of water, the water content changed slightly with the increase of capillary pressure (Figure 4-5). Figure 4-6 shows that volumetric water content at 1 bar is consistent with the particle density and porosity. For example, Olympia and TS-2 soils showed the highest residual water

contents of $0.255 \text{ cm}^3/\text{cm}^3$ and $0.385 \text{ cm}^3/\text{cm}^3$ at 1 bar, which corresponds to the lowest bulk densities ($2.41 \text{ g}/\text{cm}^3$ and $2.08 \text{ g}/\text{cm}^3$) and highest porosities ($0.594 \text{ cm}^3/\text{cm}^3$ and $0.572 \text{ cm}^3/\text{cm}^3$), respectively. However, the residual water content in CS-1 and TS-2 soil columns was defined to approach 0 by the RETC code, as shown in Table 4-4. This result might be explained by the fact that the water content presented a gradual decrease and no evidence of reaching residual saturation during the whole range of residual saturation value. The representative van Genuchten (VG) and Brook-Corey (BC) fitting curves for experimental MRC data are shown in Figure 4-7.

Residual Mineral Oil Saturation in Two-Phase (Oil-Water) Systems

EPRI mineral oil was used as the representative LNAPL in the two-phase residual saturation experiments. Column conditions and experiment results are listed in Table 4-5. The residual mineral oil saturations ranged from $0.092 \text{ cm}^3/\text{cm}^3$ for TS-2 soil to $0.218 \text{ cm}^3/\text{cm}^3$ for FR-9 soil (Figure 4-8). Although TS-2 bore a high total carbon content (10.59%), it had the lowest particle density ($2.08 \text{ g}/\text{cm}^3$) among all the soil samples, which resulted in a low bulk density ($1.025 \text{ g}/\text{cm}^3$) and high porosity ($0.583 \text{ cm}^3/\text{cm}^3$) of the TS-2 soil column. Olympia soil column had a high porosity ($0.532 \text{ cm}^3/\text{cm}^3$), but the residual oil saturation was relatively high ($0.165 \text{ cm}^3/\text{cm}^3$), which was attributed to its relative uniform particle size distribution. Compared to TS-2, Olympia had a more uniform particle size distribution (C_u was 5.47 for Olympia, lower than that of TS-2 ($C_u = 12.0$)), and a much lower mean particle size (d_{50} was 0.29 mm for Olympia, and 1.08 mm for TS-2) (Table 4-3).

Table 4-4. Summary of soil water retention parameters obtained for van Genuchten and Brooks-Corey equations.

Soil Identifier	Bulk Density (g/cm ³)	Particle Density (g/cm ³)	Van Genuchten Parameters				Brooks-Corey Parameters			
			θ_{sat}	θ_{res}	α	n	θ_{sat}	θ_{res}	H _b (cm)	λ
F-70 OS	1.741 (±0.000)*	2.63 (±0.01)	0.343	0.069	0.023	5.63	0.343	0.068	25.8	0.30
Mead/Bell	1.792 (±0.002)	2.74 (±0.24)	0.324	0.121	0.031	2.55	0.324	0.111	20.1	1.12
Kalispell	1.587 (±0.002)	2.59 (±0.02)	0.401	0.000	0.006	1.42	0.401	0.178	94.3	1.07
Olympia	1.075 (±0.001)	2.41 (±0.02)	0.594	0.001	0.006	1.32	0.594	0.255	86.2	1.78
FR-9	1.625 (±0.000)	2.68 (±0.01) 2.65 [†]	0.387	0.089	0.152	2.22	0.387	0.088	6.0	0.85
CS-1	1.388 (±0.000)	2.56 (±0.01) 2.53 [†]	0.451	0.000	0.004	1.40	0.451	0.000	101.1	4.28
LAI-3	1.676 (±0.000)	2.69 (±0.07) 2.75 [†]	0.381	0.099	0.157	1.74	0.381	0.098	5.6	1.44
TS-2	0.978 (±0.000)	2.08 (±0.19) 2.29 [†]	0.550	0.000	0.027	1.10	0.550	0.000	21.7	11.48

* standard deviation (s. d. = $\sigma/\sqrt{n-1}$)

[†] TetraTech values

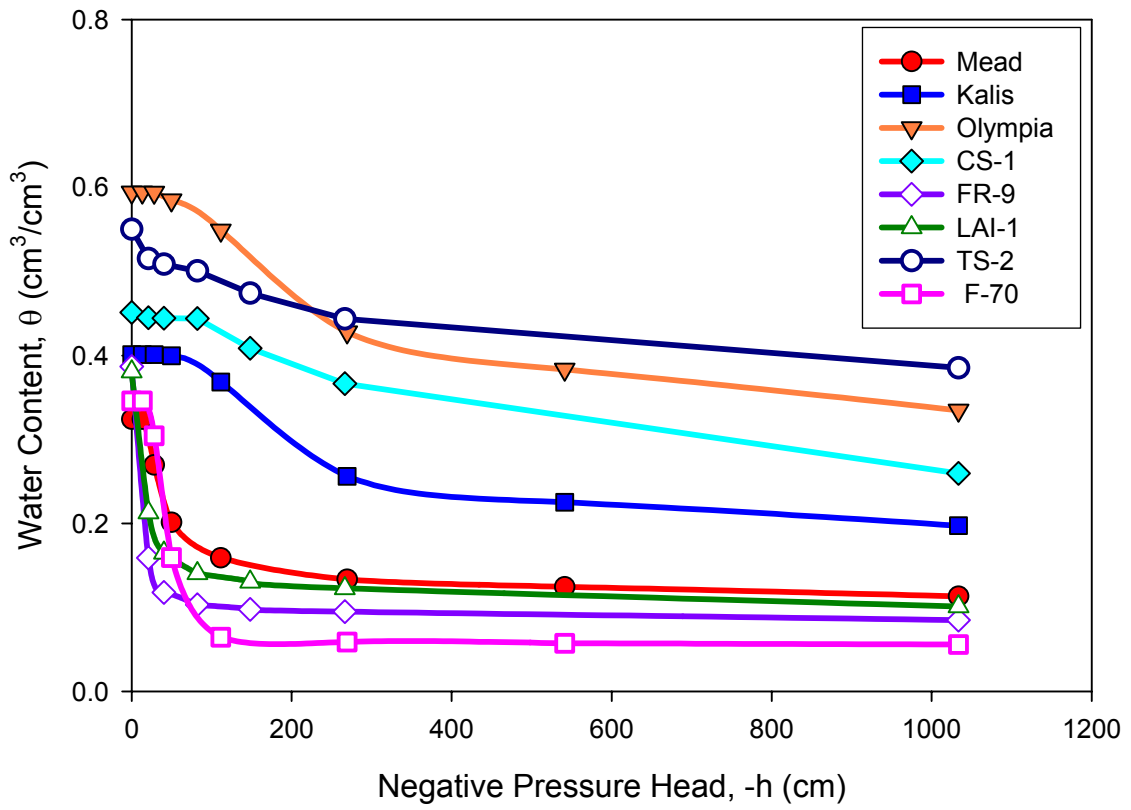


Figure 4-5. Soil water retention (release) curves of soils.

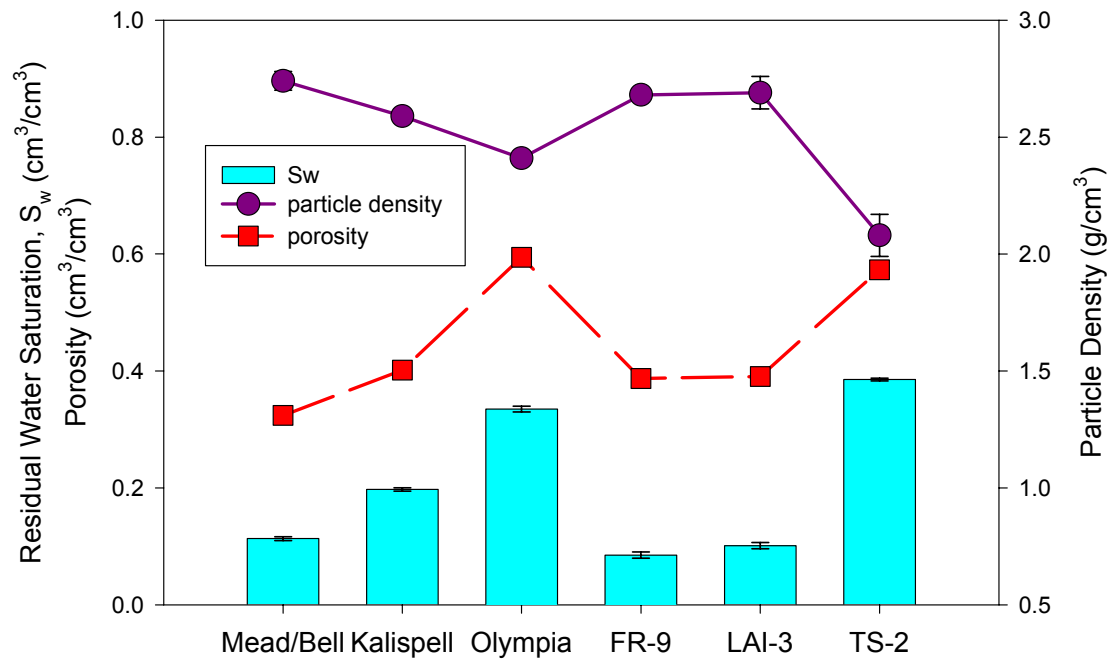


Figure 4-6. Relationship between residual water saturation and particle density and porosity in air-water-soil systems.

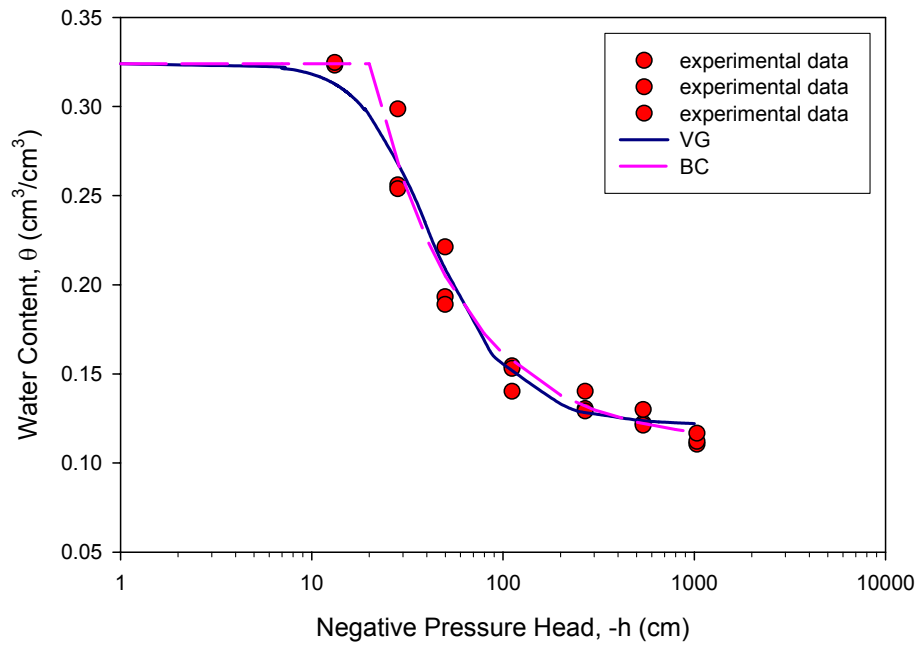


Figure 4-7. Representative van Ganuchten (VG) and Brook-Corey (BC) fitting curves for MRC (Mead/Bell).

Table 4-5. Summary of EPRI mineral oil residual saturation values in two-phase (water-oil) systems.

Soil Identifier	Bulk Density (g/cm ³)	Porosity (cm ³ /cm ³)	Water Content (θ_w) (cm ³ /cm ³)	Water Saturation (S_w) (cm ³ /cm ³)	Residual Oil Content (θ_o) (cm ³ /cm ³)	Residual Oil Saturation (S_o) (cm ³ /cm ³)	Residual Oil Conc. (mg/kg)
F-70 OS [†]	1.640 (±0.016)*	0.380 (±0.006)	0.319 (±0.015)	0.840 (±0.026)	0.061 (±0.001)	0.160 (±0.026)	36,984 (±5,169)
F-70 OS [‡]	1.656 (±0.018)*	0.375 (±0.007)	0.312 (±0.016)	0.831 (±0.028)	0.063 (±0.009)	0.169 (±0.028)	38,223 (±5,139)
Mead/Bell	1.683 (±0.016)	0.380 (±0.016)	0.325 (±0.020)	0.854 (±0.021)	0.055 (±0.006)	0.146 (±0.021)	29,086 (±3,192)
Kalispell	1.460 (±0.018)	0.448 (±0.002)	0.402 (±0.008)	0.898 (±0.018)	0.046 (±0.008)	0.102 (±0.018)	27,056 (±5,079)
Olympia	1.162 (±0.004)	0.532 (±0.012)	0.444 (±0.010)	0.835 (±0.000)	0.088 (±0.002)	0.165 (±0.000)	66,840 (±1,974)
FR-9	1.576	0.422	0.330	0.782	0.092	0.218	51,508
LAI-3	1.594 (±0.003)	0.420 (±0.13)	0.369 (±0.006)	0.879 (±0.013)	0.051 (±0.007)	0.121 (±0.013)	28,100 (±3,929)
TS-2	1.025	0.583	0.529	0.908	0.054	0.092	46,390

* standard deviation (s. d. = $\sigma/\sqrt{n-1}$)

[†] Determined by pre- and post-entrapment gravimetric method.

[‡] Determined based on analysis of pre- and post-entrapment tracer tests.

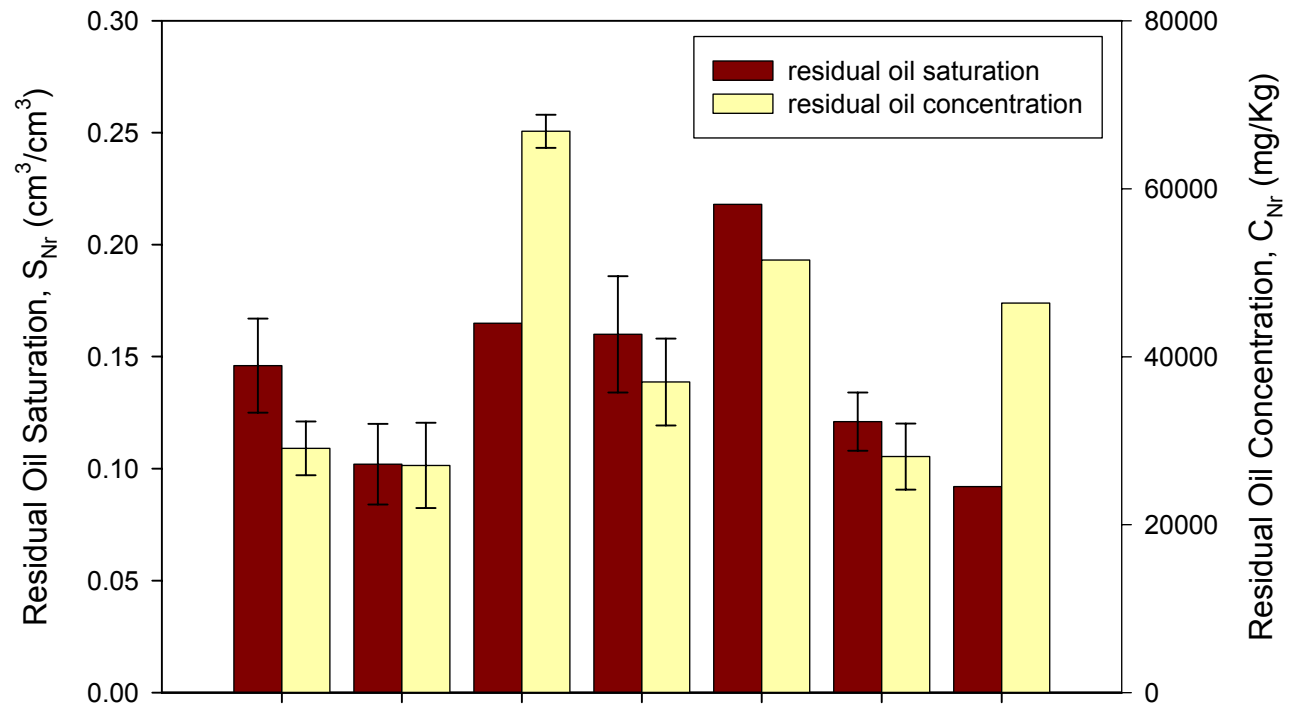


Figure 4-8. Residual mineral oil saturation in oil-water two-phase systems.

In order to seek the correlations between residual oil saturation and soil properties, both the linear (Equation 4-10) and nonlinear regression models (Equation 4-11) were evaluated for two-phase experiment data using SigmaPlot 2000 (Systat Software Inc). Parameters considered in the regressions included total carbon content (TC), characteristic particle size (d_{50} and d_{10}), particle size distribution coefficient (C_g and C_u), intrinsic permeability (k_i) and total trapping number (N_T).

$$Y = a_0 + a_1x_1 + a_2x_2 + \dots + a_nx_n \quad (4-10)$$

$$Y = a_0 + a_1x_1^{b_1}x_2^{b_2}\dots x_n^{b_n} \quad (4-11)$$

$$Y = a_0 + a_1x_1^{b_1}x_2^{b_2}\dots x_{n-2}^{b_{n-2}} + a_2x_{n-1} + a_3x_n$$

where, Y is the dependent variable, which is residual oil saturation here, a_1, a_2, \dots, a_n and b_1, b_2, \dots, b_n are coefficients, and x_1, x_2, \dots, x_n are variables, which refer to as the oil and soil properties here. The linear model has been used by Steff et al. (1999) and Chevalier and Fonte (2000) employed the nonlinear model to correlation the residual oil saturation to oil and soil properties.

The linear regressions between residual oil saturation (S_N) and individual parameters are listed in Table 4-7. The values in the Table represent the coefficients of corresponding parameters. The R^2 values ranged from approximately 0 to 0.218, which shows little correlations between the residual oil saturation and individual parameters. However, Steff et al. (1997) found a significant linear correlations between the residual pure organic saturation and oil surface tension (air-water interfacial tension) in air-organic liquid systems in synthetic polytetrafluoroethylene (PTFE) cores (data were obtained by Morrow (1976)), with R^2 value equal to 0.922. This discrepancy could attributed to the different systems in these two research efforts. Systems investigated in

this study containing complex mixture oil phase and natural soil solid are much more complicated. Therefore, the residual oil saturation should be the results of interactions of various factors. Based on this hypothesis, the correlations between the residual saturation and various parameter combinations were investigated. Selected linear and nonlinear correlations between residual oil saturation and parameter combinations are listed in Table 4-8 and 4-9. The regression results show that correlations incorporated parameters in terms of particle size or particle size distribution such as d_{50} , d_{10} , C_g , and C_u or even k_i (Case 4-7-10, 4-8-7, 4-8-8), resulted in better fit to experimental data, indicating that the particle size distribution of soils is relatively important. The quality of fit of models in Case 4-7-10 and 4-8-8 to the experimental data are shown in Figure 4-9a, b. The estimated and experimental S_N values fit very well ($R^2 = 0.918$). These results suggest that residual oil saturation in two-phase systems is primarily determined by the soil properties including total carbon content and particle size parameters. From the sign of the coefficient of each parameter, it could be qualitatively observed that higher total carbon content and smaller particle size could lead to lower the residual oil saturation. However, since too many variables are involved, these two correlations are not so meaningful in predicting the residual NAPL saturation from soil properties. This might be explained by the fact that the residual saturation data are not sufficient to achieve a statistically conclusion.

The residual oil saturation values were also expressed as solid-phase concentrations (g_{oil}/g_{soil}). The conversion from residual oil saturation to residual oil concentration was based on the following relationship:

$$C_{oil} \left(\frac{g_{oil}}{g_{soil}} \right) = S_{Nr} \left(\frac{cm^3_{oil}}{cm^3_{void}} \right) \cdot \rho_{oil} \left(\frac{g_{oil}}{cm^3_{oil}} \right) \cdot \phi \left(\frac{cm^3_{void}}{cm^3_T} \right) \cdot \rho_{soil}^{-1} \left(\frac{cm^3_T}{g_{soil}} \right) \quad (4-12)$$

Table 4-6. Linear Correlations between residual oil saturation and representative individual parameters in two-phase (water-oil) systems.

Case ID	TC (%)	d_{50} (mm)	d_{10} (mm)	C_g	C_u	k_i (cm ²)	N_T	a_0 †	R^2
4-6-1	-4.405×10^{-3} *							0.1484	0.139
4-6-24		-6.476×10^{-2}						0.1688	0.218
4-6-3			1.185×10^{-3}					0.1417	0
4-6-4				2.105×10^{-2}				0.1148	0.089
4-6-5					-5.404×10^{-3}			0.1620	0.200
4-6-6						-3.405×10^4		0.1549	0.107
4-6-7							-93.12	0.1439	0

* Values in table represent the coefficients of corresponding variables.

† a_0 is the constant term in the linear regression model

Table 4-7. Selected linear correlations between residual oil saturation and parameter combinations in two-phase (water-oil) systems.

Case ID	TC (%)	d ₅₀ (mm)	d ₁₀ (mm)	C _g	C _u	k _i (cm ²)	N _T	a ₀ [†]	R ²
4-7-1	-1.226×10 ⁻³ *	-5.504×10 ⁻²						0.1666	0.224
4-7-2	-5.334×10 ⁻³		-8.053×10 ⁻²					0.1628	0.167
4-7-3	-3.967×10 ⁻³			1.753×10 ⁻²				0.1913	0.269
4-7-4	-1.323×10 ⁻²				1.855×10 ⁻²			0.1148	0.089
4-7-5	-3.589×10 ⁻³					-2.496×10 ⁴		0.1568	0.191
4-7-6		-6.004×10 ⁻²	4.40×10 ⁻²					0.1612	0.221
4-7-7		-1.102×10 ⁻¹				3.877×10 ⁴		0.1729	0.249
4-7-8	-4.539×10 ⁻³						-3.142×10 ²	0.1556	0.148
4-7-9	3.875×10 ⁻²	-0.2964		0.209	-3.271×10 ⁻²	1.706×10 ⁵		0.2373	0.539
4-7-10	7.269×10 ⁻²	-1.528	5.125	0.1205	8.382×10 ⁻²	-1.936×10 ⁵		-0.5463	0.918

* Values in table represent the coefficients of corresponding variables.

[†] a₀ is the constant term in the linear regression model

Table 4-8. Representative nonlinear correlations between residual oil saturation and parameter combinations in two-phase(water-oil) systems.

Case ID	Correlations	R ²
4-8-1	$S_N = -4.546 \times 10^{-2} TC^{6.778 \times 10^{-4}} d_{50}^{2.501} + 0.1492$	0.258
4-8-2	$S_N = -4.546 \times 10^{-2} TC^{6.778 \times 10^{-4}} d_{50}^{2.501} + 0.1492$	0.037
4-8-3	$S_N = 2.918 \times 10^{-2} TC - 6.165 \times 10^{-2} C_g^{-0.3241} C_u^{0.7419} + 0.2502$	0.510
4-8-4	$S_N = -1.826 C_g^{-1.804 \times 10^{-2}} C_u^{1.482 \times 10^{-2}} + 1.993$	0.341
4-8-5	$S_N = 0.0537 TC - 6.082 \times 10^{-3} d_{50}^{-0.0874} C_u^{1.877} + 0.1668$	0.459
4-8-6	$S_N = 2.278 \times 10^{-3} TC - 0.1583 C_g^{-0.2394} C_u^{0.4177} - 6.186 \times 10^2 N_T + 0.3743$	0.537
4-8-7	$S_N = 0.0901 TC - 0.124 d_{50}^{0.491} C_u^{0.917} + 2.235 \times 10^5 k_i + 0.2044$	0.702
4-8-8	$S_N = 0.09995 TC - 2.026 d_{50} + 2.654 d_{10}^{0.6348} C_g^{0.0469} C_u^{0.340} - 0.3481$	0.918

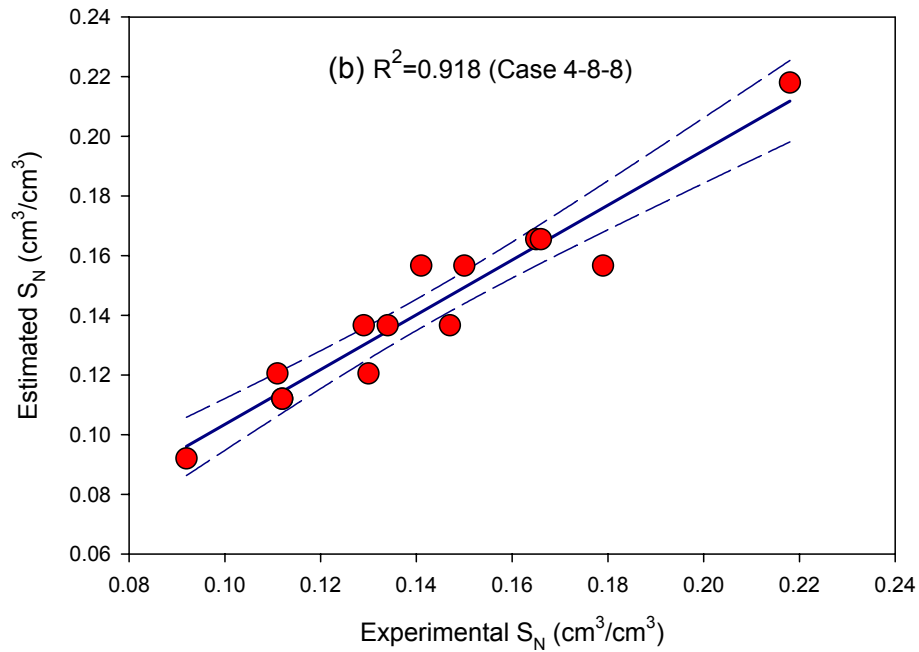
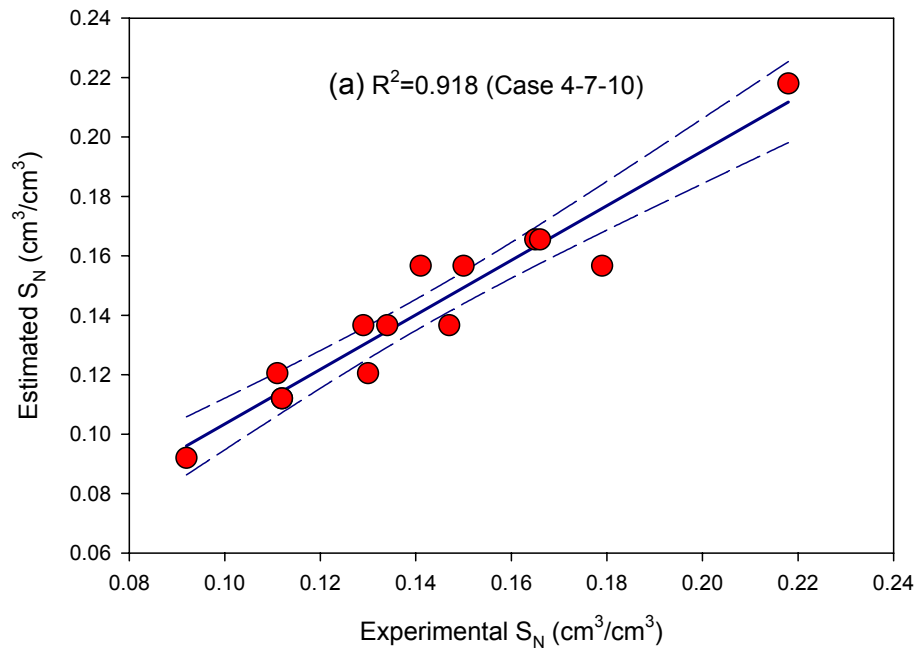


Figure 4-9. Representative correlations between residual oil saturation and soil or oil properties in two-phase (water-oil) systems (solid lines represent fit curves and dash lines represent 95% confidence level) (a) linear correlations (Case 4-7-10); (b) nonlinear correlations (Case 4-8-8).

where C_{oil} is the oil concentration, ϕ is the porosity and ρ_{soil} is the soil particle density. From the mineral oil concentration and mineral oil saturation data shown in Table 4-5, high residual oil saturations did not necessarily mean high residual oil concentrations, and low residual oil saturations were not definitely corresponding to low residual oil concentrations. For example, sample TS-2, which had the highest porosity ($0.53 \text{ cm}^3/\text{cm}^3$) and lowest bulk density ($1.025 \text{ g}/\text{cm}^3$) (Table 4-5), yielded a relatively high residual oil concentration ($46,390 \text{ mg}/\text{kg}$) despite its very low residual oil saturation ($0.054 \text{ cm}^3/\text{cm}^3$). This could be attributed to the relatively high total pore volume (55.1 cm^3) compared to other soils tested. These results demonstrate the importance of considering both the oil concentration as well as the residual oil saturation when developing regulatory guidelines for mineral oil contaminated sites.

Residual Mineral Oil Saturation in Three-Phase (Air-Oil-Water) Systems

Both EPRI and “New” Franklin mineral oil was used in the air-oil-water three-phase experiments. Figure 4-10 shows the capillary pressure-oil saturation curves for these two mineral oils in Mead/Bell, Kalispell, Olympia soils at negative pressures ranging from 0 to -250 cm. The initial oil saturations of these three soils were much lower than that of the reference F-70 Ottawa sand, i.e, the residual water saturation at the end of the water drainage of these three soils were much higher than that of the F-70. The residual oil saturations obtained for the all the soils ranged from $0.045 \text{ cm}^3/\text{cm}^3$ for EPRI mineral oil in TS-2 to $0.216 \text{ cm}^3/\text{cm}^3$ for EPRI mineral oil in Kalispell (Figure 4-11a, b and Table 4-9, 10). In general, the observed saturations values are consistent with data reported by Wilkins et al. (1995), for which residual water and NAPL saturations in

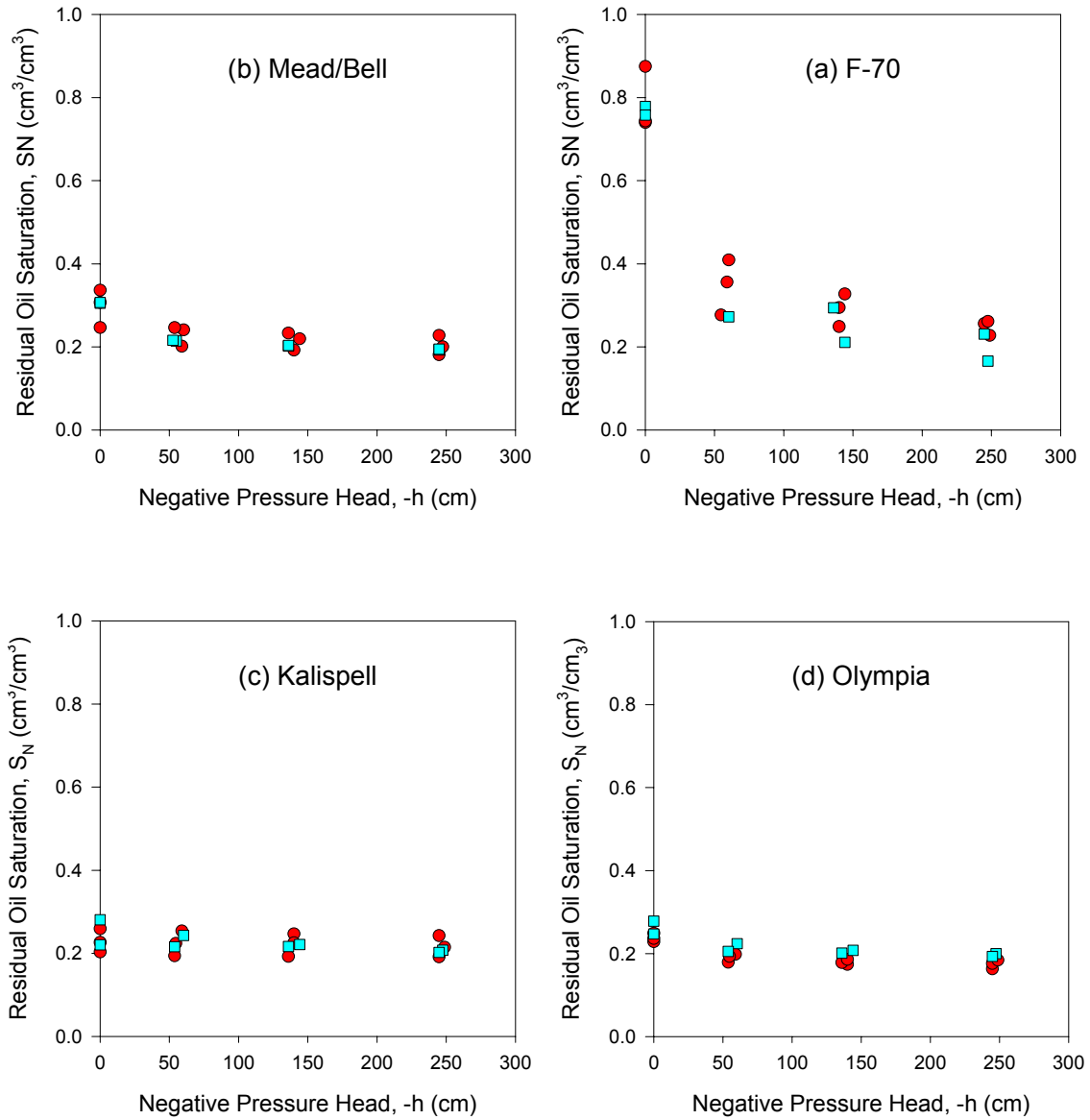


Figure 4-10. Mineral oil saturation during the oil-drainage process in three-phase (air-oil-water) systems (dots represent EPR data, and Squares represent Franklin (New) data).

three-phase systems ranged from 8 to 16% and 4 to 10%, respectively, in coarse to fine grained sands. However, most three-phase saturation measurements reported in the literature have focused on coarse textured soils and aquifer materials containing little, if any, organic carbon.

Both linear and nonlinear correlations between residual oil saturation (S_N) and soil and mineral oil properties were investigated in three-phase systems using SigmaPlot 2000 (Systat Software Inc.), as described in the two-phase experiment section (Equation 4-10, 11). First, correlations between residual mineral oil saturation and individual property parameters were developed. Compared to two-phase systems, the antecedent water saturation, S_{wi} , (the water saturation prior to the oil injection) was considered as a variable besides other representative oil and soil properties based on the fact that antecedent water saturation was reported to be a significant factor influencing the residual non-wetting phase saturation (Steffy et al., 1997; van Geel and Sykes, 1997; van Geel and Roy, 2002). Table 4-11 shows that TC , d_{50} and C_u had relatively higher R^2 values compared to the other parameters (0.580, 0.693 and 0.615, respectively), and R^2 value for S_{wi} was medium high, which implicates that these four parameters (S_{wi} , TC , d_{50} and C_u) should have relatively strong correlations with residual oil saturation. Mineral oil properties or related parameters such as viscosity and total trapping number exhibited no significant effect. Analysis of variance (ANOVA) result found no significant difference between the residual EPRI oil saturation and residual Franklin oil saturation at a significant level of 0.05 with a P value of 0.399 (Minitab, 2004). Hence, the following linear and nonlinear parameter combination analysis was mainly concentrated on S_{wi} , TC , d_{50} and C_u . Selected linear and nonlinear correlations between residual saturation and parameter combinations

are shown in Tables 4-12 and 4-13. The correlations were found to be improved compared to the correlations with individual parameters. Correlations including d_{50} and/or C_u (4-12-2, 3, 4, 5, 6, 7 and 4-13-2, 3, 4, 5) exhibited stronger correlations than that not including d_{50} and C_u (4-12-1 and 4-13-1), indicating particle size and particle size distribution played a significant role in controlling the mineral oil entrapment in soils. From the linear correlations, the coefficients of d_{50} and C_u were negative, which implicated that the larger soil particle size and less uniform particle size distribution resulted in lower residual oil saturation. Similarly, the negative coefficient of S_{wi} , indicating the higher antecedent water content (lower initial oil content), generally caused lower residual saturation. Coefficient of TC showed both negative and positive signs. In Case 4-5, 6, 7, which exhibited strong correlations, TC had positive coefficient, that means, the higher the total carbon content, the more NAPL entrapped. This result is in agreement with common knowledge that organic carbon in soil tends to “accommodate” the NAPLs. Strong correlations were observed in Case 4-12-7 and 4-13-5, which had a R^2 value of approximately 0.90 (Figure 4-12a, b). These results reveal that the residual mineral oil saturations are controlled by the total carbon content (TC), particle size (d_{50}) or particle size uniform degree (C_u) and antecedent water content (S_{wi}).

Comparison between the residual mineral oil saturation data in three-phase and two-phase systems by ANOVA reveals that there is no significant difference between these two groups of data at a significant level of 0.05 ($P = 0.012$). This observation conflicts with the literature (Mercer and Cohen, 1990), which may be attributed to the method used to measure the residual oil saturation (Davis, 1994; Adamski et al., 2003).

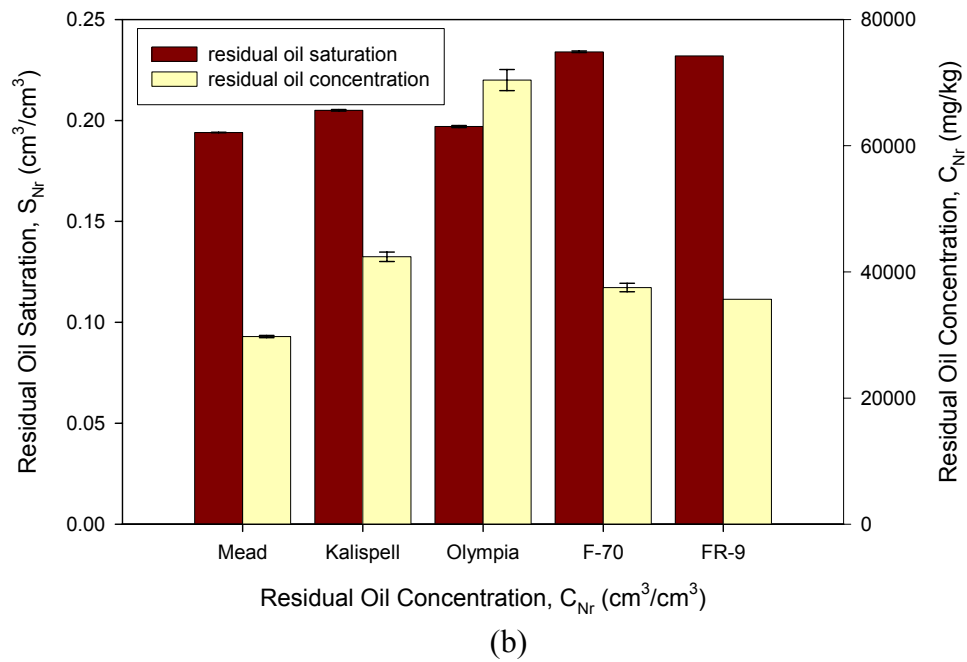
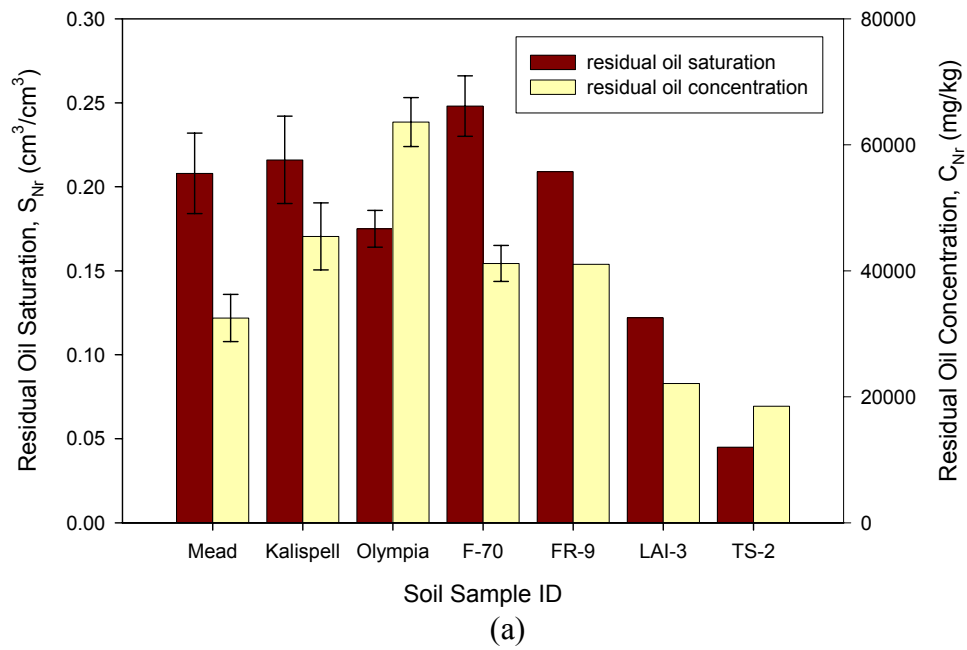


Figure 4-11. Residual mineral oil saturation in three-phase (air-oil-water) systems (a) EPRi mineral oil; (b) Franklin mineral oil.

Table 4-9. Summary of EPRI mineral oil residual saturation values in three-phase (air-water-oil) systems.

Soil Identifier	Bulk Density (g/cm ³)	Porosity (cm ³ /cm ³)	Residual Water Content (θ_w) (cm ³ /cm ³)	Residual Water Saturation (S_w) (cm ³ /cm ³)	Residual Oil Content (θ_o) (cm ³ /cm ³)	Residual Oil Saturation (S_o) (cm ³ /cm ³)	Residual Oil Conc. (mg/kg)
F-70 OS	1.769 (±0.008)*	0.332 (±0.003)	0.056 (±0.007)	0.170 (±0.020)	0.082 (±0.006)	0.248 (±0.018)	41,146 (±2,856)
Mead/Bell	1.845 (±0.000)	0.327 (±0.000)	0.137 (±0.002)	0.418 (±0.005)	0.068 (±0.008)	0.208 (±0.024)	32,502 (±3,743)
Kalispell	1.601 (±0.000)	0.382 (±0.000)	0.221 (±0.017)	0.580 (±0.045)	0.082 (±0.010)	0.216 (±0.026)	45,443 (±5,326)
Olympia	1.208 (±0.000)	0.499 (±0.000)	0.331 (±0.006)	0.663 (±0.013)	0.087 (±0.005)	0.175(±0.011)	63,592 (±3,883)
FR-9	1.667	0.371	0.068	0.183	0.077	0.209	41,024
LAI-3	1.736	0.357	0.089	0.249	0.043	0.122	22,096
TS-2	1.089	0.503	0.435	0.865	0.023	0.045	18,505

* standard deviation (s. d. = $\sigma/\sqrt{n-1}$)

Table 4-10. Summary of Franklin mineral oil residual saturation values in three-phase (air-water-oil) systems.

Soil Identifier	Bulk Density (g/cm ³)	Porosity (cm ³ /cm ³)	Residual Water Content (θ_w) (cm ³ /cm ³)	Residual Water Saturation (S_w) (cm ³ /cm ³)	Residual Oil Content (θ_o) (cm ³ /cm ³)	Residual Oil Saturation (S_o) (cm ³ /cm ³)	Residual Oil Conc. (mg/kg)
F-70 OS	1.779 (± 0.000)*	0.329 (± 0.000)	0.052 (± 0.003)	0.159 (± 0.009)	0.077 (± 0.001)	0.234 (± 0.004)	37,508 (± 677)
Mead/Bell	1.845 (± 0.000)	0.327 (± 0.000)	0.129 (± 0.004)	0.396 (± 0.013)	0.063 (± 0.000)	0.194 (± 0.001)	29,747 (± 171)
Kalispell	1.601 (± 0.000)	0.382 (± 0.000)	0.206 (± 0.001)	0.539 (± 0.004)	0.078 (± 0.001)	0.205 (± 0.004)	42,392 (± 757)
Olympia	1.209 (± 0.000)	0.499 (± 0.000)	0.289 (± 0.015)	0.579 (± 0.031)	0.098 (± 0.002)	0.197 (± 0.005)	70,391 ($\pm 1,678$)
FR-9	1.845	0.327	0.063	0.194	0.076	0.232	35,649

* standard deviation (s. d. = $\sigma/\sqrt{n-1}$)

Table 4-11. Linear Correlations between residual oil saturation and representative individual parameters in there-phase (air-water-oil) systems.

Case ID	S_{wi} (cm ³ /cm ³)	TC (%)	d_{50} (mm)	d_{10} (mm)	C_g	C_u	Viscosity (cP)	k_i (cm ²)	a_0 †	R^2
4-11-1	-0.1318 *								0.2565	0.373
4-11-2		-1.579×10^{-2}							0.2250	0.580
4-11-3			-0.2022						0.2695	0.693
4-11-4				5.493×10^{-2}					0.192	0.008
4-11-5					1.29×10^{-2}				0.1816	0.018
4-11-6						-1.554×10^{-2}			0.2568	0.615
4-11-7							-4.389×10^{-3}		0.2685	0.032
4-11-8								-2.149×10^{-5}	0.2333	0.296

* Values in table represent the coefficients of corresponding variables.

† a_0 is the constant term in the linear regression model

Table 4-12. Selected linear correlations between residual oil saturation and parameter combinations in there-phase (air-water-oil) systems.

Case ID	S_{wi} (cm ³ /cm ³)	TC (%)	d_{50} (mm)	C_u	a_0 †	R^2
4-12-1	-0.02392	-0.0141			0.2304	0.585
4-12-2	-0.2438			-3.349×10^{-2}	0.3309	0.788
4-12-3		-7.619×10^{-3}	-0.1421		0.2597	0.767
4-12-4			-0.1381	-8.955×10^{-3}	0.2802	0.828
4-12-5	-0.1111 *	3.269×10^{-3}	-0.1949		0.3101	0.863
4-12-6		0.02451	-0.1855	-2.932×10^{-2}	0.3360	0.896
4-12-7	-0.03512	0.0215	-0.1933	-0.02343	0.3366	0.900

* Values in table represent the coefficients of corresponding variables.

† a_0 is the constant term in the linear regression model

Table 4-13. Representative nonlinear correlations between residual oil saturation and parameter combinations in three-phase (air-water-oil) systems.

Case ID	Correlations	R ²
4-13-1	$S_N = -0.2382S_{wi}^{4.907}TC^{0.1507} + 0.2169$	0.613
4-13-2	$S_N = -1583d_{50}^{1.111}TC^{0.06237} + 0.2422$	0.797
4-13-3	$S_N = -1.12d_{50}^{0.0657}C_u^{0.04198} + 1.291$	0.875
4-13-4	$S_N = -0.04822TC^{1.529 \times 10^{-4}}d_{50}^{0.7617}C_u^{0.5305} + 0.2362$	0.818
4-13-5	$S_N = -0.0281S_{wi} + 0.0209TC - 0.1651d_{50}^{0.3726}C_u^{0.4545} + 0.3739$	0.901

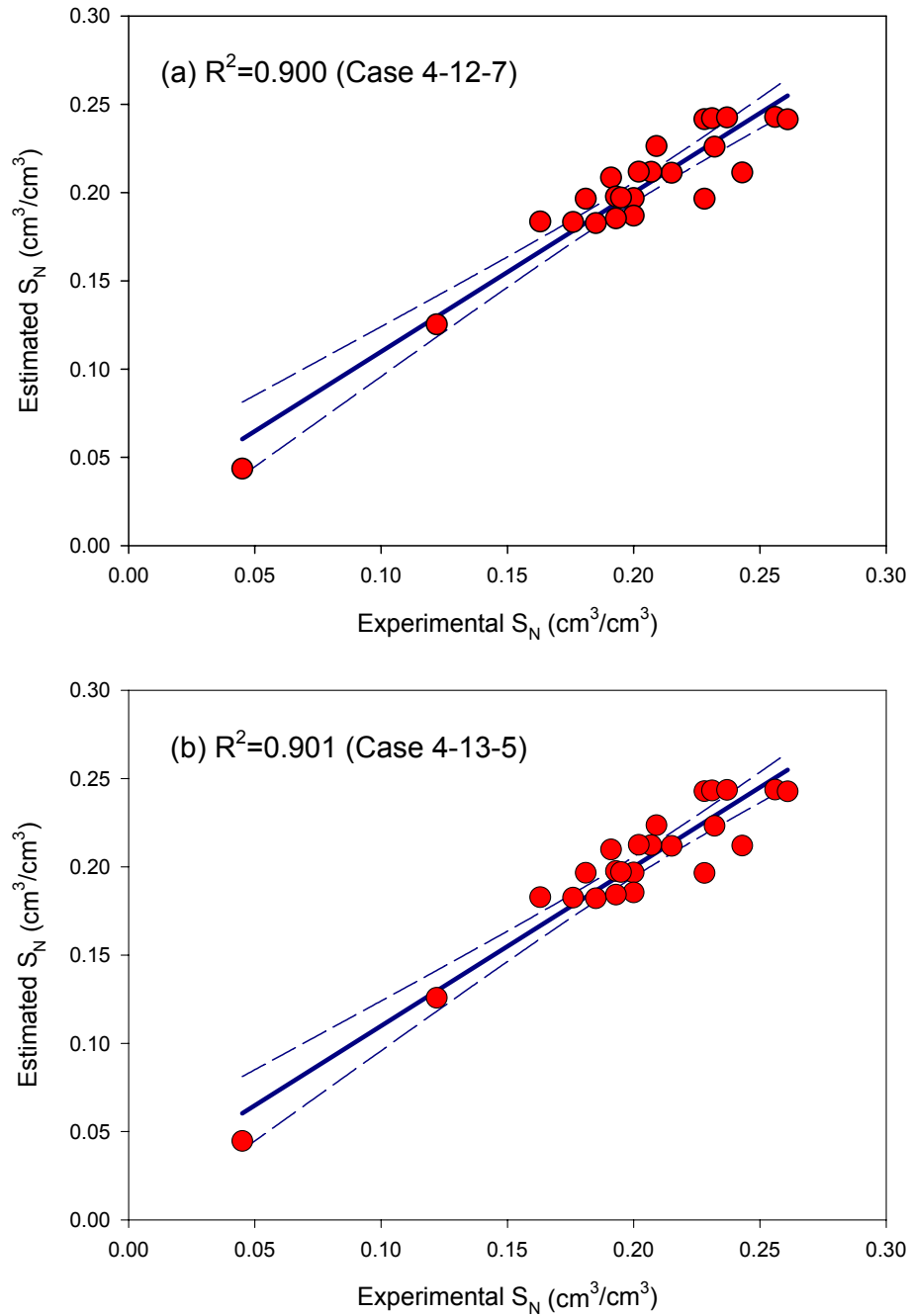


Figure 4-12. Representative correlations between residual mineral oil saturation and oil/soil properties in there-phase (air-water-oil) systems (solid lines represent fit curves and dash lines represent 95% confidence level) (a) linear correlations (Case 4-12-7); (b) nonlinear correlations (Case 4-13-5).

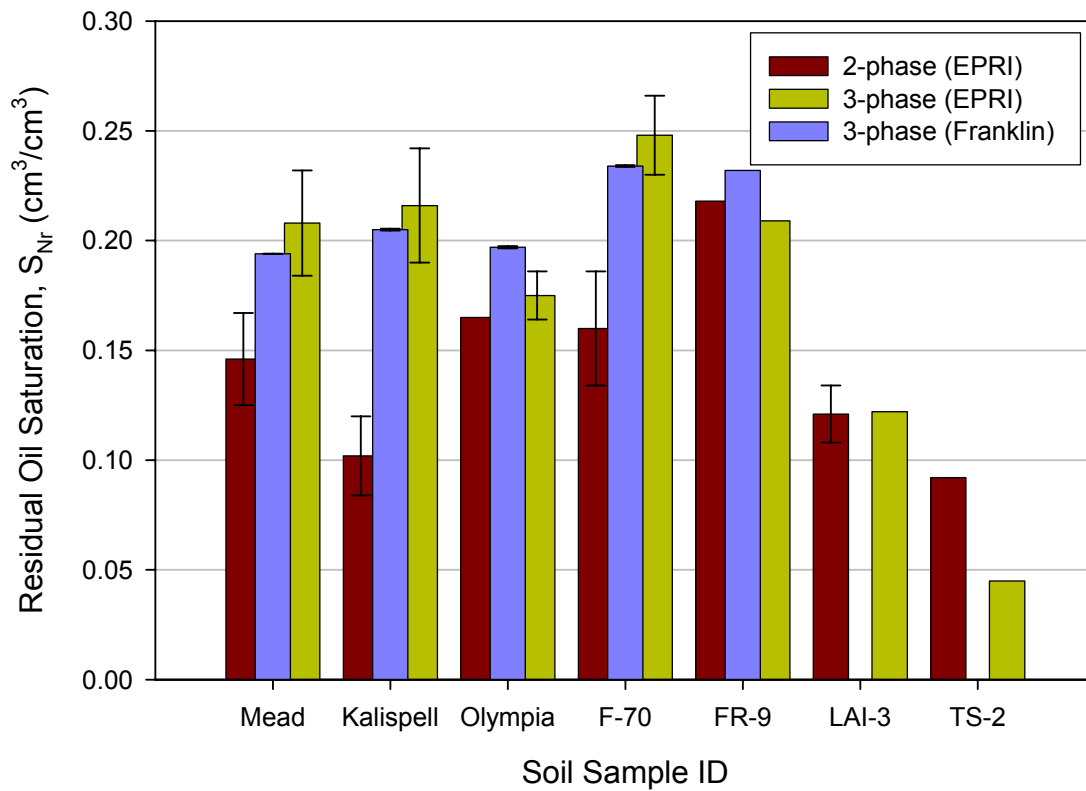


Figure 4-13. Residual mineral oil saturation in both two- and three-phase systems.

Summary and Conclusions

Mineral oils are slightly viscous light nonaqueous liquids (LNAPLs). The densities of mineral oils were very similar, ranging from 0.868 to 0.883 g/cm³, while the viscosity ranged from 13.34 to 18.72 centipoise (cP) at 22°C. The measured Franklin mineral oil-water interfacial tensions ranged from 23.8 to 36.1 dyens/cm, which are lower than those of the commonly pure NAPL such as PCE and TCE (35 to 50 dynes/cm). This result could be attributed to the existence of impurities. However, EPRI oil-water IFT was over 40 dynes/cm, which is a little higher than the value of typical commercial mineral oils. This result suggests that EPRI mineral oil may be highly refined.

The seven soil samples are mainly composed of particles ranging from 0.05 to 2 mm (sand fraction), and CS-1, LAI-3 and TS-2 contained relatively high gravel fraction (> 2 mm), which was 42.75, 28.03% and 29.10%. TS-2 soil has the lowest particle density (2.08 g/cm³), which can result in high porosity. TS-2 also bears a high total carbon content (10.59%).

The residual mineral oil saturations were in the range of 5% to 25%, which were consistent with the data in the literature of residual oil saturation. Statistic analysis to experimental data reveals relatively strong correlations between residual oil saturation and soil properties, especially in three-phase systems. In the systems evaluated herein, residual oil saturationa were not determined by a specific parameter, but the combinations of parameters, which indicates that the soil and/or mineral oil properties contribute to the mineral oil residual saturation together. In general, total organic carbon, soil particle size and particle size distribution play significant role. In three-phase

systems, except for the total carbon and particle sized contribution, the effect of antecedent water saturation (or the initial oil saturation) should not be neglected.

Overall, this study provided more extensive data on the oil/soil property quantification and residual oil saturation evaluation, which provides valuable information in LNAPL contaminant sites characterization and assessment. The preliminary correlations between residual oil saturation and oil/soil properties can serve as useful tools in predicting the NAPL residual saturation from measurable soil and/or NAPL properties.

CHAPTER V

EVALUATION OF COAL TAR RESIDUAL SATURATION IN POROUS MEDIA

Introduction

Coal tars are viscous liquids (or semi-solid) with densities slightly greater than that of water. They are usually a black to dark brown in color with a naphthalene-like odor. There are various types of coal tars, the density, viscosity and chemical composition of which depend on their origin and extent of weathering (Table 5-1). Coal tars are complex mixtures of hundreds to thousands of different chemicals. Most of the identified organics are polycyclic aromatic hydrocarbons (PAHs), including acenaphthene, anthracene, fluorine, fluoranthene, naphthalene, phenanthrene and pyrene, which account up to 64% of coal tar (McGowan et al., 1996) (Table 5-2.). Other chemical constituents include aromatic volatile organic compounds (VOCs), phenols, heterocyclic oxygen, sulfur and nitrogen compounds, present primarily in asphaltenes. Lee et al. (1992b) investigated the partitioning properties of eight coal tars from META Environmental Inc. The observed constituent concentrations may vary significantly from one MGP site to another, Table 5-3 shows the concentrations of the primary constituents in coal tar (Mahjoub et al., 2000). Most of these organics, particularly PAHs, are potential carcinogens. Therefore, the presence of coal tar, as a dense nonaqueous phase liquid (DNAPL) in the subsurface at former manufactured gas plant (MGP) sites, is not

only a subject of interest to both regulators and the regulated companies, but also a serious concern to public health.

Coal tar NAPLs can exist as a “free product” or as a “residual product” in the subsurface. Cohen and Mercer (1990) used the terminology “mobile NAPL”, which corresponds to the regulatory term “free product”. Cohen and Mercer (1990) also define mobile NAPL as the amount of NAPL that is above “residual saturation” and is able to flow in a porous media. They further defined residual saturation in a porous medium below the water table (i.e., in a two liquid-phase system consisting of water and NAPL) as the amount of NAPL that is immobile, and is trapped by capillary forces as discontinuous ganglia under ambient groundwater flow conditions. Similarly, residual product is defined as separate phase material present in amounts (e.g., concentration or saturation) below its residual saturation point in a porous medium. These definitions present challenges for the field personnel who must quickly, consistently, and accurately observe and record the presence of “free product” or “residual product”, or absence of NAPL in their site investigation efforts.

Physical-chemical properties of NAPL and porous media govern the movement and entrapment of NAPLs, and therefore determine the amount of NAPL that constitutes “residual saturation”. Gravity, capillary pressure and hydrodynamic forces, as well as NAPL density and viscosity, collectively influence NAPL migration and retention characteristics in porous media. Although several constitutive relationships have also been provided to describe the entrapment and residual saturation of NAPLs in two- and three-phase systems (Wipfler and van der Zee, 2001; van Geel and Roy, 2002), more direct correlations to predict the residual NAPL saturation from NAPL and soil properties

are required, especially from environmental remediation perspective. Zytner et al. (1993) measured the retention of PCE, TCE and gasoline in different soils and observed that the “retention capacity” increased with an increase in NAPL density, soil porosity and a decrease in soil bulk density. A few empirical correlations have been developed to relate the residual oil saturation to representative soil and water properties. Steff et al. (1997) obtained strong linear correlations between residual oil saturation and surface tension and the inverse of Bond number in organic-air systems base on literature data (Morrow, 1976). In Morrow’s systems (1976), simple pure organics (n-pentane, n-heptane, n-octane, n-decane, n-dodecane, n-tetradecane and dioctyl ether) were used as the oil phase and synthetic polytetrafluoroethylene (PTFE) was the solid phase. Chevalier and Fonte (2000) developed several correlations between residual saturation of Soltrol, which is a mixture of saturated hydrocarbons, in silica sands with capillary and gravitational forces, and grain size parameters. However, all these correlation models are focused on pure organics or low viscosity mixtures and “ideal” solid phase (uniform particle size distribution, no organic carbon).

There are very limited data available for the residual saturation of high viscous NAPL such as coal tar in porous media. The available residual saturation data for coal tars and other relevant NAPLs were summarized in Table 2-3. From these data, it is clear that oil, petroleum products and chlorinated solvents have been examined in detail, resulting in the reporting of residual saturation values for different soils and soil types. These data suggest that NAPL residual saturation increases as the permeability or median grain size of the soil decreases. Only a few residual saturation studies are reported for coal tar in unconsolidated porous media (Table 2-3), with values ranging from 0.29 to

Table 5-1. Reported physical properties of coal tars.

MGP Site	Density (g/cm ³)	Viscosity (cP)	References
Stroudsburg, PA	1.017 (15.5°C)	19.0 (7°C)	Villaume, 1985
META	1.06-1.43 (24°C)	34-6600 (40°C)	Lee et al., 1992
Stroudsburg, PA	0.994 (30°C)	9.94 cSt (30°C)	Nelson et al., 1996
Baltimore, MD	1.045 (25°C)	9.5 cSt (37°C)	Barranco and Dawson, 1999
NY New York (construction site)	1.084 (25°C)	NA	Zheng and Powers, 1999
New York	1.043 (25°C)	NA	Zheng and Powers, 1999
France	1.3	NA	Mahjoub et al., 2000
Pennsylvania	1.051 (25°C)	19.4 (25°C)	Hugaboom and Powers, 2002

Table 5-2. Representative organic concentration in coal tar (Lee et al., 1992).

Organic compounds	Range (mg/kg)
Monocyclic	13-25,300
Polycyclic	
2 and 3 rings	6,800-218,000
3 rings	12,000-110,000
Nitrogen PAHs	70-1,000
Sulfur PAHs	0-4,000

Table 5-3. Example of major organic constituents of the coal tar (Mahjoub et al., 2000).

Compounds	Concentration (mg/kg)
PAH	
Naphthalene	17,000
Acenaphtylene	1,200
Acenaphtene	720
Fluorene	4,900
Phenanthrene	14,000
Anthracene	5,700
Pluoranthrene	8,700
Pyrene	6,100
Benzo(a)anthracene	3,600
Chrysene	3,300
BTEX	
Benzene	920
Toluene	1,200
Ethyle-benzene	47
Xylene	1,700
Phenols	
Phenol	1,300
Cresols	1,800
2,4-Dimethylphenol	420

0.77 (Barranco et al., 1997; Hugaboom and Powers, 2002). Compared to the coal tar found in most MGP sites, the tar investigated in these two studies had relatively low viscosities, slightly higher than 10 cP. In addition, the solid phase consisted of clean coarse quartz sands. No residual coal tar saturation data are available for natural field soils.

The overall objective of this study is to quantify properties of nine soil samples and six coal tar samples from former MGP sites, and evaluate the residual coal tar saturation in field soil samples in two-phase (water-tar) systems. Soil properties characterized include particle density, particle size distribution, total carbon, specific surface area, cationic exchange capacity, and capillary pressure-saturation relationship. Tar properties quantified include tar density, viscosity, surface tension and tar-water interfacial tension. Correlations between the residual saturation and representative properties of coal tar and soil samples will be developed and evaluated.

Materials and Methods

Materials

Coal tar samples were received from ten MGP sites, identified by locations as Albany, Auburn, Cape May, Charleston, Fairfield, Saranac, Shippensburg, Waterbury and Winsted. Of these thirteen coal tar samples, tars from three of the MGP sites (Albany, Waterbury and Winsted) were solids. Two samples were obtained from Auburn, Cape May and Charleston. For these cases, only the second samples were analyzed. Tar samples were received in metal jars or glass jars. Prior to use, the coal tar samples that contained a separate water phase were centrifuged at 1300 rpm for 15 minutes and the

standing water was removed with a disposable glass pipet. Volatile and semi-volatile organics in Auburn, Cape May, Charleston, Fairfield, Saranac and Shippensburg coal tars were analyzed by META Environmental Inc, and the analytical results are listed in Appendix A-F.

Paired soil samples were received from nine different MGP sites (Albany, Auburn, Cape May, Charleston, Fairfield, Saranac, Shippensburg, Waterbury and Winsted). The soils were pretreated as described in Chapter IV, and stored in glass wide mouth jars and labeled for future use. The quantities of coal tar and soil received from each site are summarized in Table 5-4.

Reagents, including ammonium chloride (NH_4Cl), potassium chloride (KCl), potassium iodide (KI) and calcium chloride (CaCl_2), were obtained from Fisher Scientific Company (Pittsburg, PA), and used as received. All aqueous solutions used in tar-water two-phase column experiments were prepared with degassed Nanopure DI water (Barnsted, Berkeley Springs, WV) as described in the Materials section in Chapter IV. 0.045 M (500 mg/L) CaCl_2 solution was used as the background solution, and 0.01 M KI solution was used as the non-reactive tracer solution.

Methods

Particle Size Analysis:

Each soil sample was performed particle size analysis using sieves analysis (Gee and Bauder, 1986) as described in the Methods section in Chapter IV. Soil particles retained on the No. 5 sieve (> 4 mm) was discarded, and soils through the No. 5 sieve were stored in glass jars for later use.

Particle Density

Soil particle densities were measured by the pycnometer method (Blake and Hartge, 1986) as described in Chapter IV. Density measurement for each soil sample was run in triplicate.

Total Carbon:

Total carbon (TC) content was determined using the Shimadzu Model 500 Total Organic Carbon (TOC) Analyzer following the procedure described in Chapter IV. Soil samples for TC analysis were sieved through No. 20 sieve. TC analysis for each soil sample was performed in duplicate.

Specific Surface Area:

Specific surface area (SSA) measurements were performed using the ASAP 2010 surface area analyzer (Micromeritics, Norcross, GA), as described in Chapter IV. Soil samples for SSA analysis were sieved through No. 20 sieve. Each soil sample was measured for SSA in duplicate.

Cation Exchange Capacity:

Cation exchange capacity (CEC) of each soil sample was measured using a procedure described by Pennell et al. (1991). An Inductively Coupled Argon Plasma (ICAP) Tracer Analyzer (Thermo Jarrell Ash Co.) was used to analyze the concentration of Calcium (Ca), Magnesium (Mg), Sodium (Na), Aluminum (Al) and Potassium (K). Approximately 1 g air-dried soil was weighed (Mettler-Toledo, AG245

analytical balance) and placed in a 50 mL polyethylene centrifuge tube containing approximately 20 mL 1 M NH₄Cl solution. The soil and NH₄Cl solution were mixed with a high-speed touch mixer (Fisher, Model 232) for about 2 minutes. The supernatant was transferred to another centrifuge tube. The above procedure was repeated twice to the precipitates to completely extract the cationic ions (Ca, Mg, Na, Al, K) in soil. Approximately 50 mL supernatant was collected in a polyethylene centrifuge tube and filtered through a 0.2 µm pore size filter. One drop concentrated HNO₃ was added to the filtered solution and mixed completely. Reference solutions with a concentration of 1000 µg/mL (ppm) (High Purity Standards Inc.) of Ca, Mg, Na, Al, K were diluted to produce a mixed standard solution series (0, 10, 100, and 500 ppm). The concentration for each cationic ion was analyzed at the characteristic wavelength of each ion. Each soil sample was extracted in duplicate for cation detections.

Moisture Release Curve:

Water saturation-capillary pressure relationship in the air-water system of each soil sample was determined using a Tempe cell system (Soil Moisture Equipment Corp., Santa Barbara, CA) as described by Klute (1986). The detailed protocol was described in the Method section in Chapter IV. F-70 Ottawa sand was used as the reference soil and each soil sample was measured in duplicate.

Table 5-4. Amounts of soil and coal tar samples received from participating utilities.

Coal Tar Identifier	Utility Name	Coal Tar	Soil
Albany	NIMO	3.78 L (1 gal.)*	3.78 L (1 gal.)
Auburn (I)	NISOURCE	4 X 0.94 L (1 qt.) [†]	2 L
Auburn (II)	NISOURCE	1 L	-----
Cape May	First Energy	4 X 0.5 L	5 X 1L
Charleston (I)	SCE&G	8 X 0.24 L (8 oz.) [†]	8 X 0.24 L (8 oz.)
Charleston (II)	SCE&G	1 L	-----
Fairfield	Allient Energy	3.78 L (1 gal.)	4 X 1 L
Portland	NI Source	3.78 L (1 gal.)	-----
Saranac	NYSEG	16 X 0.24 L (8 oz.)	2 L
Shippensburg	PP&L	8 X 0.24 L (8 oz.)	0.94 L (1 qt.)
Waterbury	NE Utilities	3.78 L (1 gal.)*	2 X 0.94 L (1 qt.)
Winsted	NE Utilities	3.78 L (1 gal.)*	2 X 1 L

* Albany, Waterbury and Winsted coal tar contained large fraction of solids; soils were run with Shippensburg coal tar.

[†] Auburn I and Charleston I coal tar samples were very viscous, replaced with a second sample.

Tar Density:

The density of each coal tar sample was determined by using 25 mL wide mouth cylindrical pycnometers (Fisher Scientific, Pittsburg, PA). The measurement protocol is the same as that of mineral oil measurements, as described in Chapter IV.

Viscosity:

Coal tar viscosity was determined using a rheometer (Rheostress, Model RS75, Haake, Paramus, NJ) equipped with a double gap cylinder sensor (Model DG 41). The temperature was maintained at 22°C using a recirculating water bath (Model C25, Haake, Paramus, NJ). Viscosities were measured at shear rates ranging from 0.8 to 1000 s⁻¹. Viscosity measurements at each shear rate were within 10% of the mean, consistent with a Newtonian liquid as described in ASTM method D5018-89 (1999). Therefore, viscosities of six coal tar samples at a shear rate of 200 s⁻¹ were measured in duplicate.

Surface Tension:

The surface tension (ST) of coal tar was determined by the du Nouy ring method, as described in the Methods section in Chapter IV. Nanopure DI water was used as the reference liquid to calibrate the instrument. Each coal tar sample was measured in duplicate.

Interfacial Tension:

The interfacial tension (IFT) between coal tar and water was determined using the drop volume method (Hool et al., 1992). The general protocol was similar, as described

in Methods section in Chapter IV, although the experiment set up was different. Since coal tar is heavier than water, the experiment could be set up by injecting water into coal tar using an up-flow mode. Since coal tar is a dark, the water drops could not be observed within the coal tar phase. Therefore, coal tar was injected in a down-flow mode with the tip immersed in water contained in a 100 mL glass beaker. The time required for 5 drops to form and detach from the end of the tip immersed in the Nanopure DI water solution was recorded. A total of 30 drops were counted during each measurement. The instrument was calibrated by measuring the DI water surface tension and dodecane-water interfacial tension.

Two-Phase (Water-Tar) Residual Saturation Experiments

Two-phase column experiments were conducted to measure the residual saturation of coal tar in soils. Both Kontes borosilicate glass columns and stainless steel columns were used. The glass column has the advantage of providing visual observation of the imbibition processes, but may leak when used with high viscosity fluids. Although one cannot see inside the stainless steel column, it provides a strong seal and is suitable for experiments conducted at high temperature and high pressure (Figure 5-1).

The experiment protocol for two-phase (water-tar) residual saturation was similar to that described in two-phase (water-mineral oil) residual saturation experiments in Chapter IV. Since coal tars have densities greater than that of water, the coal tar was injected into the bottom of the column in an up-flow mode until coal tar was observed at the top outlet of the column. The column was then rotated 180° and another 20 mL coal tar was injected into the bottom of the column. Due to the high viscosity, the coal tars



(a) Kontes glass column



(b) Stainless steel column

Figure 5-1. Glass (Teflon endplates) and aluminum (stainless steel endplates) columns used to measure coal tar residual saturation.

were injected at a low flow rate (20 mL/hr). During the water flushing process, coal tar saturated columns were flooded in a down-flow mode at a flow rate was 8 mL/min to prevent the buoyancy effect, Then, the column was rotated 180° and flushed with water in a down-flow mode. This process was repeated several times until no free coal tar was observed in the effluent. Approximately 40 pore volumes of water were flooded through each column during the water flood process.

All of the two-phase (water-tar) residual saturation experiments were conducted at room temperature ($22 \pm 1^\circ\text{C}$) except for Charleston soil/tar paired samples. Each column containing Charleston tar was heated to 40°C by wrapping the column with a heating tape connected with a custom manufactured feedback heat controller for at least 24 hours before water flushing. The two-phase residual saturation experiment for each soil sample was performed in duplicate. The experimental matrix for two-phase residual saturation experiments is shown in Table 5-5.

Results and Discussion

Soil Properties

Since soil properties are known to influence NAPL displacement in porous media, all the nine MGP-site soil samples were characterized for particle size analysis, particle density (ρ_s), total carbon (TC), cation exchange capacity (CEC), N_2/BET specific surface area (SSA) and capillary pressure-water saturation (P_c - S_w) relationships. From particle size analysis, according to the United States Department of Agriculture (USDA) particle size classification, over 90% of the particles were sand size fraction (2-0.05 mm) in

Table 5-5. Experimental matrix for two-phase (water-tar) residual saturation experiments

	Column Identifier	Soil	Coal tar
Paired Samples	Auburn	Auburn	Auburn
	Cape May	Cape May	Cape May
	Charleston *	Charleston	Charleston
	Fairfield	Fairfield	Fairfield
	Saranac	Saranac	Saranac
	Shippensburg	Shippensburg	Shippensburg
Unpaired Samples	Albany	Albany	Shippensburg
	Waterbury	Waterbury	Shippensburg
	Winsted	Winsted	Shippensburg

* during Charleston soil/tar paired residual saturation experiment, coal tar was injected at 40°C.

Auburn and Cape May soils, and over 80% of sand fractions in Charleston and Fairfield soil samples. The gravel fraction (> 2 mm) ranged from 0.6% for Cape May to 44.6% for Shippensburg soil (Table 5-6). If combine the USDA (Table 5-6) and USCS (Universal Soil Classification System) (Figure 5-2 and Table 5-6) classification results, the gravel fractions in the range of 2-4.75 mm were 23.4% and 19.6% for Albany and Saranac soil, respectively. These gravel fractions were retained in soils during the air-water and coal tar-water two-phase experiments, where soils passing through No. 5 sieve (< 5 mm) were used. The coefficient of uniformity, C_u , ranged from 1.25 for Cape May to 20.00 for Shippensburg soil, indicating that Cape May is a relatively uniform sand, while Shippensburg has the most broad particle size distribution among all the nine soil samples. The coefficient of uniformity (C_u) of Albany was also as high as 14.29. The coefficient of gradation (C_g) of these nine evaluated soil samples ranged from 0.62 for Waterbury and 1.67 for Fairfield soil. These results reveal that Auburn, Cape May, Fairfield, Saranac, and Winsted soils are well-graded soils with relatively continuous distributed particle size, whereas Albany, Shippensburg and Waterbury are poorly-graded soils (Figure 5-3).

Soil particle densities fell within the range of 2.32 to 2.80 g/cm³, and are consistent with the particle densities of field soils reported in the literature (Marshall et al., 1996). Waterbury has the highest particle density of 2.80 g/cm³, which generally corresponded to a high bulk density and low porosity (low pore volume) in subsurface. Shippensburg displayed the lowest particle density of 2.32 g/cm³, which could result in a low bulk density and high porosity (or high pore volume).

Total carbon content in the nine soil samples was distributed widely, ranging from 0.07% for Cape May soil to 14.85% for Shippensburg soil, which appeared dark gray in color. Cation Exchange Capacities (CEC) of the nine MGP-site soil samples ranged from 7.09 meq/100g for Shippensburg soil to 105.1 meq/100g for Auburn soil. Specific surface areas (N_2 /BET) were in the range of 1.31 m^2/g for Winsted soil to 11.65 m^2/g for Saranac soil (Table 5-7). These SSA values were similar to that of Kaolinite (3-15 m^2/g) (Hillel, 1998).

Moisture Release Curves

The moisture release curves (MRCs) for all the nine soil samples and F-70 Ottawa sand, which was used as a reference soil, are shown in Figure 5-4. The volumetric water content of soil samples decreased rapidly once the air entry pressure (bubbling pressure) had been reached. At capillary pressures exceeding 200 cm of water, the volumetric water content exhibited almost no change, indicating that the water content had reached residual water content.

When the MRCs were plotted on a semi-log scale (log scale for negative pressure head axis), changes in water content at low capillary pressure can be seen more clearly (Figure 5-4b). Compared all the semi-log scale MRCs, Cape May exhibited the steepest drop in volumetric water content when the capillary pressure just exceed the bubbling pressure and the lowest residual water content. This behavior was attributed to the fact that Cape May had a d_{50} value of 0.20 mm and coefficient of uniformity (C_u) value of 1.25, which indicates a fine and uniform sand. In contrast, Albany, Saranac, Shippensburg and Waterbury soils exhibited a more gradual reduction in volumetric

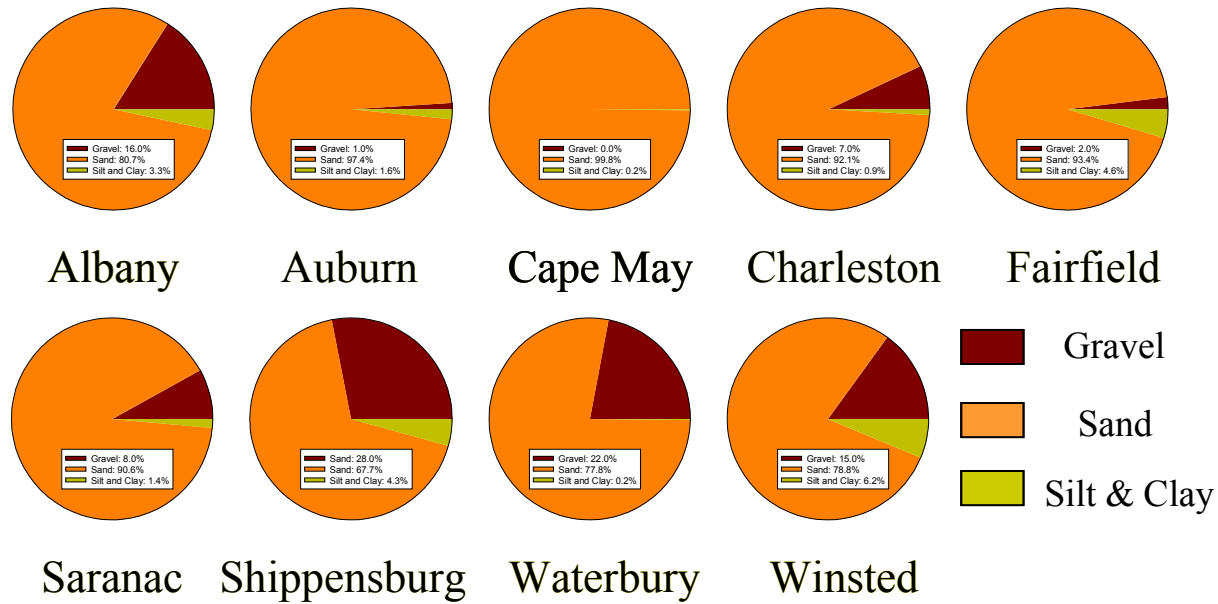


Figure 5-2. Textural classification of soils collected from nine MGP sites based on the Universal Soil Classification System (USCS) (Gravel: 76.2-4.75 mm; Sand: 4.75-0.075 mm; Silt and Clay: < 0.075 mm).

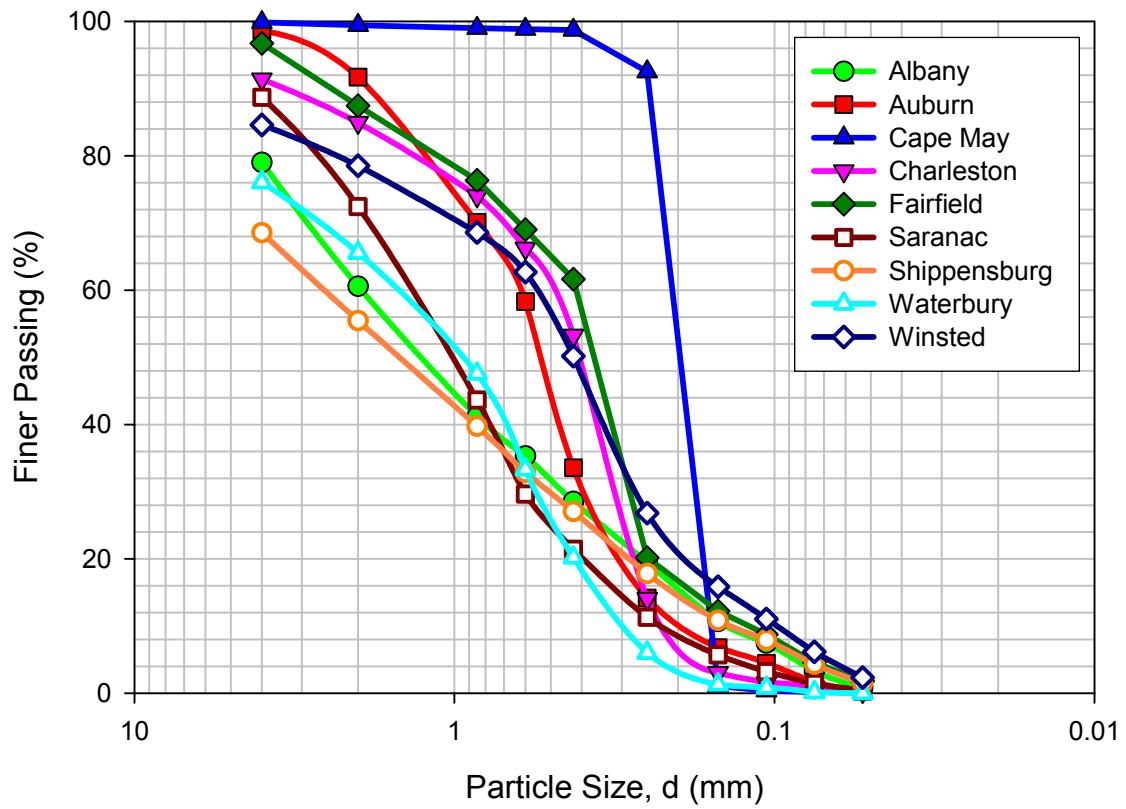


Figure 5-3. Particle size distribution curves of soil samples collected from nine MGP sites.

Table 5-6. Physical properties of soils based on particle size (sieve) analysis.

Soil Identifier	d ₆₀ (mm)	d ₅₀ (mm)	d ₁₀ (mm)	C _u [†]	C _g [‡]	USDA Particle Size Classification			USCS Particle Size Classification		
						% Gravel > 2 mm	% Sand 2-0.05 mm	% Silt+Clay < 0.05 mm	% Gravel 76.2-4.75 mm	% Sand 4.75-0.075 mm	% Silt+Clay < 0.075 mm
Albany	2.00	1.36	0.14	14.29	0.76	39.4	59.9	0.7	16.0	80.7	3.3
Auburn	0.57	0.51	0.18	3.17	1.33	8.3	91.5	0.2	1.0	97.4	1.6
Cape May	0.22	0.20	0.16	1.25	1.01	0.6	99.3	0.1	0.0	99.8	0.2
Charleston	0.48	0.41	0.23	2.09	0.93	15.1	84.7	0.2	7.0	92.1	0.9
Fairfield	0.42	0.37	0.12	3.50	1.67	12.6	85.6	1.8	2.0	93.4	4.6
Saranac	1.49	1.08	0.23	6.48	1.09	27.6	72.0	0.4	8.0	90.6	1.4
Shippensburg	2.60	1.60	0.13	20.00	0.74	44.6	53.9	1.5	28.0	67.7	4.3
Waterbury	1.63	0.97	0.30	5.43	0.62	34.5	65.5	0.0	22.0	77.8	0.2
Winsted	0.55	0.43	0.10	5.50	1.33	21.5	76.2	2.3	15.0	78.8	6.2

[†] Coefficient of uniformity, $C_u = d_{60}/d_{10}$

[‡] Coefficient of gradation, $C_g = d_{30}^2/(d_{60} \times d_{10})$

Table 5-7. Physical-chemical properties of nine MGP-site soil samples (sieved through No. 20 sieve).

Soil Identifier	Particle Density (g/cm ³)	Total Carbon (TC) (%)	Cation Exchange Capacity (CEC) (meq/100g)	N ₂ /BET Surface Area (m ² /g)
Albany	2.57 (±0.06)*	0.88	45.42	11.65
Auburn	2.58 (±0.06) *	0.50	7.09	7.47
Cape May	2.64 (±0.05)	0.07	not measured	not measured
Charleston	2.62 (±0.04)	0.56	18.08	7.36
Fairfield	2.73 (±0.02)	0.99	84.29	6.51
Saranac	2.61 (±0.09)	2.68	56.48	10.33
Shippensburg	2.32 (±0.10)	14.85	105.1	5.89
Waterbury	2.80 (±0.03)	1.17	21.86	2.10
Winsted	2.56 (±0.10)	3.72	35.36	1.31

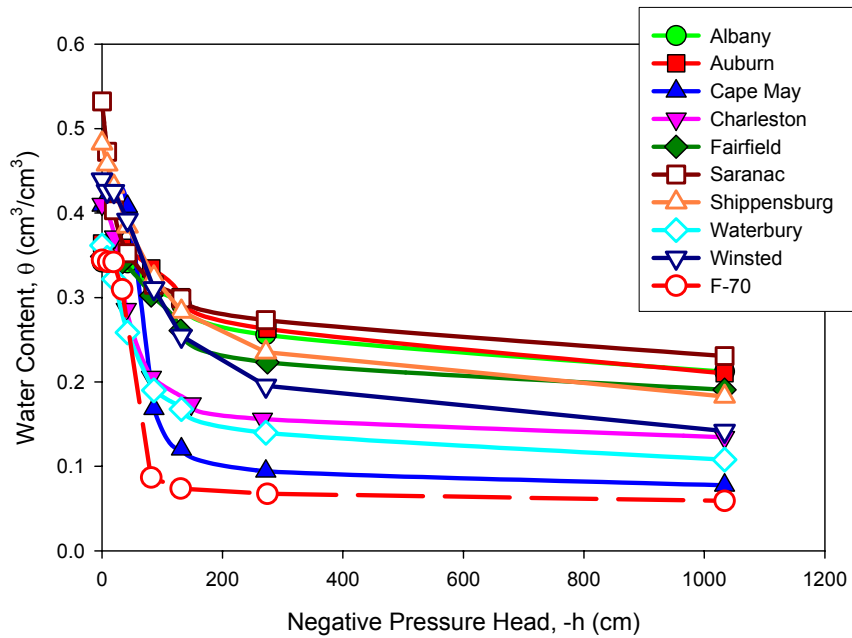
* standard deviation (s.d. = $s/\sqrt{n-1}$)

water content and higher residual water saturation. This behavior is due to their relative broader particle size distribution.

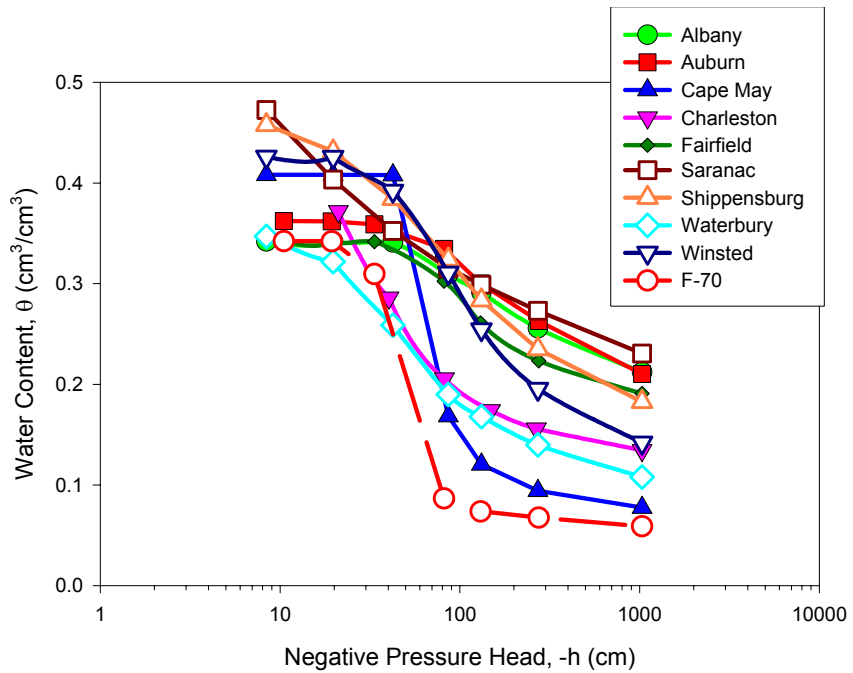
The experimental capillary pressure-saturation relationships were fit to van Genuchten (VG) and Brooks-Corey (BC) equations using the RETC code (van Genuchten et al., 1991). From the RETC fitting of the MRC data (Table 5-8), the bubbling pressure ranged from 3.6 cm for Saranac soil to 57.5 cm for Fairfield soil. Saranac, which possessed the lowest bulk density and highest porosity (or highest pore space), allowed for easy entry of air. The saturated volumetric water contents ranged from 0.344 cm³/cm³ for Fairfield soil to 0.534 cm³/cm³ for Saranac soil, which was in agreement with the bulk density and porosity values. At the capillary pressure of 1 bar, the Saranac soil contained the highest water content compared to the other eight soil samples. This result could be attributed to the high porosity of Saranac soil column. Representative van Genuchten (VG) and Brooks-Corey (BC) fitting curves for MRC for are shown in Figure 5-5.

Coal Tar Properties

Properties of three coal tar samples (Albany, Waterbury and Winsted) were not measured because these samples were actually mixtures of soil particles, water and tar. It was impossible to separate free phase tar from the solid particles, and hence, these coal tar samples were not characterized or used in subsequent experiments. The remaining seven tar samples were analyzed for density (ρ_{CT}), viscosity (η), surface tension (ST) and interfacial tension (IFT).



(a)



(b)

Figure 5-4. Soil water retention (release) curves of soils collected from nine MGP sites (a) normal scale; (b) semi-log scale.

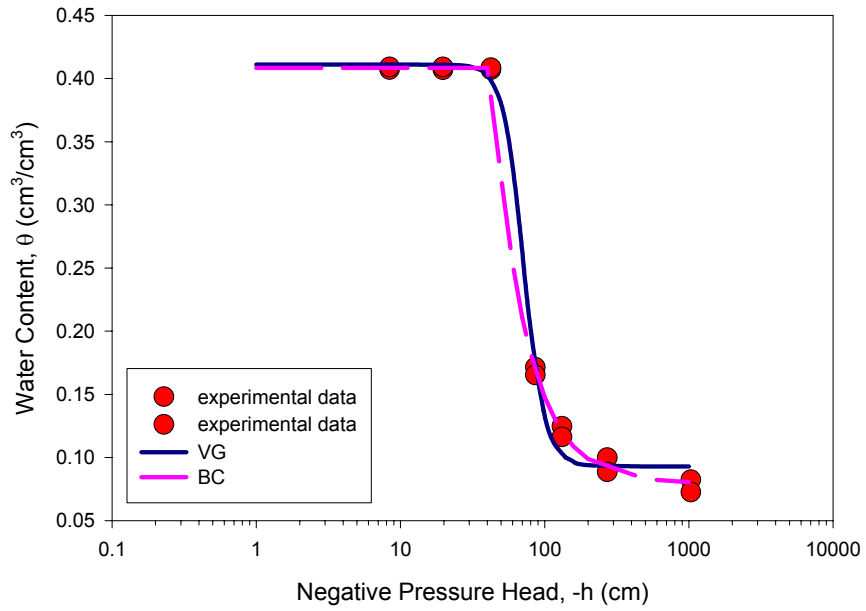


Figure 5-5. Representative van Ganuchten (VG) and Brooks-Corey (BC) fitting curves for MRC.

Table 5-8. Soil water retention characteristics obtained from van Genuchten and Brooks-Corey equations.

Soil Identifier	Bulk Density (g/cm ³)	van Genuchten Parameters [†]				Brooks-Corey Parameters			
		θ_{sat}	θ_{res}	α	n	θ_{sat}	θ_{res}	h_b (cm)	λ
Albany	1.691 (± 0.007)	0.344	0.196	0.0313	1.96	0.342	0.094	49.9	4.07
Auburn	1.640 (± 0.000)*	0.365	0.188	0.009	1.91	0.362	0.123	56.9	2.89
Cape May	1.557(± 0.000)	0.411	0.093	0.0145	6.36	0.408	0.079	42.3	0.55
Charleston	1.423 (± 0.009)	0.413	0.138	0.0314	2.39	0.391	0.129	23.7	1.03
Fairfield	1.722 (± 0.000)	0.346	0.187	0.0111	2.38	0.344	0.174	57.5	1.24
Saranac	1.221 (± 0.000)	0.534	0.190	0.1264	1.42	0.532	0.149	3.6	4.59
Shippensburg	1.168 (± 0.008)	0.478	0.122	0.0313	1.52	0.457	0.089	23.7	2.72
Waterbury	1.788 (± 0.000)	0.360	0.100	0.0326	1.91	0.343	0.091	23.3	1.44
Winsted	1.411 (± 0.000)	0.435	0.130	0.0146	2.15	0.421	0.112	48.2	1.31

Coal tar samples were slightly denser than water, with measured tar densities ranged from 1.054 g/cm³ for Cape May to 1.104 g/cm³ for Charleston at 22°C. The measured viscosities at 22°C ranged from 32.0 cP for Shippensburg tar to approximately 427 cP for Charleston tar. The measured viscosities were all greater than those reported values in previous studies (i.e., 19.4 cP and 16.6 cP at 25°C) (Barranco et al., 1997; Hugaboom and Powers, 2002). The higher viscosity samples evaluated herein are far more representative of coal tars typically encountered at former MGP sites. Charleston tar was the most viscous (425 cP) and heaviest tar (1.104 g/cm³) among all the coal tar samples (Table 5-9).

The surface tension (tar-air) and interfacial tension (tar-water) of the six tar samples ranged from 23.44 dynes/cm for Auburn tar to 34.35 dynes/cm for Fairfield tar, and 20.73 dynes/cm for Charleston tar to 26.36 dynes/cm for Auburn tar at 22°C, respectively (Table 5-9). The interfacial tensions were lower than pure NAPLs, whose interfacial tensions are generally in the range of 35 to 50 dynes/cm (Mercer and Cohen, 1990; Demond and Linder, 1993). Also, tar-water interfacial tensions were lower than some mixture NAPLs such as mineral oils, which implies that there could be more surface active materials in coal tars than in mineral oils. For example, mineral oils are primarily composed of saturated hydrocarbons, the surface active molecules usually exist as impurities, whereas surface active molecules such as asphaltenes are a considerable fraction in coal tar. Hence, coal tar-water IFT is generally lower than that of mineral oil-water (~30-46 dynes/cm) (Table 4-2). Differences in density, viscosity and interfacial tension could result in very different behavior of coal tar in subsurface compared to other mixed and pure NAPLs typically encountered in environmental remediation.

Residual Tar Saturation in Two-Phase (Water-Tar) Systems

Coal tar samples from Auburn, Cape May, Charleston, Saranac and Shippensburg were analyzed with the corresponding soil from the same location (paired samples) in order to provide residual tar saturation data to particular MGP sites. Since coal tars from Albany, Waterbury and Winsted sites were not suitable for analysis, residual saturation measurements for these three soils were obtained with Shippensburg tar (unpaired samples). This approach allowed for the evaluation of residual saturation of a single coal tar as a function of different soils. Auburn and Saranac tar residual saturation experiments were conducted in Kontes glass columns due to their relatively low viscosity, whereas the remaining experiments were conducted in stainless steel columns. Due to the high viscosity of Charleston tar, the stainless steel column was heated to 40°C during the water displacement process to allow for water entry and displacement for tar.

The residual tar saturations ranged from 0.077 cm³/cm³ for Saranac soil to 0.226 cm³/cm³ for Charleston soil, while the corresponding residual tar concentration ranged from 16,218 mg/kg for Waterbury soil to 79,317 mg/kg for Charleston soil (Table 5-10 and Figure 5-6). The most viscous tar (Charleston tar) exhibited the highest residual saturation of 0.226 cm³/cm³, indicating that the viscosity could play a significant role in the residual tar saturation. Cape May tar exhibited a relative high residual saturation value of 0.192 cm³/cm³ although its viscosity (51.0 cP) is much lower compared to Charleston tar, which could be due to the fine and uniform grain size of Cape May soil as discussed in the soil property section. Saranac tar had the lowest residual saturation (0.077 cm³/cm³). This observation could be explained by the fact that Saranac tar possessed a relatively low viscosity (63 cP) compared to Charleston and Fairfield tars,

and Saranac soil contained a relative high gravel fraction (2-4.75 mm), the lowest bulk density (1.227 g/cm^3) and highest porosity ($0.530 \text{ cm}^3/\text{cm}^3$). The residual saturations of Shippensburg tar in Shippensburg and Winsted soils were $0.156 \text{ cm}^3/\text{cm}^3$ and $0.182 \text{ cm}^3/\text{cm}^3$, respectively, although Shippensburg tar possesses the lowest viscosity (32.0 cP). These results could be attributed to the high carbon contents of these two soil samples (14.85% for Shippensburg and 3.72% for Winsted). This implies a relatively strong correlation between the soil carbon content and residual tar saturation. Based on the images of extruded soil cores (Figure 5-7, 5-8, 5-9), the soil cores appeared darker in color after coal tar entrapment. The color change of Charleston soil core was the most dramatic due to the high coal tar residual saturation.

In order to correlate the residual tar saturation to soil and tar properties, both linear and non-linear fit (SigmaPlot 2000, Systat Software Inc) relationships were evaluated as described in Chapter IV (Equation 4-10, 11). Due to the number of possible variables and complexity of the system, total carbon (TC), characteristic size (d_{50}), coefficient of gradation (C_g), coefficient of uniformity (C_u) and intrinsic permeability (ki) were defined as soil properties. Similarly, tar viscosity (η) and interfacial tension (γ) were identified as potentially tar properties. First, linear regression was used to correlate the residual tar saturations to individual soil or tar property as well as dimensionless parameter (total trapping number, N_T). The R^2 values of these correlations ranged from 0.005 to 0.239 as shown in Table 5-11, indicating weak correlations between the residual tar saturation and individual parameters. Therefore, correlations were developed between residual tar saturation and representative parameter combinations. For the correlations with parameter combinations, fewer soil and oil property parameters were selected. Total

Table 5-9. Physical properties of coal tar samples.

Coal Tar Identifier	Density (g/cm ³), 22°C	Viscosity [†] (cP), 22°C	Surface Tension [‡] (dynes/cm), 22°C	Interfacial Tension (dynes/cm), 22°C
Albany	Not measured	Not measured	Not measured	Not measured
Auburn	1.066 (±0.002)	63.6 (±0.1)	33.75 (±0.09)	26.63 (±1.23)
Cape May	1.054 (±0.001)	51.0 (±0.1)	23.44 (±0.07)	22.61 (±0.10)
Charleston	1.104 (±0.002)	425.3 (±0.7)	26.67 (±0.98)	20.73 (±0.43)
Fairfield	1.062 (±0.002)	144.6 (±0.8)	34.35 (±0.26)	23.24 (±0.31)
Portland	1.054 (±0.000)	34.7 (±0.1)	Not measured	Not measured
Saranac	1.062 (±0.000)	62.9 (±1.4)	33.63 (±0.52)	24.14 (±0.94)
Shippensburg	1.076 (±0.000)	32.0 (±0.1)	34.17 (±0.35)	21.88 (±0.11)
Waterbury	Not measured	Not measured	Not measured	Not measured
Winsted	Not measured	Not measured	Not measured	Not measured

* standard deviation (s.d. = $s/\sqrt{n-1}$)

[†] Haake Rheostress 75, shear rate = 200 1/s, [‡] Cahn DCA-322

Table 5-10. Summary of coal tar residual saturation measurements in two-phase (water + tar) systems.

Soil Identifier	Bulk Density (g/cm ³)	Porosity (cm ³ /cm ³)	Tar Viscosity (cP)	Water Saturation (S_w) [‡] (cm ³ /cm ³)	Residual Tar Saturation (S_{Nr}) (cm ³ /cm ³)	Residual Tar Concentration (C_{Nr}) (mg/kg)
Albany ^{†•}	1.766 (±0.006)	0.342 (±0.001)	32.0 (±0.1)	0.841 (±0.012)	0.159 (±0.012)	48,081 (±2,783)
Auburn	1.497 (±0.022)	0.420 (±0.008)	63.6 (±0.1)	0.841 (±0.012)	0.159 (±0.012)	48,081 (±2,783)
Cape May [•]	1.646 (±0.130)	0.383 (±0.004)	51.0 (±0.1)	0.808 (±0.024)	0.192 (±0.024)	52,821 (±8,349)
Charleston [•]	1.400 (±0.171)	0.435 (±0.25)	116.3 (±0.4) [§]	0.774 (±0.028)	0.226 (±0.028)	79,317 (±18,058)
Fairfield [•]	1.795 (±0.009)	0.343 (±0.001)	144.6 (±0.8)	0.869 (±0.041)	0.131 (±0.042)	26,824 (±8,663)
Saranac	1.227 (±0.016)	0.530 (±0.006)	62.9 (±1.4)	0.923 (±0.008)	0.077 (±0.008)	34,732 (±3,778)
Shippensburg	1.278 (±0.005)	0.451 (±0.003)	32.0 (±0.1)	0.844 (±0.048)	0.156 (±0.026)	59,399 (±10,124)
Waterbury ^{†•}	1.928 (±0.020)	0.298 (±0.006)	32.0 (±0.1)	0.841 (±0.012)	0.158 (±0.008)	16,218 (± 470)
Winsted [†]	1.526 (±0.011)	0.396 (±0.004)	32.0 (±0.1)	0.818 (±0.012)	0.182 (±0.013)	50,823 (±2,647)

* standard deviation (s.d. = $s/\sqrt{n-1}$)

† Residual saturation data for Waterbury, Winsted and Albany soils were obtained using Shippensburg coal tar.

‡ In a two-phase (water + tar) system, the sum of the water saturation and tar saturation must equal unity.

§ Viscosity of Charleston at 40°C; column was heated to 40°C to allow for water to displace coal tar.

• Soil core sent to Lehigh University for coal tar dissolution studies.

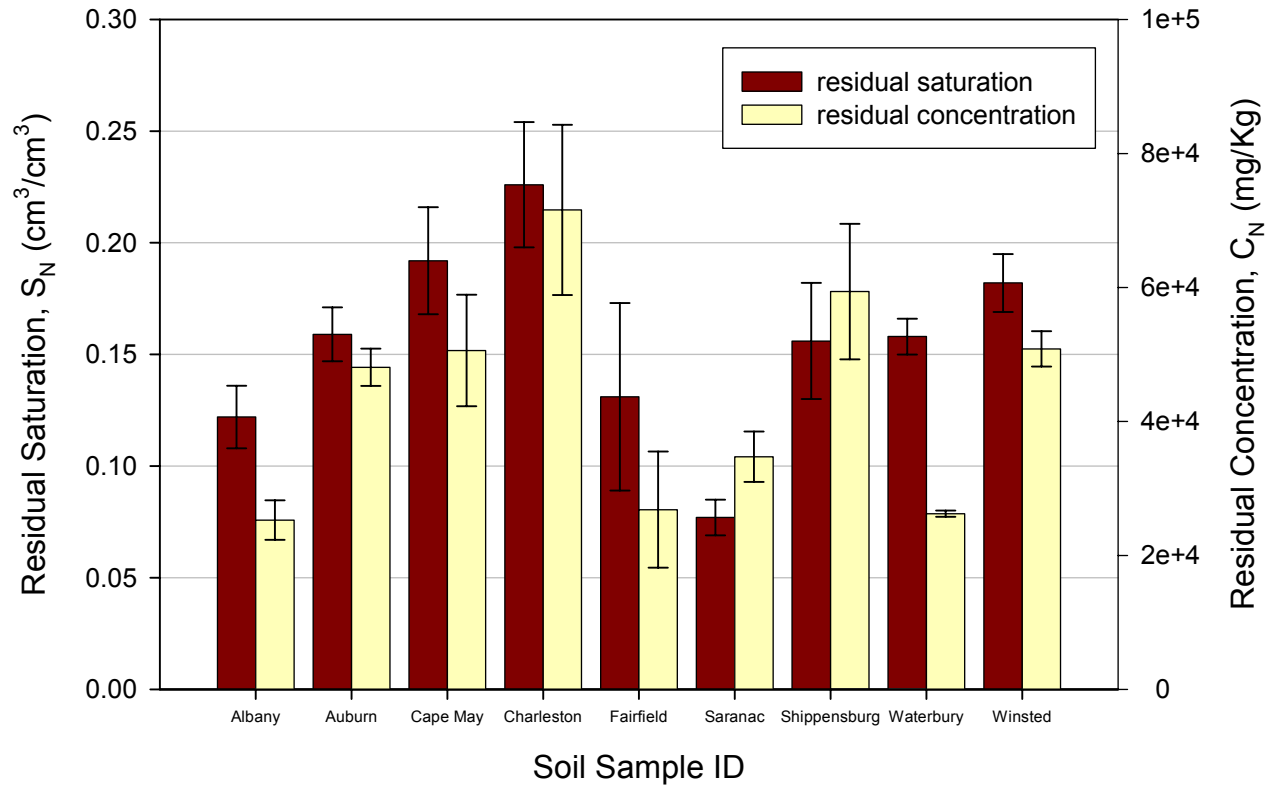


Figure 5-6. Residual saturation and residual concentration of six coal tar samples in two-phase (water-tar) systems.

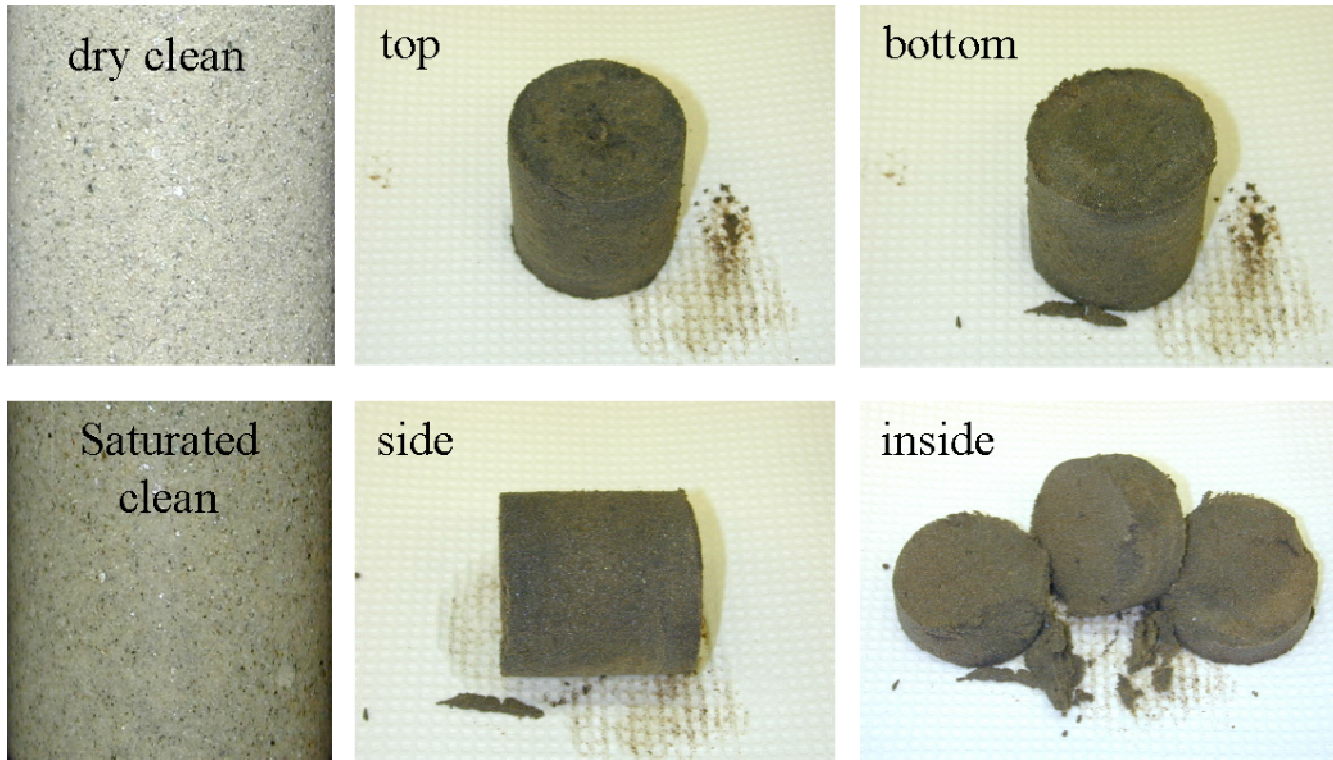


Figure 5-7. Images of air-dry and water-saturated Cape May (clean), and the extruded soil core at residual coal tar saturation.

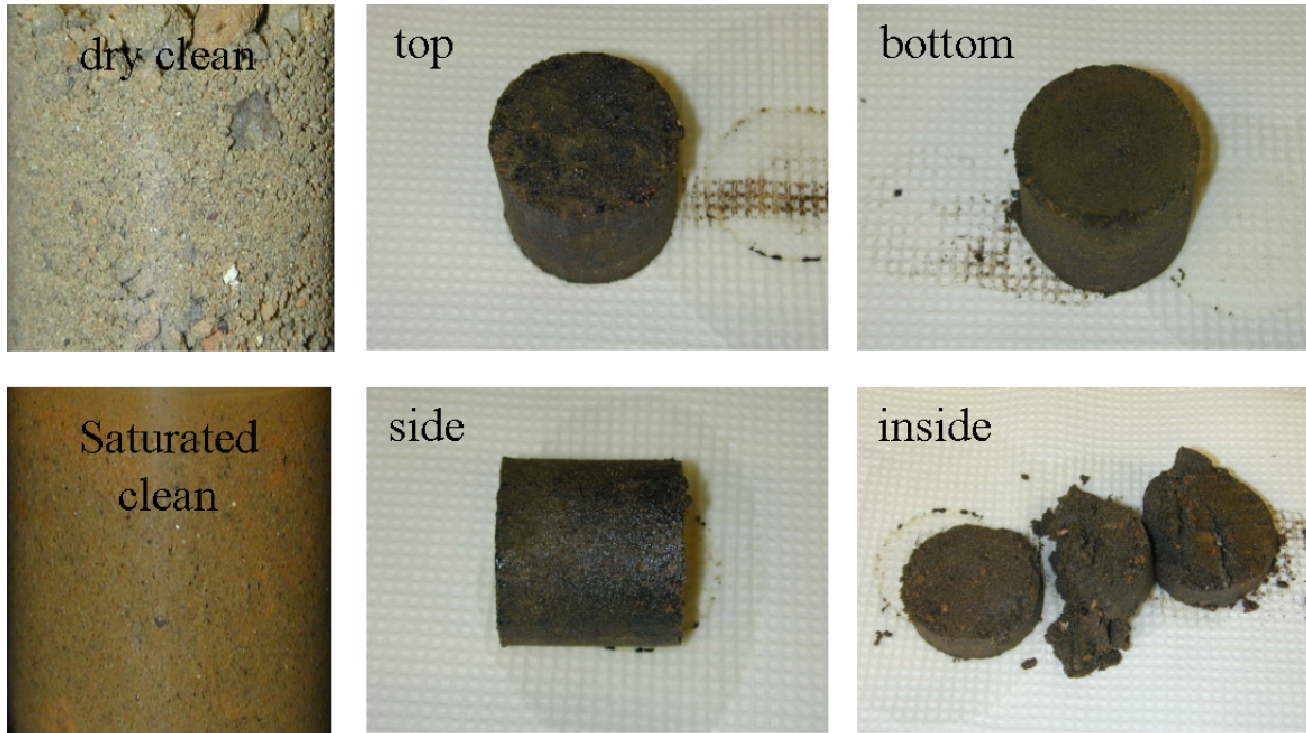


Figure 5-8. Images of air-dry and water-saturated Charleston soil (clean), and the extruded soil core at residual coal tar saturation.

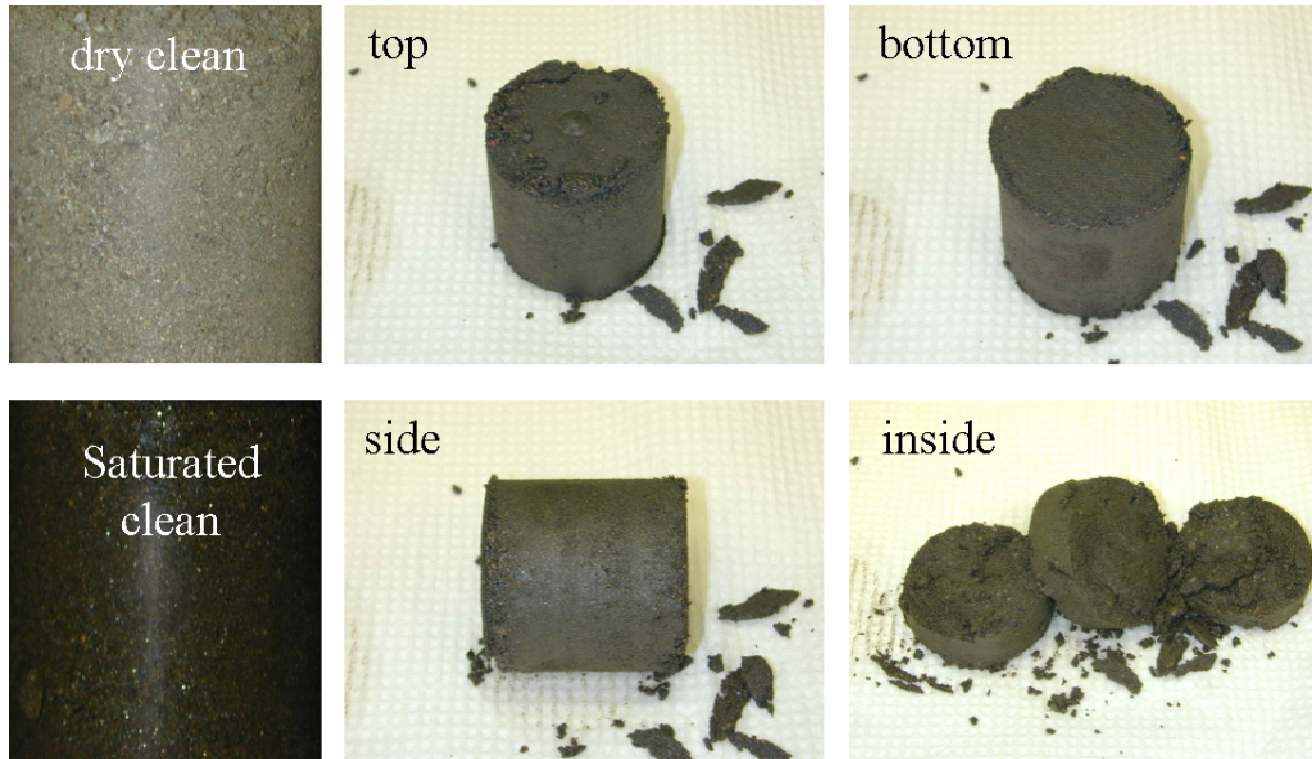


Figure 5-9. Images of air-dry and water-saturated Winsted soil (clean), and the extruded soil core at residual coal tar saturation (Shippensburg coal tar).

carbon content (TC) and characteristic particle size (d_{50}) were identified as soil properties, and tar viscosity (η) and tar-water interfacial tension (γ) were designated as coal tar properties. Selected linear and nonlinear correlations are listed in Table 5-12 and 5-13. Linear correlations (Table 5-12) were generally found to better fit the experimental data than nonlinear correlations (Table 5-13). In linear correlations, correlations incorporate both the soil and tar properties (Case 5-12-5, 5-12-6) were stronger than those just involved soil or tar properties (Case 5-12-1, 2, 3, 4), suggesting that residual tar saturations are dependent upon both soil and tar properties. Neglect either of soil or tar properties will cause wrong prediction of the residual tar saturation. Figure 5-10a shows the correlation ($R^2 = 0.628$) between the model estimated (Case 5-12-5) S_N and all experimental data. The experimental data for paired and unpaired samples were also statistically analyzed separately, as shown in Table 5-14. Representative correlations for paired and unpaired samples were showed in Figure 5-10b and c, with a R^2 value of 0.844 and 0.735, respectively. From case 5-14-1 (Figure 5-10b) and 5-14-4 (Figure 5-10c), both total carbon (TC), tar viscosity (η) and tar-water IFT (γ) bear positive coefficients, while characteristic size (d_{50}) has negative coefficient. This observation implicates that residual tar saturation in soil increases with increasing total carbon content, tar viscosity and tar-water IFT and decreasing particle size, which is in agreement with the correlations between residual mineral oil saturation and soil properties as discussed in Chapter IV.

Dimensionless Parameter Estimation

Assuming a completely water wetting porous medium (i.e., $\cos\theta$ equals to 1), the capillary number (N_{Ca}), bond number (N_B) and total trapping number (N_T) could be

estimated according to Equations 2-22, 23, 27. Comparing data given in Table 5-15, the capillary numbers for the nine soil columns were similar, ranging from 3.04×10^{-6} to 3.77×10^{-6} . In contrast, the Bond number, which was largely dependent on intrinsic permeability, varied by a three-orders-of-magnitude, from 6.96×10^{-9} for Cape May soil column to 5.27×10^{-6} for Saranac soil. The capillary number and Bond number values were similar for Charleston, Shippensburg, Saranac, and Waterbury oil columns, hence, both dimensionless groups contributed equally to the total trapping number. For Cape May soil-tar column, the Bond number was nearly three-orders-of-magnitude lower than the capillary number due to its very low intrinsic permeability, thus, the total trapping number was controlled by the capillary number. Therefore, the resulted total trapping numbers were on the same order for all the soils, varying from 3.35×10^{-6} to 9.04×10^{-6} , which were very low values compared to the critical value for NAPL mobilization reported by Pennell et al. (1996) for PCE. According to Pennell et al.(1996), the critical value of total trapping number required to initiate DNAPL mobilization fell within the range of 2×10^{-5} to 5×10^{-5} , while complete displacement of NAPL was observed as total trapping number approached 1×10^{-3} . In order to remove more coal tar from the residual tar saturation state, it is necessary to greatly increase the capillary number or Bond number, which could be implement by changing the solid phase wettability, tar-water interfacial tension, displacing fluid viscosity and Darcy velocity. These will be addressed in the following two chapters (Chapter VI and VII).

Based on the analysis of the residual saturation data, coal tar viscosity is a very important factor determining the coal tar entrapment, which was not incorporated into the

Table 5-11. Linear Correlations between residual tar saturation and representative individual parameters in two-phase (water-tar) systems (all data).

Case ID	TC (%)	d ₅₀ (mm)	C _g	C _u	η (cP)	k _i (cm ²)	N _T	γ (dynes/cm)	a ₀	R ²
5-11-1	-6.957×10 ⁻⁴								0.1577	0.005
5-11-2		-4.382×10 ⁻²							0.1886	0.247
5-11-3			-1.146×10 ⁻²						0.1678	0.007
5-11-4				-2.34×10 ⁻³					0.1718	0.099
5-11-5					1.767×10 ⁻⁴				0.1386	0.239
5-11-6						-2.765×10 ⁴			0.1691	0.150
5-11-7							-8.157×10 ³		0.1943	0.110
5-11-8								8.027×10 ⁻³	-0.0467	0.098

* values in table represent the coefficient of corresponding variables.

Table 5-12. Selected linear correlations between residual tar saturation and parameter combinations in two-phase (water-tar) systems (all data).

Case ID	TC (%)	d_{50} (mm)	d_{10} (mm)	η (cP)	γ (dynes/cm)	N_T	a_0	R^2
5-12-1	4.052×10^{-3} *	-6.653×10^{-2}					0.1942	0.346
5-12-2	4.280×10^{-3}	-5.622×10^{-2}	-8.053×10^{-2}	1.363×10^{-4}			0.1726	0.471
5-12-3				2.206×10^{-4}	4.199×10^{-3}	-1.366×10^4	-0.0929	0.534
5-12-4				1.561×10^{-4}	3.915×10^{-3}		-0.0418	0.259
5-12-5		-3.585×10^{-2}		1.248×10^{-4}	9.459×10^{-3}	-1.016×10^4	-0.0202	0.628
5-12-6	4.66×10^{-3}	-8.517×10^{-2}			1.417×10^{-2}		0.1510	0.621

* values in table represent the coefficient of corresponding variables.

Table 5-13. Selected nonlinear correlations between residual oil saturation and parameter combinations in two-phase (water-tar) systems (all data).

Case ID	Correlations	R ²
5-13-1	$S_N = 0.895 \times 10^{-2} TC^{-52.88} d_{50}^{30.80} \eta^{7.874} \gamma^{4.165} + 0.1376$	0.478
5-13-2	$S_N = -6.787 \times 10^{-2} TC^{-0.1299} d_{50}^{0.8714} \eta^{-3.215 \times 10^{-2}} + 0.1974$	0.284
5-13-3	$S_N = 0.4642 TC^{5.84 \times 10^{-4}} d_{50}^{-3.87 \times 10^{-3}} - 1.048 \times 10^2 \eta^{-1.891} \gamma^{9.207} - 4.5$	0.204
5-13-4	$S_N = 4.277 \times 10^{-2} 3TC - 5.701 \times 10^{-2} d_{50} + 41.62 \eta \gamma + 0.1738$	0.436

Table 5-14. Selected correlations between residual tar saturation and parameters in paired and unpaired two-phase (water-tar) systems.

Case ID	Correlations	R ²
	<u>For paired samples:</u>	
5-14-1	$S_N = 1.272 \times 10^{-2} TC - 0.1631d_{50} + 6.840 \times 10^{-5} \eta + 1.340 \times 10^{-2} \gamma - 0.1195$	0.844
5-14-2	$S_N = 5.126TC^{-3.449} d_{50}^{1.812} \eta^{1.026} \gamma^{0.8192} + 0.1195$	0.652
5-14-3	$S_N = 3.328TC^{-3.476} d_{50}^{1.828} + 3.328\eta^{1.036} \gamma^{0.8844} + 0.1196$	0.652
	<u>For unpaired samples:</u>	
5-14-4	$S_N = 2.949 \times 10^{-3} TC + 5.400 \times 10^{-2} d_{50} + 0.1980$	0.725
5-14-5	$S_N = 0.245TC^{3.864 \times 10^{-2}} d_{50}^{-0.1197} - 0.1026$	0.656

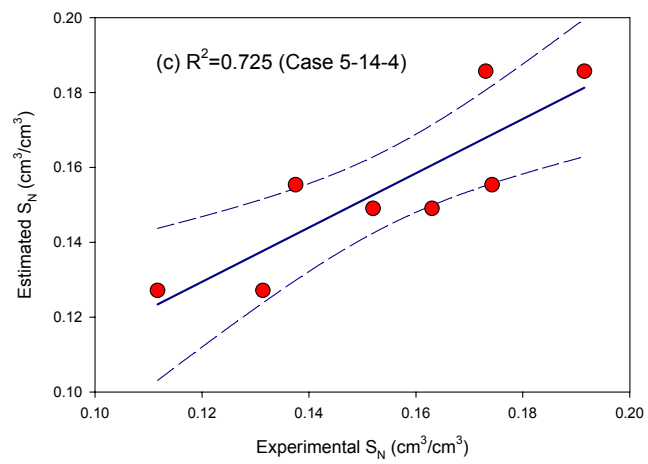
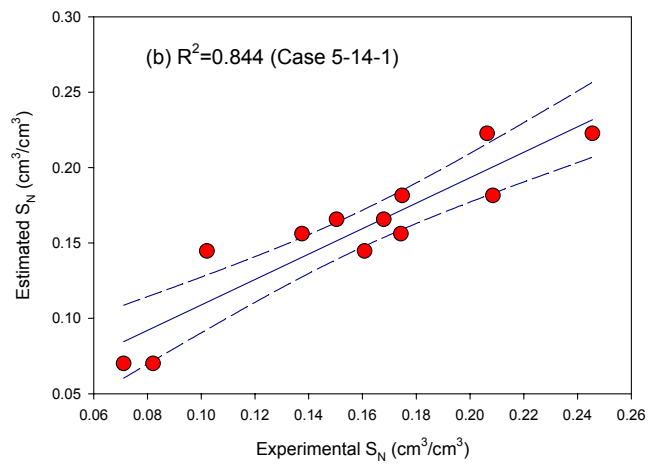
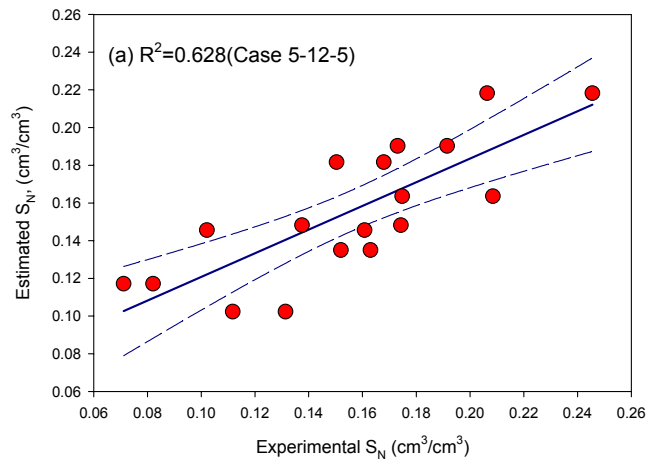


Figure 5-10. Representative linear correlations between residual tar saturation and soil/tar properties (solid lines represent fit curve and dash lines represent 95% confidence level) (a) all data; (b) paired samples; (c) unpaired samples.

Table 5-15. Capillary number, Bond number and total trapping numbers in coal tar soil columns.

Soil Identifier	Capillary Number (N_{Ca})	Capillary Number (N_B)	Capillary Number (N_T)
Albany	3.04×10^{-6}	3.02×10^{-7}	3.35×10^{-6}
Auburn	3.45×10^{-6}	2.18×10^{-7}	3.67×10^{-6}
Cape May	3.51×10^{-6}	6.96×10^{-9}	3.52×10^{-6}
Charleston	3.59×10^{-6}	2.82×10^{-6}	6.41×10^{-6}
Fairfield	3.48×10^{-6}	2.85×10^{-7}	3.77×10^{-6}
Saranac	3.77×10^{-6}	5.27×10^{-6}	9.04×10^{-6}
Shippensburg	3.04×10^{-6}	1.35×10^{-7}	4.04×10^{-6}
Waterbury	3.04×10^{-6}	1.75×10^{-7}	4.79×10^{-6}
Winsted	3.04×10^{-6}	4.98×10^{-7}	3.54×10^{-6}

total trapping number. The trapping number is derived under the assumption that the shear forces in this system are negligible. Adams (1975) proposed a new dimensionless parameter (F), which incorporated the oil-water viscosity ratio in viscous crude oil-water systems. This point will be discussed in more detail in Chapter VII.

Summary and Conclusions

Quantification of the properties of coal tar reveals that coal tars are highly viscous DNAPLs, and their physical properties vary significantly from site to site. The measured densities of the coal tar samples were slightly higher than water, ranging from 1.054 g/cm³ for Cape May to 1.104 g/cm³ for Charleston. Viscosities of the six coal tar samples exhibited a broad distribution, ranging from 32 cP for Shippensburg to 425 cP for Charleston at 22°C. These values are much higher than most of the reported coal tar viscosity values and are more representative of tar viscosities typically encountered at MGP sites. Charleston tar had the highest viscosity, which turned out to be the most difficult coal tar to displace from the soil columns during the two-phase residual saturation experiments. The tar-water IFT ranged from 22.55 to 27.83 dynes/cm, which is lower than that of pure NAPLs (35-50 dynes/cm). Characterization of soil properties shows that Auburn, Cape May, Charleston, Fairfield, and Saranac soil contain primarily sand size particles, while Shippensburg and Waterbury soil bear relatively high fraction of gravel. The residual tar saturations were in the range of 0.077 cm³/cm³ for Saranac tar to 0.226 cm³/cm³ for Charleston tar, which were consistent with the reported residual saturation values of other NAPLs. Compared to literature reported residual tar saturations usually obtained from coal tar in coarse quartz sand, data obtained in this study are more

representative of the residual tar saturation in field. Correlations between residual tar saturation and soil/tar properties shows that particle size distribution, total carbon content, tar-water interfacial tension and tar viscosity play an important role in residual tar saturation in porous media.

However, how to further remove coal tar from the residual tar saturation, will conventional remediation technologies work well at the MGP sites. Based on the total trapping number analysis, the mobilization of coal tar is likely to be very difficult. These issues will be investigated in more detail in Chapters VII.

CHAPTER VI

SOLUTION CHEMISTRY EFFECTS ON THE INTERFACIAL PROPERTIES OF COAL TAR-WATER-SILICA SYSTEMS AND RESIDUAL COAL TAR SATURATION IN POROUS MEDIA

Introduction

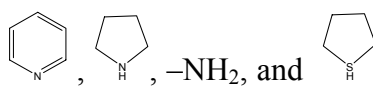
The fate and transport of NAPLs in subsurface depends not only on physical characteristics of the NAPL (e.g., density, viscosity) and porous medium (e.g., grain size, pore size distribution), but also on interfacial properties such as NAPL-water interfacial tension (IFT) and surface wettability. Interfacial properties determine the pressure required for one liquid to displace another from the pore space, which is referred to as entry pressure or displacement pressure. When the NAPL displaces or is displaced by the water phase, NAPL tend to occupy the center of big pores in a water wetting media, and low NAPL-water IFT also enhance the NAPL movement. Hence, IFT and wettability play a significant role on the amount of NAPL entrapment in and removal from porous media (Anderson, 1987a; Demond and Roberts, 1991; Demond et al., 1994; Pankow and Cherry, 1996). Since the liquid-liquid IFT and solid wettability are very sensitive to the aqueous solution pH and ionic strength (Barranco et al., 1997; Lord, 1997; Lord et al., 1997a, b, 2000; Barranco and Dawson, 1999; Hugaboom and Powers, 2002), the aqueous chemistry of the system may play a significant role in the NAPL residual saturation in porous medium.

Reservoir wettability and oil-water IFT are considered to be two of the most important factors governing enhanced oil recovery (EOR). A considerable amount of research has been undertaken to investigate the effects of interfacial chemistry and wettability on oil recovery (Morrow, 1975; Anderson, 1987a, b, c; Buckley et al., 1989; Morrow, 1990; Buckley, 1994, 2001; Buckley and Liu, 1998; Skauge et al., 1999; Buckley and Wang, 2002). Compared to EOR, research on effect of solution chemistry on NAPL entrapment and removal is less addressed. Lord and coworkers (1997a, b, 2000) investigated the IFT, wettability and capillary pressure-saturation (P_c - S) relationship changes as a function of pH in air-water-quartz and *o*-xylene-water-quartz systems in the presence of organic acid (octanoic acid) and organic base (dodecylamine). Both IFT and contact angle were observed to vary with pH and organic acid or base concentration. In these systems, two key mechanisms were believed to determine the IFT and wettability: 1) the speciation of surface-active compounds as a function of solution pH, and 2) physicochemical properties of mineral surfaces. At low pH, the neutral form of an organic acid (HA) is the dominant species, while organic bases protonate to form positively charged ions (BH^+). At high pH, organic acids dissociate to form negatively charged conjugate base (A^-), and the organic base exists in the neutral form (B). Acidic and basic functional groups of mineral surfaces can also deprotonate or protonate depending on the pH of aqueous phase. For example, the silanol groups ($\equiv SiOH$) on a silica surface can dissociate to form a negative species ($\equiv SiO^-$) when the pH is above the point of zero charge (PZC) of silica, which is in the range of pH 2.0 to 3.0 (Hirassaki, 1991; Ramaswami et al., 1994; Skauge et al., 1999). When the solution pH is lower than PZC, the silica surface carries a net positive charge ($\equiv SiOH_2^+$) (Buckley et al., 1989).

Therefore, the silica surfaces are negatively charged in the typical ground water pH range (pH 5-7).

Solid surface wettability in the presence of two immiscible liquid phases, which is defined as the measurement of the preferential tendency of one of the fluids to spread or adhere to the surface, is dependent on the interactions between the solid, water and oil surfaces. Classic DLVO (Derjaguin-Landau (1941)-Verwey-Overbeek (1948)) theory, incorporating electrostatic and van der Waals forces, has been widely used to predict the wettability of solid surfaces in oil-water two-phase systems (Buckley et al., 1989; Hirasaki, 1991; Basu and Sharma, 1996; Ward et al., 1999; Zheng, et al., 2001b; Drummond and Israelachvili, 2002). The change of IFT between oil and water phase with pH has been attributed to the surface-active properties of different species accumulated at the NAPL-water interface.

With respect to coal tar, the constituents with acid or base characteristics are primarily contained in asphaltenes. Asphaltenes have been found to account for a significant fraction of coal tar. Peters and Luthy (1993) measured a 34% of asphaltene content in coal tar from an MGP site in Stroudsburg, PA. Zheng and Powers (2003) reported asphaltene contents of 20.9% and 36.4% for coal tars from Pennsylvania and New York MGP sites, respectively. Asphaltenes are generally defined as insoluble in n-pentane and soluble in toluene, and consist of condensed aromatic nuclei systems with numerous polar functional groups containing N, O, S atoms, such as $-OH$, $-O-$, $-C=O$,

 etc. (Bunger and Li, 1981). These functional groups can act as organic acids or bases, and may be protonated or deprotonated forming neutrally,

positively or negatively charged groups. Figure 6-1 shows a conceptual structure of an asphaltene molecule.

Compared to pure nonionic organic compounds, such as benzene, dodecane, PCE and TCE, complex mixtures containing ionizable polar groups greatly influence the relative adhesion of fluids to the solid surface, as well as IFT between organic mixture and water with the change of aqueous solution chemistry. Bottle tests, adhesion tests and contact angle measurements are three methods widely used to evaluate the solid phase wettability in oil-water system (Morrow, 1990). Bottle tests visually assess the wetting conditions at different pH after equilibrating coal tar, water and clean quartz sand three-phase system. At low pH, coal tar was observed to coat the sand grains, which were identified as oil-wetting conditions; while at high pH, coal tar was found to be separated from the sand, which indicated water-wetting conditions (Powers et al., 1996; Hugaboom and Powers, 2002). Adhesion tests are also qualitative experiments, which evaluate the surface wettability by observing the tendency of oil droplet to adhere to a quartz plate when withdrawn by a syringe. If the droplets are detached completely without fluid left on the slide, non-adhesion is defined; otherwise, the slides are considered to be adhesive (Morrow, 1990). Zheng et al. (2001a) performed adhesion tests to one coal tar sample and four creosote samples at different pH and found that the wetting alteration (from non-adhesion to adhesion or *vice versa*) happened at approximately pH 5 for four of the five samples, while pH 7.2 to the other creosote sample. At the same time, classic DLVO theory including electrostatic and van der Waals forces was utilized to predict the pH corresponding to wetting reversal of quartz sand in coal tar or creosote-water-quartz sand

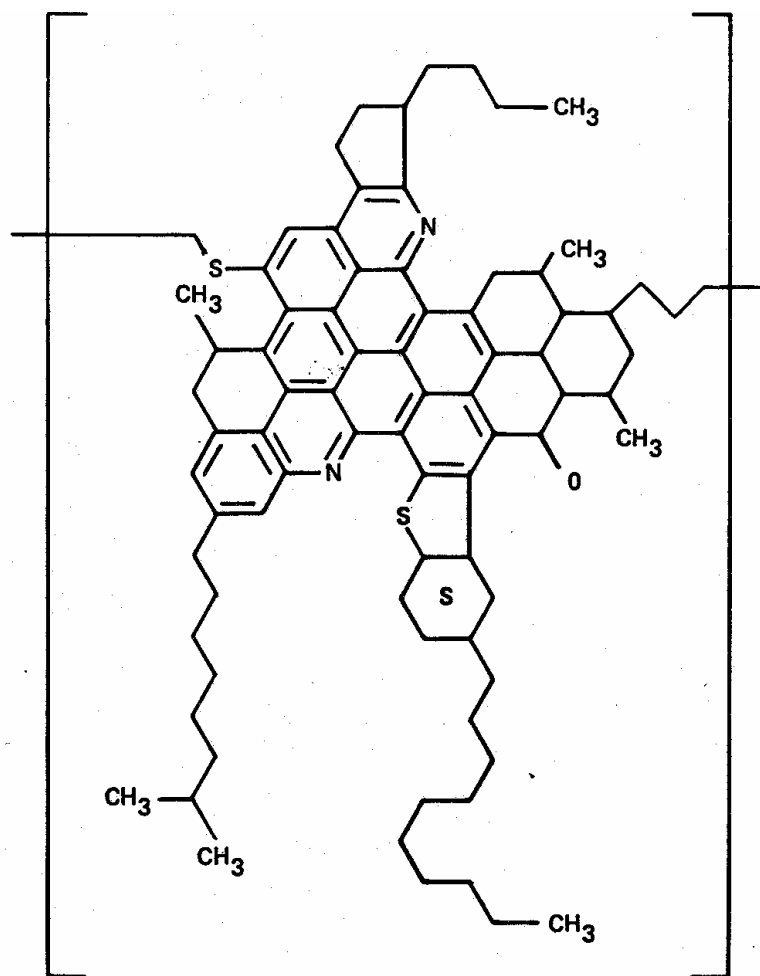


Figure 6-1. Hypothetical structure of a petroleum asphaltene
 (Chemical formula: $(C_{79}H_{92}N_2S_2O)_3$, molecular weight: 3449 g/mole)
 (Bunger and Li, 1981)

systems. By defining the pH at which the total interacting pressure between the NAPL and quartz is zero as the wetting reversal pH, the errors of wetting reversal pH values between model prediction and adhesion tests were within 0.4 pH units for four of the five samples. As the most universal measure of surface wettability, contact angle data in tar-water-silica system are limited. Barranco et al. (1997, 1999) measured the static contact angle of coal tar on quartz slides in an aqueous system. Contact angle values displayed a decrease from approximately 20° to less than 10° over the range of pH 3.4 to pH 12.4. These contact angle values indicated strongly water-wetting conditions of this system over the pH range evaluated.

With respect to the IFT, coal tar-water IFT is generally much lower than those between pure nonpolar organic compounds and water, which are generally in the range of 35-50 dynes/cm (Demond and Lindner, 1993). At pH 7.0, the IFT between coal tar and water is reported to be in the range of 20-25 dynes/cm (Barranco et al., 1997; Barranco and Dawson, 1999; Hugaboom and Powers, 2002; Zheng and Powers, 2003). The difference of IFT between coal tar-water and pure nonpolar organic-water has been attributed to the accumulation of polar components in coal tar (such as asphaltenes) at the coal tar-water interface (Demond and Lindner, 1993; Barranco et al., 1997; Barranco and Dawson, 1999; Zheng, et al., 2001b; Hugaboom and Powers, 2002; Zheng and Powers, 2003). Surface active molecules such as asphaltenes are thought to be held by an energy barrier which prevents desorption of these molecules from the coal tar-water interface (Davies and Rideal, 1963). Barranco et al. (1997, 1999) observed no significant changes in the IFT between coal tar and water over a range of pH 3.4 to 9.1, with an average IFT value of 23.5 dynes/cm. Above pH 9.1, IFT dropped sharply to 0.6 dynes/cm at pH 12.4.

A similar trend of IFT as a function of pH was observed by Zheng and Powers (2003). Within the range of pH 3.8 to 9.8, the tar-water IFT showed no apparent variation with pH, while decreased sharply when pH was above pH 10. The tar-water IFT was less than 8 dynes/cm near pH 12 (Zheng and Powers, 2003). At low pH, the IFT reduction was attributed to the protonization of organic bases; while at high pH, the anionic organic acid was responsible for the IFT reduction. The tar-water IFT is suggested to be more sensitive to organic acids at high pH than to the organic bases at low to neutral pH (Barranco and Dawson, 1999; Zheng and Powers, 2003).

Ionic strength is another important factor that may impact the interfacial properties and wettability. Gaonkar (1992) observed the IFT values were approximately 23 dynes/cm and 16 dynes/cm for a commercial soybean oil-water system in the absence and presence of NaCl (3%), respectively. Lord et al. (1997b) found the addition of 0.5 M NaCl to an *o*-xylene-water system resulted in an IFT reduction of 3.2 dynes/cm. Standal et al. (1999a, b) used isooctane as a surrogate to simulate the crude oil phase and added 1-naphthoic acid, 5-indanol or quinoline to investigate the effect of salt on quartz slide wettability and oil-water IFT. A maximum increase of 25° in contact angle was found with the addition of 0.5 M NaCl in oil (amended with 5-indanol)-water-quartz slide systems over a pH range of 5 to 9, and the oil-water IFT reductions due to the NaCl (0.5 M) addition were less than 4 dynes/cm in all these systems. This observation was attributed to a “salting out” effect. That is, the salt ions in the aqueous solution create ionic fields that attract surrounding water molecules and hence reduce organic-water interaction, which results in the reduction of organic aqueous solubility and accumulation of these components at the oil-water interface, thereby reducing the oil-water IFT.

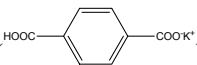
Different results of ionic strength effect were reported for nonpolar organics. Gaonkar (1992) observed IFT increases less than 1 dyne/cm at 5, 20, and 50°C in the presence of 3% NaCl in a purified oil-water system. The slight increase in IFT was attributed to the negative adsorption of NaCl at the oil-water interface. Barranco et al. (1997, 1999) found that the measured contact angles of TCE and PCE on quartz decreased from 26 to 10° and 32 to 10° as ionic strength increasing from 2×10^{-6} M to 1.0 M, respectively, while the DNAPL-water IFT values increased sharply as ionic strength greater than 0.1 M. It was interpreted that IFT between TCE or PCE and water was proportional to the solubility of NAPL in water according to the empirical models (Demond and Linder, 1993; Seo and McCray, 2002).

Overall, very limited data have been reported on the interfacial properties and wettability of coal tar-water-solid systems. The purpose of this study was to assess the effect of pH and ionic strength on the wettability of silica surfaces and coal tar-water IFT. Asphaltene contents, acid and base numbers were quantified for each coal tar sample. Zeta potentials of the six coal tar samples were measured as a function of pH in a 0.01 M NaCl aqueous solution to obtain the point of zero charge (PZC). Correlations between these measured parameters and coal tar physical properties such as density and viscosity were developed by best fitting the experiment data using SigmaPlot 2000 (Systat Software Inc). To evaluate the impact of acidic and basic components in coal tars on solid surface wettability and liquid-liquid IFT, 5-indanol and quinoline were added to one of the coal tar samples (Saranac coal tar). Contact angle of Saranac tar on silica glass slides in aqueous solution and tar-water IFT were measured as a function of aqueous solution pH and concentration of organic base or acid added. Compared to stearic acid and

dodecylamine, which have been used in previous studies (Lord et al., 1997b, 2000; Zheng and Powers, 2003), 5-indanol and quinoline are expected to better mimic the aromatic and acidic/basic nature of asphaltenes. In addition, changes in wettability of silica glass in the presence of coal tar and water were examined in the context of interactive forces between two surfaces. Hydration force was incorporated into the classic DLVO forces (electrostatic force and van der Waals force). Finally, the capillary pressure-saturation (P_c - S) relationships were investigated for Saranac coal tar in F-70 Ottawa sand to assess the effect of pH on coal tar entrapment in porous media. Three scaling approaches, which prediction the P_c - S relationship in tar-water-Ottawa sand systems from that of the air-water-Ottawa sand systems, were compared.

Materials and Methods

Materials

Coal tar samples obtained from six MGP sites (Auburn, Cape May, Charleston, Fairfield, Saranac and Shippensburg) were used in this study (Table 5-4). Naphthotic acid, 5-indanol, quinoline and 70% perchloric acid (HClO_4) were obtained from Aldrich Chemical Company (Milwaukee, MI) and used as received. Relevant properties of naphthotic acid, 5-indanol, and quinoline were listed in Table 6-1. All the other reagents, including inorganic chemicals such as sodium chloride (NaCl), sodium acetate (CH_3COONa), sodium bibasic phosphate (NaH_2PO_4), sodium monobasic phosphate (NaHPO_4), sodium bicarbonate (NaHCO_3), sodium carbonate (Na_2CO_3), potassium hydrogen phthalate () (OC(=O)c1ccc(cc1)C(=O)[O-].[K+]), sodium perchlorate (NaClO_4), sodium hydroxide

(NaOH), potassium hydroxide (KOH), acetic acid (CH₃COOH), concentrated hydrochloric acid (HCl), concentrated nitric acid (HNO₃), and organic reagents, including n-pentane, iso-propanol, toluene, methyl isobutyl ketone (MIBK) as well as pH buffer standards including pH 4.01, pH 7.00, pH 10.00 standard solution were obtained from Fisher Scientific Company (Pittsburg, PA) and used as received. All the solutions were prepared using deionized-distilled water that was treated with a Barnsted Nanopure System (Dubeque, IA) to remove any residual organic contaminants. F-70 (40-270 mesh) Ottawa sand was obtained from U.S. Silica Company (Berkeley Springs, WV), and used as received.

Methods

Solution Preparation

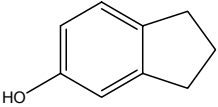
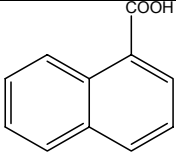
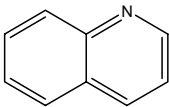
Aqueous buffer solutions were prepared with the following acid/base pairs: CH₃COOH/CH₃COONa, NaH₂PO₄/NaHPO₄, and NaHCO₃/Na₂CO₃, which have been widely used to give a specific range of pH (Xie and Morrow, 1999; Hugaboom and Powers, 2002). Three stock buffer solutions, made from three different equi-molar acid/base pairs (CH₃COOH/CH₃COONa, NaH₂PO₄/NaHPO₄, NaHCO₃/Na₂CO₃) were prepared to achieve a pH of 4.6 ± 0.1 , 7.0 ± 0.1 and 10.0 ± 0.1 , respectively (Table 6-2). Each stock solution possessed a total Na⁺ concentration of 0.01 M. Stock solutions were diluted by a factor of 10 prior to use. NaOH and HCl were used to adjust the pH to an expected value. To obtain values of pH less than 4.6, 0.1 M HCl was added drop by drop to the CH₃COOH/CH₃COONa buffer solution. Ionic strength of solution was adjusted by NaCl.

Contact Angle Measurements

The contact angle of coal tar droplets on glass microscope slides (Fisher Scientific, Pittsburg, PA) immersed in water was measured using a goniometer equipped with a CCD camera and lens assembly (Ramé-Hart, Inc., Mountain Lakes, NJ). Prior to use, each glass microscope slide was soaked in a 5 M HNO₃ solution for at least 24 hours and rinsed thoroughly with Nanopure DI water. After cleaning, the slide was soaked in a buffered water solution at a specified pH (pH 2.6, 3.5, 4.6, 7.0, 10.0), which was measured using a pH meter (Accumet Model-50, Fisher Scientific, Pittsburg, PA). Five drops of coal tar were added to an aluminum dish and soaked in a 100 mL beaker containing approximately 80 mL of buffer solution and the glass slide. Care was taken to prevent direct contact of coal tar with the glass slide. The tar-water-glass system was allowed to equilibrate for 24 hours. For coal tar containing either organic acid or base, a certain amount of 5-indanol or quinoline (1, 5, 10, 20% (wt)) was added to coal tar, mixed completely with a glass rod, and allow to equilibrate for at least 24 hours prior to the contact angle and IFT measurements.

Contact angle measurements were obtained using a sessile drop method (Adamson, 1990). In this method, a glass microscope slide was positioned horizontally inside a cubic optic glass cell (5 cm × 5 cm × 5 cm) (Fisher Scientific, Pittsburg, PA), supported by a Teflon bar. The cell was filled with approximately 80 mL of buffer solution that had been pre-equilibrated with the coal tar. Five coal tar droplets were formed on the microscope slide using a micro syringe (Hamilton Co., Reno, Nevada) (Figure 6-2a). By adjusting the position of the cell horizontally, a digitized image of each drop was captured after an equilibration period of 15 minutes using a personal computer

Table 6-1. Chemical specification for 5-indanol, 1-naphtoic acid and quinoline.

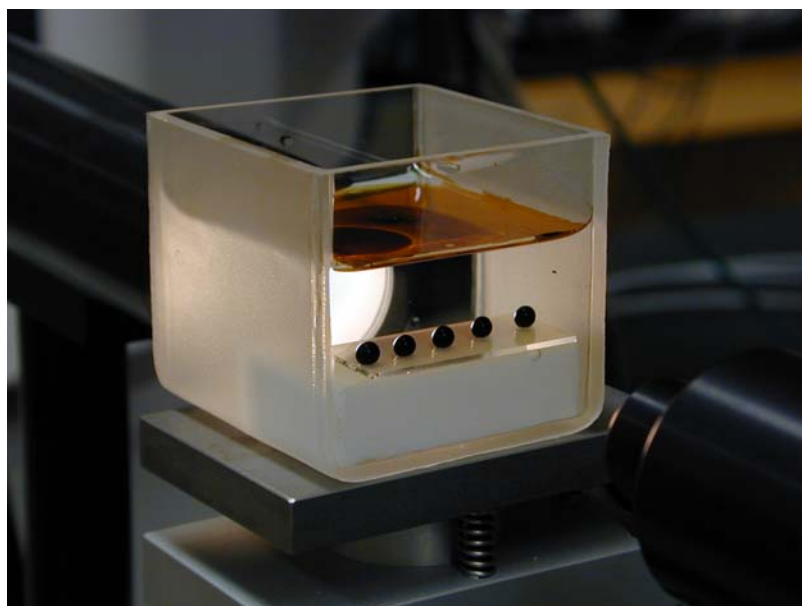
Organic compound	Structure	Purity	Log K_{ow} †	p K_a ‡
5-indanol		99%	2.99	10.3
1-naphtoic acid		>97%	3.05	3.7
quinoline		>97%	2.03	4.9

† KowWin, Syracuse Research Corporation, 2004.

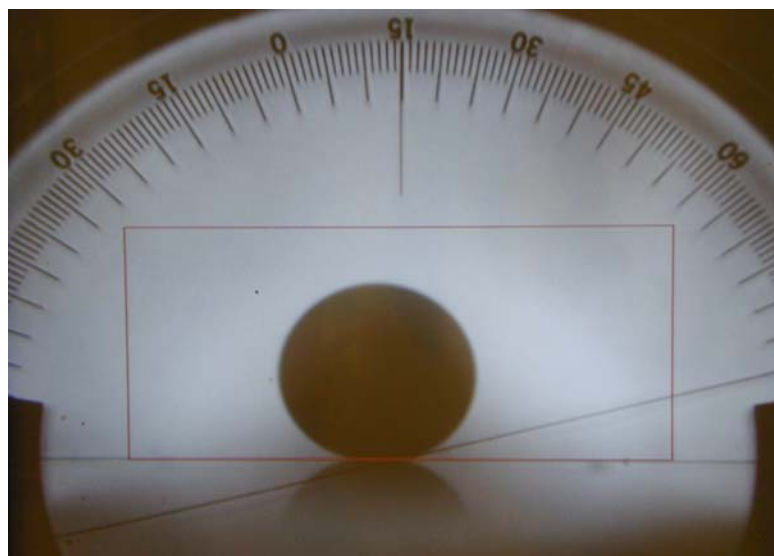
‡ SPARC, Hilal, S.H., and S.W. Karickhoff. 2003.

Table 6-2. Stock buffer solution used in this study.

pH	Solution formulation	Ionic Strength (M)
4.6 ± 0.1	0.01 M CH ₃ COOH + 0.01 M CH ₃ COONa	0.010
7.0 ± 0.1	0.0033 M NaH ₂ PO ₄ + 0.0033 M Na ₂ HPO ₄	0.013
10.0 ± 0.1	0.0033 M NaHCO ₃ + 0.0033 M Na ₂ CO ₃	0.013



(a)



(b)

Figure 6-2. Contact angle measurements (a) Sessile drop method for contact angle measurement; (b) Representative digitized images obtained from goniometer.

connected to the goniometer apparatus (Figure 6-2b). Both left and right contact angle of each droplet were measured. The reported contact angle was calculated by taking the mean of the left and right contact angles for all of the five droplets.

Interfacial Tension

Coal tar-water IFT as a function of pH was measured using the drop volume method, as described in the Method section in Chapter IV. Five droplets were counted in each measurement, and thirty drops in total were recorded for each tar-water pair.

Zeta-Potential Measurements

Zeta-potential measurements were performed using an emulsion procedure similar to that described by Parra-Barraza et al. (2003). Approximately 50 mg of coal tar were contacted with 15 mL ethanol contained in a 40 mL glass vial and mixed with a high speed touch mixer (Fisher Sci., Model 232) for about 2 minutes and then sonicated for one hour. A 0.5 mL aliquot of the emulsion was then transferred to 50 mL of buffer solution containing 0.01 M NaCl and sonicated for 30 minutes. The sonicated emulsion was conditioned for 20 minutes prior to zeta potential measurements. Zeta potential was measured using a ZetaPlus (Brookhaven Instruments Co., Holtsville, NY). For this procedure, charged coal tar droplets in the emulsion move between two oppositely charged electrodes. The electrophoretic mobility of the droplets was determined by measuring the Doppler shift in scattered light that results from the movement of droplets in the applied electric field. The zeta-potential was calculated from the measured electrophoretic mobility according to the Smoluchowski equation (Equation 6-1).

$$\zeta = \frac{U\eta}{\varepsilon} \quad (6-1)$$

where ζ is the zeta potential (V), U is the electrophoretic mobility ($\text{m}^2 \text{s}^{-1} \text{V}^{-1}$), η is the viscosity of the emulsion (N s m^{-2}), and ε is the permittivity of the solution ($\text{C}^2 \text{N}^{-1} \text{m}^{-2}$) (Hunter, 1987). Prior to the coal tar sample measurements, the instrument was calibrated by using a latex microsphere standard material from Malvern Instruments Ltd. (Southborough, MA), which had a zeta potential of 50 ± 5 mV.

Asphaltene Separation and Quantification

Asphaltene separation was performed following procedures similar to those described in American Society of Testing Material (ASTM) Method D2007-03 (2003). Approximately 60 mL of n-pentane was added to a disposable aluminum dish that contained approximately 5 g of each coal tar sample. The n-pentane and coal tar were mixed by hand with a glass rod for a period of 5 minutes. Each dish was then covered with aluminum foil to minimize evaporation of n-pentane and the mixture was allowed to stand for 30 minutes at room temperature (22 ± 1 °C). The n-pentane soluble fraction was removed by vacuum filtration through a nylon filter membrane (Millipore Inc., Billerica, MA) with an opening of 20 μm . The filtration assembly included a Gelman 47 mm magnetic filter tunnel, a 1 L filtration flask whose side arm was connected to a Millipore vacuum pressure pump. The solids retained on the filter (asphaltenes) were transferred to a disposable aluminum dish and left uncovered in an exhaust fume hood for several days until the weight change was less than 0.01 g. Asphaltene determinations were obtained in duplicate for each coal tar sample.

Acid Number Determination

Acid number was defined as the quantity of base, expressed as mg KOH/g sample, required to titrate a sample to a specified end point. The acid numbers of each coal tar sample and Saranac tar with 5-indanol or quinoline addition were determined using a nonaqueous potentiometric titration method described in ASTM method D664-01 (2001). The equipment used for acid number titration included an Accumet pH meter (Model-50), a glass body calomel reference electrode (Accumet) filled with iso-propanol saturated with NaClO₄ and a glass electrode with Ag/AgCl reference (Accumet).

The acid number titrant was prepared by dissolving approximately 2.8 g KOH into 1000 mL of iso-propanol. The titration solvent was prepared by adding 500 mL of HPLC grade toluene and 6 mL of water to 494 mL of HPLC grade anhydrous iso-propanol. The standard solution was prepared by dissolving approximately 0.2 g accurately weighed potassium hydrogen phthalate (KHP) in 500 mL of Nanopure DI water. The spiking solution was prepared by dissolving approximately 0.5 g naphthotic acid into the titration solvent to obtain a 100 mL solution.

Prior to titration, the pH meter was calibrated with pH 4.01 and pH 7.00 buffer standards, and then set to “mV” mode for electromotive force (EMF) measurements. The titrant was first calibrated with approximately 60 mL of the KHP standard solution in triplicate. The two electrodes were then inserted into the KHP standard solution contained in a 100 mL glass beaker. Titrant was added to the KHP standard solution using a 100 μ L gas-tight syringe (Hamilton) with a 90-s pause between each incremental addition (generally 0.1 mL). The volume of the titrant added per increment was also varied depending on the rate of the EMF change during the previous addition. The needle

of the syringe was kept under the solution surface during injection. The beaker was covered with parafilm and the solution was gently mixed with a magnetic stir bar throughout the titration. Titrant was added until the difference between the EMF values of two consecutive readings was less than 1 mV. After finishing the titrant calibration, 1 mL of spiking solution was added to approximately 50 mL titration solvent, mixed completely and titrated with calibrated titrant. The titration protocol was similar to that described for titrant calibration. To start the coal tar titration, approximately 1 g accurately weighed coal tar sample was transferred to a 100 mL glass beaker containing approximately 60 mL of titration solvent, and mixed using a magnet stir plate for one hour. The sample solution was spiked with 1 mL spike solution and titrated by the calibrated titrant.

The molar concentration of titrant (N) was calculated as:

$$N = \frac{1000 \times W_{KHP}}{MW_{KHP} \times V_{eq}} \quad (6-2)$$

where, W_{KHP} is the weight (g) of KHP in 50 mL of KHP standard solution, MW_{KHP} is the molecular weight of KHP (204.23 g/mole), and V_{eq} is the amount (mL) of titrant consumed by 50 mL KHP standard solution at the equivalence point.

The equivalent point corresponds to the inflection point on a plot of EMF versus cumulative volume of titrant added. In order to determine the equivalent point, the derivative of each point on the EMF-titrant volume curve was calculated and plotted as a function of the cumulative volume of titrant added. The cumulative volume of titrant added, corresponding to the peak in the derivative curve, was the equivalent volume V_{eq} .

Based on the concentration of titrant (N) calculated according to Equation 6-2, the acid number (AN) of coal tar, in terms of KOH/g tar, was calculated as following:

$$AN = \frac{(V_{eq} - b_{eq}) \times N \times MW_{KOH}}{W_{oil}} \quad (6-3)$$

where, V_{eq} is the amount of titrant (mL) consumed by coal tar sample solution spiked with 1 mL of the spiking solution at the equivalence point, b_{eq} is the amount of titrant (mL) consumed by 1 mL of spiking solution (referred to naphthotic acid dissolved titration solvent solution in acid number titration) at the equivalent point, MW_{KOH} is the molecular weight of KOH (56.1 g/mol), and W_{oil} is the weight (g) of coal tar added in titration solvent.

Acid number was performed in duplicate for each coal tar sample.

Base Number Determination

Base number was defined as the quantity of acid, expressed as mg KOH/g sample, required to titrate a sample to a specified end point. Base numbers of six coal tar samples and Saranac tar with 5-indanol or quinoline addition were determined by nonaqueous potentiometric titration, based on procedures described in ASTM method D4739-02 (2002) and published methods (Bruss and Wyld, 1957; Zheng and Powers, 1999). Experiment apparatus used for base number titration were similar to that used in acid number titration. In base number titration, methyl isobutyl ketone (MIBK) was used as the titration solvent. The base number titrant was prepared by dissolving approximately 5 mL of 70% $HClO_4$ into 1000 mL of MIBK. The standard solution was prepared by dissolving 0.4 g KHP into 500 mL acetic acid, and the spiking solution was prepared by dissolving approximately 1.6 g quinoline into MIBK to make a 250 mL solution.

The titration protocol was similar to that described for the acid number. The base number (BN), also expressed in terms of KOH/g tar, was calculated as:

$$BN = \frac{(V_{eq} - b_{eq}) \times N \times MW_{KOH}}{W_{oil}} \quad (6-4)$$

Base number was performed in duplicate for each coal tar sample.

Capillary Pressure-Residual Saturation Experiments.

Capillary pressure–saturation (P_c - S) relationships were determined at three different pHs (4.6 ± 0.1 , 7.0 ± 0.1 and 10.1 ± 0.1) at room temperature (22 ± 1 °C). Saranac coal tar was used as the NAPL phase, and F-70 Ottawa sand was used as the porous media. A stainless steel column was used, similar to that used in the coal tar-water two-phase experiments described in Chapter V (Figure 6-3). The primary difference was that both water drainage and spontaneous imbibition curves were obtained.

During the water drainage process, a coal tar reservoir was connected to the bottom of the column and pressure was applied to the coal tar reservoir. The air pressure was increased in increments from zero cm of water to a specific value when coal tar appeared at the top outlet of column. At each pressure, water produced was collected in a graduated cylinder and weighed every 24 hours until the change in water weight was less than 0.1 g. The water imbibition process was started at the pressure where the water drainage process stopped. The pressure on the coal tar reservoir was incrementally reduced to zero cm of water. At each pressure, the water level in the graduated cylinder was recorded every 24 hours, until the water change was less than 0.1 g (Figure 6-3).



Figure 6-3. Capillary pressure-saturation experimental apparatus used for Saranac coal tar-water-Ottawa sand system at pH 4.7, 7.0 and 10.0.

Results and Discussion

Characterization of Coal Tar Acid/Base Properties

Asphaltene Quantification

The measured asphaltene content of six coal tar samples from six different MGP sites are listed in Table 6-3. Asphaltene contents ranged from 33.6% for Cape May tar to 60.9% for Charleston tar. The measured asphaltene content of Charleston tar was much higher than the previously reported coal tar asphaltene contents (Peters and Luthy, 1993; Zheng, 2001; Zheng et al., 2001; Zheng and Powers, 2003). The measured viscosity and asphaltene content showed a strong linear correlation ($R^2 = 0.93$) (Figure 6-4a), which indicate that asphaltene content contribute to viscosity. In addition, a linear correlation was obtained between coal tar density and asphaltene content ($R^2 = 0.88$) (Figure 6-4b). This relation could also be attributed to the aggregation of polar molecules in the asphaltenes. Previous experimental results of other researchers revealed that viscosity of petroleum- or coal-derived liquids, including coal tar, were dependent upon asphaltene content and composition (Thomas, and Granoff, 1978; Krzyżanowska and Marzec, 1978; Bockrath et al., 1980; Sheu and Storm, 1995; Werner, et al., 1998). Thomas, and Granoff (1978) reported a linear relationship between the logarithms of dynamic viscosity of coal conversion products and asphaltene contents (wt%). Krzyżanowska and Marzec (1978) found that the kinematic viscosity of coal liquid fitted a straight line when plotted against asphaltene content (wt%). Bockrath et al. (1980) isolated asphaltene from different coal-derived products and then mixed them with a mixture solvent to investigate the effect of asphaltene content and composition on liquid viscosity. The natural logarithms of relative viscosity (viscosity of solution to that of solvent) was found to fit a linear correlation with

Table 6-3. Asphaltene content, acid and base number, as well as point of zero charge of the six coal tar samples.

Coal Tar Identifier	Asphaltene (wt%)	Acid Number (mg KOH/g)	Base Number (mg KOH/g)	PZC
Auburn	39.0 (± 3.8)*	0.29 (± 0.11)	2.09 (± 0.11)	3.9
Cape May	33.6 (± 0.4)	0.55 (± 0.11)	1.31 (± 0.36)	4.1
Charleston	60.9 (± 0.2)	0.22 (± 0.05)	1.72 (± 0.16)	4.0
Fairfield	43.2 (± 0.4)	0.47 (± 0.17)	2.88 (± 0.65)	4.1
Saranac	36.9 (± 0.9)	0.68 (± 0.02)	1.36 (± 0.37)	4.0
Shippensburg	40.3 (± 0.9)	0.50 (± 0.14)	0.12 (± 0.01)	2.9

* standard deviation (s. d. = $\sigma/\sqrt{n-1}$)

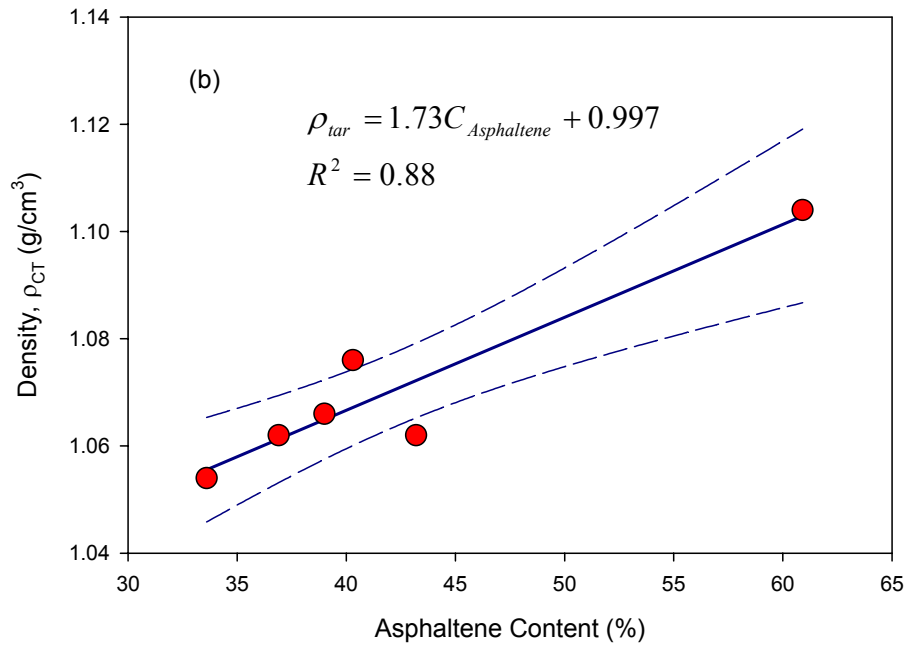
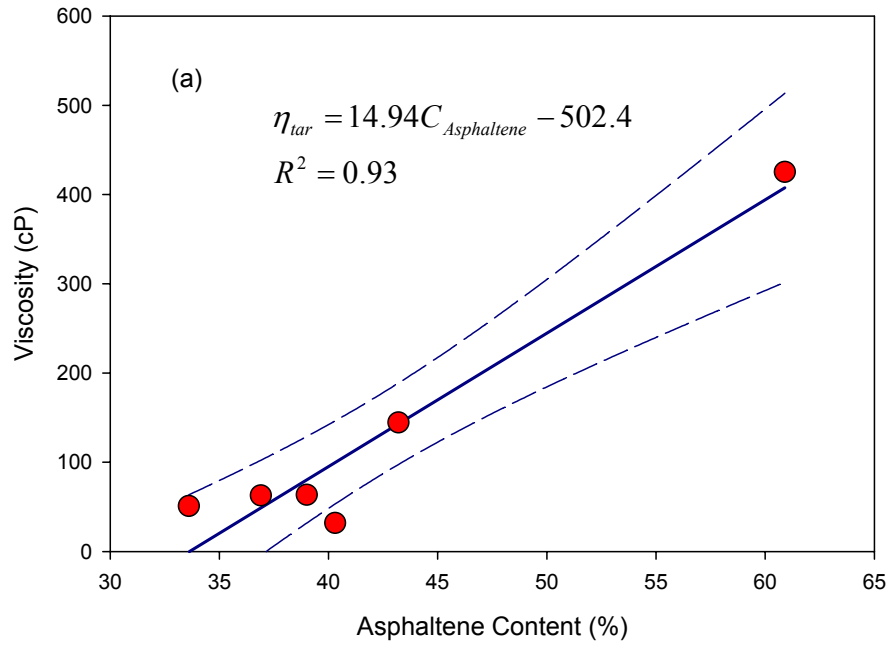


Figure 6-4. Viscosity (a) and density (b) versus asphaltene content (Solid lines represent the linear regression curve, and the dash lines represent 95% confidence levels).

the asphaltene concentration (g asphaltene/mL solvent). Sheu and Storm provided an equation (Equation 6-5) to fit the relative viscosity, η_r ($=\eta/\eta_s$, where η and η_s are the solution viscosity and solvent viscosity, respectively) and asphaltene volume fraction ϕ in a system with asphaltene dissolved in organic solvent.

$$\eta_r^m = 1 + K\phi \quad (6-5)$$

where m is the fitting parameter, when $m = 1$, a linear relationship yield. Generally, polar components have been found to be concentrated in the higher molecular-weight components such as asphaltene in coal-derived liquids. Due to hydrogen bonding between phenols and pyridine-like molecules within the asphaltenes, polar molecules tend to aggregate or self-associate and result in a high viscosity of coal tar (Bockrath et al., 1980). As for density, although asphaltene content contribution is important, the effect of aromatic and polar fraction is significant, too (Peramanu et al., 1999). That might explain why the correlation between asphaltene content and density is not as good as that between asphaltene content and viscosity.

Point of Zero Charge

Zeta potential of six coal tar samples as a function of pH were measured at a temperature of 22°C with a NaCl concentration of 0.01 M. The point of zero charge (PZC) of each coal tar sample was determined by fitting smooth curve to the experimental data and interpolating the pH of zero zeta potential. The measured zeta potential curve of Saranac as a function of pH is shown in Figure 6-5. The PZC was approximately pH 4.0 herein. When pH was lower than 4.0, the tar phase presented a positive charge. When pH was higher than 4.0, the tar phase was negatively charged. The PZC values for the six coal tar samples ranged from 2.9 to 4.1 (Table 6-3). Shippensburg

tar had the lowest PZC (pH 2.9) among the six coal tars. The PZC values of the remaining five coal tar samples were similar to reported PZC values (pH 4.2 and 4.3) of two other coal tars (Zheng et al., 2001; Hugaboom and Powers, 2002; Zheng and Powers, 2003). Figure 6-5 gave the measured zeta potential curve of Saranac as a function of pH. The point correspondent to the zero zeta potential was the PZC, which was approximately pH 4.0. When pH was lower than 4.0, the tar phase presented a positive charge. When pH was higher than 4.0, the tar phase was negatively charged.

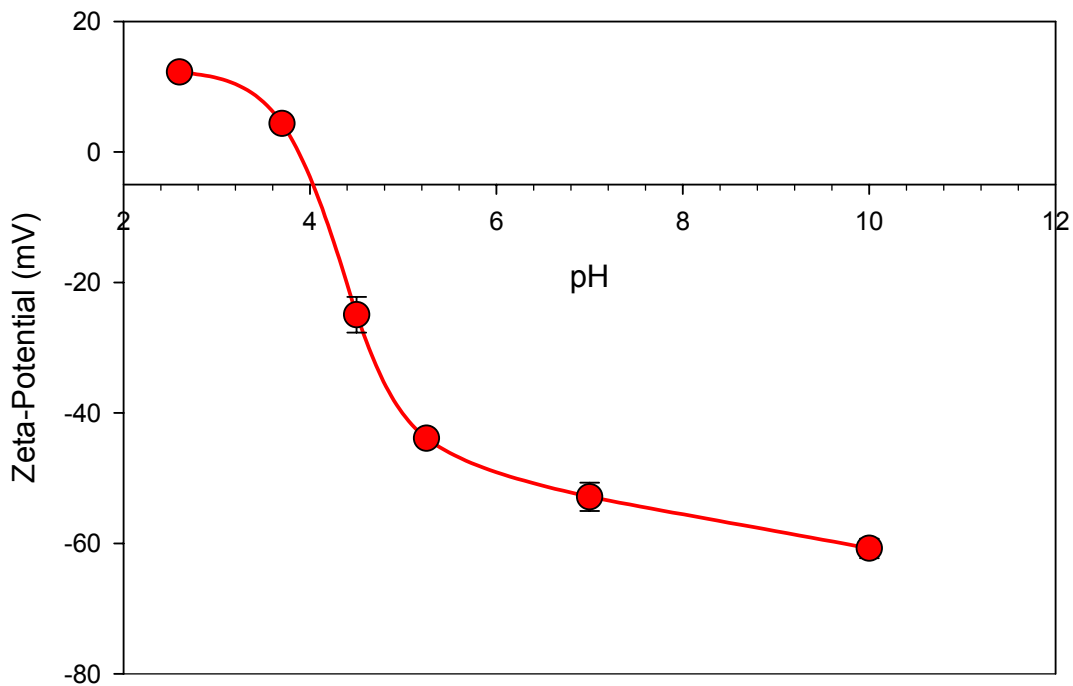


Figure 6-5. Zeta potential as a function of pH for Saranac tar.

Acid Number and Base Number

Figure 6-6 shows representative titration curves obtained in acid and base number determination. The inflection point and peak of the derivative curve were distinct for the KHP standard solution, which indicated a strong acid. The inflection point of tar sample was obtained after adding 1 mL of spiking solution, but was still not as sharp as that of the KHP, which indicated that coal tar exhibited weaker acid/base properties. As a measurement of the acid or basic constituents in petroleum products, acid number and base number are used as guides in quality control of product performs, reservoir wettability prediction in oil recovery (Dubey and Doe, 1993). Application of acid number and base number concept into the petroleum product remediation in environmental science and technologies is a new topic. Very limited research has been performed to the acid, base number analysis to oil contaminants in environment (Zheng and Powers, 1999; Zheng, 2001)

The acid numbers of the six coal tar samples ranged from 0.22 mg KOH/g tar for Charleston tar to 0.68 mg KOH/g tar for Saranac tar. The base numbers were generally higher, ranging from 0.12 mg KOH/g tar for Shippensburg tar and 2.88 mg KOH/g tar for Fairfield tar. The acid number and base number of the six coal tar samples were listed in Table 6-3. Compared to literature values, the acid and base numbers for coal tars obtained here were slightly higher than crude oil, but lower than creosote (Skauge et al., 1999; Zheng, 2001). In general, the acid number of crude oil increases with increasing base number (Skauge et al., 1999). The relationship between acid number and base number obtained in this study and literature data for crude oil, coal tar and creosote are shown in

Figure 6-7. A linear correlation was obtained using the SigmaPlot 2000 (Systat Software Inc) ($R^2 = 0.89$).

The acid and base numbers as a function of asphaltene content (wt%) for coal tar examined in this study and literature data for coal tar or crude oil (Skauge et al., 1999; Zheng, 2001; Yang et al. 2002) are shown in Figure 6-8. Skauge et al. (1999) reviewed data of 11 crude oil samples and found that acid and base numbers generally increased with increasing asphaltene content. However, Yang et al. (2002) observed weak correlations between acid or base number and asphaltene content for 25 crude oils. In general, coal tars contain higher fractions of asphaltenes than crude oil, but this does not necessarily result in higher acid and base numbers. Also, no clear correlations have been found between acid, base numbers and asphaltene content of coal tar samples (Zheng, 2001). One explanation for these observations is that the degree of aggregation may be different for different asphaltenes. Specifically, as asphaltene content increases, the number of sites with acidic or basic properties may decrease due to hydrogen bonding between O or N atoms at adjacent asphaltene molecules, which could be referred to as self-association (Sheu and Mullins, 1995).

The base to acid number ratio (BN/AN) is generally considered a reasonable indicator of PZC of crude oil or coal tar. In general, the PZC increases as the BN/AN ratio increases (Dubey and Doe, 1993; Buckley, 1994; Zheng, 2001). The coal tar PZC values increase with increasing BN/AN ratio when the BN/AN ratio is less than 4. When the BN/AN ratio is greater than 4, the PZC values do not change. PZC values are believed to depend on the coal tar chemical properties, including absolute values of the acid, base numbers, the BN/AN ratio and pK_a .

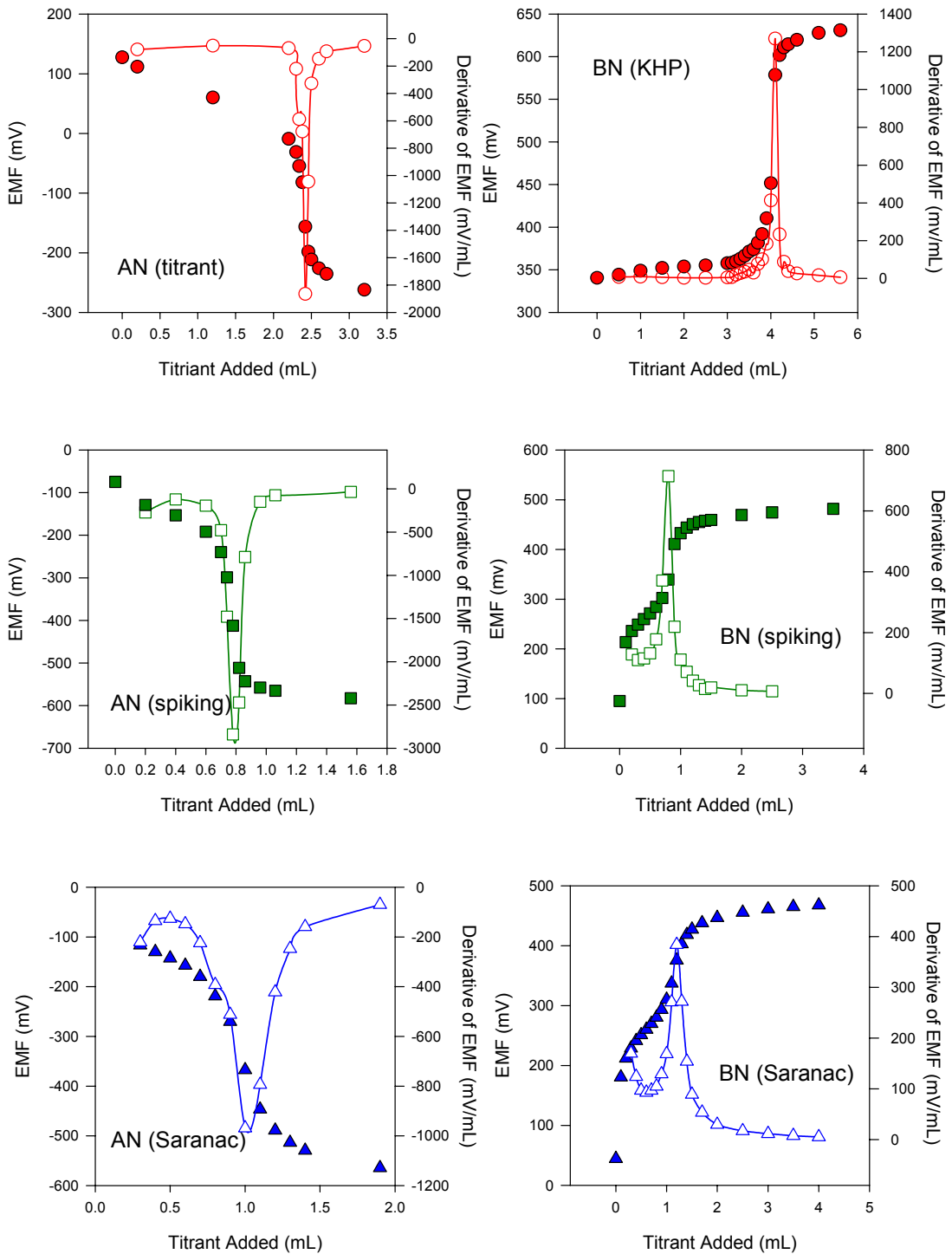


Figure 6-6. Acid- and base number determination by nonaqueous potentiometric titration.

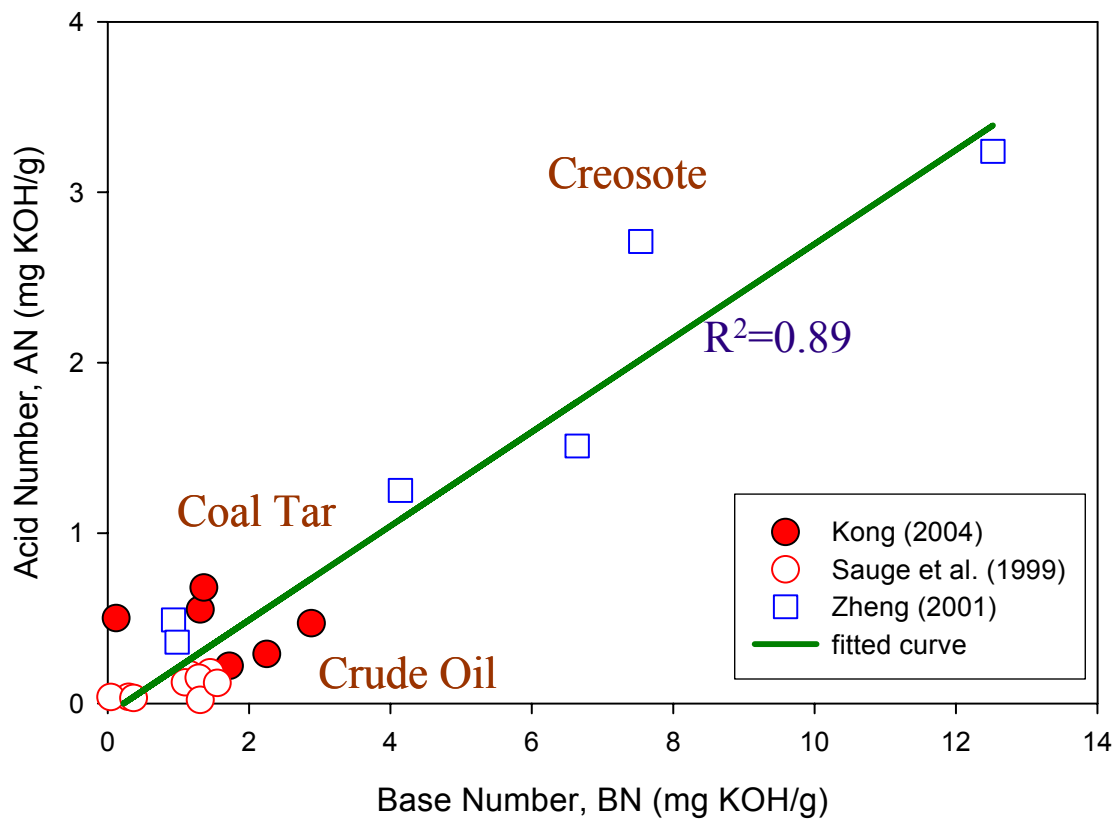


Figure 6-7. Correlations between acid and base numbers.

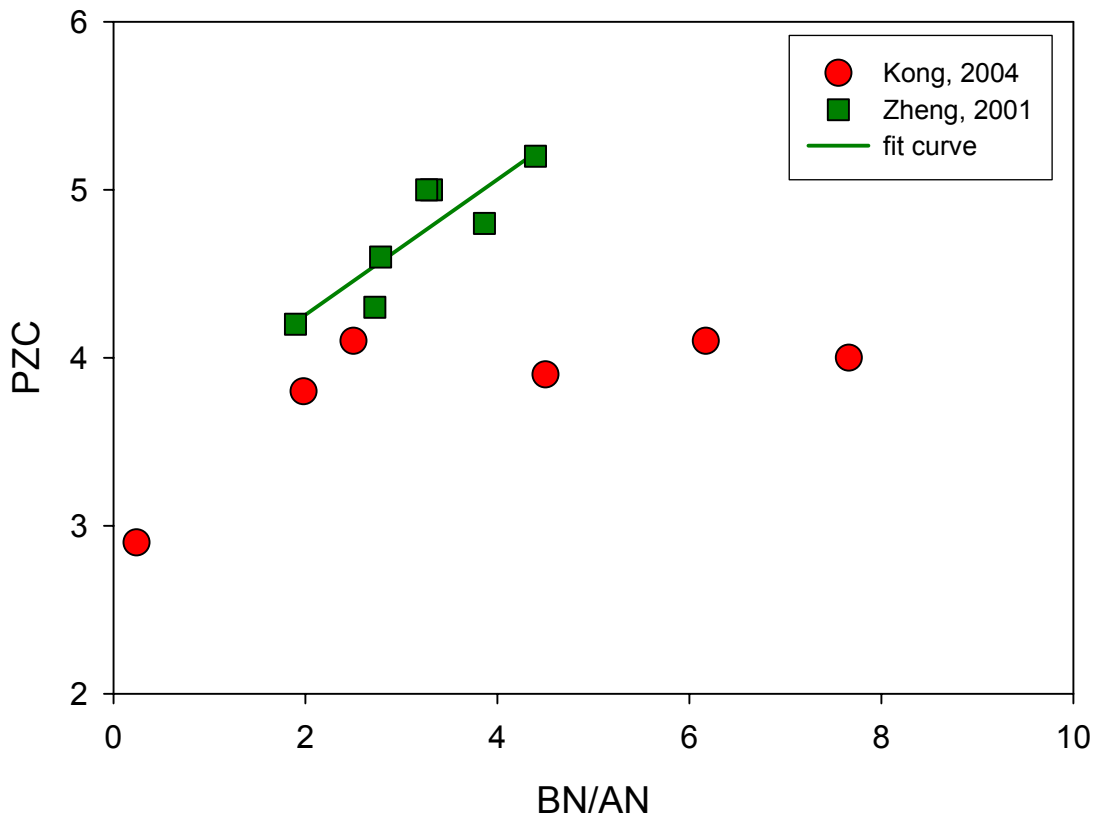


Figure 6-9. PZC as a function of BN/AN ratio (straight line represents the fitting curve for Zheng's data (2001)).

Effect of pH and Ionic Strength on Contact Angle

Effect of pH on Contact Angle

Static contact angle measurements were obtained for the six coal tar samples using microscopy glass slides as the solid surface. The slides were placed in solutions with a specified pH (pH 2.5, 3.5, 4.7, 7.0, 10.0) and a constant NaCl concentration of 0.01 M. In the pH range of 2.5 to 10.0, the contact angles of tar-water-glass systems were in the range of 10.9 to 28.9° for all the coal tar samples, which is consistent with strongly water-wetting conditions (Table 6-4). These data are in agreement with static contact angle measurements reported by Barranco et al. (1997) and Barranco and Dawson (1999), who reported that contact angle values ranged from 18 to 4° in the pH range of 3.4 to 12.4 in coal tar-water-quartz slide system.

The wetting of surfaces by water and oil depends on the surface forces, including van der Waals, electrostatic, and structural or solvation forces (Buckley et al., 1989; Hirasaki, 1991; Israelachvili, 1995; Hohshima and Furusawa, 1998; Zheng et al., 2001; Drummond and Israelachvili, 2002). The thickness and stability of water films existing between the oil (nonwetting phase) and the solid surface are contributed by these forces. The collapse of a thin water film can result in the wettability alteration. The overall interaction energy (W) could be written as

$$W = W_{vdw} + W_{edl} + W_{hyd} \quad (6-6)$$

where, W_{vdw} , W_{edl} and W_{hyd} represent the interaction energy (J) between two surfaces caused by van der Waals force, electric double layer force and hydration force, respectively.

Table 6-4. Contact angles of the six coal tar samples on glass slides as a function of aqueous solution pH.

Coal Tar ID	pH 2.5	pH 3.5	pH 4.7	pH 7.1	pH 10.0
Auburn	13.1 (± 1.6) [*]	18.2 (± 1.5)	18.6 (± 1.2)	13.1 (± 1.9)	12.2 (± 0.9)
Cape May	11.6 (± 2.0)	16.4 (± 1.6)	22.2 (± 2.4)	13.4 (± 2.0)	12.9 (± 1.4)
Charleston	14.7 (± 1.7) [†]	19.3 (± 2.3)	25.5 (± 2.5)	14.0 (± 1.9)	14.6 (± 1.8)
Fairfield	10.1 (± 1.2)	24.6 (± 3.0)	28.9 (± 1.7)	13.1 (± 1.4)	14.3 (± 1.7)
Saranac	13.7 (± 0.9)	21.2 (± 1.1)	22.0 (± 1.8)	14.2 (± 2.3)	12.1 (± 2.2)
Shippensburg	23.8 (± 1.4)	20.5 (± 1.6)	14.4 (± 2.0)	12.3 (± 0.8)	11.4 (± 1.1)

* standard deviation (s. d. = $\sigma/\sqrt{N-1}$)

† measured at pH 2.0.

The non-retarded van der Waals interaction energy (W_{vdw}) between two infinite flat plates can be expressed as

$$W_{vdw}(D) = -\frac{A}{12\pi D^2} \quad (6-7)$$

where, A is the Hamaker constant (J), and D is the separation distance between two parallel surfaces (m).

The electrostatic force is caused by the interaction between the electric double layers of two surfaces, and varies with solution pH, ionic strength and oil composition (Hiemenz, 1986; Israelachvili, 1995). The Poisson-Boltzmann equation (Equation 6-8) is generally used to describe the electrostatic potential as a function of distance from the plate.

$$\frac{d^2\psi}{dx^2} = -\frac{2zen \sinh\left(\frac{ze\psi}{kT}\right)}{\epsilon_r \epsilon_0} \quad (6-8)$$

where ψ is the potential (V), x is the distance from the surface (m), z is the valence of ion, e is the elementary electric charge (C), n is the number density of the ions (mole m^{-3}), ϵ_r is the relative permittivity of solution ($\text{C N}^{-1} \text{m}^{-1}$), ϵ_0 is the permittivity of a vacuum ($\text{C N}^{-1} \text{m}^{-1}$), k is the Boltzmann constant (J/K), and T is the absolute temperature (K). Assuming $ze\psi < kT$, the electric double layer interaction energy (W_{edl}) in a 1:1 electrolyte solution can be written as:

$$W_{edl}(h) = \frac{64n_0 kT \gamma_{i0} \gamma_{j0}}{\kappa} \exp(-\kappa h) \quad (6-9)$$

$$\kappa = \left(\frac{2ne^2}{\epsilon_r \epsilon_0 kT} \right)^{1/2}$$

$$\gamma_0 = \frac{\exp(ze\psi_0 / 2kT) - 1}{\exp(ze\psi_0 / 2kT) + 1}$$

where the subscript i and j represent two interacting surfaces, respectively, κ is the Debye-Hückel parameter, ψ_0 is the potential at the surface (Hiemenz, 1986; Hohshima and Furusawa, 1998).

Structural forces are complicated and not well understood. They could result from hydrophobicity of the surface, or hydrogen bonding, or steric force, etc, and could be attractive or repulsive. For hydrophilic surfaces, the hydration force appears at separation distances below 3-4 nm, and is generally exponentially repulsive (Israelachvili, 1995; Basu and Sharma, 1996). The empirical expression for the hydration interaction energy between two hydrophilic surfaces (W_{hyd}) is as following (Israelachvili, 1995).

$$W_{hyd} = +W_0 e^{-h/\lambda_0} \quad (6-10)$$

where λ_0 and W_0 are coefficients depending on the surfaces.

In many circumstances, DLVO theory, which incorporates van der Waals and electrostatic forces, successfully describes the interactions between two surfaces (Buckley et al., 1989; Ward et al., 1999; Zheng, 2001; Zheng et al., 2001). When the separation between two surfaces is below 5 nm, DLVO theory alone may become insufficient, and the hydration force should be considered (Buckley et al., 1989; Drummond and Israelachvili, 2002). The interaction energy curve as a function of separation distance between coal tar surface and a silica glass surfaces in 0.01 M NaCl solution according to DLVO theory is shown in Figure 6-10a. Hamaker constant in oil-water-silica system is reported in the range of 0.5 to 1.5×10^{-20} J (Buckley et al., 1989; Hirasaki, 1991; Zheng, 2001; Zheng et al., 2001). The Hamaker constant in this

calculation was selected as 1.0×10^{-20} J. To estimate the electric double layer interaction, the measured zeta potential (ψ_i) for Saranac tar was used. The surface zeta potential of glass (ψ_j) as a function of pH in a 0.01 M NaCl solution were obtained from Buckley et al. (1989). All the parameters used in the interaction energy calculations are listed in Table 6-5. At high pH, the repulsive electrostatic force between the negatively charged coal tar and glass surface become dominant due to the dissociated form of the organic acid (A^-). The coal tar must overcome the energy barrier in order to approach the glass surface. At low pH, the organic basic constituents in coal tar exist as their conjugate acid form (BH^+) and organic acid stays at neutral form (HA), the attractive electrostatic interaction between positively charged coal tar and negatively charged glass surface is likely to make the water film between the coal tar and glass surface less stable and lead to a relatively higher contact angle (less water-wetting). In the energy-distance curve (Figure 6-10a), no energy barrier appeared at pH 2.5 and pH 3.4, which implies that coal tar could approach the glass surface and result in an oil-wetting condition. However, a strong water-wetting condition was observed by contact angle values obtained over the pH range evaluated. Therefore, at low pH, the classic DLVO theory was not sufficient to explain the observed contact angle values. Due to the high concentration of H_3O^+ at low pH, the silica surface (SiO^-) may form a strong hydration layer. At the same time, the presence of surface active constituents in coal tar may cause the tar surface to be more hydrated. Thus, the dehydration energy must be overcome for coal tar to approach the glass surface. If this does not occur, the surface will remain water-wetting. Therefore, at pH 2.5 and pH 3.4, an exponentially decreasing hydration energy, as described in Equation (6-10), was incorporated into the energy-distance curve shown in Figure 6-10b.

The value of λ_0 is generally in the range of 0.6-1.1 nm for 1:1 electrolytes such as NaCl, and W_0 depends on the hydration of the surfaces but is usually below 0.003-0.03 J/m² between two hydrophilic surfaces (Israelachvili, 1995). The λ_0 was assumed to be 0.6 nm, and a value of 0.003 J/m² was used for W_0 for this simulation (Table 6-5). An energy barrier appeared after including the hydration energy into the overall interaction energy, indicative of a water-wetting condition even at low pH. In addition to the hydration force, the steric force at low pH may contribute to repulsive force between the coal tar surface and glass surface. The surface active constituents in coal tar accumulated at the tar-water interface can form a “brush-like” surface, which was observed by scanning a bitumen surface in water (Liu et al., 2003). Thus, the steric repulsive force between the extruded positively charged amine head group and silica surface at low pH cannot be neglected, which also contributes to the water film stability at low pH (Israelachvili, 1995).

Although the glass surface displayed strong water-wetting conditions, small changes in contact angle were observed at both low and high pH (Figure 6-11). The pH at which the maximum contact angle occurred was consistent with the PZC. This observation is in agreement with literature report that the wettability transition occurred one pH unit or less above the PZC (Dubey and Doe, 1993). When the solution pH was greater than the PZC of tar, electric repulsive forces between the coal tar and glass surface prevented the coal tar from approaching the glass surface, resulting in a slight decrease in contact angle. For pH values lower than the PZC, the contact angle displayed an apparent increase as pH increased from 2.5 to 4.6. The behavior could result from the competition between the hydration force and DLVO forces. Depending on the amount of organic base functional groups, the hydration force may exceed the electrostatic force

Table 6-5. Parameters used in interaction energy estimation.

Parameters	Values	Zeta potential (mV)	Quartz [†]	Coal tar [‡]
Hamaker constant, A (J)	1.0×10^{-20}	pH 2.6	-17	12.24
electrolyte concentration, (M)	0.01	pH 3.4	-27	4.35
Debye-Hückel parameter, κ (m^{-1})	3.29×10^8	pH 4.5	-37	-24.9
λ_0 (nm)	0.6	pH 5.25	-37	-43.89
W_0 (J/m^2)	0.003	pH 7.0	-37	-52.88
Temperature, T (K)	298	pH 9.8	-37	-60.77
relative permittivity of solution, ϵ_r ($CN^{-1}m^{-1}$)	78.41	[†] Buckley et al., 1989. [‡] Kong, 2004		
permittivity of a vacuum, ϵ_0 ($CN^{-1}m^{-1}$)	8.85×10^{-12}			

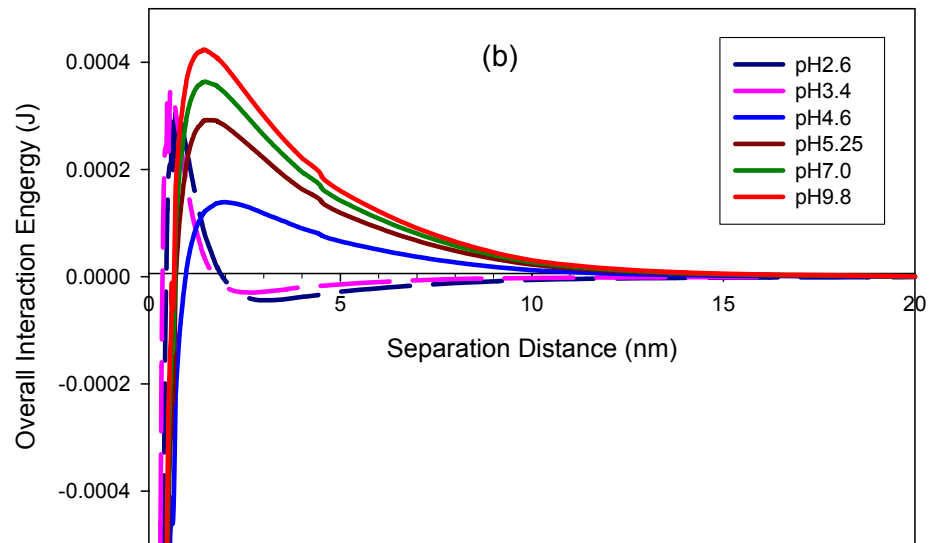
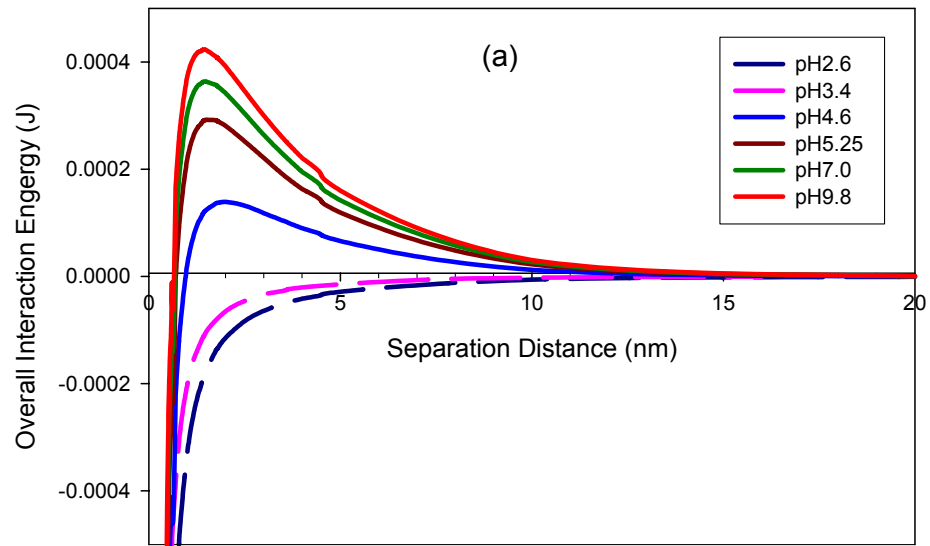


Figure 6-10. Overall interaction energy between silica glass slide and coal tar as a function of separation distance accounting for (a) electrostatic and van der Waals forces (DLVO forces); (b) Both DLVO forces and hydration force.

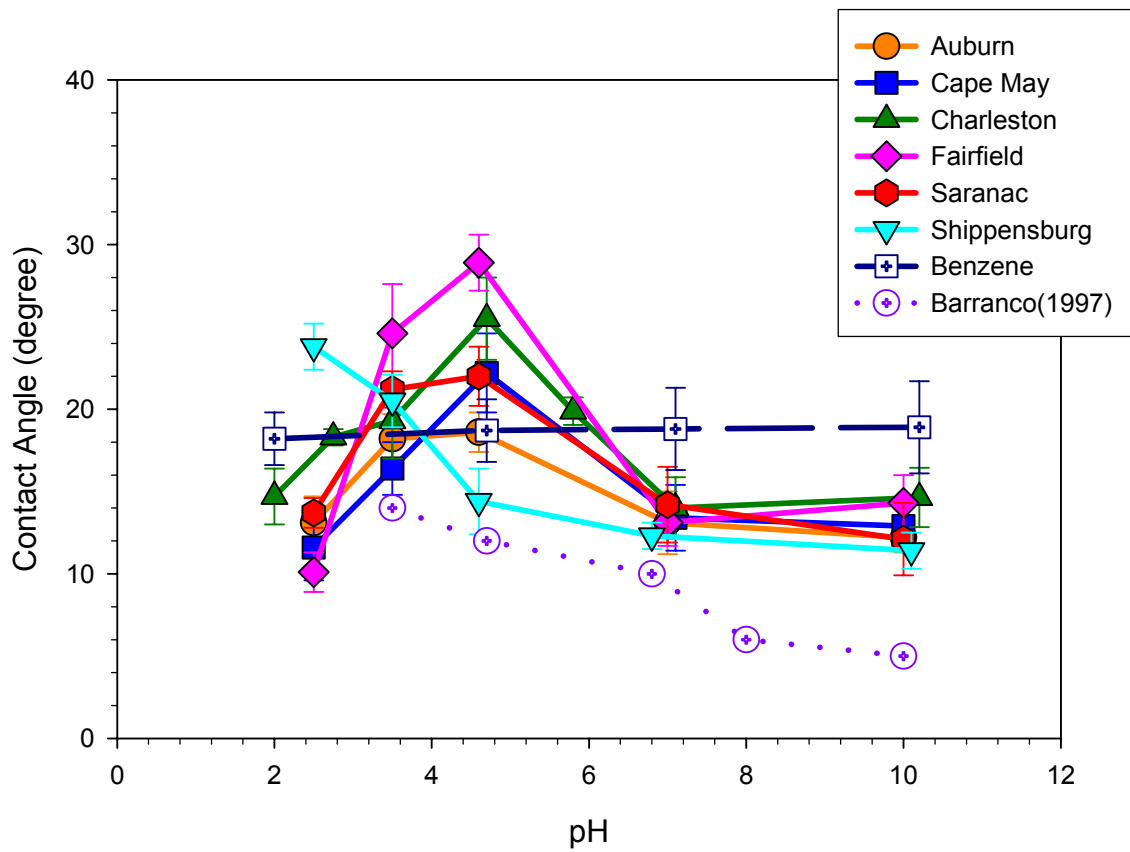


Figure 6-11. Static contact angle as a function of pH for coal tar from six MGP sites.

between coal tar and solid surface, and thereby lead to a more water-wetting condition at very low pH. For the Shippensburg coal tar, the contact angle decrease at low pH during the pH evaluated was not observed due to its relatively low PZC (pH 2.9) and base number (0.12 mg KOH/g tar).

Effect of Organic Acid or Base Addition on Contact Angle

5-indanol (organic acid) and quinoline (organic base) were added to separate samples of Saranac tar at concentrations of 1, 5, 10 and 20% (wt%). The contact angle of coal tar amended with 1% and 10% 5-indanol on a microscopic glass slide in water solution at different pH is listed in Table 6-6. No significant difference with the addition of 5-indanol was found at a significant level of 0.05 through one-way analysis of variance (ANOVA) using Minitab 14 (Minitab, 2004) at pH 2.5 ($P = 0.384$), 7.0 ($P = 0.230$) and 10.0 ($P = 0.944$). At pH 4.6, although statistically significant difference was found ($P = 0.007$), the change of contact angle was less than 6° with the addition of 5-indanol (1% and 10%), which indicates no wettability alternation occurred (Figure 6-12a). At low pH, the added neutral form of 5-indanol is the dominant species; hence it would not be expected to alter the electrostatic force between the coal tar and solid surface, which is caused by the protonated base form and negatively charged glass surface. At high pH, the repulsive force between anionic 5-indanol forms and negatively charged glass surface increased with increasing 5-indanol concentration. However, the contact angle for original coal tar was as low as 13° when pH was greater than 7.0, contact angle lower than this value is hard to be measured due to the existence of impurity, heterogeneity and roughness on the glass surfaces (Standal et al., 1999a). Following the addition of

quinoline to coal tar, the contact angle at a specified pH increased with the increasing amount of quinoline added (Table 6-7). This observation is in agreement with the previous discussion. At low pH, protonated base form (BH^+) with a positive charge is the dominant species. More quinoline was added, the positively charged species increased. Consequently, the attractive interaction between the coal tar (+) and glass (-) surface becomes stronger, and leads to a less water-wetting condition. For example, at $\text{pH } 2.5 \pm 0.1$ the contact angles between coal tar and glass surface were 12.7, 12.8, 39.5, 61.2 and 79.4° with the addition of 0, 1, 5, 10, and 20% (wt) quinoline, respectively. For the coal tar samples without quinoline addition, a slightly decrease in contact angle was obtained when the pH was less than 4.6 ± 0.1 . With the addition of quinoline, the reduction in contact angle at pH values less than 4.6 became less pronounced and no longer observed following addition of quinoline more than 5% (wt). This observation supports the hypothesis that competition between hydration (sorption of H_3O^+) and electric double layer interactions between the protonated cationic quinoline and the silica surface. At low quinoline addition (1% wt), the relationship between contact angle and a function of pH was similar to that of the Saranac tar without quinoline addition (Figure 6-12b). These results indicate that the quinoline concentration was not sufficient to alter the counteracting effect of the hydration and electrostatic forces. At quinoline concentration greater than 5% (wt), the electrostatic attractive force between the protonated-base species and negatively-charged glass surface became sufficient to overcome the hydration force, resulting in a less water-wetting condition. At high pH, the addition of quinoline did not significantly affect the contact angle because the electrostatic force did not change with the addition of quinoline. At high pH, quinoline exists as neutral form (B),

Table 6-6. Effect of 5-indanol concentration on contact angle of Saranac coal tar on glass slides in 0.01 M NaCl solution.

5-indanol concentration (wt%)	pH 2.5	pH 3.5	pH 4.6	pH 7.1	pH 10.0	pH 11.6
0	13.7 (± 0.9) [*]	21.2 (± 1.1)	22.0 (± 1.8)	14.2 (± 2.3)	12.1 (± 2.2)	—
1	14.8 (± 2.0)	19.0 (± 1.0)	22.3 (± 1.3)	15.5 (± 3.0)	12.8 (± 1.2)	13.0 (± 1.3)
10	15.5 (± 1.6)	24.9 (± 2.2)	28.1 (± 1.8)	14.3 (± 1.3)	13.2 (± 1.6)	12.3 (± 1.8)

* standard deviation (s. d. = $\sigma/\sqrt{n-1}$)

Table 6-7. Effect of quinoline concentration on contact angle of Saranac coal tar on glass slides in 0.01 M NaCl solution.

Quinoline concentration (wt%)	pH 2.5	pH 3.5	pH 4.6	pH 7.1	pH 10.0
0	13.7 (± 0.9) [*]	21.2 (± 1.1)	22.0 (± 1.8)	14.2 (± 2.3)	12.1 (± 2.2)
1	12.8 (± 1.3)	20.6 (± 1.9)	21.7 (± 2.0)	17.0 (± 1.8)	12.3 (± 2.0)
5	39.5 (± 1.6)	40.3 (± 2.4)	33.8 (± 2.7)	23.3 (± 2.6)	12.8 (± 1.4)
10	61.2 (± 2.1)	57.5 (± 2.9)	55.8 (± 1.4)	40.9 (± 2.8)	14.9 (± 1.9)
20	79.4 (± 3.5)	72.4 (± 3.1)	60.9 (± 3.8)	47.9 (± 3.7)	12.7 (± 1.3)

^{*} standard deviation (s. d. = $\sigma/\sqrt{n-1}$)

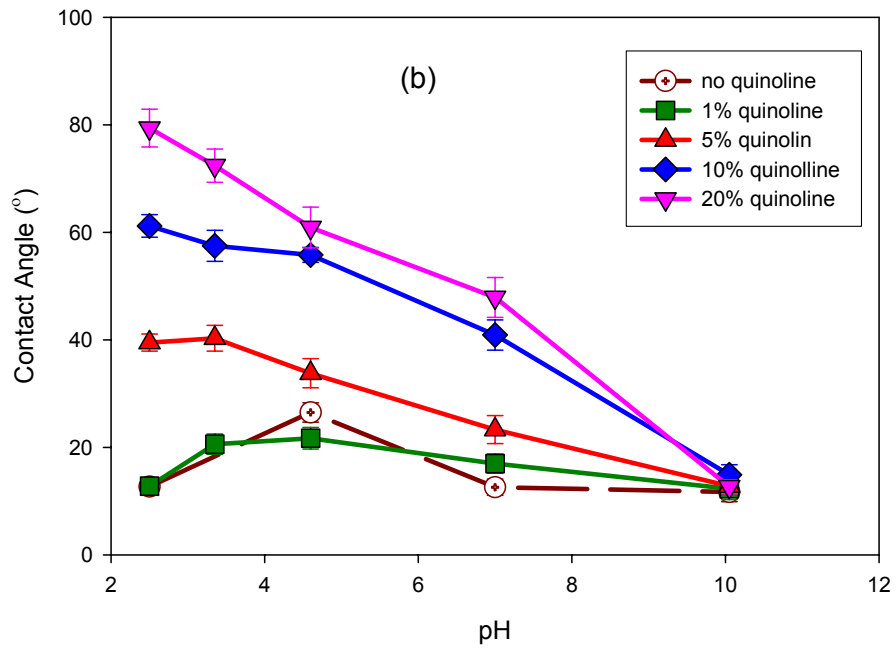
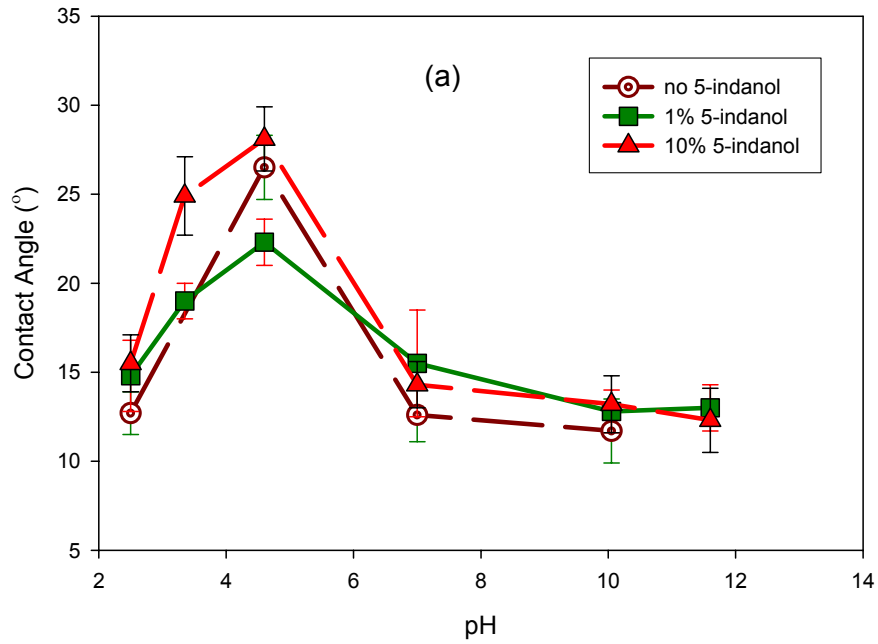


Figure 6-12. Contact angle as a function of pH with the addition of 5-indanol (a) and quinoline (b) to Saranac coal tar.

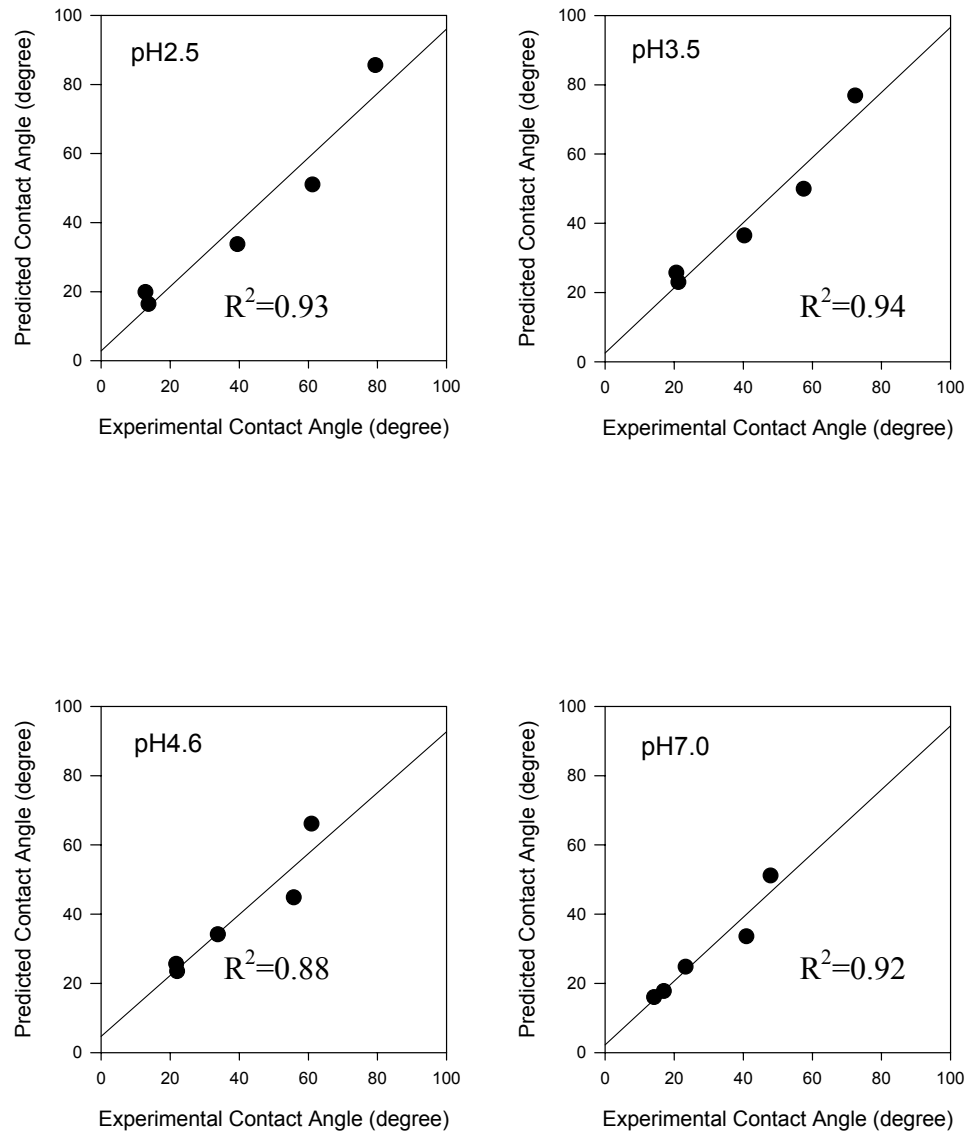


Figure 6-13. Correlations between contact angle and AN, BN and addition of quinoline to Saranac coal tar.

which does not change the repulsive force between the coal tar and glass surfaces.

In order to evaluate the relationship between contact angle and acidic and basic constituents in coal tar, correlations between contact angle and BN/AN ratio as well as 5-indanol or quinoline concentration were developed. Wettability is believed to relate to the BN/AN ratio rather than AN or BN separately (Buckley, 1994; Skauge et al., 1999). The following equation was employed:

$$\omega = a_1(BN / AN) + a_2(Q) + a_3 \quad (6-11)$$

where, ω refers to the contact angle ($^\circ$), Q is the amount of quinoline added (wt%), and a_1 , a_2 , a_3 are fitting coefficients determined by fitting experimental data to Equation (6-11). Figure 6-13 shows that the model-predicted contact angle values using Equation (6-11) fit measured contact angle values within the low to neutral pH range very well, where R^2 is nearly equal to 1. The strong correlation illustrates that contact angle is sensitive to the acid and base constituents in coal tar phase, particularly at high base (quinoline) constituent content (Q).

Effect of Ionic Strength on Contact Angle

Contact angles of Saranac tar on glass slide in the absence and presence of NaCl (0.5M) were measured. The measured contact angles exhibited a slightly decrease with increasing ionic strength (Figure 14a). This trend could be easier to be observed when Saranac tar was amended with 10% quinoline (Figure 14b). For example, at pH 4.6 ± 0.1 , the contact angle was 64.0 , 55.8 , 47.0 and 30.2° at a NaCl concentration of 0, 0.01, 0.1 and 0.5 M, respectively (Table 6-8). These observations could be attributed to the electrostatic force, steric effect and “salting out” effect.

The addition of salt to an aqueous solution can break the existing H-bonding between water molecules and polar organic compounds, which results in the “salting out” of organic polar compounds or polar functional groups from the aqueous phase (Gaonkar, 1992; Standal et al., 1999; Moran et al., 2000). On the other hand, if the polar group is ionized, the electrical repulsive potential of the interface and steric force tend to expel the adsorption of ionized polar molecules from accumulating at the interface (Davies and Rideal, 1963). Buckley et al. (1989) measured the zeta potential values of crude oil droplets and suspensions of microscope slide glass. The absolute values of zeta potential at the oil and glass surfaces were observed decreasing as the NaCl concentration increasing, indicating less ionized species at the oil and glass surfaces with increasing salinity. In the tar-water-glass systems considered here, asphaltenes containing in coal tar are complex molecules with many polar atoms such as N and O, which could form H-bonding with water molecules, resulting in the accumulation of this molecules at the tar-water interface. As the salt concentration in solution increase, some of the existing H-bonding break, causing a self-association of the asphaltene molecules (Roberts et al., 1996a, b; Sheu and Mullins, 1995). Therefore, the surface-active molecules at the interface decrease with the increasing of ionic strength. In addition, the ionized groups accumulated at the coal tar-water interface could prevent the “salted out” ions or functional groups from locating at the interface due to the repulsive electrostatic force.

Over a pH range of 2.5 to 7.0, the protonated base form (BH^+) was prevented from entering the aqueous phase due to the “salting out” effect, whereas the repulsive electrostatic force and steric effect limited the accumulation of the positively charged basic groups at the tar-water interface. Hence the HB^+ constituent might be forced back

into the coal tar phase. Consequently, the attractive interaction between the positively charged tar phase and negatively charged silica surface was reduced, leading to a less oil-wetting and more water-wetting condition as salinity increased (Figure 6-14).

Effect of pH and Ionic Strength on Tar-Water IFT

Effect of pH on Tar-Water IFT

The IFT of each coal tar sample was measured as a function of pH at constant NaCl concentration of 0.01 M. The measured IFTs ranged from 13.8 to 26.4 dynes/cm over the pH range considered (Table 6-9). These values are much lower than the IFT between the pure nonpolar organic chemicals and water, such as TCE, PCE, and benzene with IFT of 32.8, 47.5 and 35.0 dynes/cm, respectively (Demond and Lindner, 1993). These data suggest that the polar function groups in coal tar accumulate at the tar-water interface, and thereby lowered the IFT between tar and water as compared to pure nonpolar organic chemicals.

At both high and low pH, the IFTs were lower than in neutral pH range (Figure 6-15). This observation was attributed to the existence of deprotonated organic acid species at higher pH, and ionized basic organic compounds at low pH. Lord et al. (2000) observed that dodecylamine partitioned into *o*-xylene, and exhibited minimal activity at the *o*-xylene-water interface, while the protonated dodecylamine species remained in the aqueous phase and resulted in an IFT reduction. Zheng and Powers (2003) suggested that deprotonated acids and protonated bases are more surface-active than their corresponding neutral forms. In tar-water systems investigated herein, at low pH, the positively charged protonated organic base form (BH^+) are likely responsible for the IFT reduction.

Table 6-8. Effect of NaCl concentration on the contact angle of Saranac coal tar (amended with 10% (wt) quinoline) on glass slides.

NaCl Concentration (M)	pH 2.5	pH 3.5	pH 4.6	pH 7.1	pH 10.0
0	68.5 (±1.6)*	64.8 (±1.0)	64.0 (±2.4)	48.0 (±1.6)	12.3 (±1.6)
0.01	61.2 (±2.1)	57.5 (±2.9)	55.8 (±1.4)	40.9 (±2.8)	14.9 (±1.9)
0.1	55.8 (±4.7)	51.8 (±3.2)	47.0 (±5.0)	13.2 (±1.6)	12.3 (±1.8)
0.5	55.3 (±1.9)	47.2 (±3.9)	30.2 (±3.8)	14.2 (±1.0)	13.0 (±1.4)

* standard deviation (s. d. = $\sigma/\sqrt{n-1}$)

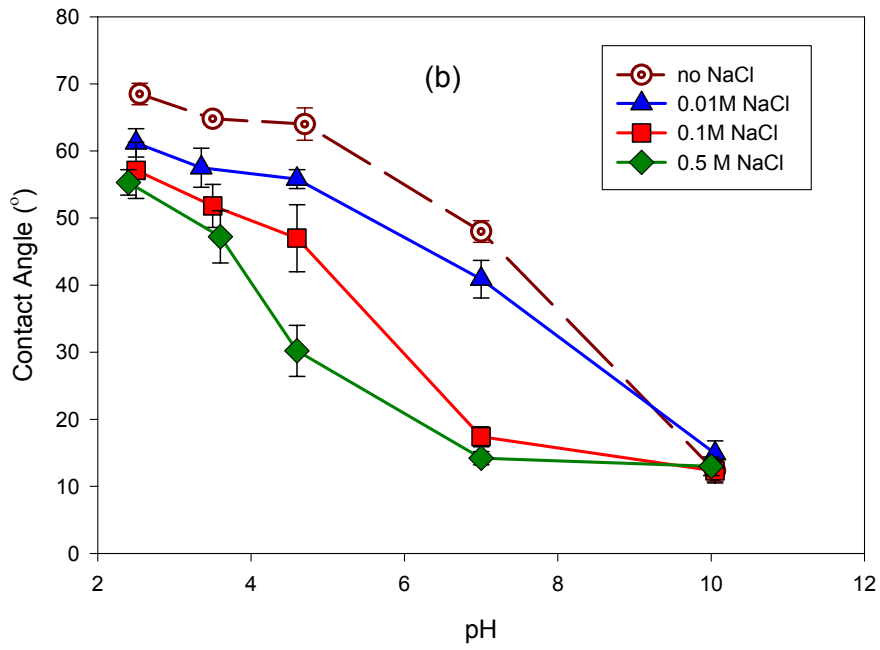
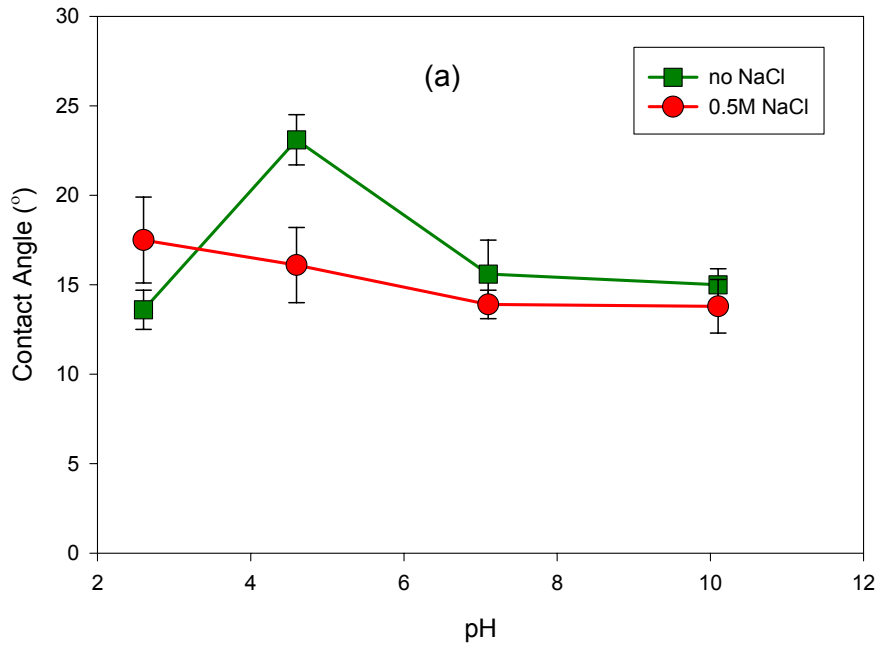


Figure 6-14. Contact angles of Saranac tar (a) and Saranac tar amended with 10% (wt) quinoline (b) on microscope glass slide as a function of aqueous pH at different NaCl concentrations.

Table 6-9. Tar-water IFT as a function of pH for six coal tar samples.

Coal Tar ID	pH 2.6	pH 4.6	pH 7.0	pH 10.0
Auburn	17.78 (± 0.11) [*]	26.12 (± 0.29)	26.36 (± 1.23)	18.43 (± 0.51)
Cape May	17.03 (± 0.01)	22.91 (± 0.99)	22.61 (± 0.10)	15.51 (± 0.20)
Charleston	18.78 (± 0.56) [†]	21.90 (± 0.69)	20.73 (± 0.43)	15.61 (± 0.72)
Fairfield	13.81 (± 0.14)	23.75 (± 1.36)	23.24 (± 0.31)	17.59 (± 0.27)
Saranac	18.48 (± 0.23)	23.73 (± 0.30)	24.14 (± 0.94)	14.24 (± 0.56)
Shippensburg	22.05 (± 0.18)	22.82 (± 0.16)	21.88 (± 0.11)	17.93 (± 0.29)

* standard deviation (s. d. = $\sigma/\sqrt{n-1}$)

† measured at pH 2.0.

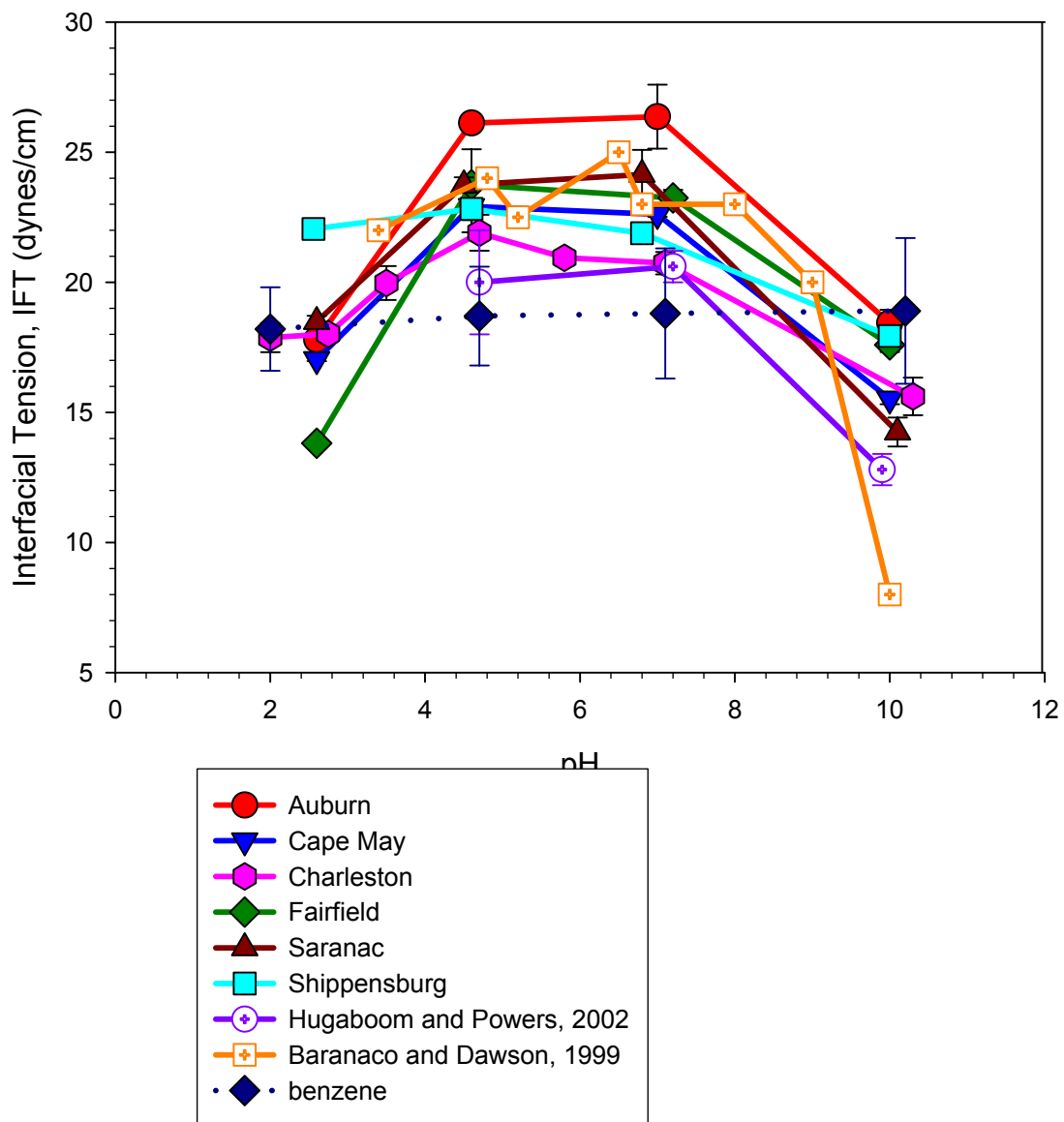


Figure 6-15. Interfacial tension (IFT) as a function of pH for six coal tar samples.

Similarly, at high pH, the negatively charge conjugate base (A^-) of organic acid (HA) may be responsible for the observed IFT reduction. Barranco and Dawson (1999) also suggested that the tar-water IFT was more sensitive to acidic organic compounds at high pH than basic organic compounds at neutral to low pH.

Effect of Organic Acid/Base Addition on Tar-Water IFT

5-indanol (organic acid) and quinoline (organic base) were added to separate samples of Saranac tar at concentrations of 1, 5, 10 and 20% (wt%). The addition of 5-indanol and quinoline caused the reduction in IFT between coal tar phase and water with a NaCl concentration of 0.01 M at different pH. The reduction in IFT increased with the concentration of 5-indanol or quinoline. For example, at pH 7.0 ± 0.1 , IFT was 24.1, 23.5, 18.2, 15.9, and 12.5 dynes/cm with 0, 1, 5, 10, 20% (wt) addition of 5-indanol, respectively (Table 6-10, Figure 6-16a). IFT decreased from 24.1 dynes/cm to 14.1 dynes/cm as the addition of quinoline increased from 0 to 20% (wt) (Table 6-11, Figure 6-16b). The IFT reduction can attributed to the accumulation of surface active species such 5-indanol or quinoline at the tar-water interface. The more surface active molecules at the tar-water interface, the more the reduction of IFT. The Gibbs adsorption equation describes the relationship between the IFT reduction and the concentration of surface active species at the interface (Davies and Rideal, 1963):

$$-d\gamma = RT\left(\sum_i \Gamma_i d \ln(a_i)\right) \quad (6-12)$$

where γ is the interfacial tension ($N m^{-1}$), R is the universal gas constant ($8.31 J mol^{-1} K^{-1}$), Γ_i is the surface excess of species i ($mol m^{-2}$), and a_i is the activity of species i adsorbed at the interface ($mol L^{-1}$). The Gibbs equation implies that the IFT reduction is

proportional to the concentration of surface active species at the interface. Quinoline and 5-indanol, which were added to Saranac coal tar, could act as surface active species, accumulating at the tar-water interface and thereby reducing the tar-water IFT. Since the exact composition of Saranac coal tar is unknown, it is difficult to predict the organic acid or base constituent effect on IFT using the existing empirical correlations. Peters and Luthy (1993) proposed a pseudo-component simplification by representing the coal tar as a single component. Applying the pseudo-component concept, a reasonable linear correlation between the tar-water IFT and amount of 5-indanol or quinoline added at pH 7.0 was obtained ($R^2 = 0.93$ and 0.97 for 5-indanol and quinoline addition, respectively) (Figure 6-17). This indicates that the IFT was largely controlled by the surface active species which accumulate at the tar-water interface.

Comparing the effect of amending species (i.e. 5-indanol and quinoline) on the magnitude of IFT reduction, it was observed that 5-indanol had a slightly greater impact than quinoline (Figure 6-18). This difference likely results from their structural difference between the compounds. For 5-indanol, the oxygen atom is not incorporated within the ring structure, while the nitrogen atom in quinoline is located on the hetero-ring. As a result, both an inductive effect caused by the O atom and a resonance effect caused by the electron in O atom and π -electrons on aromatic ring exist for 5-indanol, whereas only a resonance effect exists in quinoline. Thus H-bonding between 5-indanol and water may be stronger than that between quinoline and water (Schwarzenbach et al., 2003), which could result in greater accumulation of 5-indanol at the tar-water interface.

The same linear regression used Equation (6-11) was employed to the IFT as a function of BN/AN ratio and amount of acid or base added to Saranac coal tar. Figure 6

Table 6-10. Effect of 5-indanol concentration on IFT between Saranac tar (added with 10% wt 5-indanol) and water with 0.01 M NaCl.

Addition of 5-indanol in coal tar (wt%)	pH 2.5	pH 4.6	pH 7.0	pH 11.0
0	18.48 (± 0.23) [*]	23.73 (± 0.30)	24.14 (± 0.94)	14.24 (± 0.56) [†]
1	19.34 (± 0.22)	23.54 (± 0.53)	23.49 (± 0.70)	11.22 (± 0.16)
5	17.56 (± 0.22)	19.13 (± 0.28)	18.18 (± 0.10)	11.23 (± 0.16)
10	15.12 (± 0.14)	15.99 (± 0.11)	15.86 (± 0.09)	12.85 (± 0.08)
20	12.60 (± 0.23)	12.41 (± 0.24)	12.25 (± 0.07)	9.87 (± 0.15)

^{*} standard deviation (s. d. = $\sigma/\sqrt{n-1}$)

[†] measured at pH 10.0

Table 6-11. Effect of quinoline concentration on IFT between Saranac coal tar (amended with 10% (wt) quinoline) and water with 0.01 M NaCl.

Addition of quinoline in coal tar (wt%)	pH 2.5	pH 4.6	pH 7.0	pH 11.0
0	18.48 (± 0.23) [*]	23.73 (± 0.30)	24.14 (± 0.94)	14.24 (± 0.56) [†]
1	20.24 (± 0.26)	23.18 (± 0.28)	22.59 (± 0.06)	14.32 (± 0.31)
5	20.82 (± 0.20)	20.84 (± 0.16)	20.20 (± 0.10)	12.09 (± 0.17)
10	18.50 (± 0.43)	18.45 (± 0.13)	17.85 (± 0.16)	12.38 (± 0.20)
20	15.59 (± 0.22)	14.57 (± 0.11)	14.14 (± 0.03)	8.65 (± 0.10)

^{*} standard deviation (s. d. = $\sigma/\sqrt{n-1}$)

[†] measured at pH 10.0.

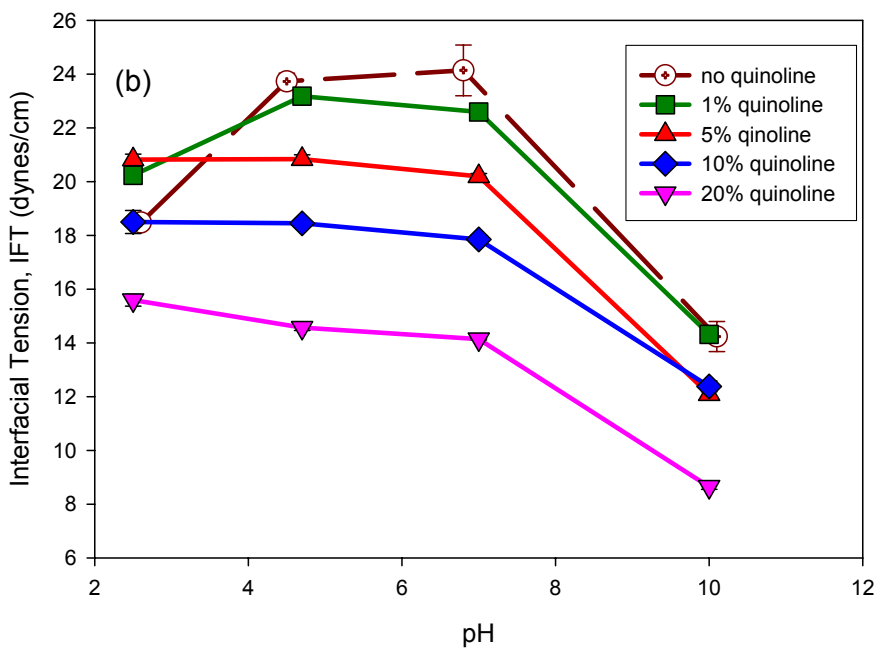
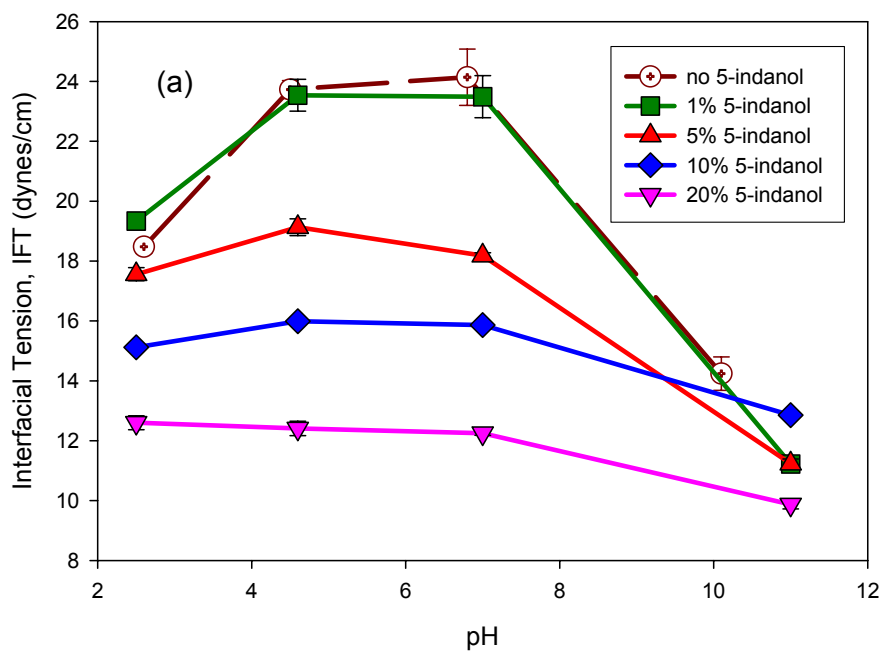


Figure 6-16. IFT as a function of pH with the addition of 5-indanol (a) or quinoline (b) to Saranac tar.

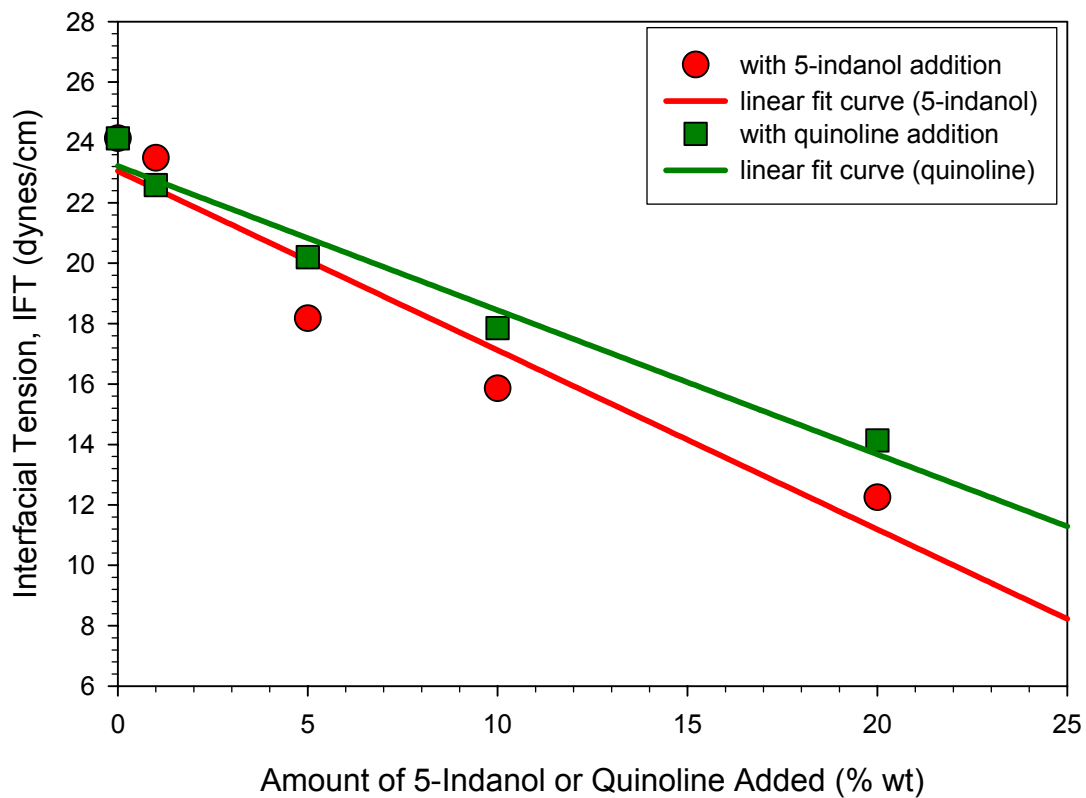


Figure 6-17. Correlations between tar-water IFT and the amount of 5-indanol or quinoline added to Saranac tar at pH 7.0 ($R^2=0.92$ for linear fit of data with 5-indanol addition, and $R^2=0.97$ for linear fit of data with quinoline addition).

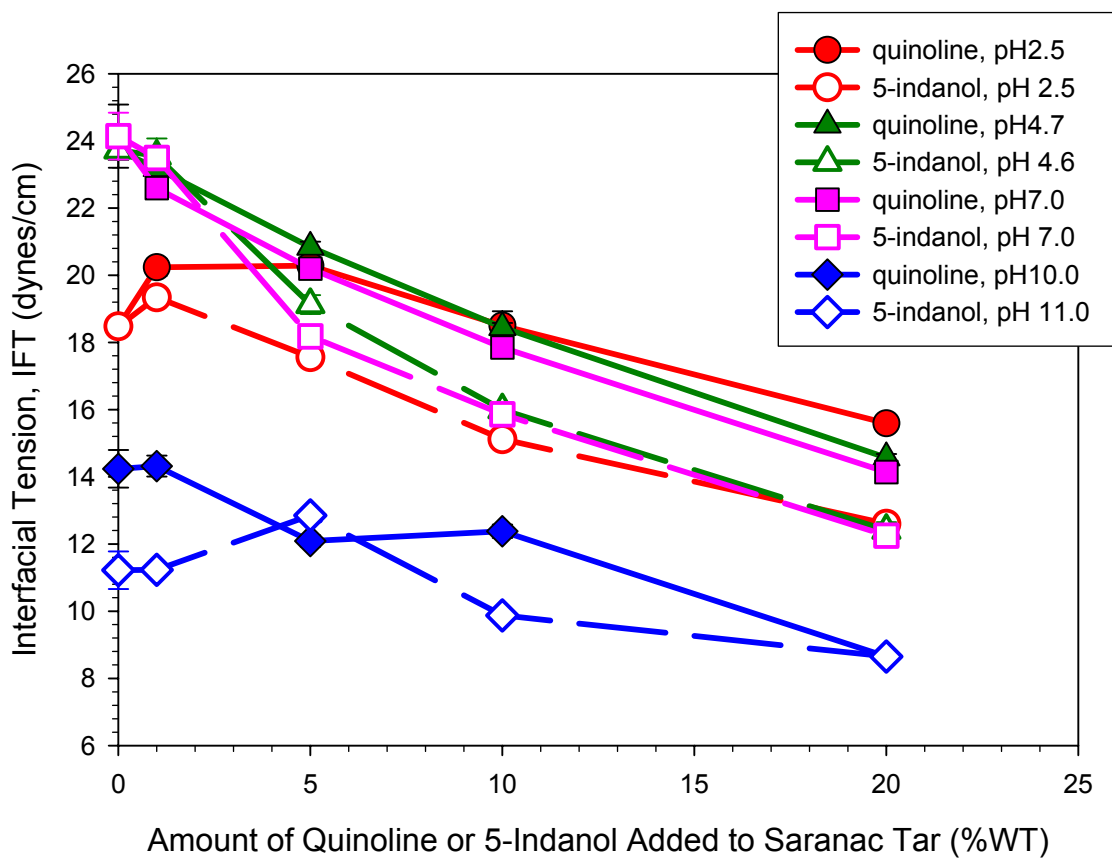


Figure 6-18. Comparison of IFT reduction with the addition of quinoline or 5-indanol to Saranac tar as a function of pH.

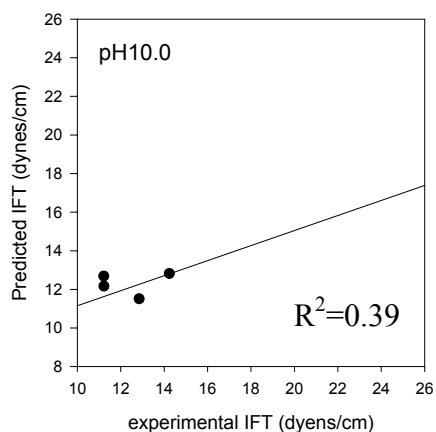
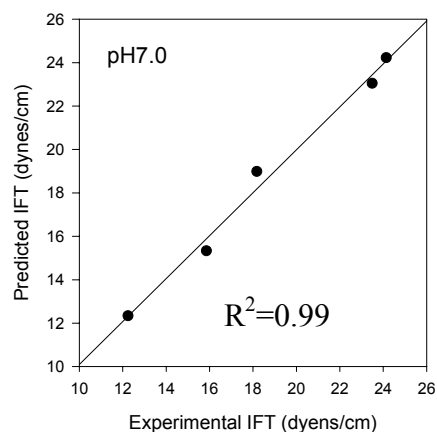
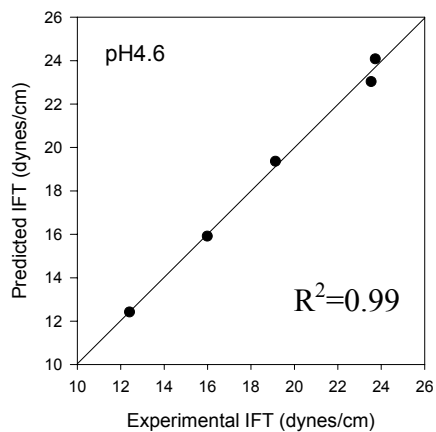
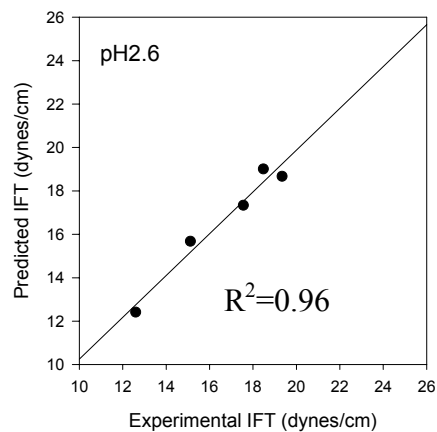


Figure 6-19. Correlations between IFT and AN, BN, addition of 5-indanol to Saranac coal tar.

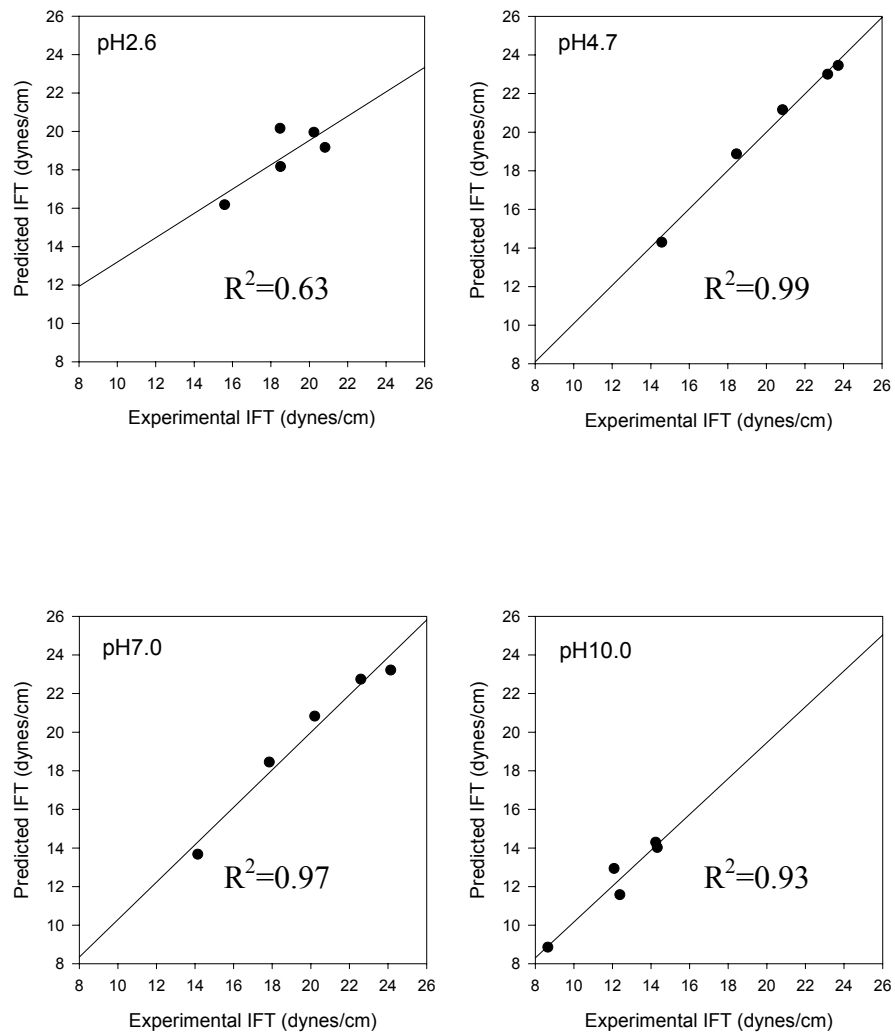


Figure 6-20. Correlations between IFT and AN, BN, addition of quinoline to Saranac coal tar.

19 and 6-20 show that the IFT was strongly correlated to the BN/AN ratio and amount of acid or base added at low to neutral pH. In general, the IFT increased with increased BN/AN and addition of 5-indanol or quinoline.

Effect of Ionic Strength on IFT

The IFT between Saranac tar and water was measured in the absence and presence of NaCl (0.5 M) over a pH range of 2.5 to 10.0. The measured tar-water IFT shows that IFT increase with increase ionic strength. For example, the IFT increased from 23.7 dynes/cm with no NaCl added to 29.2 dynes/cm with a NaCl concentration of 0.5 M at pH 4.7 (Table 6-12 and Figure 6-21a). This observation could be explained by the electrostatic force, steric effect and “salting out” effect. As discussed in previous section, tar-water IFT is proportional to the concentration of surface active molecules at the tar-water interface. As ionic strength increased, some of the H-bonding could break, resulting in fewer surface active molecules accumulating at the tar-water interface, and thereby caused the tar-water IFT increasing (Sheu and Mullins, 1995; Roberts et al., 1996 a, b). In addition, the ionized groups accumulated at the coal tar-water interface could prevent the “salted out” ions or functional groups from locating at the interface due to the repulsive electrostatic force. To evaluate this hypothesis, 10% of quinoline was added to both Saranac tar and benzene (a nonionizable organic liquid). Over a pH range of 2.5 to 7.0, the tar-water IFT showed a slightly increase (less than 1 dynes/cm) when NaCl concentration was lower than 0.1 M, and more pronounced increase (~7 dynes/cm) when the NaCl concentration was increased to 0.5 M (Figure 6-21b). For benzene-water systems, an IFT reduction of approximately 4 dynes/cm was observed when 0.5 M NaCl

was added to the aqueous solution over a pH range of 2.5 to 10.0 (Figure 6-21c). This finding is consistent with literature data in other pure non-ionizable organic-water systems, such as *o*-xylene-water and isooctane-water systems (Lord, et al., 1997b; Standal, et al., 1999a). Benzene, *o*-xylene and isooctane are nonionizable compounds. Therefore, the electrostatic force between the neutral oil phase and the “salted out” surface active ions are negligible. Under this circumstance, the “salting out” effect is dominant and can result in more surface active compounds accumulating at the interface and reduce the oil-water IFT. Therefore, contact angle and IFT in systems containing coal tars behavior differently from those containing nonionizable organics with respect to variation in ionic strength.

Effect of pH on Capillary Pressure-Saturation Relationships in Coal Tar-Water-Silica Sand System

Capillary pressure-saturation (P_c - S) relationships were investigated in Saranac coal tar-water-F-70 Ottawa sand system at pH 4.6 ± 0.1 , pH 7.0 ± 0.1 and pH 10.0 ± 0.1 at room temperature (22 ± 1 °C). Saranac coal tar was selected as the representative coal tar in this experiment. The P_c - S relationship during water drainage and spontaneous imbibition process was shown in Figure 6-22.

By fitting the experimental data during water drainage process to the Brook-Corey equation (Equation 2-12), the entry pressures of the nonwetting phase at different pH in tar-water system were obtained (Table 6-14). Compared to the water drainage curve in air-water system, the coal tar entry pressures in F-70 Ottawa sand were higher than the air entry pressure in the same sand. The coal tar entry pressures ranged from 36.8

Table 6-12. Effect of NaCl concentration on the IFT between Saranac coal tar and water.

NaCl concentration (M)	pH 2.5	pH 4.6	pH 7.0	pH 10.1
0	18.42 (± 0.23) [*]	23.73 (± 0.60)	24.14 (± 0.94)	14.24 (± 0.56)
0.5	13.93 (± 0.08)	29.18 (± 0.20)	28.42 (± 0.16)	14.31 (± 0.37)

^{*} standard deviation (s. d. = $\sigma/\sqrt{n-1}$)

Table 6-13. Effect of NaCl concentration on the IFT between Saranac coal tar (amended with 10% (wt) quinoline) and water.

NaCl concentration (M)	pH 2.5	pH 4.6	pH 7.0	pH 10.1
0	18.42 (± 0.23) [*]	17.94 (± 0.06)	17.67 (± 0.12)	12.87 (± 0.06)
0.01	18.50 (± 0.43)	18.45 (± 0.13)	17.85 (± 0.16)	12.38 (± 0.20)
0.1	19.14 (± 0.14)	18.90 (± 0.16)	18.15 (± 0.16)	9.22 (± 0.17)
0.5	25.24 (± 0.30)	25.08 (± 0.13)	23.25 (± 0.18)	9.98 (± 0.13)

^{*} standard deviation (s. d. = $\sigma/\sqrt{n-1}$)

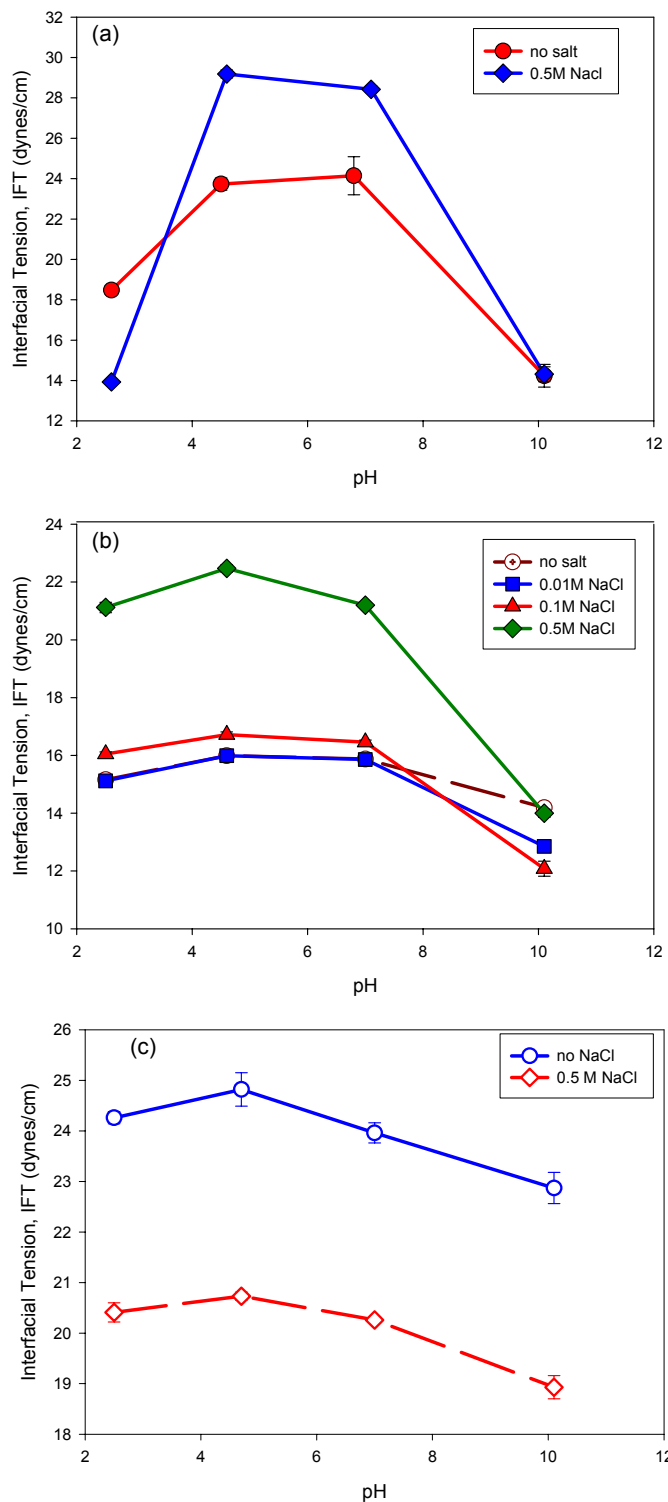


Figure 6-21. IFT between Saranac and water as a function of pH at two different NaCl concentrations (a) Saranac tar without quinoline amended; (b) Saranac tar amended with 10% quinoline; (c) benzene amended with 10% quinoline.

cm of water at pH 4.7 to 56.5 cm of water at pH 10.0, which was consistent with the wettability results at different pHs. The contact angle values decreased as pH increase from pH 4.7 to pH 10.0, which corresponding to a wettability varied from relatively less water wetting to more water wetting. At pH 4.7, the silica sand was relatively more oil-wetting, which indicated easier entry of coal tar. At pH 10.0, the sand was more water-wetting, which may result in a higher coal tar entry pressure. In previous experiments (Demond and Roberts, 1991), the entry pressures of the nonwetting phase (dodecane, o-xylene, TCE and n-butyl acetate) decreased with decreasing oil-water interfacial tension. But in this experiment, the entry pressure increased with decreasing interfacial tension. The data suggested that tar-water interfacial tension was not the only factor governing the nonwetting phase entry pressure, and wettability effects could dominant the IFT effect. In addition, the high viscosity of coal tar might contribute to the overall high entry pressure values.

With respect to residual water saturation during the water drainage process, the residual water saturation in tar-water system was much higher than that in air-water system. For the coal tar-water system, the residual water saturation values ranged from $0.589 \text{ cm}^3/\text{cm}^3$ at pH 4.7 to $0.817 \text{ cm}^3/\text{cm}^3$ at pH 10.0. The trend of residual saturation decrease with pH increasing was in agreement with the contact angle decrease (water wetting conditions increase) with increasing pH. However, the residual water saturation values were higher than the literature reported values in coal tar-water system (Barranco and Dawson, 1999; Hugaboom and Powers, 2002). To explain this apparent contradicts, the following two aspects need to be considered: 1) Coal tar used in this study has a viscosity of 63 cP, whereas the viscosity of coal tar used in other studies are less than 20

cP; 2) F-70 Ottawa sand used herein had a lower mean particle size and broader range of particle size distribution than those used in literature (Table 6-15).

During the water imbibition process, the water saturation remained constant when the capillary pressure decreased from 200 cm to 50 cm of water. This observation was interpreted that capillary forces no longer acted to imbibe water into the media once coal tar wetting occurred (Barranco and Dawson, 1999). The residual coal tar saturation ranged from 0.10 cm³/cm³ at pH 10.0 to 0.38 cm³/cm³ at pH 4.7, which was consistent with relatively higher water wetting condition of Ottawa sand at pH 10.0 and lower water wetting condition at pH 4.7. However, the residual coal tar saturation values at pH 7.0 and pH 10.0 were 0.18 cm³/cm³ and 0.10 cm³/cm³, respectively, which were much lower than reported values, which were approximately 0.30 in Hugaboom and Powers' experiment (2002) and over 0.50 cm³/cm³ in Barranco's work (1999). Due to the high nonwetting phase viscosity and small medium pore size, the coal tar tend to form viscous finger or channels through the column, which results in a higher water residual saturation and low coal tar saturation. Dekker and Ritsema (1995) reported that fingerlike wetting patterns was restricted to fine over coarse-textured soils and homogeneous sandy soils. This was confirmed by taking apart the column after the experiments, and some areas of the soil core were found to be bypassed by coal tar.

Leverett's scaling factor has been widely used to predict the capillary pressure-saturation (P_c - S) relationship in an organic-water system based on that measured for air-water system. In the previously investigated systems, the viscosity ratio of organic and water was approximately equal to 1 so that the effect of viscosity ratio on relative permeability could be neglected (Demond and Roberts, 1991). In this study, Leverett's

function was first applied to high viscosity ratio NAPL-water system. Three approaches of scaling were considered. In case I, an IFT ratio was used as scaling factor, $\frac{(\gamma)_{tar/water}}{(\gamma)_{air/water}}$.

In this case, the scaled capillary pressure $P_{air/water}$ ($P_{tar/water} = \frac{(\gamma)_{tar/water}}{(\gamma)_{air/water}} P_{air/water}$) was

substitute for the capillary pressure $P_{air/water}$ and the water saturation data (S) were not changed. The resulted P - S data were then fit into the van Genuchten equation (Equation 2-13) using SigmaPlot 2000. The fitting parameters are listed in Table 6-16. The resulted P_c - S relationships from the air-water systems should describe the corresponding P_c - S relationship in the tar-water systems according to Leverett's function. However, Figure 6-23a shows that this scaling approached failed to describe the experimental data in tar-water system. Demond and Roberts (1991) used effective water saturation in the place of water saturation to reduce the effect of residual saturation and found the scaling P_c - S_e relationship fit the experiment data well, which was not the case in Saranac tar-water system (Figure 6-23b). Case II: Contact angle (ω) was added to the scaling factor,

$\frac{(\gamma \cos \omega)_{tar/water}}{(\gamma \cos \omega)_{air/water}}$, and no observable improvement were found (Figure 6-23c, d). In case

III, considering the high tar-water viscosity ratio compared to commonly encountered oil-

water system, a viscosity ratio term, $\left(\frac{\eta_{tar}}{\eta_{water}}\right)^{0.4}$ (Abrams, 1975), was incorporated into

the scaling factor and resulted in a new scaling factor, $\frac{(\gamma \cos \omega)_{tar/water}}{(\gamma \cos \omega)_{air/water}} \left(\frac{\eta_{tar}}{\eta_{water}}\right)^{0.4}$. It was

found that the scaled curve fit the experiment data well, especially at pH 4.7 and pH 7.0.

From the three scaling approaches applied here, it showed that the high tar-water

viscosity ratio might be responsible for the failure of the scaling from air-water system in Case I and II. In order to improve the prediction, it is necessary to reduce the occurrence of viscous fingering and seek better scaling factors.

The three scaling approaches were also compared statistically using the Root Mean Square Error (RMSE) (Karagunduz et al., 2001):

$$RMSE = \sqrt{\frac{1}{n-1} \sum_{i=1}^n (M_i - P_i)^2} \quad (6-12)$$

where, M is the measured value, P is the predicted value and n is the number of measured data points. Figure 6-25 shows the RMSE of each scaling approach at pH 4.7, pH 7.0 and pH 10.0. The RMSE in Case III is much lower than those in Case I and Case II, which indicate the scaling factor incorporating viscosity ratio factor predicts the experiment data much better in tar-water-sand systems. Case I and Case II shows no significant difference at a significant level of 0.05 ($P = 0.976$) in one-way ANOVA analysis (Minitab, 2004).

In general, the capillary pressure-saturation relationships are considered to be dependent on fluid phase properties, porous media pore size and pore distribution, interfacial properties, as well as drainage and imbibition rate. The fluid phase, porous medium and experiment method will greatly influence the experimental results (Dullien, 1992). In the coal tar-water system, the high viscosity ratio between the coal tar and water phase could have caused viscous fingering and resulted in misestimate of the coal tar residual saturation in porous medium.

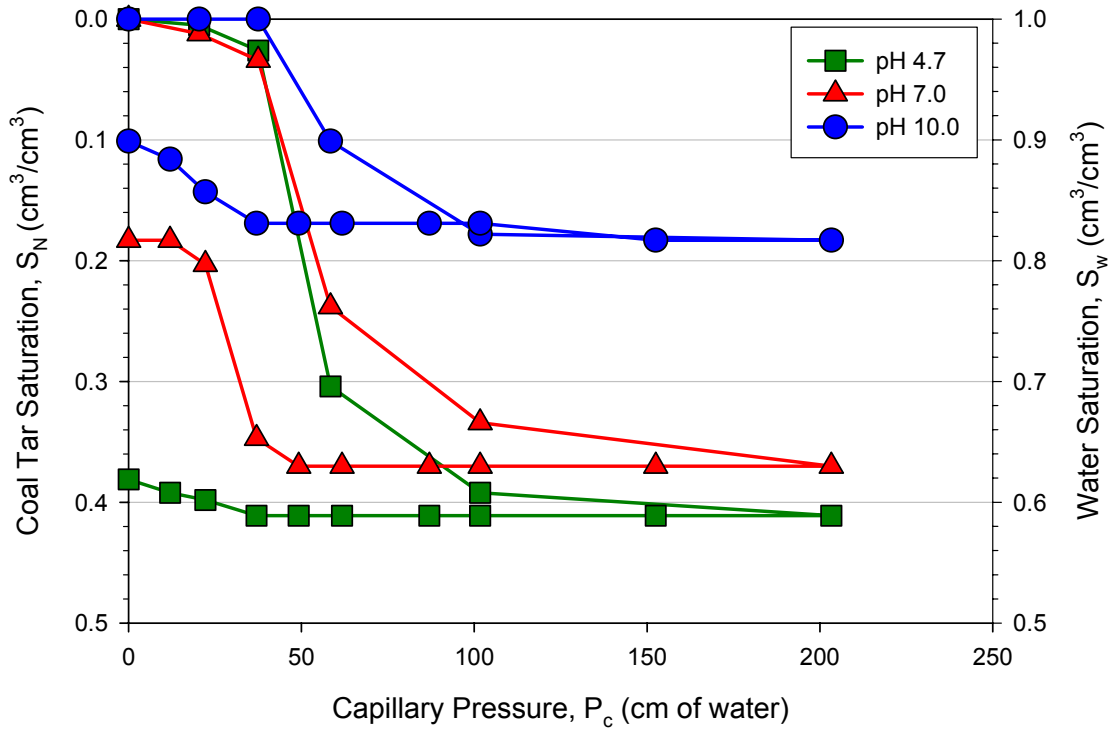


Figure 6-22. Capillary pressure-saturation relationships in coal tar-water-F-70 Ottawa sand system at pH 4.7, 7.0, 10.0.

Table 6-14. Comparison of measured and predicted drainage capillary pressure entry pressure in Saranac tar-water-Ottawa sand system.

Systems	IFT (dynes/cm)	Contact angle (°)	H _b (cm of H ₂ O)	Residual water saturation, S _{Nr} (cm ³ /cm ³)
Air-water (pH 4.7)	72.6	--	25.5	0.248
Air-water (pH 7.0)	72.6	--	29.7	0.164
Air-water (pH 10.0)	72.6	--	27.8	0.137
Tar-water (pH 4.7)	23.73 (±0.30)*	22.0 (±1.8)	36.8	0.589
Tar-water (pH7.0)	24.14 (±0.94)	14.2 (±2.3)	51.0	0.630
Tar-water (pH 10.0)	14.24 (±0.56)	12.1 (±2.2)	56.5	0.817

* standard deviation (s. d. = $\sigma/\sqrt{n-1}$)

Table 6-15. Comparison of residual saturation of water and coal tar during water drainage and imbibition process.

Coal Tar properties Density (g/cm ³), viscosity (cP)	Porous medium	Residual water saturation during drainage (cm ³ /cm ³)	Residual coal tar saturation during imbibition (cm ³ /cm ³)	Literatures
1.062 g/cm ³ (22°C) 61.0 cP (22°C)	F-70 Ottawa sand, 0.053-0.425mm, d _m =0.2mm	0.59 at pH 4.7 0.63 at pH 7.0 0.82 at pH 10.0	0.38 at pH 4.7 0.18 at pH 7.0 0.10 at pH 10.0	Kong, 2004
1.045 g/cm ³ (25°C) 9.9 cP(37°C)	Median grained quartz sand, 0.075-2 mm, d _m =0.4mm	0.20 at pH 3 0.30 at pH 7 0.30 at pH 12	0.77 at pH 3 0.66 at pH 7 0.52 at pH 12	Barranco, 1999
1.051 g/cm ³ (25°C) 19.4 cP (25°C)	50% 30 to 40 mesh (0.600 to 0.425 mm) and 50% of 40 to 50 mesh (0.425 to 0.300 mm)	0.12 at pH 4.7 0.14 at pH 7.2 0.13 at pH 9.9	0.47 at pH 4.7 0.30 at pH 7.2 0.29 at pH 9.9	Hugaboom, 2002

Table 6-16. Parameters fitted to van Genuchten equation in air-water-F-70 and tar-water-F-70 systems using different scaling factors

pH	Parameters	Air-Water	Tar-Water		
			Case I $\frac{(\gamma)_{tar/water}}{(\gamma)_{air/water}}$	Case II $\frac{(\gamma \cos \omega)_{tar/water}}{(\gamma \cos \omega)_{air/water}}$	Case III $\frac{(\gamma \cos \omega)_{tar/water}}{(\gamma \cos \omega)_{air/water}} \left(\frac{\eta_{tar}}{\eta_{water}} \right)^{0.4}$
pH 4.7	θ_{sat}	0.345	0.345	0.345	0.345
	θ_{res}	0.058	0.058	0.058	0.058
	n	4.414	4.414	4.414	4.414
	α	0.0349	0.1067	0.1048	0.1777
pH 7.0	θ_{sat}	0.345	0.345	0.345	0.345
	θ_{res}	0.058	0.058	0.058	0.058
	n	4.414	4.414	4.414	4.414
	α	0.0349	0.1150	0.1081	0.1818
pH 10.0	θ_{sat}	0.345	0.345	0.345	0.345
	θ_{res}	0.058	0.058	0.058	0.058
	n	4.414	4.414	4.414	4.414
	α	0.0349	0.0219	0.0206	0.0346

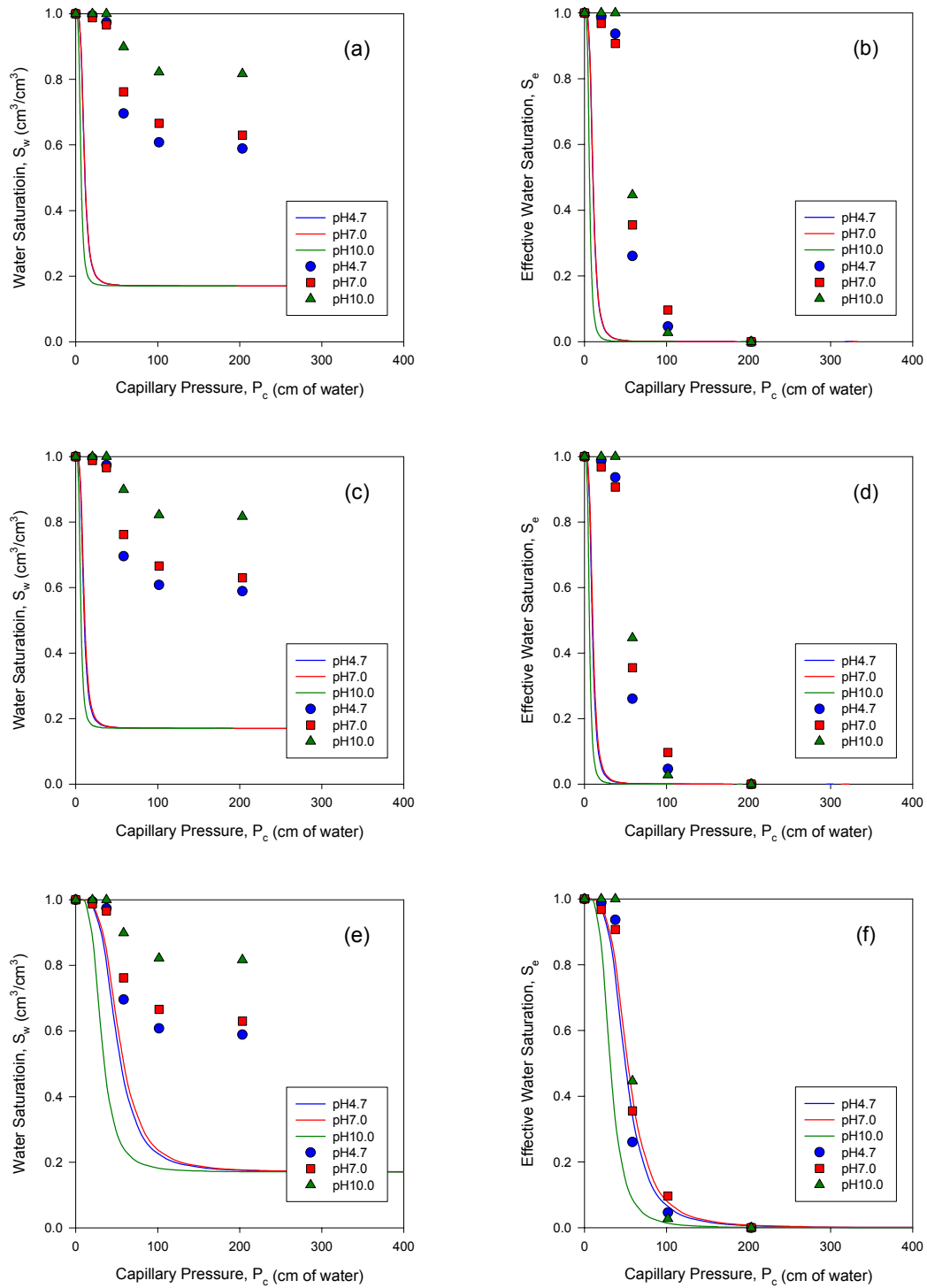


Figure 6-24. Scaled capillary pressure-saturation relationships (lines represents predicted P_c - S relationships from that in air-water system, dots represents experimental data). (a)(b) Case I; (c)(d) Case II; (e)(f) Case III.

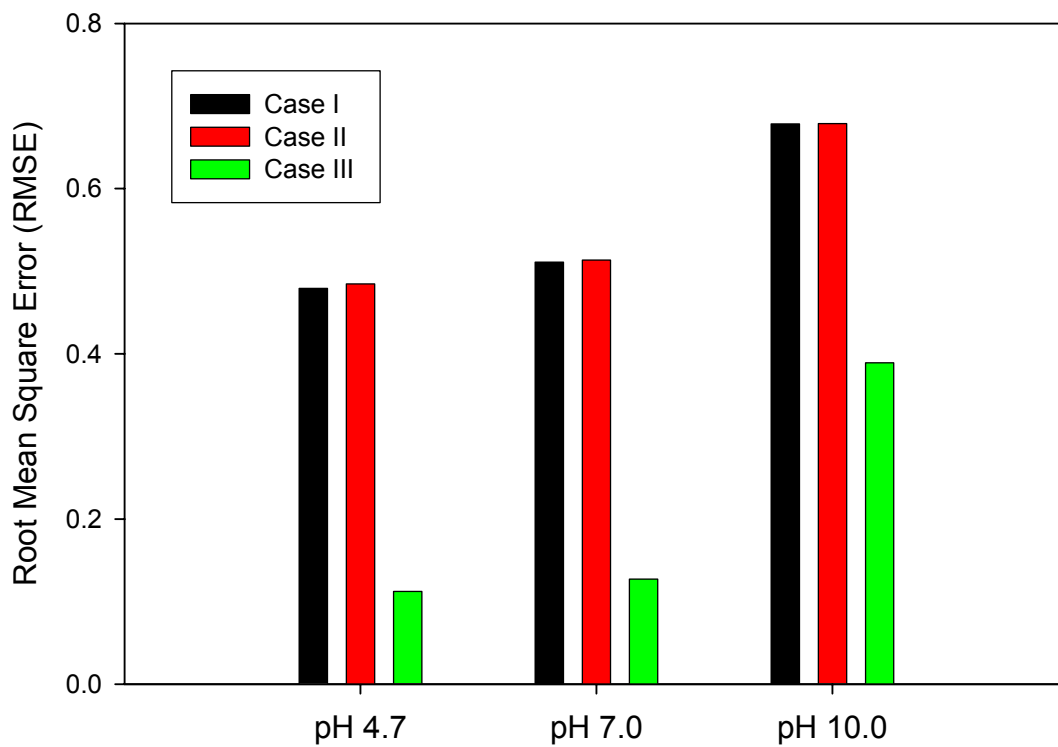


Figure 6-25. Root Mean Square Error (RMSE) of three different scaling approaches at pH 4.7, 7.0 and 10.0.

Summary and Conclusions

Wettability and interfacial properties in oil-water-solid systems are dependent upon the oil composition, aqueous solution chemistry, as well as solid surface characteristics. As aqueous solution chemistry changes, the acidic or basic functional groups in the oil phase and on the solid surface can be protonated or deprotonated into anionic or cationic or neutral species. Consequently, the interactive forces between the oil phase and solid surface change, leading to the change of adhesion or spreading of oil on the solid surface. At the same time, these species can accumulate at the oil-water surface and reduce the oil-water IFT. In coal tar, asphaltenes are believed to be the constituents that not only affect the physical properties of coal tar such as viscosity and density, but also responsible for wettability and IFT changes with pH due to the existence of acidic and basic functional groups.

Contact angle was used as a quantitative index of the glass wettability. A reduction of contact angle at both low and high pH was observed. At high pH, the contact angle reduction was attributed to the electrostatic repulsive force between the deprotonated organic acid species (A^-) and negatively charged glass surface, while at low pH, the combination of hydration force and electrostatic force are proposed to be responsible. However, the contact angles were lower than 30° in the tar-water-silica system over the evaluated pH range in this experiment, which indicated water wetting condition. The mechanisms of pH effect on contact angle were explored by addition of 5-indanol and quinoline into the coal tar phase. The addition of 5-indanol did not impact the contact angle, while the addition of quinoline resulted in a more oil-wetting and less water-wetting condition, especially at low pH. These observations could be attributed to

electrostatic force between the coal tar phase and glass surface. The contact angle in tar-water-glass system was also observed to increase with the increasing of ionic strength.

Tar-water IFT also presented a reduction at both low and high pH, which indicated the dissociation of acid or base constituents was responsible for the IFT reduction. The addition of 5-indanol and quinoline generally decreased the IFT due to the increase of surface active constituent accumulation at the tar-water interface. Ionic strength presents no significant effect on IFT when ionic strength is less than 0.5 M, which implicates that the ionic strength effect will be negligible at commonly encountered groundwater systems.

The experimental results on pH and ionic strength effect on contact angle and IFT implies that the aqueous chemistry including pH and ionic strength is not sufficient to enhance the removal of coal tar in the subsurface system with silica sand. On the other hand, for different porous media, such as minerals rich of alumina, hematite, calcite, or Brucite, which have PZC of 7 to 9, 6 to 9, 8 to 9.5 and 12, respectively, the effects could be very different (Hirasaki, 1991). In oil recovery industry, oil reservoirs were found to change from water-wet to oil-wet with the change of solution of pH or ionic strength (Morrow et al., 1986, Morrow, 1991). Thus, at some MGP sites with porous medium other than silica, aqueous chemistry could be an effective option for controlling the entrapment and removal of coal tar.

To date, coal tar capillary pressure-saturation relationship investigations have been conducted mainly in coarse quartz sand and low viscosity tars in literature (Barranaco and Dawson, 1999; Hugaboom and Powers, 2002). The experiments described here conducted the water drainage and imbibition process to highly viscous coal

tar and a relatively fine quartz sand system. The experiment results show that coal tar residual saturation in porous media is dependent on wettability and interfacial properties of the system. However, the potential of viscous fingering and channeling of coal tar may be an issue, which effects the reproducibility of these experiments. Analysis of P_c - S relationship shows that the commonly used scaling factor including IFT and contact angle is not adequate to predict the P_c - S relationship in tar-water systems from that in corresponding air-water systems. The incorporation of viscosity ratio of NAPL and water greatly helped.

CHAPTER VII

EFFECTS OF TEMPERATURE AND SURFACTANT ADDITION ON COAL TAR PROPERTIES, RESIDUAL SATURATION AND RECOVERY FROM POROUS MEDIA

Introduction

Almost every city in the United States had a manufactured gas plant (MGP), and these sites are often located in the downtown areas of the cities (USEPA, 2000). Although many former MGP sites have been or are currently being investigated and/or remediated, a large number remain unaddressed. To select an effective and economic remediation technology to specific MGP sites is of primary concern.

The difficulties in MGP site remediation are greatly determined by the unique physical and chemical properties of MGP residuals. As the significant byproducts of MGP sites, coal tars have very high viscosities, which hinder the removal of coal tar from contaminated sites. In addition, as complex DNAPLs, coal tars can behave very differently in porous media from those commonly encountered DNAPLs such as TCE and PCE. As discussed in the previous chapter (Chapter VI), coal tar density and viscosity are primarily determined by the asphaltene content and composition in coal tar. Asphaltenes are also responsible for the acidic/basic properties of coal tar, which vary with environmental aqueous chemistry. Considering the coal tar composition, including

asphaltene content, depends upon their origins and weathering, the MGP site remediation technologies will be varied from site to site, which requires comprehensive NAPL and site characterization.

The entrapment and displacement of DNAPL in subsurface is controlled by a complex interplay among capillary, gravitational and viscous forces (Villaume, 1985; Mercer and Cohen, 1990; Pankow and Cherry, 1996). Dimensionless parameters such as the capillary number (N_{Ca}) and Bond number (N_B) are widely used to predict the NAPL displacement during water-flooding in porous media (Table 2-5) (Reed and Healy, 1976; Ng et al., 1978; Morrow and Songkran, 1981; Chatzis and Morrow, 1984; Dawson and Roberts, 1997). On the basis of experimental observation, residual oil is generally displaced when N_{Ca} is greater than 5×10^{-3} (Ng et al., 1978). Pennell et al. (1996) incorporated the relative permeability into the Bond number, and proposed the total trapping number (N_T), defined as the summation of capillary number and Bond number (Equation 2-26, 27). The critical value of N_T required to initiate PCE mobilization was within the range of 2×10^{-5} to 5×10^{-5} , while complete displacement of PCE occurred when the value of N_T approached 1×10^{-3} (Pennell et al., 1996). For NAPL with densities similar to that of water, it is necessary to increase the ratio of viscous to capillary forces (i.e. increase the capillary number), which can be achieved by increasing the flooding flow rate or aqueous phase viscosity, reducing the oil-water interfacial tension or by changing the wettability of the media. Flooding rates are limited by the permeability of the porous media, increasing the displacing phase viscosity may reduce the permeability and result in media clogging. However, IFT can be lowered several orders-of-magnitude by using appropriate surfactants. Surfactants have been widely used

in both oil recovery and NAPL remediation. Surfactant enhanced aquifer remediation (SEAR) is a technology designed to recover free-phase NAPL trapped in aquifer by IFT reduction and/or micelle solubilization (Saripalli et al., 1997; Bettahar et al., 1999; Dwarakanath et al., 1999; Lee et al., 2001a; Fu and Imhoff, 2002). Surfactants are amphiphilic molecules, which can greatly reduce the NAPL-water IFT by the adsorption of surfactants at the NAPL-water interface. The selection of appropriate surfactants is determined by remediation requirement. In general, the selection criteria include environmental acceptability and bioavailability, low adsorption on soil particles, cost, ability to reduce IFT (if mobilization is desired) and high contaminant solubilization. Anionic surfactants are the most commonly used surfactants in enhanced oil recovery (EOR) and SEAR because they are stable, cheap, and relatively resistant to retention (Lake, 1989; Rouse et al., 1993; Pennell et al., 1994; Dwarakanath et al., 1999; Istok and Field, 1999; Lee et al., 2001b; Ramsburg, 2002; Hirasaki and Zhang, 2003).

For viscous NAPL, only the reduction of IFT is not sufficient to enhance the NAPL removal. Due to the high viscosity contrast between the coal tar phase and the aqueous phase, the displacing aqueous phase tends to bypass the coal tar phase and leave large areas unswept during the water flooding, which results in incomplete and inefficient coal tar displacement. This effect is attributed to the viscous fingering or channeling, which stems from the hydrodynamic instability of the fluid front due to the large viscosity difference between the displacing and displaced phase (Lake, 1989; Martel et al., 1998; Giese and Powers, 2002). This hydrodynamic instability can be evaluated by the mobility ratio of water phase to oil water, which is defined according to Equation (2-28). In the displacement process, lower mobility ratios (less than 1) favor NAPL

recovery. In order to reduce the hydrodynamic instability and improve the water flooding efficiency, it is essential to reduce the NAPL-water viscosity ratio.

Considering the reduction of NAPL viscosity, temperature elevation (thermal technologies) is an extensively used approach. Thermal methods depend on several displacement mechanisms, but the most important one is the reduction of viscosity (Ekmondson, 1965; Lake, 1989; Sleep and Ma, 1997). Viscosity decreases exponentially as temperature increases, which implies that the higher the viscosity, the more reduction with temperature, the lower the viscosity, the less reduction (Laker, 1989). Therefore, in an oil-water system, the reduction of viscous oil is greater than that of the aqueous phase with increasing temperature, which leads to significant reduction of oil-water viscosity ratio. In practice, thermal remediation methods, including combustion, steam or hot water flushing/displacement, have been used at MGP sites (USEPA, 2000; Young et al., 2002). Hot water flushing was applied to the Brodhead Creek MGP site in Stroudsburg, Pennsylvania for one year, and more than 1,500 gallons of coal tar were recovered. The initial tar volume was unknown due to the sampling difficulties and subsurface heterogeneity. The operation ceased until the increase in cumulative recovery of coal tar dropped to less than 0.5% per pore volume of flushed water (USEPA, 2000). Leuschner et al. (1997) reported a 23% removal of coal tar by enhanced water flood at elevated temperatures.

Another widely used mobility control method is polymer solutions. Polymers have been widely used in enhanced oil recovery (EOR), and are often combined with the surfactant flushing, which is referred to as micelle/polymer (MP) flushing (Mungan et al., 1960; Slater and Farouq Ali, 1970; Chou and Shah, 1981; Hesselink and Faber, 1981;

Lakatos et al., 1981; Lake, 1989; Liu, 1995). Xanthan gum, hydrolyzed polyacrylamide (HPAM) and copolymers of acrylic acid and acrylamide are the three polymers, which have been used in EOR (Lake, 1989). The use of polymer solutions in aquifer remediation to increase the NAPL removal efficiency is a relatively new technology (Martel et al., 1998; Giese and Powers, 2002; Young et al., 2002). Based on a laboratory study by Giese and Powers (2002), the final saturation of coal tar or creosote decreases from more than 40% after water flooding to approximately 19% after approximately 800 ppm xanthan gum solution flushing. During a pilot-scale study at a former MGP site in Bloomington, Illinois, it was found that more than 80% of the coal tar (with a viscosity of 65 cP and a density of 1.08 g/cm³ at 24°C) was removed after polymer/surfactant flushing (0.13% xanthan gum + 4% AlfoterraTM 123-8 PO Sulfate surfactant + 8% 2-butanol + 0.08% CaCl₂) combined with temperature elevation (35°C) (Young et al., 2002).

Although a few enhanced water flooding methods have been utilized for MGP site remediation, no reported research has been conducted to investigate the coal tar mobilization in the context of capillary, gravitational and viscous forces. Compared to most of the previous studies (Dawson and Roberts, 1996; Pennell et al., 1996), which were mainly concentrated on less viscous NAPLs with viscosities similar to that of water, the coal tar-water system may behave differently with respect to capillary, and viscous forces. It is generally assumed that shear forces, which would be a function of the viscosity contrast between the aqueous and NAPL phase, are negligible. For high viscosity coal tars, the high viscosity ratio between coal tar and water phase may develop normal viscous stress at the menisci of the coal tar droplet and change the pressure

difference between two menisci (Ng et al., 1978). To investigate the viscosity effect, Abrams (1975) incorporated the viscosity ratio into capillary number to form a dimensionless group referred to as “F”. This dimensionless group (F) was evaluated in oil-water system with oil/water viscosity ratio ranged from approximately 0.01 to 30. The residual oil saturation left by waterflood of a water-wet rock was found to be governed by the value of this group, which indicates the viscosity ratio exerts an influence on the oil displacement in a system with oil/water viscosity ratio not close to one.

The purpose of this study was to investigate the effect of heating on coal tar properties, including density, viscosity, tar-water interfacial tension, glass surface wettability, and residual coal tar saturation. The effect of surfactant addition on coal tar coal tar-water interfacial tension and corresponding residual saturation was also evaluated. Xanthan gum was combined with surfactant solution to increase the capillary number and reduce the tar-water viscosity ratio. In order to help to develop effective remediation technologies to former MGP sites, coal tar mobilization was evaluated in terms of capillary number, total trapping number and viscosity ratio.

Materials and Methods

Materials

Charleston coal tar has the highest viscosity (425 cP at 22°C) among the six coal tar samples received from different MGP sites. During the previous tar-water two-phase experiments (Chapter IV), residual saturation of Charleston tar at 40°C is even higher than that of the other five coal tar samples at 22°C. Hence, Charleston coal tar is the most

difficult tar to remove from the porous media. Based on the assumption that if the temperature and surfactant addition showed great enhancement to the Charleston tar removal, their effect on other less viscous coal tars should be more significant, and the potential for the application of these technologies to the MGP sites remediation would be promising, Charleston coal tar was selected as the representative coal tar in this study.

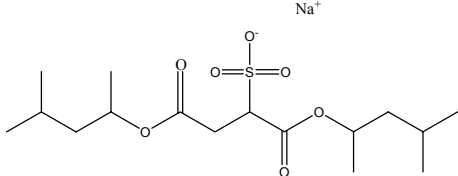
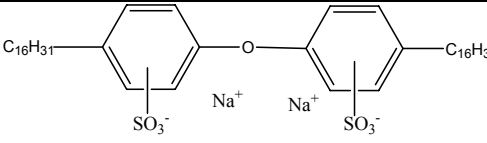
Three anionic surfactants were evaluated for the coal tar displacement herein based on previous work in both enhanced oil recovery and NAPL remediation (Lee et al., 2001a; Rouse et al., 2001; Ramsburg, 2002; Hirasaki and Zhang, 2003)). Surfactant Aerosol MA-80I (sodium dihexylsulfosuccinate in a mixture of isopropanol and water) was donated by Cytec Industries. Steol CS-330 (sodium laureth ($n \geq 3$) sulfate) was obtained from Stepan Company, and Dowfax 8390 (disodium n-hexadecyl diphenyloxide disulfonate) was purchased from Dow Chemical Company. All of the surfactants were used as received. Table 7-1 lists relevant properties of these surfactants. Xanthan gum was purchased from Fisher Scientific Company in the form of a powder. Ottawa sand, 20-30 mesh and F-70 (40-270 mesh) was purchased from U. S. Silica Co. and was used as received.

Methods

Effect of Temperature on Coal Tar Properties

Density and viscosity of Charleston coal tar and water solution with or without surfactant, tar-water interfacial tension and contact angle of Charleston coal tar on microscope glass slide were measured in the temperature range of 22°C to 50°C. The detailed analysis protocols were described in Chapter IV and Chapter VI. During the

Table 7-1. Characteristics of surfactants used in study.

Trade Name	Active Ingredient	Molecular Formula	Molecular Structure	Molecular Weight (g/mol)	Critical Micelle Concentration, CMC (mM)	Manufacturer
Aerosol MA-80I	Sodium di(1,3-dimethylbutyl) sulfosuccnate	$C_{16}H_{29}O_4SO_3Na$		388.46	NA	Cytec Inc.
Steol CS-330	Sodium polyethoxyethyl dodecylsulfate	$(C_2H_4O)_n C_{12}H_{25}OSO_3Na$	NA	422	1.06	Stepan Co.
Dowfax 8390	Disodium n-hexadecyl diphenyloxide disulfonate	$C_{16}H_{33}C_{12}H_7O(SO_3Na)_2$		598	0.5	Dow Chemical Co.

density measurements, temperature was controlled by immersing the tested pycnometer in a water bath on a hot plate, and monitored using a fluoropolymer-coated mercury thermometer (Fisher Scientific Co.). During viscosity measurements, temperature was varied using a recirculating water bath attached to the Rheometer cell. During contact angle measurements, the optic glass cell, containing with tar, water and glass slide was heated on the sand bath on the hot plate, and temperature was measured using a thermometer. Each measurement was run in duplicate.

Phase Behavior (Salinity Scan)

Interfacial tension (IFT) reductions are fundamental to NAPL displacement strategies. Lowering interfacial forces allows flows to overcome the capillary forces entrapping NAPLs. The phase behavior experiment incorporated anionic surfactants and electrolytes for IFT reduction. Winsor type III microemulsion is the optimum condition for NAPL remediation. In this studies, Aerosol MA-80I, Steol CS-330 and Dowfax 8390 were chosen as the surfactants, and NaCl and CaCl₂ were used as the electrolytes.

Salinity scan experiments were conducted in 10 mL graduated (0.1 mL) centrifuge tubes (Fisher Scientific Co.), in which equal volumes (5 mL) of coal tar and surfactant solution containing various amounts of NaCl and CaCl₂ were added (Figure 7-1). These mixtures were equilibrated on Lab Quake shaker trays for 24 hours and allowed to settle for a period of 24 hours, or until no further phase separation occurred. The final phase volumes were recorded and equilibrated samples were analyzed for tar-water IFT and tar viscosity.

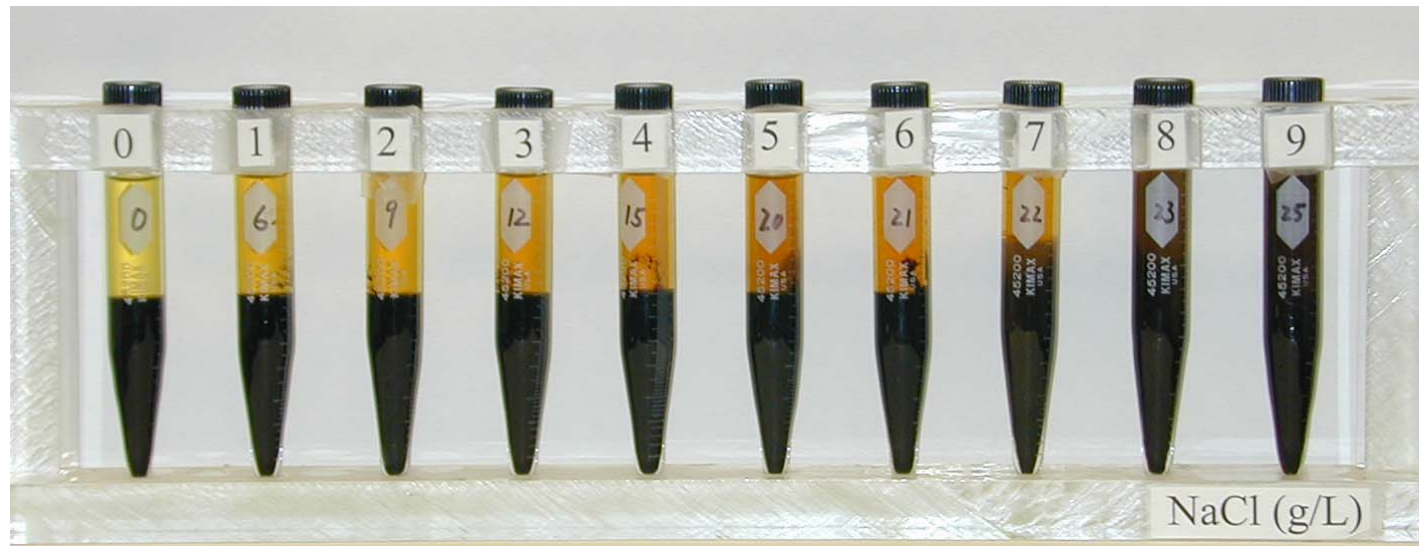


Figure 7-1. Representative salinity scan experiment with 10% MA-80I surfactant, 1g/L CaCl_2 and NaCl.

IFT Measurements

When IFT is less than 1 dynes/cm, the IFT values were measured by pendant drop method (Adamson, 1990). The pendant drop method was performed using a goniometer (Ramé-Hart, Inc., Mountain Lakes, NJ). The aqueous solution was contained in a rectangular optic cuvette, and placed on the specimen stage. Coal tar was gently introduced in to the cell through a tungsten-carbide tip (Caiser Tool Company, CA), which was connected to a 1 mL Hamilton gas tight syringe through stainless steel fittings. The syringe was mounted vertically above the aqueous cuvette. The tip was submerged under the water surface so that the coal tar droplet formed completely in the aqueous solution. The image of the drop was captured using a personal computer connected to the goniometer apparatus. The dimensions of the drop was measured and the IFT was calculated by using the following equation (Adamson, 1990):

$$\gamma = \frac{\Delta\rho g d_e^2}{H} \quad (7-1)$$

where, $\Delta\rho$ is the density difference between the coal tar phase and aqueous phase. d_e is the equatorial diameter of the coal tar droplet, and H is a shape-dependent quantity, which was determined empirically through the quantity S ($S=d_s/d_e$), where d_s is the diameter measured at a distance d_e up from the bottom of the drop (Figure 7-2).

Permeability Measurement

The permeability of 20-30 mesh Ottawa sand packed columns were measured using constant head method at different stages during coal tar displacement experiment (Klute and Dirksen, 1986). The four stages were i) when the column was saturated with water prior to coal tar injection; ii) after the water-flood of coal tar contaminated column;

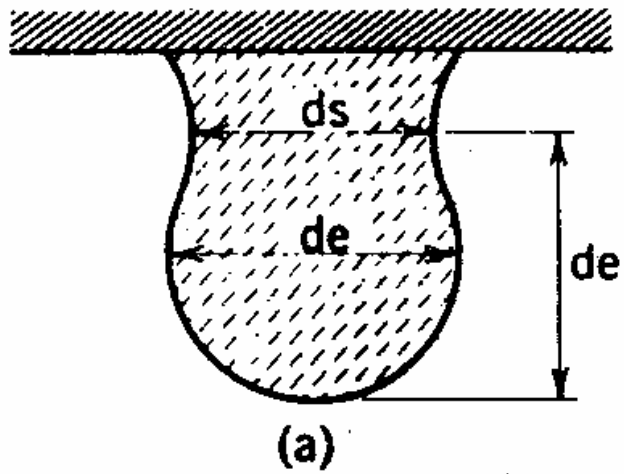


Figure 7-2. Schematic shape of a pendant drop of one fluid formed in another (d_e is the equatorial diameter of the pendant droplet, and d_s is the diameter measured at a distance d_e up from the bottom of the drop).

iii) after surfactant flushing (CS-330); iv) after surfactant/polymer (CS-330/xanthan gum) flushing. To establish constant head conditions, a 1 L DI water reservoir was connected with the top inlet of the stainless steel column through a teflon tubing. The bottom outlet of the column was connected with the atmosphere, with the height of the effluent tubing fixed. The height of the water reservoir was adjusted in order to obtain different flow rates. The water produced from the column was collected and weighed, and the time interval for water collection was also recorded. The flow rate was then determined based on the water produced and time interval. Flow rate was measured in triplicate at each head. Head loss was determined measuring the height difference between the surface of the water reservoir and water outlet of the column. Ten data points (flow rates and corresponding head loss values) were collected by changing the height of the water reservoir. The flow rate (Q) was converted to Darcy velocity (q) according to Equation (7-2), and the head gradient ($\Delta H/\Delta x$) was also calculated. Darcy velocity was plotted against the head gradient, the conductivity was then determined by linear regression according to Darcy's Law (Equation 7-2). Finally, the permeability was calculated according to Equation (7-3).

$$q = \frac{Q}{A} = -K \frac{\Delta H}{\Delta x} \quad (7-2)$$

$$K = \frac{k\rho g}{\eta} \quad (7-3)$$

where q is the Darcy velocity (cm/s), Q is the flow rate (cm³/s), A the cross section area of the column (cm²), K is the conductivity (cm/s), ΔH is the head loss (cm), Δx is the column length in the flow direction (cm), k is the permeability (cm²), ρ (g/cm³) and η (cP) are density and viscosity of flowing fluid, respectively. The obtained permeability value

prior to coal tar injection was compared with available literature reported values and theoretic estimation using Kozeny-Carman (Equation 2-23).

Coal Tar Displacement Experiments

The column experiment apparatus used in the displacement studies was similar to that employed for the tar-water two-phase column experiments (See Chapter IV). Column experiments were conducted at three different temperatures (22, 35 and 50°C). The 35 and 50°C temperatures were obtained by performing the experiment in a 35°C constant temperature room, and in a temperature control chamber (Lab-Line Instruments, Inc), respectively. Temperatures were monitored by measuring the temperature of influent/effluent solutions during experiment using a fluoropolymer-coated mercury thermometer (Fisher Scientific). The experimental protocol was as follows: column was first firmly packed and completely water saturated as described in Chapter IV, coal tar was then injected into the column at a flow rate of 3 mL/min at 50°C in the temperature control chamber in order to achieve uniform coal tar distribution inside the column. If applicable, the column was then allowed to cool to the desired flushing temperature prior to the water displacement flood. The column was then flooded with water (with a NaCl concentration of 0.01 M) at a flow rate of 5 to 6 mL/min until no free phase coal tar was observed at the column effluent. Non-reactive tracer (KI) experiments were performed before the coal tar injection and after the water flooding. The residual coal tar saturation was calculated by comparing the retardation factors of these two tracer breakthrough curves as described in Chapter IV. The water flood was followed by a series of surfactant and/or surfactant/polymer floods at flow rates ranging from 2 to 15 mL/min.

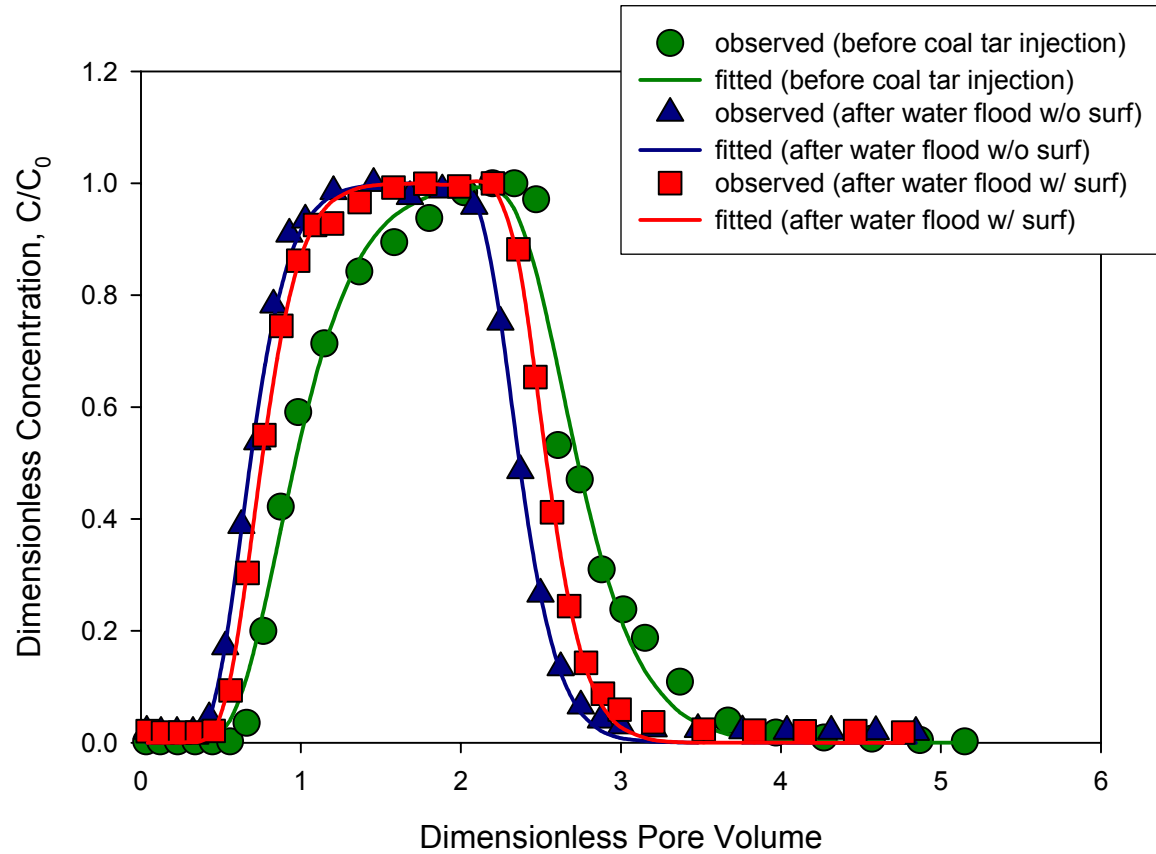


Figure 7-3. Representative KI tracer BTCs for determining the residual coal tar saturation in Charleston tar-water-Ottawa sand (20-30 mesh) system (Retardation factors R_F are 1.01, 0.71 and 0.78 for system before coal tar injection, after water flood without surfactant, and after water flood with surfactant, respectively).

The residual coal tar saturation was determined by either KI tracer test method or gravimetric method as described in Chapter IV. Figure 7-3 shows representative breakthrough curves (BTCs) of non-reactive tracer before coal tar injection, post water and surfactant flushing.

Results and Discussion

Effect of Temperature on Coal Tar and Displacing Solution properties

Effect of Temperature on Density

The liquid densities of Charleston coal tar and the surfactant solutions, including MA-80I, CS-330 and Dowfax 8390, were measured at different temperatures. Figure 7-4 shows representative relationships between solution density and temperature. The measured densities decreased as the temperature was increased from 22 to 50°C. Second-order parabolic correlations were obtained to fit this relationship between density and temperature of Charleston tar, surfactant solution and water using Sigma Plot 2000. The resulting relationships were in agreement with correlations reported in other studies (Ekmondson, 1965; Basu et al., 1996; Sleep and Ma, 1997). The equations of the curves for density (ρ) as a function of temperature (T , °C) were:

$$\rho_{tar} = 1.096 + 7.572 \times 10^{-4} T - 1.752 \times 10^{-5} T^2 \quad R^2=1.0 \quad (7-4)$$

$$\rho_{MA-80I} = 1.011 + 3.852 \times 10^{-4} T - 1.081 \times 10^{-5} T^2 \quad R^2=1.0 \quad (7-5)$$

$$\rho_{water} = 1.001 - 8.366 \times 10^{-5} T - 3.638 \times 10^{-6} T^2 \quad R^2=1.0 \quad (7-6)$$

where ρ_{tar} , ρ_{MA-80I} and ρ_{water} are the densities of Charleston coal tar, 10% MA-80I surfactant solution and water, respectively.

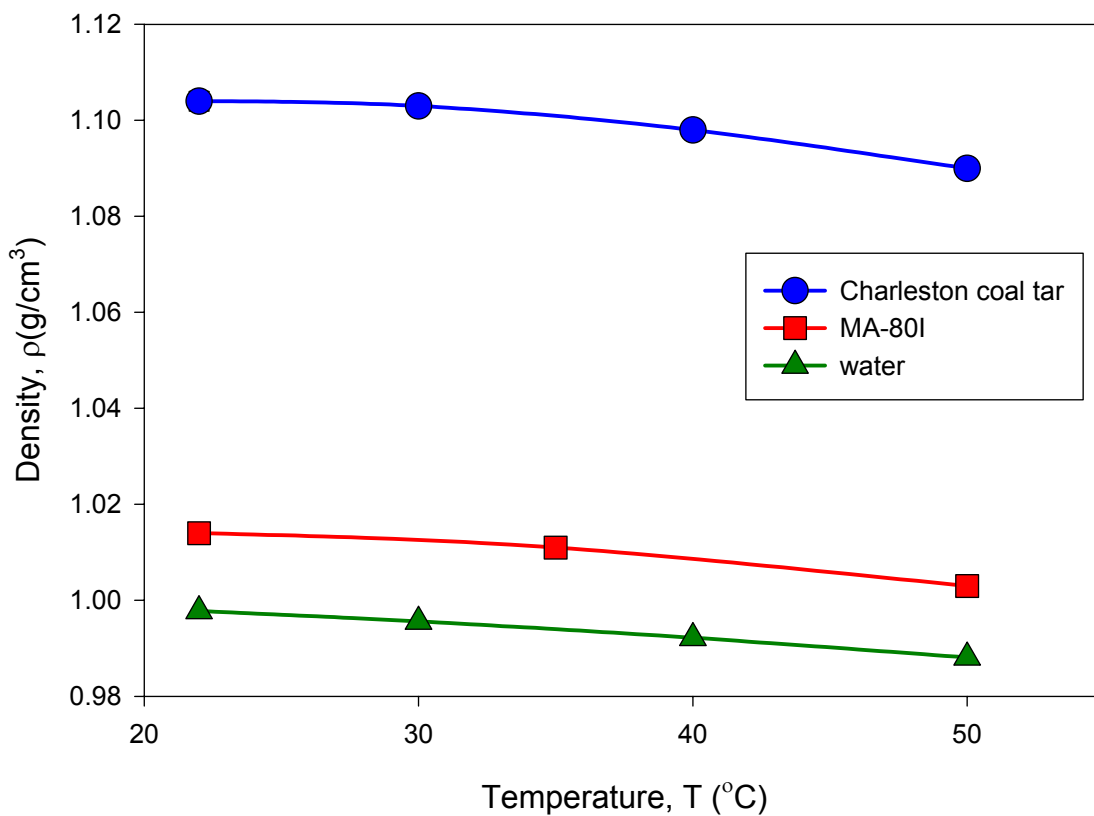


Figure 7-4. Measured density of coal tar, surfactant solution (10% MA-80I + 1g/L CaCl₂ + 3 g/L NaCl) and water (0.01 M as a function of temperature in the range of 22 to 50°C (error bars are smaller than symbols).

Effect of Temperature on Viscosity

Viscosity of three coal tar samples (Charleston, Fairfield and Cape May) as well as surfactant solutions were measured at four temperatures (22, 30, 40 and 50°C). Measured viscosities exhibited an exponential decrease as the temperature was increased from 22 to 50°C (Figure 7-5a). For tars with higher initial viscosity (at room temperature), the greater reduction in viscosity with increasing temperature was observed. For example, the viscosity of Charleston coal tar decreased 357 cP from 425 cP when temperature increased from 22 to 50°C. In contrast, the viscosity reduction for Cape May tar, which was only 42 cP from 61 cP over the same temperature range. These data indicate that the temperature effect would be more significant for more viscous tars. Figure 7-5a also showed that the reduction of viscosity of coal tar was greater at low temperature range than that at high temperature range. For example, the viscosity of Charleston coal tar decreased 197 cP when temperature was increased from 22 to 30°C, whereas a viscosity reduction of only 47 cP was observed when temperature was increased from 40 to 50°C. This observation implies that a significant improvement in flushing efficiency could be achieved by applying relative low temperature thermal treatments. The resulted viscosities of coal tar as a function of temperature were in agreement with reported viscosity data of white oils and crude oils as shown in Figure 7-5b (Ekmondson, 1965). Sleep and Ma (1997) found that the viscosity of PCE showed a relatively steady decrease with elevated temperature compared to multi-component oil phase. It was suggested that the fluid viscosities were dependent on composition (Reid et al., 1987), but no theory has been proposed to predict the variation of viscosity with temperature for multi-component systems. The viscosity-temperature correlations in this

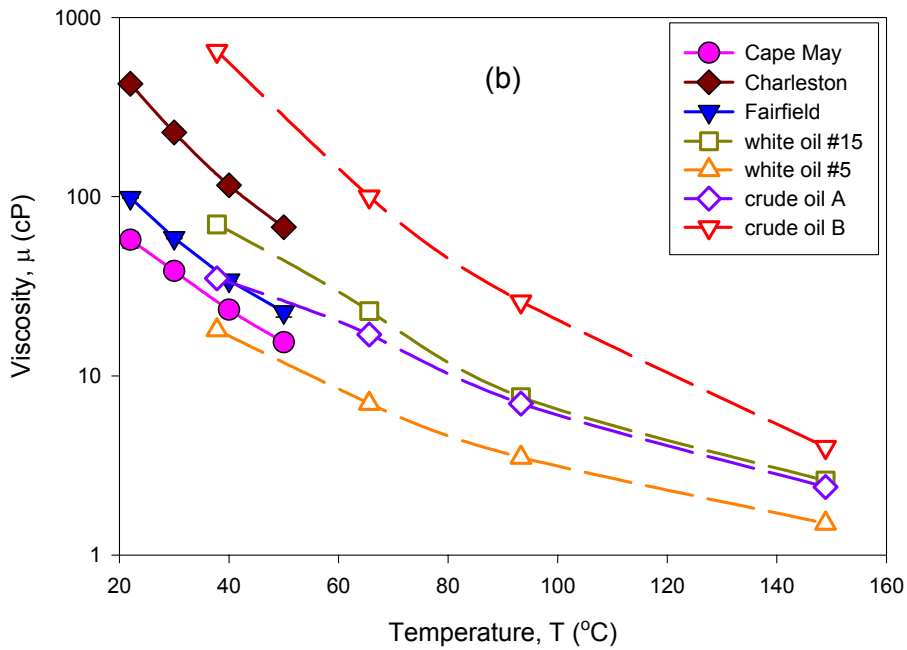
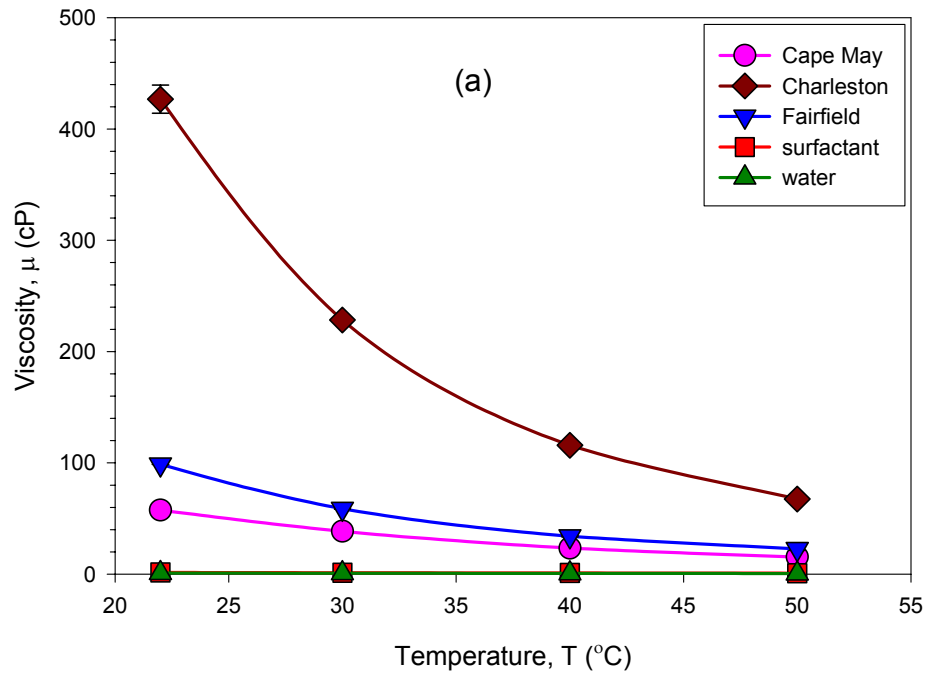


Figure 7-5. Temperature effect on viscosity (a) viscosity of coal tar (Charleston, Fairfield and Cape May), surfactant solution (10% MA-80I + 1 g/L CaCl₂ + 3 g/L NaCl) and water (0.01 M NaCl) as a function of temperature (22 to 50°C) (error bars are smaller than symbols). (b) Comparison of viscosity of coal tar to that of white oils and crude oils (white oil and crude oil data are from Ekmondson, 1965).

study were fit to the following equations based on Sigma Plot 2000:

$$\eta_{Charleston} = 2.064 \times 10^3 e^{-7.204 \times 10^{-2} \times T} \quad R^2=0.997 \quad (7-7)$$

$$\eta_{Fairfield} = 3.430 \times 10^2 e^{-5.728 \times 10^{-2} \times T} \quad R^2=0.994 \quad (7-8)$$

$$\eta_{CapeMay} = 1.670 \times 10^2 e^{-4.864 \times 10^{-2} \times T} \quad R^2=0.999 \quad (7-9)$$

$$\eta_{MA-80I} = 2.298 e^{-2.019 \times 10^{-2} \times T} \quad R^2=0.998 \quad (7-10)$$

$$\eta_{water} = 1.478 e^{-2.021 \times 10^{-2} \times T} \quad R^2=0.998 \quad (7-11)$$

where $\eta_{Charleston}$, $\eta_{Fairfield}$, $\eta_{CapeMay}$, η_{MA80-I} and η_{water} refer to the viscosity of Charleston, Fairfield, Cape May coal tar, 10% MA80-I surfactant solution and water, respectively.

Effect of Temperature on IFT

Charleston tar-water IFTs were measured as a function of temperature at pH 4.6 ± 0.1, 7.0 ± 0.1 and 10.0 ± 0.1. Figure 7-6a showed that tar-water IFTs increased slightly from 22 to 40°C at pH 4.7 and pH 7.0, and no apparent change was observed at pH 10.0. Best fit for IFT-temperature relationship over the evaluated temperature range using SigmaPlot 2000 are as follow:

$$IFT_{pH4.7} = 1.354 + 4.977 \times 10^{-1} T - 5.422 \times 10^{-3} T^2 \quad R^2=1.0 \quad (7-12)$$

$$IFT_{pH7.0} = 2.394 + 7.768 \times 10^{-1} T - 9.727 \times 10^{-3} T^2 \quad R^2=1.0 \quad (7-13)$$

No statistical relationships were found to fit the IFT-temperature relationship at pH 10.0. In general, tar-water IFTs showed little change over the temperature range from 22 to 50°C. IFT variation depends on the adsorption of surface active species at the oil-water

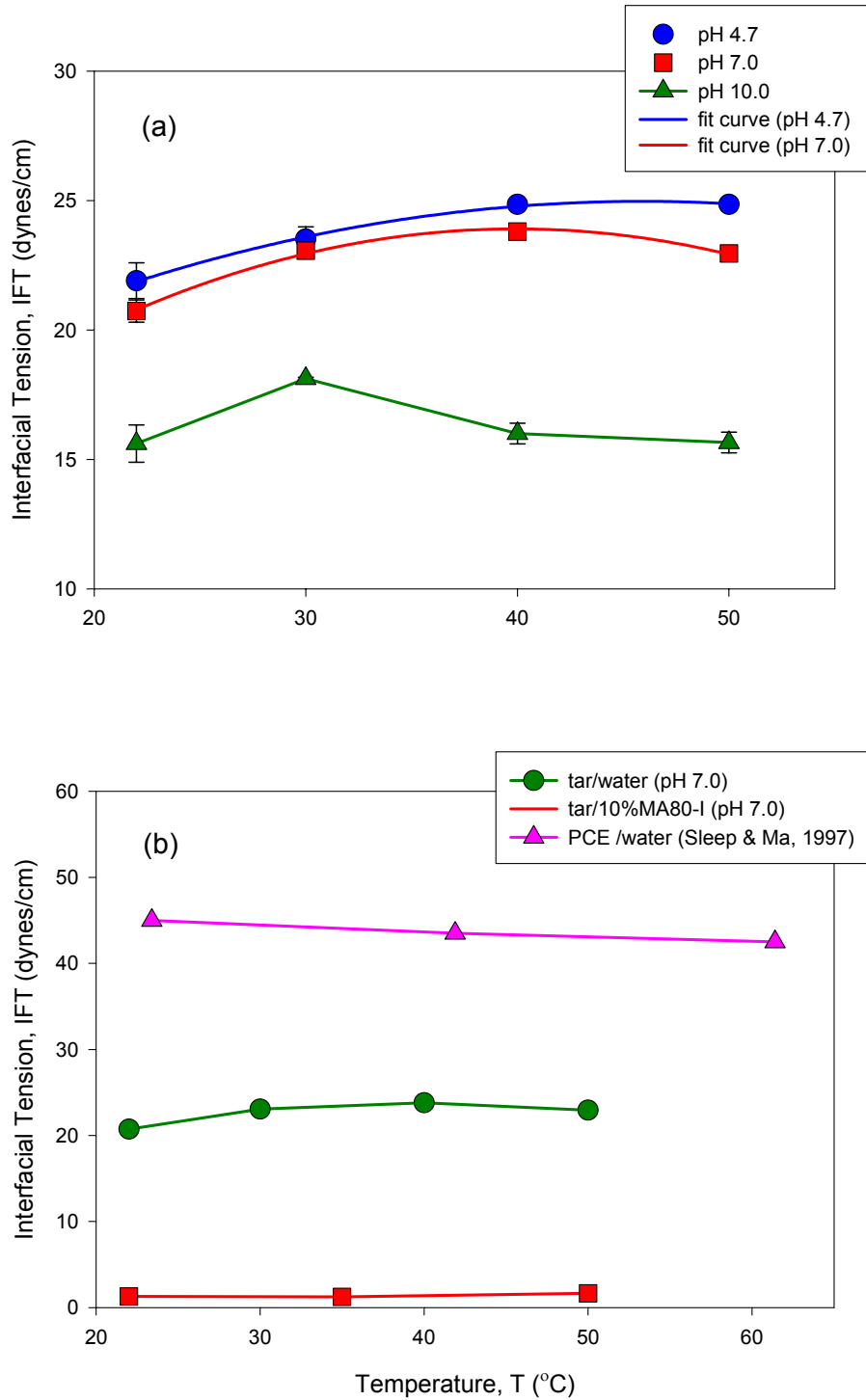


Figure 7-6. Charleston tar-water, surfactant solution IFT as a function of temperature (a) Tar-water IFT as a function of temperature at different pHs; (b) Comparison of tar-water IFT and tar-surfactant solution IFT as a function of temperature at pH 7.0.

interface (Davies and Rideal, 1963). At the same time, aging effects of the interface can impact the measured IFT (Luthy et al., 1993; Nelson et al., 1996; Sleep and Ma, 1997). So, the IFT variation with temperature is actually system specific. Various data have been reported for the oil-water IFTs as a function of temperature. McCaffery (1972) observed an approximate 1 dyne/cm decrease in IFT per 10°C increase in temperature for n-alkanes in water, and a decrease of 0.7-0.3 dynes/cm per 10°C for mineral oil and tetradecane. An IFT decreased with increasing temperature was also observed in the PCE-water system (Sleep and Ma, 1997). However, Hjelmeland and Larrondo (1986) reported that IFT between crude oil and a brine solution increased with increasing temperature under anaerobic conditions, and decreased with increasing temperature under aerobic conditions. A comparison between the IFT of coal tar-water and coal tar-surfactant systems as a function of temperature at pH 7.0 is shown in Figure 7-6b. The presence of MA-80I, surfactant greatly reduced the tar-water IFT from over 20 dynes/cm for original Charleston tar to approximately 1.5 dynes/cm, but presented little variation with temperature.

Effect of Temperature on Contact Angle

Contact angle of Charleston coal tar on glass slides was evaluated at pH 4.6 ± 0.1 , 7.0 ± 0.1 and 10.0 ± 0.1 over a temperature range of 22 to 50°C. A decrease in contact angle in tar-water-glass system with elevated temperature was observed at pH 4.7, while no difference in trends was found at pH 7.0 and 10.0 (Figure 7-7a). When the pH was higher than 7.0, the contact angle at 22°C was already very low (approximately 14°),

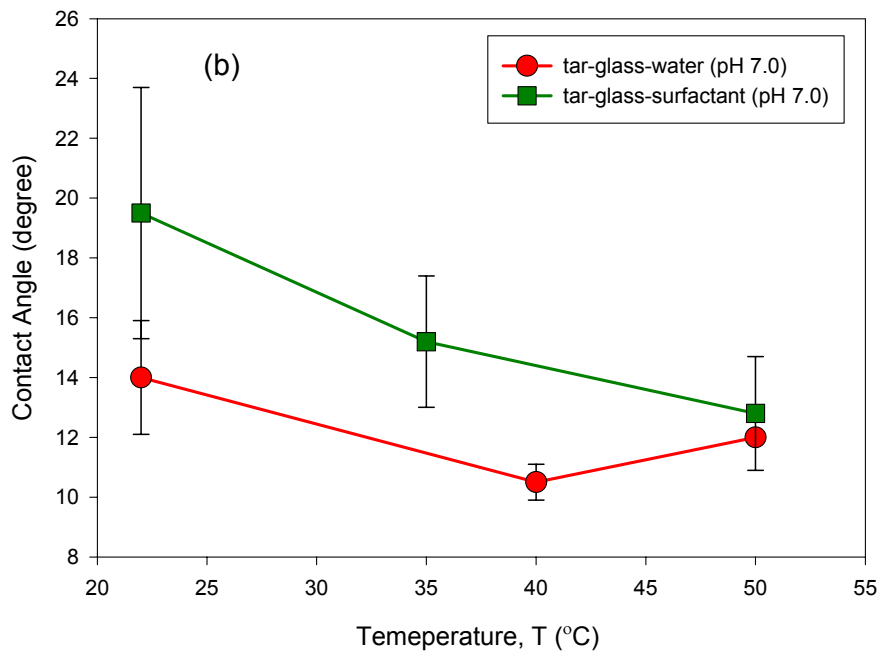
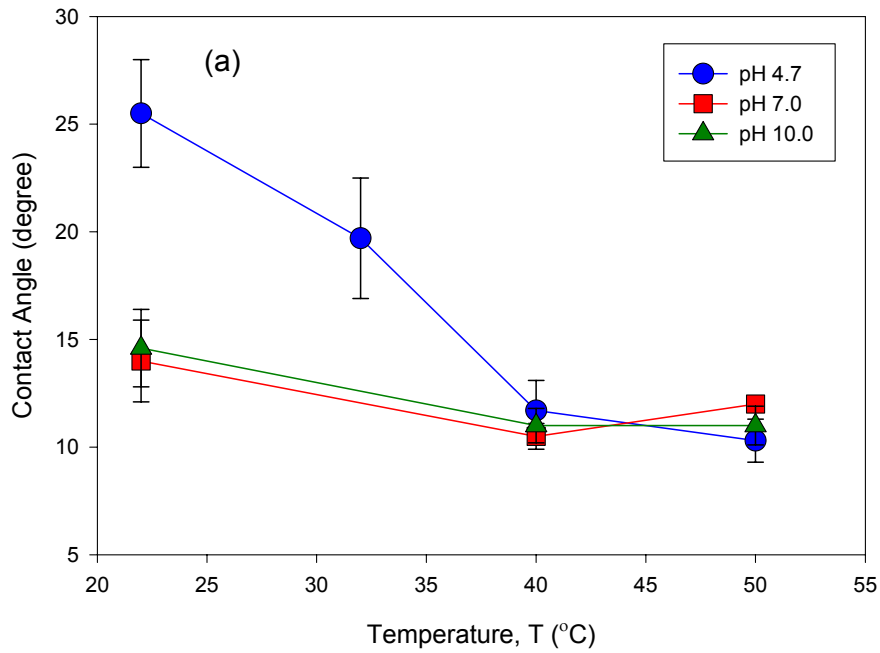


Figure 7-7. Contact angle of glass slides in Charleston tar-water and tar-10% MA80-I surfactant solution systems as a function of temperature (a) Contact angle of Charleston coal tar on glass slide in water; (b) Comparison of contact angle of Charleston coal tar on glass slide in water and surfactant solution.

it was hard to observe further reduction of contact angle with elevated temperature due to the impurity and roughness of the glass surface. The dependence of wettability on temperature is quite complex. Three possible effects of increasing reservoir temperature during thermal recovery operations have been reported: i) unaltered wettability; ii) more strongly water-wet, and iii) more strongly oil-wet (Rao, 1999). For an organic-water-glass system, contact angle change of $-0.27^{\circ}/^{\circ}\text{C}$ was observed by Poston et al. (1970). Hjelmeland and Larrondo (1986) found that an oil-wet calcite surface at 22°C changed to water-wet at 60°C , which corresponds to a contact angle reduction with increasing temperature. whereas, Rao and Karyampudi (1995) observed that a quartz surface in a heavy oil-brine system remained strongly water-wetting in the temperature range of 20 to 162°C , and exhibited strongly oil-wetting at 196°C . For air-water-silica systems, the contact angle is reported approach zero and no effect of temperature was found (Davis, 1994; Bradford et al., 1995).

When comparing the contact angle in coal tar-water-glass and coal tar-surfactant-system, the contact angle in coal tar-surfactant-glass system was observed to be higher than that in coal tar-water-glass system, which indicated that the glass surface became relatively less water-wet in the presence of surfactant (Figure 7-7b). Demond et al. (1994) observed that the presence of a cationic surfactant, cetyltrimethylammonium bromide (CTAB), caused wettability alteration from water-wet to oil-wet (contact angle changed from about 10° - 15° to 155° or 180°) in an *o*-xylene-water-quartz system, from water-wet to oil-wet. The glass surface remained water-wet in this study, although the contact angle increased.

Among the coal tar properties considered, including density, viscosity, tar-water IFT and contact angle, variations of density, tar-water IFT and contact angle with temperature in the range of 22 to 50°C were not sufficient enough to cause any considerable changes in coal tar entrapment and removal. Viscosity variation over the evaluated temperature range was most significant and expected to impact the residual saturation of coal tar in silica sands.

Residual Coal Tar Saturation during Tar Displacement Experiments

Effect of Temperature on Coal Tar Residual Saturation

Coal tar-water two-phase residual saturation experiments were performed in columns packed with either F-70 or 20-30 mesh Ottawa sand at three different temperatures (22, 35 and 50°C). The enhance of coal tar removal with elevated temperature in F-70 Ottawa sand was less significant than that in 20-30 mesh Ottawa sand over the temperature range of 22 to 50°C. Figure 7-8a shows the amount of coal tar removed and residual coal tar saturation in F-70 Ottawa sand packed columns after approximately 25 pore volumes of 10% MA-80I surfactant solution flushing. The amount of coal tar removed increased from 14.0 mL to 16.9 mL, and the corresponding residual tar saturation decreased from 31.4% to 27.6%, when temperature was increased from 22 to 50°C. For 20-30 mesh Ottawa sand columns under the same surfactant flushing and temperature conditions, the amount of coal tar removed was higher and residual coal tar was lower than those of F-70 Ottawa sand columns (Figure 7-8b). In 20-30 mesh Ottawa sand columns, the removed coal tar increase from 18.9 mL to 23.8 mL, and residual tar saturation decreased from 32.8% to 21.8%. This observation suggested that temperature

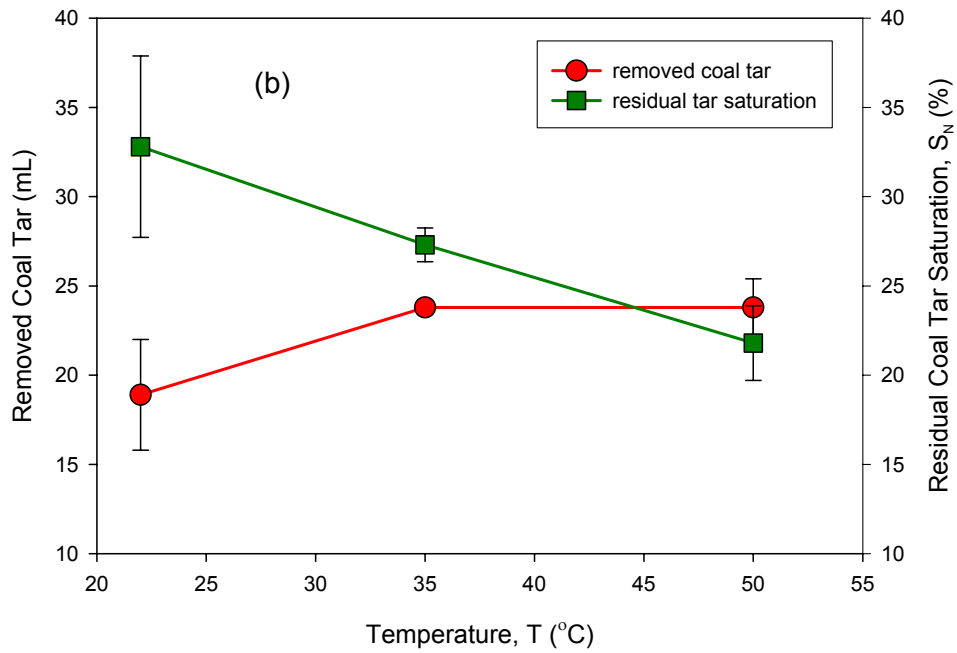
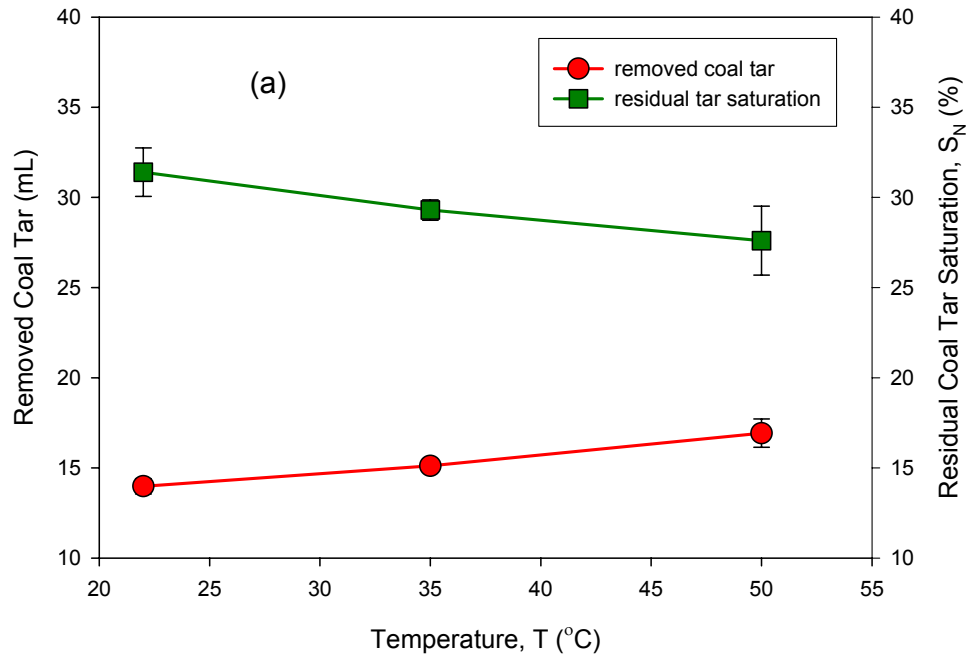


Figure 7-8. Temperature effect on Charleston coal tar removal in Ottawa sand (a) F-70 Ottawa sand; (b) 20-30 mesh Ottawa sand.

effect on NAPL removal was more significant in coarse particle porous media than in fine particle porous media.

Surfactant Screening

Both anionic and nonionic surfactants have been widely used in enhanced oil recovery and aquifer remediation. The application of nonionic surfactants at elevated temperature is usually avoided because of the cloud point effects, which is defined as the temperature above which an aqueous solution of a water-soluble surfactant becomes turbid. In this study, three anionic surfactants, including Aerosol MA-80I, Steol CS-330 and Dowfax 8390, were selected in phase behavior experiments. Aerosol MA-80I has been widely used in SEAR (Ramsburg, 2002), and Steol CS-330 has been reported to be very efficient in EOR based on their ability to greatly reduce the oil-water IFT (Hirasaki and Zhang, 2003). Dowfax 8390 was believed to not only lower the oil-water IFT but also increase the solubility of PAHs due to the aromatic rings in the surfactant structure (Lee et al., 2001a; Rouse et al., 2001). These three surfactants bear different types of hydrophobic portions, i. e., MA-80I has an aliphatic hydrophobic chain, CS-330 contains aliphatic cyclic groups, and Dowfax 8390 bears aromatic rings.

Salinity can also have pronounced effects on phase behavior of anionic surfactant solutions in contact with NAPLs. The concentration of electrolyte in the aqueous phase was determined by evaluating the tar-water IFT and viscosity reduction of equilibrated coal tar. Salt scan experiments performed on Charleston tar-surfactant solution system at room temperature ($22 \pm 1^\circ\text{C}$) showed that all surfactant solutions lowered the interfacial tension between coal tar and water from 20.7 dynes/cm to approximately 1-2 dynes/cm

(Figure 7-9a). The addition of NaCl had little effect on the observed IFT reduction. For Charleston coal tar equilibrated with 10% MA-80I + 1 g/L CaCl₂ + NaCl surfactant solution, the viscosity decreased from 425 cP to about 350 cP at a NaCl concentration of 3 g/L. Above a NaCl concentration of 3 g/L, the viscosity increased (Figure 7-9b). The measured Charleston tar-water IFT and viscosity data for MA-80I (10%wt), CS-330 (5%wt active ingredient) and Dowfax 8390 (5%wt active ingredient) as listed in Table 7-2 shows that different surfactants did not make considerable difference in tar-water IFT reduction with CaCl₂ and NaCl were added. However, when 0.2 M Na₂CO₃ was added to CS-330, tar-water IFT and tar viscosity were greatly reduced compared to other evaluated surfactant solution compositions. When a surfactant solution of 5% CS-330 active component with a Na₂CO₃ concentration of 0.2 M was mixed with Charleston coal tar, after equilibration for over 24 hours, the tar-water IFT was measured to be approximately 0.1 dynes/cm, and viscosity of tar decreased to 139 cP at 22°C. Based on the preliminary surfactant phase experiments, two surfactant solutions were used in tar displacement experiments. The selection of surfactant solution was mainly based on the effect of solution on the tar-water IFT reduction. For example, the addition of Na₂CO₃ reduced the tar-water IFT on order of magnitude lower than that with the addition of NaCl. Viscosity and cost were also considered in the surfactant solution selection. For instance, the tar-water IFT variations were within 1 dynes/cm at different NaCl concentration in the range of 0 to 9 g/L for MA-80I surfactant solution, but the viscosity is the lowest at a NaCl of concentration of 3 g/L, this NaCl concentration was thus considered as the optimum salt concentration for MA-80I surfactant solution. Dowfax 8390 is very expensive and the tar-water IFT reduction with the addition of Dowfax 8390 was similar as that of MA-80I

Table 7-2. Effect of surfactant and salt on tar-water IFT and viscosity of Charleston coal tar at room temperature ($22 \pm 1^\circ\text{C}$).

Surfactant	Salt	Salt Concentration (g/L)	IFT (dyens/cm)	Viscosity (cP)
MA-80I	1 g/L CaCl ₂ + NaCl	0	1.95 (± 0.06)*	386.2 (± 4.1)
		3	1.36 (± 0.20)	338.1 (± 0.4)
		6	1.48 (± 0.04)	384.6 (± 3.7)
		15	1.11 (± 0.07)	539.9 (± 3.8)
CS-330	1 g/L CaCl ₂ + NaCl	0	1.46 (± 0.02)	NA
		3	1.41 (± 0.05)	
		9	1.12 (± 0.03)	
CS-330	Na ₂ CO ₃	21.2	0.1	139.0 (± 0.8)
Dowfax 8390	1 g/L CaCl ₂ + NaCl	0	1.56 (± 0.01)	NA
		3	1.48 (± 0.01)	
		9	1.12 (± 0.03)	

* standard deviation (s. d. = $\sigma/\sqrt{n-1}$)

NA=not available

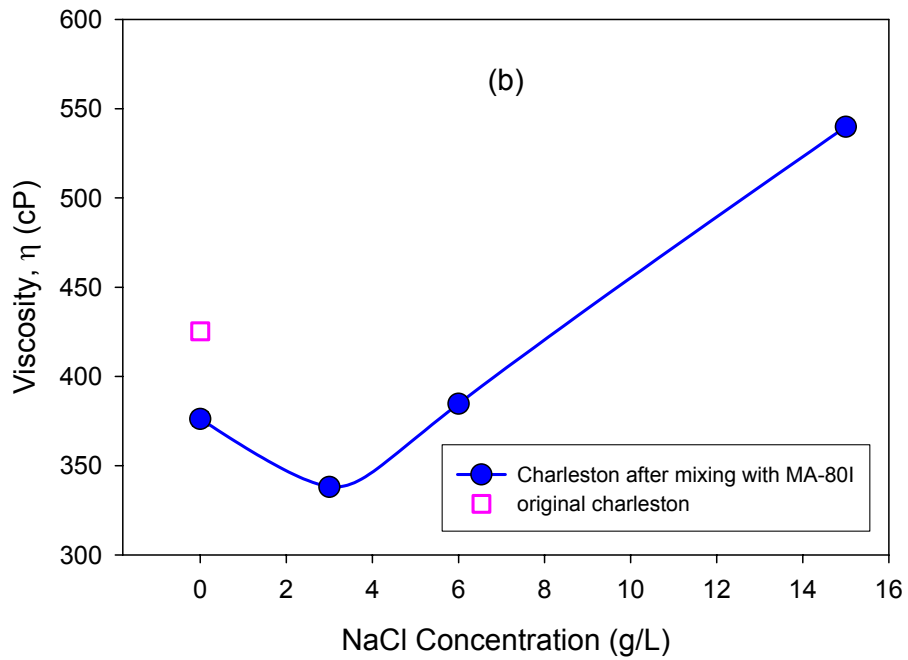
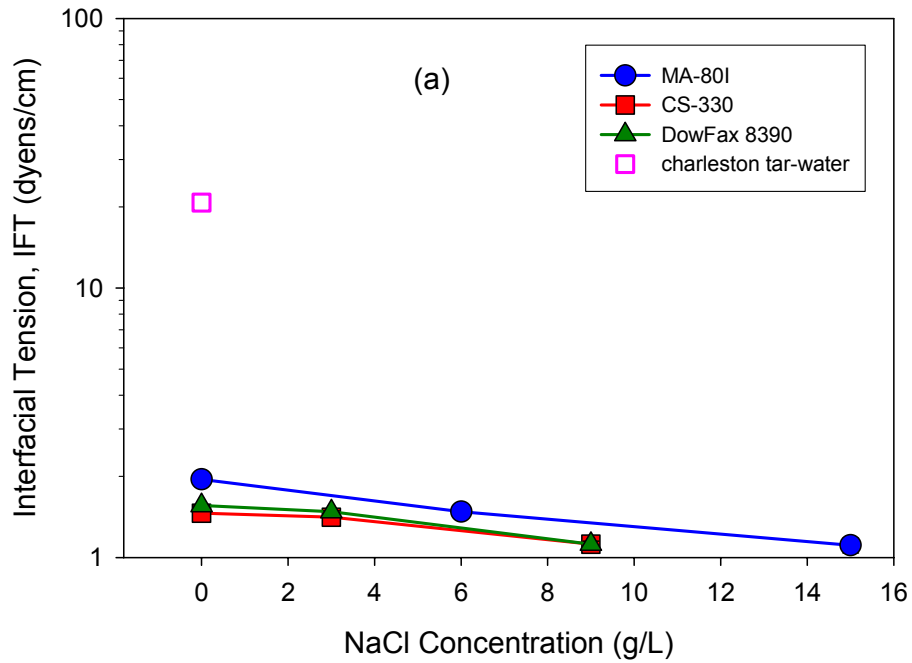


Figure 7-9. IFT and viscosity as a function of salinity in Charleston coal tar-surfactant solution system (a) IFT as a function of salinity; (b) viscosity as a function of salinity (error bars are smaller than symbols).

and CS-330, hence Dowfax 8390 was not evaluated in subsequent tar displacement experiments. These two surfactant solutions were 10% MA-80I + 1 g/L CaCl_2 + 3 g/L NaCl and 5% CS-330 active component + 21.2 g/L (0.2 M) Na_2CO_3 , designated as MA and CS in the following sections, respectively.

Effects of Surfactant Flushing on Residual Coal Tar Saturation

The coal tar contaminated columns packed with 20-30 mesh Ottawa sand after a water flood were followed by MA and CS surfactant flushing at room temperature ($22 \pm 1^\circ\text{C}$), respectively. Figure 7-10 shows that the residual saturation of coal tar was nearly 8% lower after CS surfactant solution flushing than surfactant flushing with MA. The reason could be attributed to the greater tar-water IFT reduction of CS-330 compared to MA-80I. The tar-water IFT after Charleston coal tar equilibrated with CS surfactant solution was measure to be approximately 0.1 dynes/cm, while the tar-water IFT after equilibrated with MA surfactant solution was about 1.4 dynes/cm, more than one order-of-magnitude higher. In addition, the viscosity of Charleston coal tar equilibrated with CS surfactant solution was 139 cP at 22°C , considerably lower than that of the tar equilibrated with MA solution (338 cP). From the phase behavior experiment, it was also visually observed that the Charleston tar flowed more easily in the test tubes after equilibrating with CS-330 surfactant solution. At temperature of $50 \pm 1^\circ\text{C}$, the residual coal tar saturation decrease from residual saturation after water flushing (33.9%) to 25.3% after MA surfactant solution flushing and 19.6% after CS surfactant solution flushing, which indicates approximately 6% lower in residual tar saturation for CS surfactant flushing.

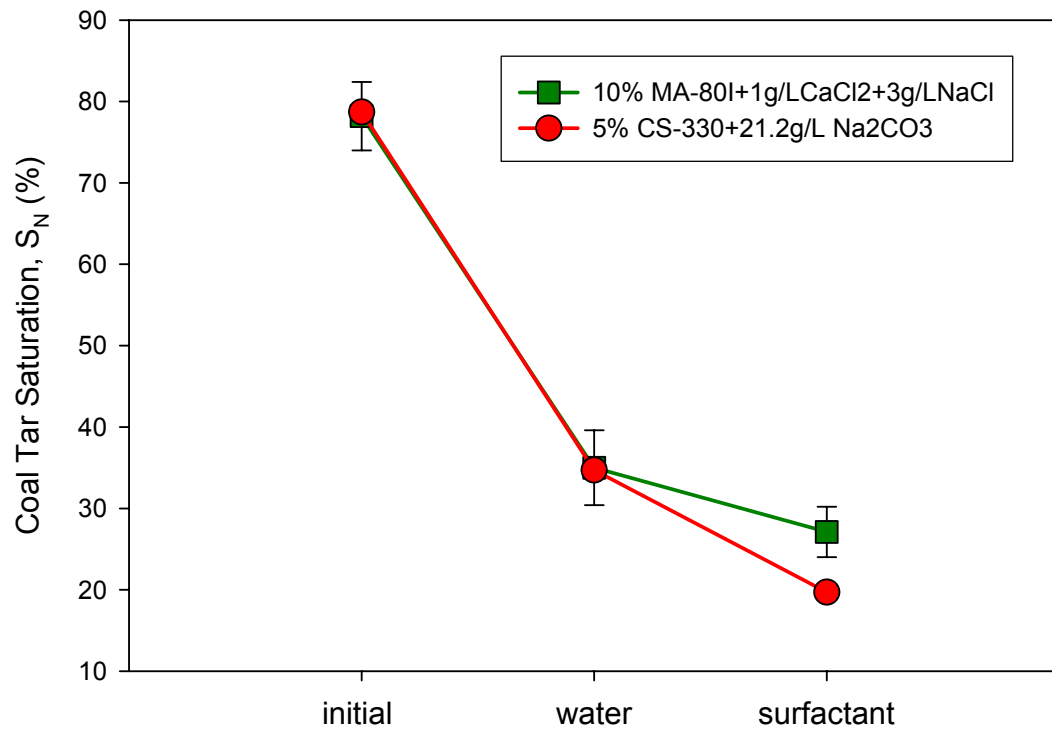


Figure 7-10. Comparison of Charleston coal tar residual saturation after different surfactant solution flushing at 22°C (“initial” means the initial coal tar saturation, “water” refers to the residual tar saturation after water (0.01M NaCl) flood, and “surfactant” corresponds to the residual tar saturation after surfactant flushing).

Polymer Solution Viscosity and Rheology

Xanthan gum is a polysaccharide widely used in micellar/polymer flushing in EOR. It was found to be the most suitable polymer for remediation of NAPL in porous media (Martel et al., 1998). Powder xanthan gum was used as the polymer in surfactant/polymer flushing in this study to increase the viscosity of the displacing phase and improve the mobility ratio, consequently achieve better displacement of viscous NAPL.

Unlike coal tar, xanthan gum solution is a non-Newtonian fluid, which means that the viscosity of xanthan gum solution changes with the applied shear rate. The viscosity of non-Newtonian fluid can decrease (shear thinning) or increase (shear thickening) with increasing shear rate. In the case of xanthan gum in water, viscosity has been shown to decrease with increasing shear rate (Martel et al., 1998; Giese and Powers, 2002).

According to the power law (Wilkinson, 1960), the shear stress and shear rate relationship for non-Newtonian fluids can be expressed as:

$$\tau = K \dot{\gamma}^n \quad (7-14)$$

where τ ($\text{g cm}^{-1} \text{s}^{-1}$) and $\dot{\gamma}$ (s^{-1}) referred to shear stress and shear rate, respectively, K is the power law constant (cP s^{n-1}) and n is the power law exponent. After substituting

Newton's law, $\tau = \mu \dot{\gamma}$, into Equation (7-12), the following expression is obtained:

$$\eta = K \dot{\gamma}^{n-1} \quad (7-15)$$

where the coefficient K and n can be estimated by measuring the viscosity as a function of shear rates.

Shear rates in porous media vary with porosity, permeability and fluid velocity. Some approximations are available to predict the shear rate in porous media. Hirassaki and Pope (1974) proposed the following model, which was most appropriate for homogeneous media of uniform grain size.

$$\dot{\gamma} = \left(\frac{3n+1}{4n} \right)^{\frac{n}{n-1}} \frac{12v}{\left(\frac{150k}{\phi} \right)^{0.5}} \quad (7-16)$$

where v is the pore water velocity (cm/s), and k (cm²) and ϕ (cm³/cm³) are the permeability and porosity of the porous media, respectively. Therefore, the viscosity of polymer solution in a specific porous media can be estimated by applying the estimated shear rate in porous media as shown in Equation (7-15).

The viscosity of xanthan gum solution as a function of shear rate, temperature and concentration on a log-log scale is shown in Figure 7-11. It can be seen that the viscosity decreased with increasing shear rate in the range from 0.08 to 1000 s⁻¹, which is indicative of shear thinning. At the same time, xanthan gum solution viscosity decreased with increasing temperature, and increased with increasing xanthan gum concentration. Higher xanthan gum concentration can yield a higher aqueous phase viscosity and higher mobility ratio, but greater viscosity decrease permeability considerably. A concentration of 500 ppm xanthan gum was selected for use in this study to achieve increased viscosity without substantial reductions in permeability. At this concentration, the estimated xanthan gum viscosities in the 20-30 mesh Ottawa sand column were approximately 15.1, 9.9 and 7.2 cP at temperature of 22, 35 and 50°C, respectively.

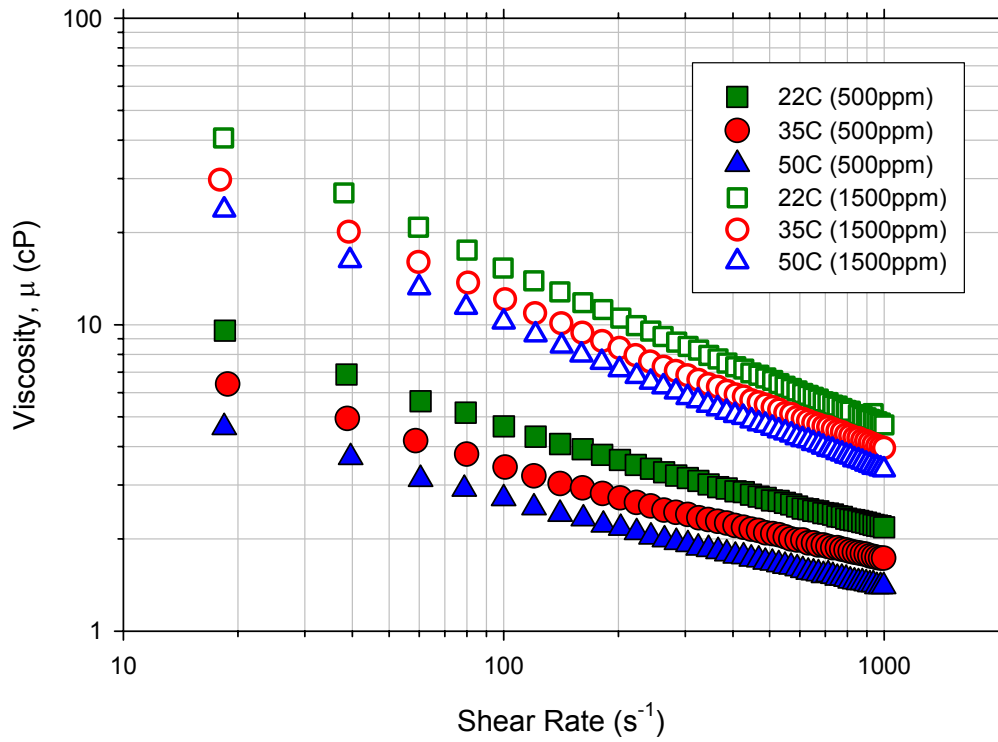


Figure 7-11. Effect of shear rate, temperature and concentration on xanthan gum solution viscosity.

Dimensionless Parameter Analysis of Coal Tar Displacement

Dimensionless group analysis was performed to evaluate tar displacement in 20-30 mesh Ottawa sand. The permeability at different stages during the flushing process is shown in Figure 7-12. The initial permeability of the water saturated column without coal tar was approximately $1 \times 10^{-6} \text{ cm}^2$. This value was in agreement with the calculated value by Kozeny-Carman equation (Equation 2-24), which is approximately $2.5 \times 10^{-6} \text{ cm}^2$ under this circumstance. The permeability in coal tar contaminated column was much lower. After entrapment of coal tar at residual saturation, the permeability decreased by almost one order-of-magnitude ($9.59 \times 10^{-8} \text{ cm}^2$). After surfactant and surfactant/polymer flushing, the measured permeabilities were 1.65×10^{-7} and $2.37 \times 10^{-7} \text{ cm}^2$, respectively, which were slightly higher than that prior to the surfactant or surfactant/polymer flushing due to the removed of residual coal tar inside the column.

Capillary number (N_{Ca}), bond number (N_B) and total trapping number (N_T) in tar-water-Ottawa sand system were calculated according to Equation (2-22), (2-23) and (2-27). The dimensionless group, F, was proposed by Abrams (1975), which was defined as following:

$$F = N_{Ca} \left(\frac{\eta_w}{\eta_o} \right)^{0.4} = \left(\frac{q \eta_w}{\gamma_{o/w}} \right) \left(\frac{\eta_w}{\eta_o} \right)^{0.4} \quad (7-17)$$

The residual oil saturation is generally independent of N_{Ca} when N_{Ca} is less than 2×10^{-5} (Ng et al., 1978). The critical value of N_T required to initiate PCE mobilization was reported to be in the range of 2×10^{-5} to 5×10^{-5} (Pennell et al., 1996). The common waterfloods of oil reservoir were operated when F was less than 1×10^{-6} . To displace residual oil from porous media, F must be raised to the range of 1×10^{-4} to 1×10^{-3}

(Abrams, 1975). Table 7-3 lists the calculated values of the dimensionless groups for each coal tar displacement column experiment. Since the density of coal tar is very close to that of water, For example, the density difference between Charleston coal tar and water was approximately 0.1 g/cm^3 during water displacement and ranged from 0.006 to 0.09 g/cm^3 during surfactant or surfactant/polymer flushing, which implies the buoyancy force in coal tar-water system may be negligible. So the Bond numbers (N_B), which is defined as the ratio of buoyancy force to capillary force, were not listed in Table 7-3, and the relationship between the residual tar saturation and N_B was not investigated, either. After the initial water flood, without surfactant or polymer, the residual coal tar saturations ranged from 33.9% to 35.3%, and the corresponding N_{Ca} , N_T and F values were approximately 10^{-6} and 10^{-7} , which are far below the reported critical values for NAPL mobilization (Abrams, 1975; Lake, 1989; Pennell et al., 1996). In order to mobilize the trapped coal tar, several approaches were utilized in order to increase the value of N_{Ca} , N_T and F . These methods include: i) surfactant flushing applied to the columns in order to reduce the tar-water IFT; ii) temperature increased to obtain lower oil-water viscosity ratio; iii) flow rates increased to increase the capillary number value; iv) xanthan gum added to achieve higher displacing phase viscosity. When CS surfactant flushing was applied, the values of N_{Ca} , N_T were increased to greater than 1×10^{-3} , and F was greater than 1×10^{-4} . Although the in PCE systems, completely displacement of TCE occurred when N_T was greater than 1×10^{-3} , coal tar residual saturations were still as high as 20%. Even if N_{Ca} , N_T decreased to greater than 1×10^{-2} and F to greater than 5×10^{-3} , the coal tar residual saturations were approximately 17%. Figure 7-13a, b, c showed the coal tar saturation as a function of N_{Ca} , N_T and F . The trends of these three figures are

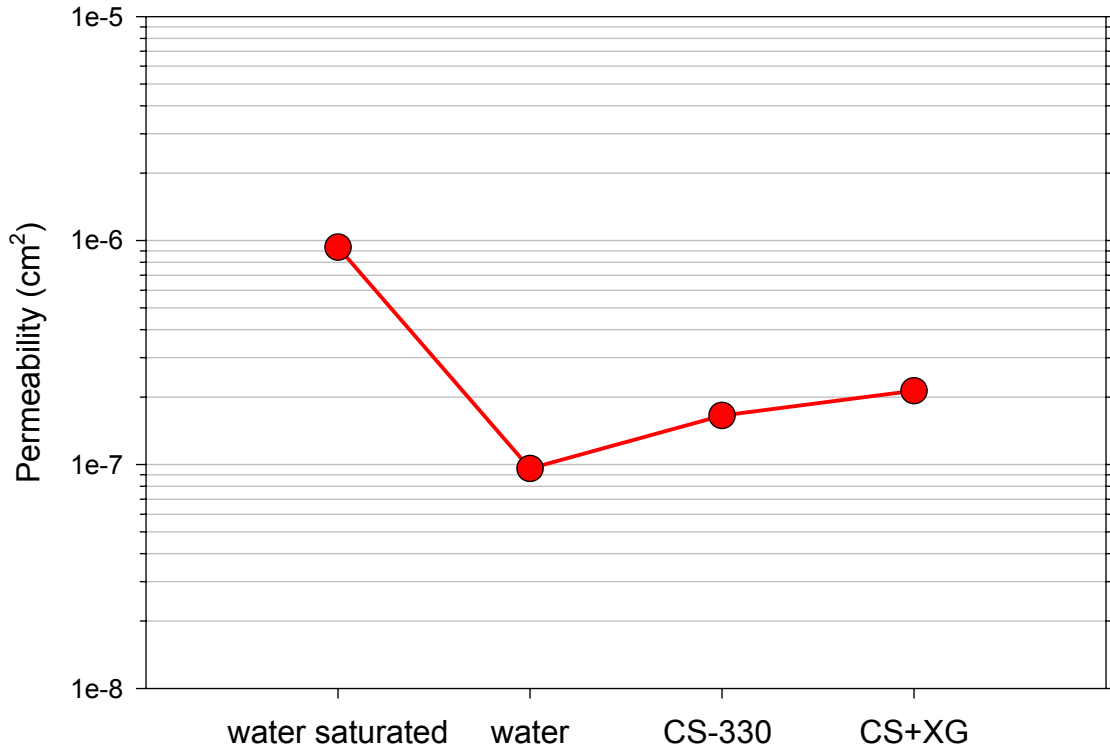


Figure 7-12. Permeability changes in column during various stage of the flushing process (“Water”, “CS-330” and “CS+XG” correspond to the permeability after water (0.01 M NaCl, CS-330 and CS-330/Xanthan gum solution flushing).

Table 7-3. Dimensionless Parameter Analysis of Coal Tar Displacement.

Column ID	Flood Solution	Bulk Density (g/cm ³)	Porosity (cm ³ /cm ³)	Initial tar saturation (%)	Residual tar saturation (%)	Flow Rate (mL/min)	Viscosity Ratio (μ_w/μ_o)	IFT (dyne/cm)	N _{Ca}	N _T	F
OS-1E	Water	1.782	0.330	78.9	35.3	5	0.00224	20.73	1.9E-6	2.1E-6	1.6E-7
OS-1F	Water	1.778	0.332	78.4	34.1	5	0.00224	20.73	1.9E-6	2.1E-6	1.6E-7
OS-3D	Water	1.782	0.329	78.8	33.9	5	0.00810	22.95	9.6E-7	1.1E-6	1.9E-6
OS-1E	CS*	1.782	0.330	78.9	19.2	10	0.0101	0.1	1.2E-3	1.2E-3	1.8E-4
OS-1F	CS	1.778	0.332	78.4	20.2	10	0.0101	0.1	1.2E-3	1.2E-3	1.8E-4
OS-3D	MA [†]	1.782	0.329	78.8	25.3	10	0.0253	1.1	5.5E-5	5.7E-5	1.2E-5
OS-3D	CS	1.782	0.329	78.8	19.6	10	0.0367	0.1	8.8E-4	9.1E-4	2.4E-4
OS-1E	CS+XG [‡]	1.782	0.330	78.9	18.0	10	0.1086	0.1	1.2E-2	1.3E-2	5.2E-3
OS-1E	CS+XG	1.782	0.330	78.9	17.7	10	0.1086	0.1	1.2E-2	1.3E-2	5.2E-3
OS-1E	CS+XG	1.782	0.330	78.9	16.9	15	0.1086	0.1	1.9E-2	1.9E-2	7.8E-3
OS-1F	CS+XG	1.778	0.332	78.4	16.5	15	0.1086	0.1	1.9E-2	1.9E-2	7.8E-3
OS-3D	CS+XG	1.782	0.329	78.8	17.4	10	0.2	0.1	5.8E-3	3.3E-3	5.8E-3

* CS: 5% CS330 active ingredient + 0.2M Na₂CO₃.

[†] MA: 10% MA-80I +1 g/L CaCl₂ + 3g/L NaCl.

[‡] XG: 500 ppm xanthan gum.

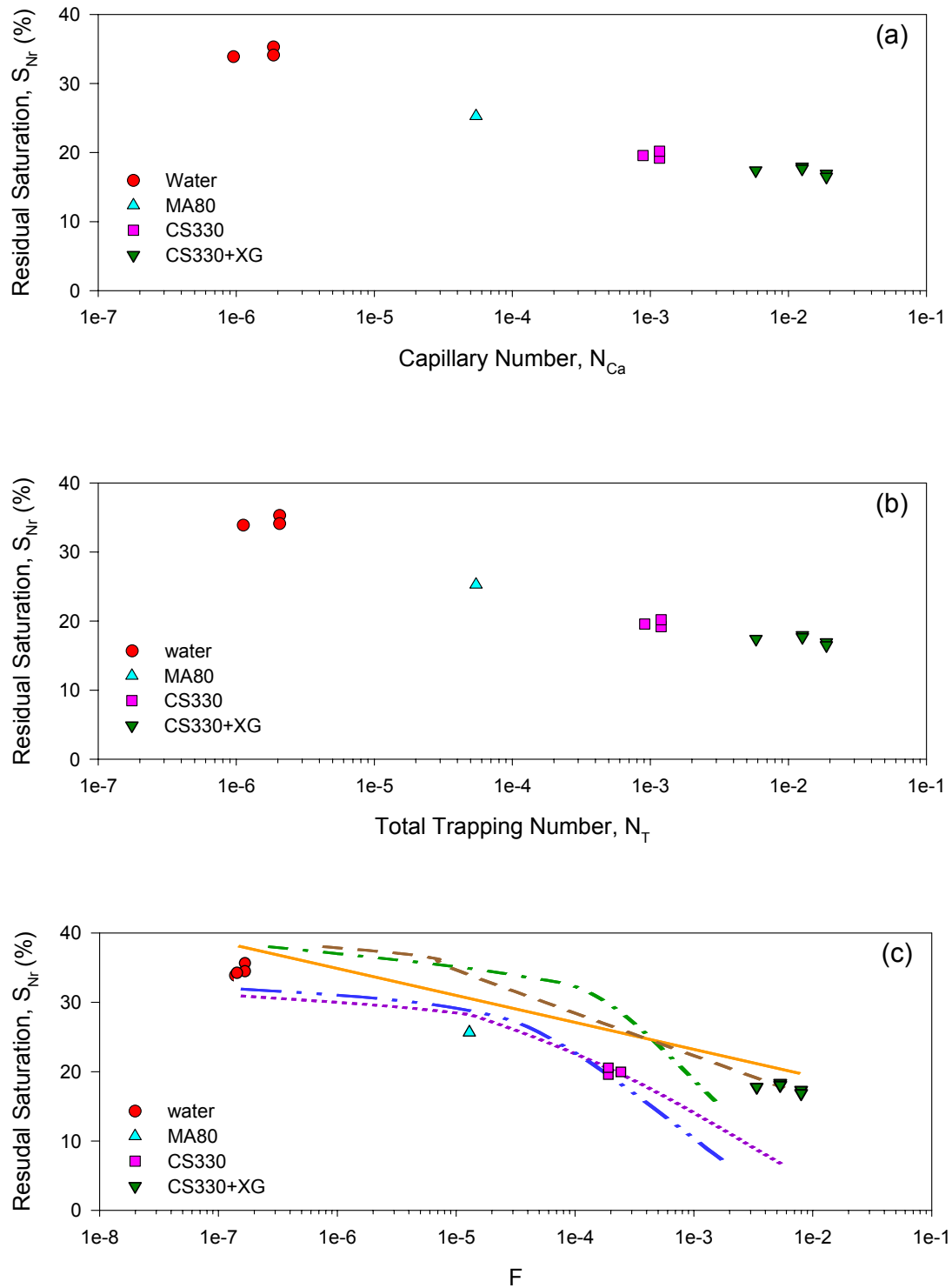


Figure 7-13. Relationships between residual coal tar saturation and (a) capillary number, (b) total trapping number, and (c) dimensionless group F (Solid or dash lines in (c) represent data for crude oil (Abrams, 1975).

very similar. Compared with the PCE desaturation curve (Pennell et al., 1996), the coal tar residual saturation as a function of N_T showed a steady and slow decrease with increasing N_T , and the coal tar showed no evidence of complete displacement over the evaluated N_T range. This result implied that coal tar behaviors very differently in the porous media from other commonly encountered pure NAPLs such as PCE and TCE. Abrams (1975) also observed crude oil residual saturations of up to 20% at F values greater than 10^{-2} (Figure 7-13c). These data indicates that it is considerably difficult to removal coal tar from the porous media than low viscosity fluids.

Summary and Conclusions

In this section, the effect of temperature and surfactant/salt or surfactant/polymer/salt addition on the coal tar removal from porous media is evaluated. Coal tar properties including density, viscosity, interfacial tension, and wettability were found to dependent on temperature. Viscosity decreased exponentially with elevated temperature in the range of 22°C to 50°C. The viscosity reduction was more significant for high viscous tars, which suggests potential benefit of thermal enhancements in viscous NAPL removal. Within the evaluated temperature range from 22°C to 50°C, coal tar residual saturation in 20-30 mesh Ottawa sand was more sensitive to temperature than in F-70 Ottawa sand. That is, more coal tar was removed from 20-30 mesh Ottawa sand with increasing temperature.

Surfactants can greatly reduce the oil-water interfacial tension. In this study, Steol CS-330 was found to reduce the Charleston tar-water IFT from 27 dynes/cm to

approximately 0.1 dynes/cm. The residual coal tar saturation in Ottawa sand after CS surfactant flushing was 8% lower than those flushed with MA surfactant solution at 22°C, and 6% lower at 50°C. Na₂CO₃ was proved to be more effective in IFT reduction than NaCl in the CS-330 surfactant solution. However, the tar-water IFT was still not low enough to achieve complete displacement of residual coal tar. More detailed salinity scan and surfactant screening experiments may help to identify more effective surfactant, polymer and salt combinations for the viscous coal tar removal from porous media.

Dimensionless group analysis showed that residual coal tar saturation decreased with increasing capillary number (N_{Ca}), total trapping number (N_T) and F value, but the decrease function was different from those of other pure NAPLs such as PCE. A complete mobilization region was not obtained based on dimensionless parameter analysis.

Although the effect of temperature and surfactant and/or polymer addition does not sound so great to achieve the complete displacement of Charleston coal tar, the results obtained in this study still provide very important information. Because Charleston coal tar has the highest viscosity (425 cP) of all the coal tar samples evaluated in this study, it actually represents the “worst case” scenario. If the residual saturation of Charleston coal tar could be reduced from approximately 35% (after water displacement flood) to less than 20% after surfactant and/or surfactant/polymer flushing, the residual saturation of other less viscous coal tars have the potential to be reduced to a lower level, which implies effective strategy to some MGP site remediation.

CHAPTER VIII

CONCLUSIONS AND RECOMMENDATIONS

Mineral oils and coal tars are viscous nonaqueous phase liquids (NAPLs). Their potential risks to human health and the environment are primarily caused by polycyclic aromatic hydrocarbons (PAHs), which exist as impurities in mineral oils and main constituents in coal tars. Thus, the presence of these organic mixtures in the subsurface can degrade the ground water quality. However, very limited data are available about the mineral oil and coal tar behavior in the subsurface. The investigations on the mechanisms governing the mineral oil and coal tar removal from the porous media are extremely lacking. Current remediation technologies are ineffective, especially to coal tar contaminated sites (former manufactured gas plants (MGPs)), and a lot of contaminated sites remain unaddressed. The research described herein focused on the quantification of properties of commercial mineral oils, MGP-site coal tars and natural soils and residual oil or tar saturations in soils, and the investigation of NAPL entrapment and displacement mechanisms. Remediation strategies including thermal method and surfactant or surfactant/polymer flushing were evaluated in a laboratory scale.

Based on the characterization data, mineral oils were classified as viscous light nonaqueous liquids (LNAPLs), with densities of approximately 0.88 g/cm^3 and viscosities ranging from 13 to 17 cP at 22°C . The oil-water IFTs ranged from 23.8 to 48.7

dynes/cm, slightly lower than the commonly pure NAPL such as PCE and TCE. Residual mineral oil saturations in two-phase (water-oil) and three-phase (air-water-oil) systems were in the range of 5% to 25%, which were consistent with literature residual oil saturation data. Correlations between residual oil saturation and representative oil and soil properties reveal that residual oil saturations are dependent upon soil total carbon content, particle size parameter (particle size and size distribution). However, most of the correlations are not strong.

Coal tars are viscous DNAPLs, with densities slightly higher than water (1.052 - 1.104 g/cm³) and viscosities much higher than water, (32 - 425 cP at 22°C). These values were much higher than most of the coal tar viscosity in other research work, and are representative of the coal tars encountered at former MGP sites. Charleston tar, which had a viscosity of 425 cP at 22°C, was the most difficult to remove during the two-phase (water-tar) displacement experiments. Residual tar saturations in two-phase systems (water-tar) were in the range of 0.13 to 0.23 cm³/cm³, which were consistent with the reported residual saturation values of other NAPLs. Compared to literature reported residual tar saturations, which were obtained in relatively uniform coarse quartz sand, this research work provided residual saturation data of field tar samples in natural soils. These data will help the risk assessment and remediation strategy to former MGP sites. Correlations between the residual coal tar saturations and tar/soil properties were developed. The results show that the residual saturations were dependent on the tar and soil properties, such as tar viscosity, tar-water IFT, soil carbon content and particle size distribution. These correlations provide tools to predict residual tar saturation from measurable soil and tar properties.

Coal tar acidic and basic properties were quantified in order to investigate the effect of aqueous solution chemistry on residual tar saturation. The data of asphaltene content, acid/base number and point of zero charge (PZC) were in agreement with the corresponding data reported for crude oils, creosotes and coal tars. Coal tar density and viscosity show significant dependence upon asphaltene content, which is attributed to the asphaltene aggregation.

Solution pH exhibited effect on silica surface wettability in the presence of coal tar and tar-water IFTs, which could be attributed to the existence of acidic or basic constituents in coal tar. Based on the contact angle data, the silica surface exhibited slightly increased water-wetting condition (i.e., contact angle reduction) when pH is greater than 7 or lower than 4 (except for Shippensburg tar). At high pH (>7), the contact angle reduction was attributed to the electrostatic repulsive force between negatively charged silica glass surface and deprotonated organic acid in coal tar. At low pH, the hydration force overweighed the electrostatic force and resulted in the contact angle reduction. Interfacial tension exhibited a reduction at both low and high pH, suggesting the dissociation of acid or base constituents was responsible. These mechanisms governing the contact angle and IFT change with pH were further evaluated by addition of 5-indanol and quinoline into the coal tar phase. Quinoline and 5-indanol functioned as organic acid and base, and served as surrogates for the surface active aromatic constituents in coal tar. From the contact angle and IFT measurements with the addition of 5-indanol and quinoline, 5-indanol addition did not effect the contact angle, while the addition of quinoline resulted in a more oil-wetting condition, especially at low pH (< 4). These observations are consistent with the hypothesis that wettability change stems from

the electrostatic interaction between the coal tar phase and silica surface. Another important observation was that the contact angle decreased slightly when pH was less than 4, which indicates that the hydration force cannot be neglected. With the addition of quinoline, this trend was less clear and disappeared when quinoline addition was greater than 5%, confirming the existence of the hydration force. The overall energy caused by van der Waals, electrostatic and hydration forces between the coal tar and glass slide surface as a function of the separation distance between these two surfaces was calculated. The resulted curves of overall energy against separation distance exhibit energy barriers for the coal tar to overcome in order to approach the glass surface at pH 2.6 and 3.4, which theoretically explains the contact angle reduction when pH is less than 4.5. For tar-water IFT, 5-indanol and quinoline acted as surface active species which accumulated at the tar-water interface, and consequently decreased the IFT. Ionic strength exhibited no significant effect on the contact angle and IFT when ionic strength was less than 0.5 M, which suggests that ionic strength effects are negligible at commonly encountered groundwater systems.

For the systems evaluated in this research, the change of contact angle with aqueous chemistry was so small that the silica surface exhibited water-wetting condition within the pH range from 2.6 to 10. The lowest IFT reduced was approximately 13 dynes/cm, which was not low enough to alter the residual tar saturations. Consequently, for MGP sites with similar media conditions, more effective remediation strategies other than aqueous chemistry variation are required in order to removal the residual coal tar.

Capillary pressure-saturation relationships were investigated for F-70 Ottawa sand. Experiment results show the effect of pH on coal tar residual saturation, which was

consistent with the wettability of the media as a function of pH. That is, residual tar saturation in F-70 Ottawa sand at pH 4.6, pH 7.0 and pH10.0 decreased from 0.38, 0.18 to 0.10 cm³/cm³, respectively, which corresponds to a contact angle decrease (more water-wetting) from approximately 24 to 14°. Although no wettability alteration was observed during the evaluated pH range based on the contact angle values, the relative wetting condition change can be seen. The residual tar saturations were much lower than in the two-phase water flood experiments, which could be due to the viscous fingering and channeling. This phenomenon was confirmed by visual observation of the sand core section. Scaling analysis based experiment data shows that the scaling factors used in simple pure organic-water systems, which incorporated IFT ratio, $\frac{(\gamma)_{tar/water}}{(\gamma)_{air/water}}$, or IFT and contact angle ratio, $\frac{(\gamma \cos \omega)_{tar/water}}{(\gamma \cos \omega)_{air/water}}$, failed to predict the experimental data, whereas scaling factor considering IFT, contact angle and viscosity ratio, $\frac{(\gamma \cos \omega)_{tar/water}}{(\gamma \cos \omega)_{air/water}} \left(\frac{\eta_{tar}}{\eta_{water}} \right)^{0.4}$, successfully fit the experimental results. This observation shows that viscosity ratio plays a significant role in the capillary pressure-saturation relationship in viscous oil-water-soil systems.

Another important part of this research was to investigate the effect of temperature and surfactant or surfactant/polymer addition on the coal tar entrapment and removal. Coal tar properties, including density, viscosity and tar-water interfacial tension and porous media wettability were found to dependent on temperature. Viscosity showed an exponential decrease with increasing temperature. In this study, three temperatures (22°C, 35°C and 50°C) within the relatively low temperature range were selected during

the coal tar displacement experiments. When temperature increased from 22 to 50°C, residual tar saturation was found to decrease from 31.4% to 27.6% in F-70 sand, from 32.8% to 21.8% in 20-30 mesh Ottawa sand. In the surfactant flushing studies, three anionic surfactants, Aerosol MA-80I, Steol CS-330 and Dowfax 8390, were tested for the ability to reduce the tar water IFT and two surfactant solutions were utilized in laboratory column experiments. CS-330 with a salinity of 21.2 g/L (0.2 M) Na₂CO₃ was found to be more effective than Aerosol MA-80I with addition of 1 g/L CaCl₂ and 3 g/L NaCl, which indicates the efficiency of surfactant flushing was not only dependent upon the surfactant-NAPL combination, but also salinity. Xanthan gum addition to the surfactant flushing solution shows further removal of the residual coal tar in sand. Due to the non-Newtonian characteristic, xanthan gum solution behavior in the porous medium was not only dependent on concentration, but also the porous medium. To select an appropriate polymer solution concentration that could increase the aqueous viscosity without plugging the pores was very important. A concentration of 500 ppm of xanthan gum solution was used in the surfactant/polymer study and found to enhance the coal tar removal from the porous media.

Dimensionless parameter analysis shows that residual coal tar saturation decreased with increasing capillary number, total trapping number and F value, but the decrease function was different from those of other simple NAPLs such as PCE. No complete mobilization was found within the evaluated total trapping number range. The residual coal tar saturation was still as high as approximately 17% when the total trapping number was higher than 10⁻². This result is in agreement with published data on

displacement of viscous oils, and indicates the difficulty in removing entrapped coal tar from porous media.

Although no complete coal tar displacement was achieved under the experiment conditions in this study, thermal technique and surfactant and/or polymer flushing, or their combinations exhibit potential to the MGP site remediation. But, it may still require further flux and plume management.

For future work

1. The systems investigated in this research are complicated, with various variables. To evaluate the mechanisms governing NAPL entrapment and removal, select more “ideal” sand (no organic content, uniform coarse sand) to start with, and then transfer to natural soils.
2. Further experiments are required to confirm the capillary pressure-saturation (P_c - S) relationship results in this research. The high tar viscosity (62 cP) and F-70 sand (relatively fine and broad particle size distribution) have the potential to result in viscosity fingering and longer experimental duration time. To start with less viscous tar and uniform sand (i.e., 20-30 mesh Ottawa sand) would help to overcome these disadvantages.
3. To further improve the coal tar removal, more detailed surfactant phase experiments would help to screen optimum surfactant solution composition, particularly salt type and concentration.
4. Further investigation of the interaction between polymer and surfactant or polymer and salt will lead to an optimum composition of the flushing solution and improve the flushing efficiency.

5. To investigate the relationship between chemical composition and coal tar physical-chemical properties will help to understand the unique properties of coal tar, and benefit to select appropriate remediation technologies to enhance coal tar removal from porous media.

APPENDIX A. PRIMARY VOLATILE AND SEMIVOLATILE ORGANICS IN AUBURN COAL TAR

Analytical Results for Volatile and Semivolatile Organics META Environmental, Inc.

Field ID:	Coal tar - 1 Auburn	Preparation Method:	EPA 3570
Client:	Lehigh U	Cleanup Method(s):	EPA 3630mod.
Project:	NAPL Mobility	Analysis Method:	GC/FID (EPA8100 mod.)
Lab ID:	10MAYR16.D	Matrix:	NAPL
File ID (PF):	10MAYR16.D	Preservation:	None
File ID (DF):	10MAYR17.D	Decanted:	No
File ID (UF):	10MAYR15.D	Sample Size:	0.0125 g
Date Sampled:		%Solid:	100%
Date Received:	3/8/02	Extract Volume:	2 mL
Date Prepared:	4/30/02	Prep DF:	50
Date Cleanup:	5/7/02	Analysis DF:	1
Date Analyzed:	11 May 2002 1:05 am	Injection Volume:	0.001 mL
Instrument:	GC_3	Batch QC:	LU020430-MB
Operator:	DB		

Analyte:	Concentration mg/kg	Q	RL mg/kg	EDL mg/kg	Comments
TARGET COMPOUNDS:					
Aliphatic (PF: C6-C8)	460		800	400	
Aliphatic (PF: C9-C12)	3,870		800	400	
Aliphatic (PF: C13-C18)	21,400		800	400	
Aliphatic (PF: C19-C36)	42,000		800	400	
Aromatic (DF: C9-C10)	15,800		800	400	
Aromatic (DF: C11-C22)	1,480		800	400	
TPH (UF: C6-C36)	342,000		800	400	
Total VPH	20,100				
Total EPH	68,800				
Total VPH & EPH	85,000				
Extraction Surrogates					
	%R		Min	Max	
Fluorobenzene (DF)	Not Spiked		50%	120%	
2-Fluorobiphenyl (DF)	Not Spiked		50%	120%	
5-alpha-Androstane (PF)	Not Spiked		50%	120%	
Fluorobenzene (UF)	Not Spiked		50%	120%	
2-Fluorobiphenyl (UF)	Not Spiked		50%	120%	
5-alpha-Androstane (UF)	Not Spiked		50%	120%	
Fractionation Surrogates					
2,5-Dibromotoluene (PF)	88%		50%	120%	
2,5-Dibromotoluene (DF)	4%		50%	120%	
2-Bromonaphthalene (DF)	263%	I	50%	120%	
1-Chlorooctadecane (PF)	86%		50%	120%	

Qualifiers:

B Analyte detected in the blank

D Analyte reported from a diluted extract

U Undetected above the detection limit

J Estimated value detected between the reporting and detection limits

E Estimated value detected above calibration range

I Concentration/Peak ID uncertain due to potential interference

RL Reporting limit is the sample equivalent of the lowest linear calibration concentration.

EDL Estimated detection limit is 50% of the RL

Total VPH = Aliphatics (C6-C12) + Aromatics (C9-C10)

Total EPH = Aliphatics (C9-C36) + Aromatics (C11-C22)

Total VPH & EPH = Total VPH + Total EPH - Aliphatics (C9-C12) Due to Range overlap

APPENDIX B. PRIMARY VOLATILE AND SEMIVOLATILE ORGANICS IN CAPE MAY COAL TAR

Analytical Results for Volatile and Semivolatile Organics META Environmental, Inc.

Field ID:	Coal tar - 10 Cape May	Preparation Method:	EPA 3580
		Cleanup Method(s):	EPA 3630mod.
Client:	Lehigh U	Analysis Method:	GC/FID (EPA8100 mod.)
Project:	NAPL Mobility	Matrix:	NAPL
Lab ID:	LU020405-07	Preservation:	None
File ID (PF):	19APRR29.D	Decanted:	No
File ID (DF):	19APRR30.D		
File ID (UF):	19APRR28.D	Sample Size:	0.0155 g
Date Sampled:		%Solid:	100%
Date Received:		Extract Volume:	2 mL
Date Prepared:	4/9/02	Prep DF:	1
Date Cleanup:	4/18/02	Analysis DF:	1
Date Analyzed:	20 Apr 2002 3:31 pm	Injection Volume:	0.001 mL
Instrument:	GC_3		
Operator:	DB	Batch QC:	LU020409-MB

Analyte:	Concentration mg/kg	Q	RL mg/kg	EDL mg/kg	Comments
TARGET COMPOUNDS:					
Aliphatic (PF: C6-C8)	1,200		12.9	6.45	
Aliphatic (PF: C9-C12)	10,900		12.9	6.45	
Aliphatic (PF: C13-C18)	20,600		12.9	6.45	
Aliphatic (PF: C19-C36)		U	12.9	6.45	
Aromatic (DF: C9-C10)	44,600		12.9	6.45	
Aromatic (DF: C11-C22)	438,000		12.9	6.45	
TPH (UF: C6-C36)	570,000		12.9	6.45	
Total VPH	56,700				
Total EPH	470,000				
Total VPH & EPH	516,000				
Extraction Surrogates					
	%R		Min	Max	
Fluorobenzene (DF)		Not Spiked	50%	120%	
2-Fluorobiphenyl (DF)		Not Spiked	50%	120%	
5-alpha-Androstane (PF)		Not Spiked	50%	120%	
Fluorobenzene (UF)		Not Spiked	50%	120%	
2-Fluorobiphenyl (UF)		Not Spiked	50%	120%	
5-alpha-Androstane (UF)		Not Spiked	50%	120%	
Fractionation Surrogates					
2,5-Dibromotoluene (PF)	56%		50%	120%	
2,5-Dibromotoluene (DF)	20%		50%	120%	
2-Bromonaphthalene (DF)	75%		50%	120%	
1-Chlorooctadecane (PF)	58%		50%	120%	

Qualifiers:

B Analyte detected in the blank

D Analyte reported from a diluted extract

U Undetected above the detection limit

J Estimated value detected between the reporting and detection limits

E Estimated value detected above calibration range

I Concentration/Peak ID uncertain due to potential interference

RL Reporting limit is the sample equivalent of the lowest linear calibration concentration

EDL Estimated detection limit is 50% of the RL

Total VPH = Aliphatics (C6-C12) + Aromatics (C9-C10)

Total EPH = Aliphatics (C9-C36) + Aromatics (C11-C22)

Total VPH & EPH = Total VPH + Total EPH - Aliphatics (C9-C12) Due to Range overlap

APPENDIX C. PRIMARY VOLATILE AND SEMIVOLATILE ORGANICS IN
CHARLESTON COAL TAR

Analytical Results for Volatile and Semivolatile Organics
META Environmental, Inc.

Field ID:	Coal tar - 2 Charleston	Preparation Method:	EPA 3570
		Cleanup Method(s):	EPA 3630mod.
Client:	Lehigh U	Analysis Method:	GC/FID (EPA8100 mod.)
Project:	NAPL Mobility	Matrix:	NAPL
Lab ID:	LU020308-02	Preservation:	None
File ID (PF):	10MAYR19.D	Decanted:	No
File ID (DF):	10MAYR20.D		
File ID (UF):	10MAYR18.D	Sample Size:	0.0108 g
Date Sampled:		%Solid:	100%
Date Received:	3/8/02	Extract Volume:	2 mL
Date Prepared:	4/30/02	Prep DF:	50
Date Cleanup:	5/7/02	Analysis DF:	1
Date Analyzed:	11 May 2002 4:24 am	Injection Volume:	0.001 mL
Instrument:	GC_3		
Operator:	DB	Batch QC:	LU020430-MB

Analyte:	Concentration mg/kg	Q	RL mg/kg	EDL mg/kg	Comments
TARGET COMPOUNDS:					
Aliphatic (PF: C6-C8)	567		926	463	
Aliphatic (PF: C9-C12)	1,630		926	463	
Aliphatic (PF: C13-C18)	2,810		926	463	
Aliphatic (PF: C19-C36)		U	926	463	
Aromatic (DF: C9-C10)	91,100		926	463	
Aromatic (DF: C11-C22)	582,000		926	463	
TPH (UF: C6-C36)	626,000		926	463	
Total VPH	93,300				
Total EPH	587,000				
Total VPH & EPH	679,000				
Extraction Surrogates					
	%R		Min	Max	
Fluorobenzene (DF)	Not Spiked		50%	120%	
2-Fluorobiphenyl (DF)	Not Spiked		50%	120%	
5-alpha-Androstane (PF)	Not Spiked		50%	120%	
Fluorobenzene (UF)	Not Spiked		50%	120%	
2-Fluorobiphenyl (UF)	Not Spiked		50%	120%	
5-alpha-Androstane (UF)	Not Spiked		50%	120%	
Fractionation Surrogates					
2,5-Dibromotoluene (PF)	81%		50%	120%	
2,5-Dibromotoluene (DF)	48%		50%	120%	
2-Bromonaphthalene (DF)	255%	I	50%	120%	
1-Chlorooctadecane (PF)	80%		50%	120%	

Qualifiers:

B Analyte detected in the blank
D Analyte reported from a diluted extract
U Undetected above the detection limit
J Estimated value detected between the reporting and detection limits
E Estimated value detected above calibration range
I Concentration/Peak ID uncertain due to potential interference
RL Reporting limit is the sample equivalent of the lowest linear calibration concentration
EDL Estimated detection limit is 50% of the RL
Total VPH = Aliphatics (C6-C12) + Aromatics (C9-C10)
Total EPH = Aliphatics (C9-C36) + Aromatics (C11-C22)
Total VPH & EPH = Total VPH + Total EPH - Aliphatics (C9-C12) Due to Range overlap

APPENDIX D. PRIMARY VOLATILE AND SEMIVOLATILE ORGANICS IN
FAIRFIELD COAL TAR

Analytical Results for Volatile and Semivolatile Organics
META Environmental, Inc.

Field ID:	Coal tar - 4M Fairfield	Preparation Method:	EPA 3570
		Cleanup Method(s):	EPA 3630mod.
Client:	Lehigh U	Analysis Method:	GC/FID (EPA8100 mod.)
Project:	NAPL Mobility	Matrix:	NAPL
Lab ID:	LU020308-04	Preservation:	None
File ID (PF):	10MAYR22.D	Decanted:	No
File ID (DF):	10MAYR23.D		
File ID (UF):	10MAYR21.D	Sample Size:	0.0161 g
Date Sampled:		%Solid:	100%
Date Received:	3/8/02	Extract Volume:	2 mL
Date Prepared:	4/30/02	Prep DF:	50
Date Cleanup:	5/7/02	Analysis DF:	1
Date Analyzed:	11 May 2002 7:40 am	Injection Volume:	0.001 mL
Instrument:	GC_3		
Operator:	DB	Batch QC:	LU020430-MB

Analyte:	Concentration mg/kg	Q	RL mg/kg	EDL mg/kg	Comments
TARGET COMPOUNDS:					
Aliphatic (PF: C6-C8)	1,350		621	311	
Aliphatic (PF: C9-C12)	3,810		621	311	
Aliphatic (PF: C13-C18)	8,190		621	311	
Aliphatic (PF: C19-C36)		U	621	311	
Aromatic (DF: C9-C10)	93,600		621	311	
Aromatic (DF: C11-C22)		U	621	311	
TPH (UF: C6-C36)	116,000		621	311	
Total VPH	98,800				
Total EPH	12,000				
Total VPH & EPH	107,000				
Extraction Surrogates					
	%R		Min	Max	
Fluorobenzene (DF)	Not Spiked		50%	120%	
2-Fluorobiphenyl (DF)	Not Spiked		50%	120%	
5-alpha-Androstane (PF)	Not Spiked		50%	120%	
Fluorobenzene (UF)	Not Spiked		50%	120%	
2-Fluorobiphenyl (UF)	Not Spiked		50%	120%	
5-alpha-Androstane (UF)	Not Spiked		50%	120%	
Fractionation Surrogates					
2,5-Dibromotoluene (PF)	85%		50%	120%	
2,5-Dibromotoluene (DF)	26%		50%	120%	
2-Bromonaphthalene (DF)	303%	I	50%	120%	
1-Chlorooctadecane (PF)	85%		50%	120%	

Qualifiers:

B Analyte detected in the blank

D Analyte reported from a diluted extract

U Undetected above the detection limit

J Estimated value detected between the reporting and detection limits

E Estimated value detected above calibration range

I Concentration/Peak ID uncertain due to potential interference

RL Reporting limit is the sample equivalent of the lowest linear calibration concentration

EDL Estimated detection limit is 50% of the RL

Total VPH = Aliphatics (C6-C12) + Aromatics (C9-C10)

Total EPH = Aliphatics (C9-C36) + Aromatics (C11-C22)

Total VPH & EPH = Total VPH + Total EPH - Aliphatics (C9-C12) Due to Range overlap

APPENDIX E. PRIMARY VOLATILE AND SEMIVOLATILE ORGANICS IN
SARANAC COAL TAR

Analytical Results for Volatile and Semivolatile Organics
META Environmental, Inc.

Field ID:	Coal tar - 5 Saranac	Preparation Method:	EPA 3570
Client:	Lehigh U	Cleanup Method(s):	EPA 3630mod.
Project:	NAPL Mobility	Analysis Method:	GC/FID (EPA8100 mod.)
Lab ID:	LU020308-06	Matrix:	NAPL
File ID (PF):	10MAYR28.D	Preservation:	None
File ID (DF):	10MAYR29.D	Decanted:	No
File ID (UF):	10MAYR27.D	Sample Size:	0.13 g
Date Sampled:		%Solid:	100%
Date Received:	3/8/02	Extract Volume:	2 mL
Date Prepared:	4/30/02	Prep DF:	50
Date Cleanup:	5/7/02	Analysis DF:	1
Date Analyzed:	11 May 2002 2:06 pm	Injection Volume:	0.001 mL
Instrument:	GC_3	Batch QC:	LU020430-MB
Operator:	DB		

Alyte:	Concentration mg/kg	Q	RL mg/kg	EDL mg/kg	Comments
TARGET COMPOUNDS:					
Aliphatic (PF: C6-C8)	146		76.9	38.5	
Aliphatic (PF: C9-C12)	94.8		76.9	38.5	
Aliphatic (PF: C13-C18)	77.0		76.9	38.5	
Aliphatic (PF: C19-C36)		U	76.9	38.5	
Aromatic (DF: C9-C10)	2,580		76.9	38.5	
Aromatic (DF: C11-C22)		U	76.9	38.5	
TPH (UF: C6-C36)		U	76.9	38.5	
Total VPH	2,820				
Total EPH	172				
Total VPH & EPH	2,900				
Extraction Surrogates					
	%R		Min	Max	
Fluorobenzene (DF)	Not Spiked		50%	120%	
2-Fluorobiphenyl (DF)	Not Spiked		50%	120%	
5-alpha-Androstane (PF)	Not Spiked		50%	120%	
Fluorobenzene (UF)	Not Spiked		50%	120%	
2-Fluorobiphenyl (UF)	Not Spiked		50%	120%	
5-alpha-Androstane (UF)	Not Spiked		50%	120%	
Fractionation Surrogates					
2,5-Dibromotoluene (PF)	86%		50%	120%	
2,5-Dibromotoluene (DF)	25%		50%	120%	
2-Bromonaphthalene (DF)	292%	I	50%	120%	
1-Chlorooctadecane (PF)	85%		50%	120%	

Qualifiers:

B Analyte detected in the blank
D Analyte reported from a diluted extract
U Undetected above the detection limit
J Estimated value detected between the reporting and detection limits
E Estimated value detected above calibration range
I Concentration/Peak ID uncertain due to potential interference
RL Reporting limit is the sample equivalent of the lowest linear calibration concentration
EDL Estimated detection limit is 50% of the RL
Total VPH = Aliphatics (C6-C12) + Aromatics (C9-C10)
Total EPH = Aliphatics (C9-C36) + Aromatics (C11-C22)
Total VPH & EPH = Total VPH + Total EPH - Aliphatics (C9-C12) Due to Range overlap

APPENDIX F. PRIMARY VOLATILE AND SEMIVOLATILE ORGANICS IN
SHIPPENSBURG COAL TAR

Analytical Results for Volatile and Semivolatile Organics
META Environmental, Inc.

Field ID:	Coal tar - 8 Shippensburg	Preparation Method:	EPA 3570
		Cleanup Method(s):	EPA 3630mod.
Client:	Lehigh U	Analysis Method:	GC/FID (EPA8100 mod.)
Project:	NAPL Mobility	Matrix:	NAPL
Lab ID:	LU020308-09	Preservation:	None
File ID (PF):	13MAYR11.D	Decanted:	No
File ID (DF):	13MAYR12.D		
File ID (UF):	13MAYR10.D	Sample Size:	0.0148 g
Date Sampled:		%Solid:	100%
Date Received:	3/8/02	Extract Volume:	2 mL
Date Prepared:	4/30/02	Prep DF:	50
Date Cleanup:	5/7/02	Analysis DF:	1
Date Analyzed:	13 May 2002 7:31 pm	Injection Volume:	0.001 mL
Instrument:	GC_3		
Operator:	DB	Batch QC:	LU020430-MB

Analyte:	Concentration mg/kg	Q	RL mg/kg	EDL mg/kg	Comments
TARGET COMPOUNDS:					
Aliphatic (PF: C6-C8)	1,380		676	338	
Aliphatic (PF: C9-C12)	7,260		676	338	
Aliphatic (PF: C13-C18)	7,340		676	338	
Aliphatic (PF: C19-C36)		U	676	338	
Aromatic (DF: C9-C10)	109,000		676	338	
Aromatic (DF: C11-C22)	221,000		676	338	
TPH (UF: C6-C36)	466,000		676	338	
Total VPH	118,000				
Total EPH	236,000				
Total VPH & EPH	346,000				
Extraction Surrogates					
	%R		Min	Max	
Fluorobenzene (DF)	Not Spiked		50%	120%	
2-Fluorobiphenyl (DF)	Not Spiked		50%	120%	
5-alpha-Androstane (PF)	Not Spiked		50%	120%	
Fluorobenzene (UF)	Not Spiked		50%	120%	
2-Fluorobiphenyl (UF)	Not Spiked		50%	120%	
5-alpha-Androstane (UF)	Not Spiked		50%	120%	
Fractionation Surrogates					
2,5-Dibromotoluene (PF)	84%		50%	120%	
2,5-Dibromotoluene (DF)	32%		50%	120%	
2-Bromonaphthalene (DF)	255%	I	50%	120%	
1-Chlorooctadecane (PF)	81%		50%	120%	

Qualifiers:

B Analyte detected in the blank

D Analyte reported from a diluted extract

U Undetected above the detection limit

J Estimated value detected between the reporting and detection limits

E Estimated value detected above calibration range

I Concentration/Peak ID uncertain due to potential interference

RL Reporting limit is the sample equivalent of the lowest linear calibration concentration

EDL Estimated detection limit is 50% of the RL

Total VPH = Aliphatics (C6-C12) + Aromatics (C9-C10)

Total EPH = Aliphatics (C9-C36) + Aromatics (C11-C22)

Total VPH & EPH = Total VPH + Total EPH - Aliphatics (C9-C12) Due to Range overlap

LITERATURE CITED

- Abrams, A. 1975. The influence of fluid viscosity, interfacial tension, and flow velocity on residual oil saturation left by waterflood. *SPE J.*, **October**: 437-447.
- Acevedo, S., X. Gutierrez, and H. Rivas. 2001. Bitumen-in-water emulsions stabilized with natural surfactants. *J. Colloid Interf. Sci.*, **242**: 230-238.
- Adamson, A.W. 1990. Physical Chemistry of Surfaces. 5th edition, John Wiley & Sons, Inc, NY. pp.777.
- Adamski, M., V. Kremese, R.J. Charbeneau. 2003. Residual Saturation: What Is It? How Is It Measured? How Should We Use It? Proceedings of the Petroleum Hydrocarbons and Organic Chemicals in Ground Water: Prevention, Assessment, and Remediation, 20th Conference and exposition, Costa mesa, CA. .
- Ahmed, N., R. McVicker, T.W. Anderson, C. Carpenter, W.L. Cohen, W. Damm, A.I. Johnson, R. Peralta and J.P. Riley. 1997. Ground Water Protection Alternatives and Strategies in the U. S. A. American Society of Civil Engineers, NY. pp. 283.
- American Society for Testing and Materials. 1999. Standard Test Method for Shear Viscosity of Coal-Tar and Petroleum Pitches. Methods ASTM D 5018-89. West Conshohocken, PA.
- American Society for Testing and Materials. 2001. Standard Test Method for Acid Number of Petroleum Products by Potentiometric Titration. Methods ASTM D 664-01. West Conshohocken, PA
- American Society for Testing and Materials. 2003. Standard Test Method for Base Number Determination by Potentiometric Titration. Methods ASTM D 4739-02. West Conshohocken, PA
- American Society for Testing and Materials. 2003. Standard Test Method for Characteristic Groups in Rubber Extender and Processing Oils and Other Petroleum-Derived Oils by the Clay-Gel Absorption Chromatographic Method. Methods ASTM D 2007-03. West Conshohocken, PA.
- Anderson, W.G., 1986. Wettability literature survey-Part 1. Rock/oil/brine interactions, and the effects of core handling on wettability. *J. Pet. Technol.*, **October**: 1125-1149.
- Anderson, W.G. 1987a. Wettability literature survey-Part 4: Effect of wettability on

- capillary pressure. *J. Pet. Technol.*, **October**: 1283-1300.
- Anderson, W.G. 1987b. Wettability literature survey-Part 5: The effects of wettability on relative permeability. *J. Pet. Technol.*, **November**: 1453-1987.
- Anderson, W.G. 1987c. Wettability literature survey-Part 6: The effects of wettability on waterflooding. *J. Pet. Technol.*, **December**: 1605-1621.
- Bachmann, J., R. Horton, R.R. van der Ploeg and S. Woche. 2000. Modified sessile drop method for assessing initial soil-water contact angle of sandy Soil. *Soil Sci. Soc. Am. J.*, **64**: 564-567.
- Bachmat, Y. 1994. Groundwater as part of the water system. p. 5-20. *In* Groundwater Contamination and Control, Zoller, U. (ed.) Marcel Dekker, Inc. NY.
- Backhus, D.A. and P.M. Gschwend. 1994. Groundwater contamination by polycyclic aromatic hydrocarbons: A case study of coal tar-contaminated site. p. 315-325. *In* Groundwater Contamination Control. U. Zoller (ed.). Marcel Dekker, Inc. NY.
- Baran, J.R., Jr., G.A. Pope, W.H. Wade, W. Weerasoorlya and A. Yapa. 1994. Micromulsion formation with chlorinated hydrocarbons of differing polarity. *Environ. Sci. Technol.*, **28**(7): 1361-1366.
- Barranco, F.T., Jr. and H.E. Dawson. 1999. Influence of aqueous pH on the interfacial properties of coal tar. *Environ. Sci. Technol.*, **33**(10): 1598-1603.
- Barranco, F.T., Jr., H.E. Dawson, J.M. Christener and B.D. Honeyman. 1997. Influence of aqueous pH and ionic strength on the wettability of quartz in the presence of dense non-aqueous-phase liquids. *Environ. Sci. Technol.*, **31**(3): 676-681.
- Bassel, M.D. and C.H. Nelson. 2000. Overview of *in situ* chemical oxidation: status and lessons learned. *In* Treating Dense Nonaqueous-Phase Liquids (DNAPLs): Remediation of Chlorinated and Recalcitrant Compounds. (Wickramanayake, G.B., A.R. Gavaskar, N. Gupta (ed.). Battelle Press, Columbus, OH.
- Basu, S., K. Nandakumar, and J.H. Masliyah. 1996. A study of oil displacement on model surfaces. *J. Colloid Interf. Sci.*, **182**: 82-94.
- Basu, S. and M.M. Sharma. 1996. Measurement of critical disjoining pressure of dewetting of solid surfaces. *J. Colloid Interface Sci.*, **181**: 443-455.
- Bear, J. 1972. Dynamics of Fluids in Porous Media. Dover Publication, Inc. NY. pp. 764.
- Bettahar, M., C. Schafer and M. Baviere. 1999. An optimized surfactant formulation for the remediation of diesel oil polluted sandy aquifers. *Environ. Sci. Technol.*, **33**(8): 1269-1273.

- Blake, G.R. and K.H. Hartge. 1986. Particle density. p. 377-382. *In Methods of Soil Analysis, Part I.* Klute, A. (ed.), 2nd edition, American Society of Agronomy, Inc, Soil Science Society of America, Inc. Madison, WI.
- Bockrath, B.C., R.B. LaCount and R.P. Noceti. 1980. Coal-derived asphaltenes: effect of phenol content and molecular weight on viscosity of solutions. *Fuel*, **59**: 621-626.
- Bradford, S.A. and F.J. Leij. 1995. Wettability effects on scaling two- and three-fluid capillary pressure-saturation relations. *Environ. Sci. Technol.*, **29**(6): 1446-1456.
- Brooks, R.H. and A.T. Corey. 1960. Hydraulic properties of porous medium. *Hydrol. Pap.* No. 3, 24., Colorado State University, Fort Collins, CO.
- Bruss, D.B. and G.E.A. Wyld. 1957. Methyl isobutyl ketone as wide-range solvent for titration of acid mixtures and nitrogen bases. *Analy. Chem.*, **29**(2): 232-235.
- Buckley, J.S. 1994. Chemistry of the crude oil/brine interface. p.33-38. *In 3rd International Symposium on Evaluation of Reservoir Wettability and Its Effect on Oil Recovery*, Laramie, WY.
- Buckley, J.S. 2001. Effective wettability of minerals exposed to crude oil. *Curr. Opin. Colloid In.*, **6**: 191-196.
- Buckley, J.S. and J. Wang. 2002. Crude oil and asphaltene xharacterization for prediction of wetting alteration. *J. Pet. Sci. Eng.*, **33**: 195-202.
- Buckley, J.S., K. Takamura and N.R. Morrow. 1989. Influence of electrical surface charges on the wettability properties of crude oils. *SPE Res. Eng.*, **August**: 332-340.
- Buckley, J.S. and Y. Liu. 1998. Some mechanisms of crude oil/brine/solid interactions. *J. Pet. Sci. Eng.*, **20**: 155-160.
- Bunger, J.W. and N.C. Li 1981. Chemistry of Asphaltenes. American Chemical Society. Washington, D. C. pp. 260.
- Chatzis, I., and N.R. Morrow, 1984. Correlation of Capillary Number Relationships for Sandstone. *SPE J.* **October**, 555-562.
- Chevalier, L.R. and J.M. Fonte. 2000. Correlation model to predict residual immiscible organic contaminants in sandy soils. *J. Hazard. Material.*, **B72**: 39-52.
- Chou, S.I. and D.O. Shah 1981. Optimal salinity of polymer solution in surfactant-

- polymer flooding process. p. 843-860. *In* Surface Phenomena in Enhanced Oil Recovery. D. O. Shah (ed.). Plenum Press, NY.
- Cline, P.V., J.J. Delfino and P.S.C. Rao. 1991. Partitioning of aromatic constituents into water from gasoline and other complex solvent mixtures. *Environ. Sci. Technol.*, **25**(5): 914-920.
- Cohen, R.M. and J.W. Mercer. 1993. DNAPL Site Evaluation. U.S. Environmental Protection Agency, Ada, OK.
- Davidson, L.B. 1969. The Effect of temperature on the permeability ratio of different fluid pairs in two-phase systems. *J. Pet. Technol.*, **August**: 1037-1046.
- Davies, J.T. and E.K. Rideal 1963. *Interfacial Phenomena*. 2nd edition. Academic Press Inc., London. pp. 480.
- Davis, E.I. 1994. Effect of temperature and pore size on the hydraulic properties and flow of a hydrocarbon oil in the subsurface. *J. Contam. Hydrol.*, **16**(1): 55-86.
- Dawson, H.E. and P.V. Roberts. 1997. Influence of viscous, gravitational, and capillary forces on DNAPL saturation. *Ground Water*, **35**(2): 261-269.
- Demond, A.H. and A.S. Linder. 1993. Estimation of interfacial tension between organic liquids and water. *Environ. Sci. Technol.*, **27**(12): 2318-2331.
- Demond, A.H., F.N. Desai and K.F. Hayes. 1994. Effect of cationic Surfactants on organic liquid-water capillary pressure-saturation relationships. *Water Resour. Res.*, **30**(2): 333-342.
- Demond, A.H. and P.V. Roberts. 1991. Effect of interfacial forces on two-phase capillary pressure-saturation relationships. *Water Resour. Res.*, **27**(3): 423-437.
- Drummond, C. and J. Israelachvili. 2002. Surface forces and wettability. *J. Colloid Interf. Sci.*, **33**: 123-133.
- Dubey, S.T. and P.H. Doe. 1993. Base number and wetting properties of crude oils. *SPE Reserv. Eng.*, **August**: 195-200.
- Dullien, F.A.L. 1992. *Porous Media Fluid Transport and Pore Structure*, Academic Press, Inc., San Diego, CA. pp. 574.
- Dumore, J.M. and R.S. Schols. 1974. Drainage capillary-pressure Functions and the influence of connate water. *SPE J.*, **October**: 437-444.
- Dwarakanath, V. and G.A. pope. 2000. Surfactant phase behavior with field degreasing solvent. *Environ. Sci. Technol.*, **34**(22): 4842-4848.

- Dwarakanath, V., K. Kostarelos, G.A. Pope, D. Shotts and W.H. Wade. 1999. Anionic surfactant remediation of soil columns contaminated by nonaqueous phase liquid. *J. Contam. Hydrol.*, **38**: 465-488.
- Dwarakanath, V., R.E. Jackson and G.A. Pope. 2002. Influence of wettability on the recovery of NAPLs from alluvium. *Environ. Sci. Technol.*, **36**(2): 227-231.
- Ekmondson, T.A. 1965. Effect of temperature on waterflooding. *J. Can. Pet.*, **November**: 236-242.
- Field, J.A., F. Boelsma, H. Baten and W.H. Rulkens. 1995. Oxidation of anthracene in water/solvent mixtures by the white-rot fungus, *Bjerkandera sp.* Strain BOS 55. *Appl. Microb. Biotechnol.*, **44**: 234-240.
- Fu, X. and P.T. Imhoff. 2002. Mobilization of small DNAPL pools formed by capillary entrapment. *J. Contam. Hydrol.*, **56**: 137-158.
- Gaonkar, A.G. 1992. Effects of salt, temperature, and surfactants on the interfacial tension behavior of a vegetable oil/water System. *J. Colloid Interg. Sci.* **149**(1): 256-260.
- Gee, G.W., and J.W. Bauder. Particle-size analysis. p. 383-398. *In Methods of Soil Analysis, Part I.* Klute, A. (ed.), 2nd edition, American Society of Agronomy, Inc, Soil Science Society of America, Inc. Madison, WI.
- Giese, S.W. and S.E. Powers. 2002. Using polymer solutions to enhance recovery of mobile coal tar and creosote DNAPLs. *J. Contam. Hydrol.*, **58**: 147-167.
- Grant, S.A. 2003. Extension of a temperature effects model for capillary pressure saturation relations. *Water Resour. Res.*, **39**(1): SBH 1-1,10.
- Grant, S.A. and A. Salehzadeh. 1996. Calculation of temperature effects on wetting coefficients of porous solids and their capillary pressure Functions. *Water Resour. Res.*, **32**(2): 261-270.
- Grimberg, S.J., W.T. Stringfellow and M.D. Aitken. 1996. Quantifying the biodegradation of phenanthrene by *Pseudomonas stutzeri* P16 in the presence of a nonionic surfactant. *Appl. Environ. Microbiol.*, **62**(7): 2387-2392.
- Guerin, T.F. 2002. A pilot study for the selection of a bioreactor for remediation of groundwater from a coal tar contaminated site. *J. Hazard, Material.*, **B89**: 241-252.
- Harkins, W.D. and F.E. Brown. 1919. The determination of surface tension (free surface

- energy), and the weight of falling drops: the surface tension of water and benzene by the capillary height method. *J. Amer. Chem. Soc.*, **41**: 499-524.
- Hatheway, A.W. 1999. Manufactured gas in California, 1852-1940: Basis for remedial action. *Practice of Periodical of Hazardous, Toxic, and Radioactive Waste Management*, **July**: 132-146.
- Hesselink, F.T. and M.J. Faber 1981. Polymer-surfactant interaction and its effect on the mobilization of capillary-trapped oil. p. 861-869. *In Surface Phenomena in Enhanced Oil Recovery*. D. O. Shah (ed.). Plenum Press, NY.
- Hiemenz, P.C. 1986. Principles of Colloid and Surface Chemistry. 2nd edition. Marcel Dekker, Inc., NY. pp. 815.
- Hilal, S.H., and S.W. Karickhoff. 2003. SPARC Performs Automated Reasoning in Chemistry. U.S. Environmental Protection Agency. Athens, GA. Available at: <http://ibmlc2.chem.uga.edu/sparc/>
- Hillel, D. 1998. Environmental Soil Physics. Academic Press, San Diego, CA. pp. 771.
- Hirasaki, G. and D.L. Zhang. 2003. Surface chemistry of oil recovery from fractured, oil-wet, carbonate formation. paper SPE 80989, presented at the SPE International Symposium on Oilfield Chemistry, Houston, TX . 5-7 Feb.
- Hirasaki, G.J. 1991. Wettability: Fundamentals and surface forces. *SPE Formation Eval.* 217-226.
- Hirasaki, G.J. and G.A. Pope. 1974. Analysis of factors influencing mobility and adsorption in the flow of polymer solution through porous media. *SPE J.*, **14**: 337-346.
- Hjelmeland, O.S. and L.E. Larrondo. 1986. Experimental investigation of the effects of temperature, pressure, and crude oil composition on interfacial properties. *SPE Reservoir Eng.*, **1**(4): 321-328.
- Hohshima, H. and K. Furusawa 1998. Electrical Phenomena at Interfaces-Fundamentals, Measurements, and Applications. Marcel Dekker, Inc., NY. pp. 628.
- Hool, K. and B. Schuchardt. 1992. A new instrument for the measurement of liquid-liquid interfacial tension and the dynamics of interfacial tension reduction. *Meas. Sci. Technol.*, **3**: 451-457.
- Hugaboom, D.A. and S.E. Powers. 2002. Recovery of coal tar and creosote from porous media: The influence of wettability. *Ground Water Monit. Rem.*, **22**(4): 83-90.

- Hunt, J.R., N. Sitar and K.S. Udell. 1988a. Nonaqueous phase liquid transport and cleanup, 1. Analysis of mechanisms. *Water Resour. Res.*, **24**(8): 1247-1258.
- Hunt, J.R., N. Sitar and K.S. Udell. 1988b. Nonaqueous phase liquid transport and cleanup, 2. Experimental studies. *Water Resour. Res.*, **24**(8): 1259-1269.
- Hunter, R. J. 1987. Foundations of Colloid Science. Oxford University Press, NY. pp 673.
- Irwin, R.J., M. van Mouwerik, L. Stevens, M.D. Seese, and W. Basham. 1998. Environmental Contaminants Encyclopedia. National Park Service, Water Resources Division, Fort Collins, CO.
- Israelachvili, J. 1995. Intermolecular and Surface Forces, Academic Press Inc., London.
- Istok, J.D. and J.A. Field. 1999. *In-situ*, field scale evaluation of surfactant-enhanced DNAPL recovery using a single-well, "Push-Pull" test. Oregon State University, Corvallis, OR.
- Jayanti, S., L.N. Britton, V. Dwarakanath and G.A. Pope. 2002. Laboratory evaluation of custom-designed surfactants to remediate NAPL source zones. *Environ. Sci. Technol.*, **36**(24): 5491-5497.
- Jimenez, I.Y. and R. Bartha. 1996. Solvent-augmented mineralization of pyrene by a *Mycobacterium sp.* *Appl. Environ. Microbiol.*, **62**(7): 2311-2316.
- Karagunduz, A., K.D. Pennell, and M.H. Young. 2001. Influence of a nonionic surfactant on the water retention properties of unsaturated. *Soils. Soil Sci. Soc. Am. J.*, **65**: 1392-1399.
- Kilbane, J.J., II. 1997. Extractability and subsequent biodegradation of PAHs from contaminations soil. 285-304.
- Klute, A. 1986. Water retention: Laboratory methods. p. 635-662. *In* Methods of Soil Analysis, Part 1. Klute, A. (ed.). 2nd edition, American Society of Agronomy, Inc, Soil Science Society of America, Inc. Madison, WI.
- Klute, A. and C. Dirksen. 1986. Hydraulic conductivity and diffusivity: Laboratory methods. p. 687-734. *In* Methods of Soil Analysis, Part 1. Klute, A. (ed.). 2nd edition, American Society of Agronomy, Inc, Soil Science Society of America, Inc. Madison, WI.
- Kool, J.B. and J.C. Parker. 1987. Development and evaluation of closed-form expressions for hysteretic soil hydraulic properties. *Water Resour. Res.*, **23**(1): 105-114.
- Kostecki, P.T. and E.J. Calabrese 1991. Hydrocarbon Contaminated Soils and

Groundwater. Lewis Publishers, Boca Raton, FL.

- Krzyżanowska, T. and A. Marzec. 1978. Coal derived group component effects on viscosity. *Fuel*, **57**: 804-805.
- Lakatos, I., J. lakatos-Szabo and J. Toth. 1981. Factors influencing polyacrylaide adsorption in porous media and their effect on flow behavior. p. 821-842. *In* Surface Phenomena in Enhanced Oil Recover. Shah, D.O. (ed.) Plenum Press, NY.
- Lake, L.W. 1989. Enhanced Oil Recovery. Englewood Cliffs, Prentice Hall, NY. pp.550.
- Lantz, S.E., M.T. Montgomery, W.W. Schultz, P.H. Pritchard, B.J. Spargo and J.G. Mueller. 1997. Constituents of an organic wood preservative that inhibit the fluoranthene-degrading activity of *Sphingomonas paucibilis* Strain EPA505. *Environ. Sci. Technol.*, **37**: 3573-3580.
- Lee, L.S., M. Hagwall, J.J. Delfino and P.S.C. Rao. 1992a. Partitioning of polycyclic aromatic hydrocarbons from diesel fuel into water. *Environ. Sci. Technol.*, **26**(11): 2104-2110.
- Lee, L.S., P.S.C. Rao and I. Okuda. 1992b. Equilibrium partitioning of polycyclic aromatic hydrocarbons from coal tar into water. *Environ. Sci. Technol.*, **26**(11): 2110-2115.
- Lee, D-H., R.D. Cody and B.L. Hoyle. 2001a. Comparison of six surfactants in removing toluene and trichlorobenzene from a sandy soil under laboratory conditions. *Can. Geotech. J.*, **38**: 1329-1334.
- Lee, P-H., S.K. Ong, J. Golchin and G.L. (sam) Nelson. 2001b. Use of solvents to enhance PAH biodegradation of coal tar-contaminated soils. *Water Res.*, **35**(16): 3941-3949.
- Lenhard, R.J. and J.C. Parker. 1988. Experimental validation of the theory of extending two-phase saturation-pressure relations to three-fluid phase systems for monotonic drainage paths. *Water Resour. Res.*, **34**(3): 373-380.
- Lenhard, R.J. 1992. Measurement and modeling of three-phase saturation-pressure hysteresis. *J. Contam. Hydrol.*, **9**: 243-269.
- Leuschner, A.P., M.W. Moeller, J.A. Gerrish, and L.A. Johnson. 1997. Case study: MGP site remediation using enhanced DNAPL Recovery. p. 607-620. *In* Contaminated soils. **2**. Kostechi, P.T., E.J. Clabrese, and M. Bonazountas (Ed.), Amherst Scientific Publishers, Amherst, MA.

- Link, A. 2000. Effect of nonionic surfactants on fission of polycyclic aromatic hydrocarbons from coal tar. *Practice of Periodical of Hazardous, Toxic, and Radioactive Waste Management*, **April**: 78-81.
- Liu, H. 1995. Enhancing oil recovery by using of polymer waterflooding. *Shiyou Kantan Yu Kaifa*, **22(2)**: 64-67.
- Liu, H.H. and J.H. Dane. 1993. Reconciliation between measured and theoretical temperature effects on soil water retention curves. *Soil Sci. Soc. Am. J.*, **57**: 1202-1207.
- Liu, J., Z. Xu, and J. Masliyah. 2003. Studies on bitumen-silica interaction in aqueous solutions by atomic force microscopy. *Langmuir*, **19**: 3911-3920.
- Lord, D.L., A.H. Demond, A. Salehzadeh and K.F. Kayes. 1997a. Influence of organic acid solution chemistry on subsurface transport properties 2. capillary pressure-saturation. *Environ. Sci. Technol.* **31(7)**: 2052-2058.
- Lord, D.L., K.F. Kayes, A.H. Demond and A. Salehzadeh. 1997b. Influence of organic acid solution chemistry on subsurface transport properties. 1. Surface and interfacial tension. *Environ. Sci. Technol.* **31(7)**: 2045-2051.
- Lord, D.L., A.H. Demond and K.F. Kayes. 2000. Effects of organic base chemistry on interfacial tension, wettability, and capillary pressure in multiphase subsurface waste systems. *Transp. Porous Media.* **38**: 79-92.
- Lowe, D.F., C.L. Oubre and C.H. Ward 1999. Surfactants and Cosolvents for NAPL Remediation, Lewis Publishers, Boca Raton, FL. pp. 412.
- Luthy, R.G., A. Ramaswami, S. Ghoshal and W. Merkel. 1993. Interfacial films in coal tar nonaqueous-phase liquid-water systems. *Environ. Sci. Technol.*, **27(13)**: 2914-2918.
- MacDonald, J.A., and M.C. Kavahaugh. 1994. Restoring contaminated groundwater: An achievable goal? *Environ. Sci. Technol.*, **28(8)**: 362A-368A.
- Mackay, D.M. and J.A. Cherry. 1989. Groundwater contamination: pump-and-treat remediation. *Environ. Sci. Technol.*, **23(6)**: 630-636.
- Mahjoub, B., M. Jayr, R. Bayard and R. Gourdon. 2000. Phase partition of organic pollutants between coal tar and water under variable experimental conditions. *Water Res.*, **34(14)**: 3551-3560.
- Marshall, T.J., J.W. Holmes, and C.W. Rose. 1996. Soil Physics. Cambridge University Press, NY. pp. 453.

- Martel, K.E., R. Martel, R. Lefebvre and P.J. Gelinas. 1998. Laboratory study of polymer solutions used for mobility control during *in situ* NAPL recovery. *GWRR*, **Summer**: 103-113.
- McCaffery, F.G. 1972. Measurement of interfacial tensions and contact angles at high temperature and pressure. *J. Can. Pet.*, **July-September**: 26-32.
- McGowan, T.F., B.A. Greer and M. Lawless. 1996. Thermal treatment and non-thermal technologies for remediation of manufactured gas plant sites. *Waste manage.*, **16(8)**: 691-698.
- Mennella, A. and N.R. Morrow. 1995. Point-by-point method of determining contact angle from dynamic Wilhelmy plate data for oil/brine/solid systems. *J. Colloid Interf. Sci.*, **172**: 48-55.
- Mercer, J.W. and R.M. Cohen. 1990. A review of immiscible fluids in the subsurface: properties, models, characterization and remediation. *J. Contam. Hydrol.*, **6**: 107-163.
- Minitab, 2004 MINITAB 14 (Demo), Minitab, State College, PA.
- Moran, K., A. Yeung, J. Czarnecki and J. Masliyah. 2000. Micron-scale tensiometry for studying density-matched and highly viscous fluids-with application to bitumen-in-water emulsions. *Colloid Surface, A*: **174(1-2)**: 147-157.
- Morrow, N.R. 1975. The effects of surface roughness on contact angle with special reference to petroleum recovery. *J. Can. Pet.*, **14(4)**: 42-53.
- Morrow, N.R. 1976. Capillary pressure correlations for uniformly wetted porous media. *J. Can. Pet.*, **October-December**: 49-69.
- Morrow, N.R. 1990. Wettability and its effect on oil recovery. *J. Pet. Technol.*,: 1476-1484.
- Morrow, N.R. and B. Songkran 1981. Effect of viscous and buoyancy forces on nonwetting phase trapping in porous media. p. 387-411 *In Surface Phenomena in Enhanced Oil Recovery*. Shah, D.O. (ed.), Plenum Press, NY.
- Mualem, Y. 1974. A conceptual model of hysteresis. *Water Resour. Res.*, **10(3)**: 514-520.
- Mualem, Y., and H.J. Morel-Seytoux. 1978. Analysis of a capillary hysteresis model based on a one-variable distribution function. *Water Resour. Res.*, **14(4)**: 605-610.
- Mungan, N., F.W. Smith and J.L. Thompson. 1960. Polymer floods. *J. Pet., Technol.*, **18(10)**: 1143-1150.

- National Library of Medicine, 1994. Hazardous Substances Data Bank. Available at:<http://sis.nlm.nih.gov/Tox/ToxHSDB.html>
- Nelson, E.C., S. Ghoshal, J.C. Edwards, G.X. Marsh and R.G. Luthy. 1996. Chemical characterization of coal tar-water interfacial films. *Environ. Sci. Technol.* **30**(3): 1014-1022.
- Ng, K.M., H.T. Davis and L.E. Scriven. 1978. Visualization of blob mechanics in flow through porous media. *Chem. Eng. Sci.* **33**: 1009-1017.
- Orkoula, M.G., P.G. Koutsoukos, M. Robin, O. Vizika and L. Cuiec. 1999. Wettability of CaCO₃ surfaces. *Colloids Surface A.* **157**: 333-340.
- Pankow, J.F. and J.A. Cherry. 1996. Dense Chlorinated Solvents and Other DNAPLs in Groundwater, Waterloo Press, Portland, OR. pp. 552.
- Parker, J.C. and R.J. Lenhard. 1987. A model for hysteretic constitutive relations governing multiphase flow 1. Saturation-pressure relations. *Water Resour. Res.*, **23**(12): 2187-2196.
- Parra-Barraza, H., D. Hernandez-Montiel, J. Lizardi, J. Hernandez, R.H. Urbina and M.A. Valdez. 2003. The zeta potential and surface properties of asphaltenes obtained with different crude oil/n-heptane properties. *Fuel*, **82**: 869-874.
- Paterson, I.F., B.Z. Chowdhry and S.A. Leharne. 1999. Polycyclic aromatic hydrocarbon extraction from a coal tar-contaminated soil using aqueous solutions of nonionic surfactants. *Chemosphere*, **38**(13): 3095-3107.
- Pennell, K.D.; R.D. Rhue; W.G. Harris. 1991. The effect of heat treatments on the total charge and exchangeable cations of calcium-, sodium-, and lithium-saturated kaolinite. *Clay Clay Miner.*, **39**(3): 306-315.
- Pennell, K.D., L.M. Abriola and W.J. Weber, Jr. 1993. Surfactant-enhanced solubilization of residual dodecane in soil column. 1. Experimental investigation. *Environ. Sci. Technol.*, **27**: 2332-2340.
- Pennell, K.D., M. Jin, L.M. Abriola and G.A. Pope. 1994. Surfactant enhanced remediation of soil columns contaminated by residual tetrachloroethylene. *J. Contam. Hydrol.*, **16**: 35-53.
- Pennell, K.D., G.A. Pope and L.M. Abriola. 1996. Influence of viscous and buoyancy forces on the mobilization of residual tetrachloroethylene during surfactant flushing. *Environ. Sci. Technol.*, **30**(4): 1328-1335.
- Peramanu, S., B.B. Pruden, and P. Rahimi. 1999. Molecular weight and specific gravity

- distribution for athabasca and Cold Lake bitumens and their saturate, aromatic resin and asphaltene fractions. *Ind. Eng. Chem. Res.*, **38**: 3121-3130.
- Peters, C.A. and R.G. Luthy. 1993. Coal tar dissolution in water-miscible solvents: experimental evaluation. *Environ. Sci. Technol.* **27**(13): 2831-2843.
- Peters, C.A. and R.G. Luthy. 1994. Semiempirical thermodynamic modeling of liquid-liquid phase equilibria: Coal tar dissolution in water-miscible solvents. *Environ. Sci. Technol.*, **28**(7): 1331-1340.
- Peters, C.A., C.D. Knightes and D.G. Brown. 1999. Long-term composition dynamics of PAH-containing NAPLs and implications for risk assessment. *Environ. Sci. Technol.*, **33**(24): 4499-4507.
- Pfannkuch, H. 1983. Hydrocarbon Spills, Their retention in the subsurface and propagation into shallow aquifers. *Office of Water Research and Technology*, Washington, D. C.
- Powers, S.E. and M.E. Tamblin. 1995. Wettability of porous media after exposure to synthetic gasolines. *J. Contam. Hydrol.*, **19**: 105-125.
- Powers, S.E., W.H. Anckner and T.F. Seacord. 1996. Wettability of NAPL-contaminated sands. *J. Environ. Eng.*, **October**: 889-896.
- Prieur, J.R. 1994. Restoration of petroleum- and solvent-contaminated aquifers: general and specific considerations. p. 627-642. *In Groundwater Contamination and Control*. Zoller, U. (Ed). Marcel Dekker, Inc., NY.
- Ramaswami, A., S. Ghoshal and R.G. Luthy. 1994. Mass transfer and biodegradation of PAH compounds from coal tar. *Water Sci. Technol.*, **30**(7): 61-70.
- Ramaswami, A., P.K. Johanson, M. Isleyen, A.R. Bielefeldt and T. Illangasekare. 2001. Assessing multicomponent DNAPL biostabilization. I. Coal tar. *J. Environ., Eng.*, **December**: 1065-1072.
- Ramaswami, A. and R.G. Luthy. 1997. Mass transfer and bioavailability of PAH compounds in coal tar NAPL-slurry systems. 1. Model development. *Environ. Sci. Technol.*, **31**(8): 2260-2267.
- Ramaswami, A., S. Ghoshal and R.G. Luthy. 1997. Mass transfer and bioavailability of PAH compounds in coal tar NAPL-slurry systems. 2. Experimental evaluations. *Environ. Sci. Technol.*, **31**(8): 2268-2276.
- Rame, E. 1997. The interpretation of dynamic contact angles measured by the Wilhelmy Plate method. *J. Colloid Interf. Sci.*, **185**: 245-251.

- Ramsburg, C.A. 2002. Development of Surfactant-Based Immiscible Displacement Technologies for Remediation of Aquifers Contaminated with Dense Non-Aqueous Phase Liquids. PhD thesis, Georgia Institute of Technology, Atlanta, GA.
- Rao, D.N., and R.S. Karyampudi. 1995. Productivity enhancing wettability control technology for cyclic steam process in the Elk Point Cummings formation, Paper 95-62, presented at the 46th Annual Technical Conference of CIM, Banff, Alberta, 14-17 May, 1995.
- Rao, D.N. 1999. Wettability effects in thermal recovery operations. *SPE Reservoir. Eval. Eng.*, **2**(5): 420-430.
- Rathmell, J.J., P.H. Braun and T.K. Perkins. 1973. Reservoir waterflood residual oil saturation from laboratory tests. *J. Pet. Technol.*, **25**: 175-185.
- Reed, R.L., and R.N. Realy. 1977. Some physicochemical aspects of microemulsion flooding: A review. p. 383-437. *In Improved Oil Recovery by Surfactant and Polymer Flooding*. Shah, D.O. and R.S. Schechter (eds.), Academic Press, NY.
- Reid, R.C., J.M. Prausnitz and B.E. Poling. 1987. Properties of gases and liquids. 4th edition, McGraw-Hill, NY. pp.741.
- Roberts, J.E., R.J. Spontak, H. Jameel, and S.A. Khan, 1996a. A novel approach to black liquor viscosity reduction using salt additives. *TAPPI J.* **79**(8), 167-174.
- Roberts, J.E., S.A. Khan, and R.J. Spontak. 1996b. Controlled black liquor viscosity reduction through salting-in. *AIChE J.* **42**(8), 2319-2326.
- Rouse, J.D., D.A. Sabatini and J.H. Harwell. 1993. Minimizing surfactant losses using twin-head anionic surfactants in subsurface remediation. *Environ. Sci. Technol.*, **27**(10): 2072-2078.
- Rouse, J.D., O.S. Hirata and K. Furukawa. 2001. Influence of diphenyloxide disulfonate surfactants on biodegradation of hydrocarbons. *Global Nest. Int. J.*, **3**(1): 23-36.
- Saripalli, K.P., M.D. Annable and P.S.C. Rao. 1997. Estimation of nonaqueous phase liquid-water interfacial areas in porous media following mobilization by chemical flooding." *Environ. Sci. Technol.*, **31**(12): 3384-3388.
- Schramm, L.L., E.N. Stasiuk and D. Turner. 2003. The influence of interfacial tension in the recovery of bitumen by water-based conditioning and flotation of athabasca oil sands. *Fuel Process. Technol.*, **80**: 101-118.
- Schwarzenbach, R.P., P.M. Gschwend, and D.M. Imboden. 2003. Environmental Organic Chemistry. John Wiley & Sons, Inc. Hoboken, NJ.

- Seo, H.S. and J.E. McCray. 2002. Interfacial Tension of Chlorinated Aliphatic DNAPL Mixtures as a Function of Organic Phase Composition. *Environ. Sci. Technol.*, **36**(6): 1292-1298.
- She, H.Y. and B.E. Sleep. 1998. The Effect of Temperature on Capillary Pressure-Saturation Relationships for Air-Water and Perchloroethylene-Water Systems. *Water Resour. Res.*, **34**(10): 2587-2597.
- Sheu, E.Y., D. A. Storm, 1995. Colloidal Properties of Asphaltenes in Organic Solvents. . *In Asphaltenes-Fundamentals and Applications*. (Sheu, E. Y. and O. C. Mullins, ed). Plenum Press NY.
- Skauge, A., S. Standal, S.O. Boe, T. Skauge and A.M. Blokhus. 1999. Effect of organic acids and bases, and oil composition on wettability. paper SPE 56673, presented at the SPE Annual Technical Conference and Exhibition, Houston, TX, 2-3 Oct, 1999.
- Slater, G.E. and S.M. Farouq Ali. 1970. Simulation of oil recovery by polymer flooding. *J. Can. Pet. Technol.*, **9**(4): 251-260.
- Sleep, B.E. and Y. Ma. 1997. Thermal variation of organic fluid properties and impact on thermal remediation feasibility. *J. Soil Contam.*, **6**(3): 281-306.
- Smith, L.A., R.E. Hinchee. 1993. In situ Thermal Technologies for Site Remediation. Lewis Publishers, Boca Raton, FL. pp.209.
- Standal, S., J. Haavik, A.M. Blokhus and A. Skauge. 1999a. Effect of polar organic components on wettability as studied by adsorption and contact angles. *J. Pet. Sci. Eng.*, **24**: 131-144.
- Standal, S.H., A.M. Blokhus, J. Haavik, A. Skauge and T. Barth. 1999b. Partition coefficients and interfacial activity for polar components in oil/water model systems. *J. Colloid Interf. Sci.*, **212**: 33-41.
- Standnes, D.C. and T. Austad. 2003. Wettability alteration in carbonates low-cost ammonium surfactants based on bio-derivatives from the coconut palm as active chemicals to change the wettability from oil-wet to water-wet conditions. *Colloid Surf. A*, **218**: 161-173.
- Steffy, D.A., D.A. Barry and C.D. Johnston. 1997. Influence of antecedent moisture content on residual LANPL saturation. *J. Soil Contam.*, **6**(2): 113-147.
- Syracuse Research Corporation, 2004. KowWin (online Demo) Available at: <http://esc.syrres.com/interkow/physdemo.htm>.

- Systat Software Inc (SSI), 2000, SigmaPlot 2000.
- Taugbol, K., T.V. Ly and T. Austad. 1995. Chemical flooding of oil reservoirs. 3. Dissociative surfactant-polymer interaction with a positive effect on oil recovery. *Colloid Surf. A*, **103**: 83-92.
- Thomas, M.G. and B. Granoff. 1978. Coal-derived product effects on viscosity. *Fuel*, **57**(2): 122-123.
- Toride, N., F.J. Leiji and M. Th. van Genuchten. 1995. The CXTFIT Code for Estimating Transport Parameters from Laboratory or Field Tracer Experiments. Research Report No. 137. U. S. Salinity Laboratory. Riverside, CA. pp. 121.
- U.S. Environmental Protection Agency (EPA) 1995. National Primary Drinking Water Regulations, Contaminant Specific Fact Sheets, Volatile Organic Chemicals - Technical Version. Office of Water, EPA 811-F-95-004-T, EPA, Washington, D.C.
- U.S. Environmental Protection Agency (EPA) 2000. A Resource for MGP Site Characterization and Remediation: Expedited Site Characterization and Source Remediation at Former Manufactured Gas Plant Sites. EPA 542-R-99-005, U.S. Environmental Protection Agency, Office of Solid Waste and Emergency Response, Washington, D.C.
- U.S. Environmental Protection Agency (EPA) 2001. Coal Tar Contamination Associated with a Former Manufactured Gas Plant Ashland/Northern States Power Lakefront. CERCLIS No. WISFN0507952, Wisconsin Department of Health and Family Services, Division of Public Health, Ashland, WI.
- van Geel, P. J. and J. F. Sykes. 1997. The importance of fluid entrapment, saturation hysteresis and residual saturations on the distribution of a lighter-than-water non-aqueous phase liquid in a variably saturated sand medium. *J. Contam. Hydrol.*, **25**(3-4): 249-270.
- van Geel, P. J. and S. D. Roy. 2002. A proposed model to include a residual NAPL saturation in a hysteretic capillary pressure-saturation relationship. *J. Contam. Hydrol.*, **58**(1-2): 79-110.
- van Genuchten, M. T. 1980, A closed-form equation for predicting the hydraulic conductivity of unsaturated soils. *Soil Sci. Soc. Am. J.*, **44**: 892-898.
- van Genuchten, M.T., F.J. Leiji and S.R. Yates. 1991. The RETC Code for Quantifying the Hydraulic Functions of Unsaturated Soils. EPA/600/2-91/065. U. S. Salinity Laboratory, Riverside, CA. pp. 95.
- Villaume, J.F. 1985. Investigations at sites contaminated with dense, non-aqueous phase

- liquids (NAPLs). *Ground Water Monit. Rev.*, **Spring**: 60-74.
- Volpe, C.D., C. Cassinelli and M. Morra. 1998. Wihelmy plate measurements on poly (N-isopropylacrylamide)-grafted surfaces. *Langmuir*, **14**: 4650-4656.
- Ward, A.D., R.H. Ottewill and R.D. Hazlett. 1999. An investigation into the stability of aqueous films separating hydrocarbon drops from quartz surfaces. *J. Pet. Sci. Eng.*, **24**: 213-220.
- Werner, A., F. Behar, J.C.de Hemptinne, and E. Behar. 1998. Viscosity and phase behavior of petroleum fluids with high asphaltene Contents. *Fluid Phase Equilib.*, **147**(1-2): 343-356.
- West, C.C. 1992. Surfactants and subsurface remediation. *Environ. Sci. Technol.*, **26**(12): 2324-2330.
- Weast, R.C., M.J. Astle, and W.H. Beyer (ed.). 1986-1987. CRC Handbook of Chemistry and Physicals, 67th edition, F-4-5, 37. CRC Press, Boca Raton, FL.
- Wilkins, M.D., L.M. Abriola and K.D. Pennell. 1995. An experimental investigation of rate-limited mass transfer during soil vapor extraction. *Water Resour. Res.*, **21**: 2159-2168.
- Wilkinson, W. L. 1960. Non-newtonian fluids; fluid mechanic, mixing and heat transfer. Pergamon Press, NY. pp. 138.
- Wipfler, E.L. and S.E.A.T.M. van der Zee. 2001. A set of constitutive relationships accounting for residual NAPL in the unsaturated zone. *J. Contam. Hydrol.*, **50**(1-2): 53-77.
- Xie, X. and N.R. Morrow. 1999. Contact angles on quartz induced by adsorption of heteropolar hydrocarbons. *J. Adhes. Sci. Technol.*, **13**(10): 1119-1135.
- Yang, S-Y., G.J. Hirasaki, S. Basu and R. Vaidya. 2002. Statistical analysis on parameters that affect wetting for the crude oil/brine/mica system." *J. Pet. Sci. Eng.*, **33**: 203-215.
- Yeom, I.T., M.M. Ghosh, C.D. Cox and K.G. Robinson. 1995. Micellar solubilization of polynuclear aromatic hydrocarbons in coal tar-contaminated soils. *Environ. Sci. Technol.*, **29**(12): 3015-3021.
- Yeom, I.T., M.M. Ghosh and C. D. Cox. 1996. Kinetic aspects of surfactant solubilization of soil-bound polycyclic aromatic hydrocarbons. *Environ. Sci. & Technol.*, **30**(5): 1589-1595.
- Young, C.M., V. Dwarakanath, T. Malik, L. Milner, J. Chittet, N. Huston and V.

- Weerasooriya 2002. *In situ* remediation of coal tar-impacted soil by polymer-surfactant flooding. The Third International Conference on Remediation of Chlorinated and Recalcitrant Compounds, Monterey, CA.
- Zheng, J. and S.E. Powers. 1999. Organic bases in NAPLs and their impact on wettability. *J. Contam. Hydrol.* **39**: 161-181.
- Zheng, J. 2001, Mechanisms That Affect the Wettability of Quartz Exposed to Coal-Derived Non-Aqueous Phase Liquids. PhD thesis. Clarkson University. NY.
- Zheng, J., S.H. Behrens, M. Borkovec and S.E. Powers. 2001a. Predicting the wettability of quartz surfaces exposed to dense nonaqueous phase liquids. *Environ. Sci. Technol.* **35**(11): 2207-2213.
- Zheng, J., J. Shao and S.E. Powers. 2001b. Asphaltenes from coal tar and creosote: Their role in reversing the wettability of aquifer systems. *J. Colloid Interf.Sci.* **344**: 365-371.
- Zheng, J., S.H. Behrens, M. Borkovec and S.E. Powers. 2001c. Predicting the wettability of quartz surfaces exposed to dense nonaqueous phase liquids. *Environ. Sci. Technol.* **35**(11): 2207-2213.
- Zheng, J. and S.E. Powers. 2003. Identifying the effect of polar constituents in coal-derived NAPLs on interfacial tension. *Environ. Sci. Technol.* **37**(14): 3090-3094.
- Zytner, R.G., Biswas, Nihar, Bewtra and K. Jatinder. 1993. Retention capacity of dry soils for NAPLS. *Environ. Technol.* **14**(11): 1073-1080.

VITA

Lingjun Kong was born in Hunan Province, China in May 1968. Her mother was a teacher, and her father was an engineer. In 1979, she entered into the best high school in the city through strict examination within top 10 among the children all over the city. The six years in high school was one of the happiest times in her life. She totally enjoyed the competitive but colorful life. In 1985, she graduated from high school with the highest score in the city, and joined Shanghai Jiao Tong University, Shanghai, China. She got her BS in Electrochemistry (Applied Chemistry) in July, 1989, and was honored to go to the Environmental Engineering program in graduate school at Shanghai Jiao Tong University without the entrance examination. Her MS thesis was focused on detergent adsorption on MgO adsorbent. After graduation, she became a teacher in Beijing Institute of Clothing Technology (original named Beijing Institute of Chemical and Textile Engineering) in April 1992. She came to the United States in 1998, and worked for Dr Kevin H. Gardner at Case Western Reserve University. Her research at CWRU was about the hematite transport in porous media. She transferred to Georgia Institute of Technology in August 1999, and has been working for Dr Kurt D. Pennell ever since then. During the first two years at Georgia Tech, she was working on the Cryptosporidium transport in porous media, and started working on a quiet different project about NAPL residual saturation in porous media from 2001. She got her PhD degree in Environmental Engineering in July, 2004.